ORNL/MD/LTR-241
Volume 1
Revision 0

MOX Test Fuel 40 GWd/MT PIE: Final Report

R.N. Morris
C.A. Baldwin
N.H. Packan

August 2003

Fissile Materials Disposition Program

Notice
This report was prepared as an account of work sponsored by an agency of the United States Government. Neither the United States Government nor any agency thereof, or any of their employees, makes any warranty, expressed or implied, or assumes any legal liability or responsibility for the accuracy, completeness, or usefulness of any information, apparatus, product, or process disclosed, or represents that its use would not infringe privately owned rights. Reference herein to any specific commercial product, process, or service by trade name, trademark, manufacturer, or otherwise, does not necessarily constitute or imply its endorsement, recommendation, or favoring by the United States Government or any agency thereof. The views and opinions of authors expressed herein do not necessarily state or reflect those of the United States Government or any agency thereof.

Revision History

Revision number	Date Issued	Reason for revision
0	August 2003	First Issue

Post Office Box 2008
Bldg. 3525, MS 6295, Room 104
Oak Ridge, TN 37831-6295
Phone: (865) 241-4237
Fax: (865) 576-7862
Email: morrisrn@ornl.gov

August 2003

Distribution

MOX Test Fuel 40 GWd/MT PIE: Final Report

The enclosed document details the MOX Test Fuel PIE that was performed on Capsules 4 and 13, which were withdrawn from the Advanced Test Reactor in March 2002 with average burnups of approximately 40 GWd/MT. This task was conducted under the DOE Fissile Materials Disposition Program (FMDP). This work was carried out at the Irradiated Fuels Examination Laboratory by the staff of the Metals and Ceramics Division of the Oak Ridge National Laboratory during the period from May 2002 though June 2003.

This is a Level-2 document as defined in the Fissile Materials Disposition Program Light-Water Reactor Mixed-Oxide Fuel Irradiation Test Project Plan, ORNL/MD/LTR-78, Rev 2.

Sincerely,

Robert N. Morris
Fissile Materials Disposition Program

Enclosure

Distribution: See Section 10 of enclosure

ORNL/MD/LTR-241
Volume 1
Revision 0

MOX Test Fuel 40 GWd/MT PIE: Final Report

R.N. Morris
C.A. Baldwin
N.H. Packan

August 2003

Oak Ridge National Laboratory

CONTENTS

FIGURES vii

TABLES xiii

ACRONYMS xv

ABSTRACT xvi

EXECUTIVE SUMMARY xvii

1. INTRODUCTION 1-1
   1.1 General 1-1
   1.2 Scope 1-1
   1.3 Gallium Migration 1-2
   1.4 Findings Concerning Code Representation and Predictions 1-2

2. PREIRRADIATION CHARACTERIZATION 2-1
   2.1 Fuel Types 2-1
   2.2 Irradiation Geometry 2-3
   2.3 Preirradiation Dimensional Data 2-7

3. IRRADIATION HISTORY FOR CAPSULES 4 AND 13 AND ACCURACY OF CARTS CODE PREDICTIONS 3-1
   3.1 Irradiation History for Phase I 3-1
   3.2 Irradiation History for Phase II 3-3
   3.3 Irradiation History for Phase III Part 1 3-5
   3.4 Irradiation History for Phase IV Part 1 3-7
   3.5. Irradiation Summary and CARTS Predictions Accuracy for Capsules 4 and 13 3-9
      3.5.1. Pellet Temperatures 3-10
      3.5.2. Pellet – Clad Interface 3-11
      3.5.3 Fuel Pin Internal Pressure 3-12

4. METROLOGY OF CAPSULES 4 AND 13 4-1
   4.1 Capsule Photo Visual Inspection 4-1
   4.2 Capsule Temperature Measurements 4-5
   4.3 Capsule Dimensional Inspection 4-5
   4.4 Capsule Gamma Scans 4-7
      4.4.1 Capsule 4 Gamma Scan 4-7
      4.4.2 Capsule 13 Gamma Scan 4-13
      4.4.3 Gamma Scanner Data Collection Orientation 4-18
   4.5 Fission Gas Measurements 4-18

4.6 Fuel Pin Photo Visual Inspections 4-21
4.7 Fuel Pin Dimensional Inspections 4-24
4.7.1 Fuel Pin Volume Measurement 4-25
4.7.2 Fuel Density Measurement 4-25

5. METALLOGRAPHY 5-1
5.1 Introduction 5-1
5.2 Sample Preparation 5-1
5.3 Results of the Polishing 5-1
5.4 Mount Etching 5-40
5.5 Gamma Scan of Mount 6219 5-43
5.6 SEM Mounts 5-45
5.6.1 Fuel Pin 7 SEM Mount 5-45
5.6.2 Fuel 16 SEM Mount 5-54
5.7 Metallographic Summary 5-61

6. RADIOCHEMISTRY RESULTS 6-1
6.1 Introduction 6-1
6.2 Gallium Analysis Results 6-1
6.3 Burnup Analysis 6-11
6.4 Capsule 4 & 13 Surface Investigation 6-11
6.5 Radiochemical Summary 6-12

7. SUMMARY AND CONCLUSIONS 7-1
7.1 Fuel and Clad Performance Found Acceptable 7-1
7.2 Permanent Clad Expansion 7-2
7.3 Clad Samples Identified for Future Testing 7-2
Sample 7-3
7.4 Summary of Adjusted Pressure and Release Fraction Measurements 7-3
Pressure 7-4

8. ACKNOWLEDGMENTS 8-1

9. REFERENCES 9-1

10. DISTRIBUTION 10-1

FIGURES

Figure 2.1 Longitudinal cross section of the as- fabricated MOX fuel. 2-2

Figure 2.2 Micrograph of unetched (left) and etched (right) as-fabricated microstructure detailing porosity distribution. 2-2

Figure 2.3 Typical MOX pellet as fabricated at LANL for the MOX test irradiation. 2-3

Figure 2.4 Capsule, fuel pin, and basket assemblies. 2-4

Figure 2.5 Capsule and fuel pin axial dimensions. 2-5

Figure 2.6 Pellet, fuel pin, and capsule radial dimensions. 2-6

Figure 3.1 Dates, effective full-power days, and accumulated burnups for Capsules 4 and 13 during the Phase-I irradiation cycles. 3-2

Figure 3.2 Dates, effective full-power days, and accumulated burnups for Capsules 4 and 13 during the Phase-II irradiation cycles. 3-4

Figure 3.3 Dates, effective full-power days, and accumulated burnups for Capsules 4 and 13 during the Phase-III Part 1 irradiation cycles. 3-6

Figure 3.4 Dates, effective full-power days, and accumulated burnups for Capsules 4 and 13 during the Phase-IV Part 1 irradiation cycles. 3-8

Figure 4.1 Side view of Capsule 4. Note the discoloration on the right 2/3 of the capsule. 4-3

Figure 4.2 Top view of Capsule 4. 4-3

Figure 4.3 Bottom view of Capsule 4. 4-3

Figure 4.4 Side view of Capsule 13. The discoloration is similar to that on Capsule 4. 4-4

Figure 4.5 Top view of Capsule 13. 4-4

Figure 4.6 Bottom view of Capsule 13. 4-4

Figure 4.7 Free air temperature measurement on Capsule 4. 4-6

Figure 4.8 Schematic of diameter measurement. 4-6

Figure 4.9 Capsule 4 mid energy gamma raster scan. 4-8

Figure 4.10 Capsule 4 high-energy gamma raster scan. 4-10

Figure 4.11 Capsule 4 mid energy gamma line scan. 4-11

Figure 4.12 Capsule 4 high-energy gamma line scan. 4-12

Figure 4.13 Capsule 13 mid energy gamma raster scan. 4-14

Figure 4.14 Capsule 13 high-energy gamma raster scan. 4-15

Figure 4.15 Capsule 13 mid energy gamma line scan. 4-16

Figure 4.16 Capsule 13 high-energy gamma line scan. 4-17

Figure 4.17 Orientation of the capsule and the gamma scanner collimator/detector. 4-18

Figure 4.18 Cross sectional view of the Fission Gas Pressure Measuring Apparatus. [Drill Schematic 3.wpg]..... 4-19

Figure 4.19 Side view of Fuel Pin 7 (foreground). Shown in the background are the components of the capsule. 4-21

Figure 4.20 Top view of Fuel Pin 7. The puncture hole can be seen. 4-22

Figure 4.21 Bottom view of Fuel Pin 7. The vertical mark on the pedestal is a nick made when sawing the capsule bottom off. 4-22

Figure 4.22 Side view of Fuel Pin 16 (foreground). Shown in the background are the components of the capsule. The small cut off piece of the capsule was used as a spacer when resolving the broken drill problem..... 4-23

Figure 4.23 Top view of Fuel Pin 16. A piece of the broken drill bit can be seen in the partially drilled hole. 4-23

Figure 4.24 Bottom view of Fuel Pin 16..... 4-24

Figure 4.25 Graph of Fuel Pin 7 diametrical measurements. 4-27

Figure 4.26 Graph of Fuel Pin 16 diametrical measurements. Both pressurized and unpressurized measurements are shown. (The unpressurized measurement had three small handling scratches at approximately 1.8, 2, and 3”, which were removed from the graph for clarity)..... 4-28

Figure 4.27 Schematic of the Fuel Pin Volume Measuring Apparatus. 4-29

Figure 5.1 Mount 6218 from Pellet 2, Fuel Pin 7. Note the rectangular island in the center, the large agglomerates, and the "halos" around the agglomerates. The sector numbers locate the pellet-clad interfaces in the next figures. 5-4

Figure 5.2 Clad sectors 1 and 2 of Mount 6218..... 5-5

Figure 5.3 Sectors 3 and 4 of Mount 6218. 5-6

Figure 5.4 Sectors 5 and 6 of Mount 6218. 5-7

Figure 5.5 Sectors 7 and 8 of Mount 6218. 5-8

Figure 5.6 Sectors 9 and 10 of Mount 6218. 5-9

Figure 5.7 Sectors 11 and 12 of Mount 6218. 5-10

Figure 5.8 Metallographic cross section prepared from Fuel Pin 7 specimen, FP-7-M-2. Note the triangle like "core" piece isolated by cracks near the center. Agglomerates are as before. ... 5-11

Figure 5.9 Metallographic cross section prepared from Fuel Pin 7 specimen, FP-7-M-3. Note the rectangle like piece isolated by cracks near the center. The black spots are pullout..... 5-12

Figure 5.10 Sectors 1 and 2 of Mount 6220. 5-13

Figure 5.11 Sectors 3 and 4 from Mount 6220. 5-14

Figure 5.12 Sectors 5 and 6 from Mount 6220. 5-15

Figure 5.13 Sectors 7 and 8 from Mount 6220. 5-16

Figure 5.14 Sectors 9 and 10 from Mount 6220. 5-17

Figure 5.15 Sectors 11 and 12 from Mount 6220. 5-18

Figure 5.16 Axial section of Fuel Pin 7, specimen FP-7-M-4. Note that the pellet dish and chamfer can be seen indicating excellent irradiation behavior. Agglomerates can be seen throughout the section. Note that they are somewhat lighter, less developed, near the pellet axis than near the clad. The black regions are pullout…. 5-19

Figure 5.17 Close up view of pellet interface showing the chamfer and dishing. The small "triangle" in the chamfer space is a potting artifact (low spot or bubble). 5-20
Figure 5.18 Mount 6221 with sector definitions. Note that in the following figures one side

(right) has less corrosion than the other (left). 5-21

Figure 5.19 Left and right side sectors 11 and 1 from Mount 6221. 5-22

Figure 5.20 Left and right side sectors 12 and 2 from Mount 6221. 5-23

Figure 5.21 Left and right side sectors 13 and 3 from Mount 6221. 5-24

Figure 5.22 Left and right side sectors 14 and 4 from Mount 6221. 5-25

Figure 5.23 Left and right side sectors 15 and 5 from Mount 6221. 5-26

Figure 5.24 Left and right side sectors 16 and 6 from Mount 6221. 5-27

Figure 5.25 Left and right side sectors 17 and 7 from Mount 6221. 5-28

Figure 5.26 Left and right side sectors 18 and 8 from Mount 6221. 5-29

Figure 5.27 Left and right side sectors 19 and 9 from Mount 6221. 5-30

Figure 5.28 Cross section of Fuel Pin 7, specimen FP-7-M-5. Note that the agglomerates can be seen throughout the cross section, even near the center. Note the large agglomerate at the 5 o'clock position. This mount also has a triangle like region broken out near the center. 5-31

Figure 5.29 Cross section of Fuel Pin 16, specimen FP-16-M-1. Note that the agglomerates can be seen through out the cross section, even near the center. This mount also has a core like region broken out near the center. 5-32

Figure 5.30 Sectors 1 and 2 of Mount 6223. 5-33

Figure 5.31 Sectors 3 and 4 of Mount 6223. 5-34

Figure 5.32 Sectors 5 and 6 of Mount 6223. 5-35

Figure 5.33 Sectors 7 and 8 of Mount 6223. 5-36

Figure 5.34 Sectors 9 and 10 of Mount 6223. 5-37

Figure 5.35 Sector 13 of Mount 6223. 5-38

Figure 5.36 Cross-section of Fuel Pin 16, specimen FP-16-M-2. Again, note that the agglomerates can be seen through out the cross-section, even near the center. Also note the trapezoid and triangle like cylinder regions isolated by cracks near the center. The black region near the bottom is pullout. 5-39

Figure 5.37 Grain structure near the pellet edge in Mount 6222 (Untreated). 5-41

Figure 5.38 Grain structure near the pellet center in Mount 6222 (Untreated). 5-41

Figure 5.39 Grain structure near the pellet edge in Mount 6225 (TIGR). 5-42

Figure 5.40 Composite photograph of etched Mount 6225 (TIGR). 5-42

Figure 5.41 Gamma scan of Mount 6219. Note the off center burnup profile. 5-44

Figure 5.42 Composite photograph of mount used for SEM/Microprobe examination. (Also discussed in the metallography section) 5-46

Figure 5.43 SEM/Microprobe scans of Site 1 in Mount 6218 5-47

Figure 5.44 Larger view of SEM/Microprobe back scatter electron image of Site 1. 5-49

Figure 5.45 SEM/Microprobe Xe scan of Site 1 in Mount 6218. 5-50

Figure 5.46 SEM/Microprobe scans for a fuel/clad region, Site 3, isolated from an agglomerate.. 5-51

Figure 5.47 SEM/Microprobe scans for an internal agglomerate at Site 2 5-52

Figure 5.48 SEM/Microprobe scans for a grain boundary at Site 4. 5-53

Figure 5.49 Composite photograph of mount used for SEM/Microprobe examination. (Note that there is no Site 4). 5-55

Figure 5.50 SEM/Microprobe scans of Site 1 in Mount 6240. 5-56

Figure 5.51 SEM/Microprobe scans of Site 3 in Mount 6240. 5-57

Figure 5.52 Mapping of Site 2, an internal agglomerate. 5-58

Figure 5.53 Comparison of internal and edge agglomerates. 5-59

Figure 5.54 SEM image of a grain boundary at Pull Out 1. 5-60

Figure 6.1 Fuel Pin 7 top cutting guide. 6-3

Figure 6.2 Fuel Pin 7 bottom cutting guide. 6-4

Figure 6.3 Fuel Pin 16 top cutting guide. 6-5

Figure 6.4 Fuel Pin 16 bottom cutting guide. 6-6

Figure 6.5 Capsule 4 wall MET mount..... 6-13

TABLES

Table 2.1 ATR-MOX Capsule Preirradiation Information 2-7

Table 2.1 (Cont.) ATR-MOX Capsule Preirradiation Information 2-8

Table 3.1 Capsule heating rates for Phase I 3-3

Table 3.2 Capsule heating rates for Phase II 3-5

Table 3.3 Capsule heating rates for Phase III Part 1 3-7

Table 3.4 Capsule heating rates for Phase IV Part 1 3-9

Table 4.1 Quick Look Metrology 4-1

Table 4.2 Capsule and Fuel Pin Numbering Status 4-2

Table 4.3 Capsule 4 and 13 Temperature Measurements 4-5

Table 4.4 Capsule Measurements 4-7

Table 4.5 Fission Gas Measurements 4-20

Table 4.6 Fuel Pin 7 and 16 Length and Weight 4-25

Table 4.7 Fuel Pin 7 Density Measurement 4-26

Table 5.1 Mount ID Numbers and Fuel Pellet Locations 5-2

Table 5.2 SEM Mount ID Numbers and Fuel Pellet Locations 5-45

Table 6.1 Fuel Pin 7 Sampling 6-7

Table 6.2 Fuel Pin 16 Sampling 6-8

Table 6.3 Radiochemical Samples for Building 2026 6-9

Table 6.4 Irradiated Clad Results 6-10

Table 6.5 Pellet Results 6-10

Table 6.6 Pellet Burnup Results 6-12

Table 6.7 Burnup Results for FP-7-P-1. 6-14

Table 6.8 Burnup Results for FP-7-P-2. 6-15

Table 6.9 Burnup Results for FP-7-P-3. 6-16

Table 6.10 Burnup Results for FP-7-C-3. 6-17

Table 6.11 Burnup Results for FP-16-P-1. 6-18

Table 6.12 Burnup Results for FP-16-P-2. 6-19

Table 6.13 Burnup Results for FP-7-C-3. 6-20

Table 7.1 Clad Samples Archived for Later Testing 7-3

Table 7.2 Adjusted Capsule and Fuel Pin Pressures and Release Fractions 7-4

ACRONYMS

APT	Average Power Test
ATR	Advanced Test Reactor
BOL	Beginning of Life
CARTS	Capsule Assembly Response-Thermal Swelling (Code)
EFPD	Effective Full Power Days
FGPMA	Fission Gas Pressure Measuring Apparatus
FMDP	Fissile Materials Disposition Program
FPMA	Fuel Pin Measuring Apparatus
GWd/MT	Giga-Watt Days per Metric Ton
HBS	High Burn-up Structure
INEEL	Idaho National Engineering and Environmental Laboratory
LANL	Los Alamos National Laboratory
LHGR	Linear Heat Generation Rate
LWR	Light Water Reactor
MCNP	Monte Carlo Neutron Photon (Code)
Mils	0.001 inches
MOX	Mixed Oxide
NRC	Nuclear Regulatory Commission
ORNL	Oak Ridge National Laboratory
PIE	Post Irradiation Examination
ppb	Parts Per Billion
ppm	Parts Per Million
PWR	Pressurized Water Reactor
RG	Reactor Grade
RMAL	Radioactive Materials Analysis Laboratory
TD	Theoretical Density
TIGR	Thermally Induced Gallium Removal
WG	Weapons Grade

ABSTRACT

This report summarizes the results of the post irradiation examination of the 40 GWd/MT MOX test capsules (numbers 4 and 13). The purpose of this examination was to document and monitor the progress of the MOX fuel test irradiation. Both capsules were examined, opened, and the fuel pin removed. Capsule 4 contained Fuel Pin 7 and Capsule 13 contained Fuel Pin 16. Both fuel pins were easily removed from the capsules and were found to be in excellent condition. Visual and dimensional inspections revealed no problems.

Determination of the fission gas release fractions (8.4 to 9.5%) and fuel pellet stack gamma scan measurements indicate that the fuel is behaving satisfactorily with respect to its irradiation history. Metallographic mounts were prepared from both fuel pins and fuel behavior was examined with no indications of excessive swelling or fuel restructuring. As was found in previous PIEs, the size distribution of plutonium-rich agglomerates is rather large, with a few examples of equivalent diameters in the 500-600 micron range.

Careful observation of the metallographic mounts indicates that the fuel swelling is as predicted. There is evidence of irradiation-induced clad expansion (creep) along with some minor pellet-clad mechanical interaction due to pellet hourglassing. The fuel grain size difference between the center and the edge was modest.

The gallium content of the clad was in the sub ppm range indicating no significant migration of gallium from the fuel to the clad. Overall, both capsules underwent the irradiation with no detrimental effects and gallium migration/effects have not proved to be an issue.

Volume 2 of this report addresses the implications of these PIE findings.

EXECUTIVE SUMMARY

The post irradiation examination (PIE) of the fourth set of two capsules in a series being irradiated by the FMDP to investigate the properties of weapons-derived plutonium in mixed-oxide (MOX) light-water reactor fuel is described in this report. This test irradiation and associated PIE series was deemed necessary because weapons-derived plutonium differs from reactor grade (RG) plutonium in both isotopic enrichment of ^{239}Pu and in trace impurities, particularly gallium. As set forth in the *Fissile Materials Disposition Program Light-Water Reactor Mixed Oxide Fuel Irradiation Test Project Plan,* ORNL/TM-13419, Rev 1, the goals include "Demonstrate the utilization of plutonium derived from weapons components in a light water reactor (LWR) environment," and "Contribute experience with irradiation of gallium-containing fuel to the data base required for resolution of generic LWR WG MOX fuel design issues." These goals are being pursued by examination of fuel pin material performance, including specific consideration of trace gallium behavior.

The MOX test capsules are irradiated in the Advanced Test Reactor (ATR) at INEEL and are being withdrawn for PIE in four phases, denoted early, intermediate, 30 GWd/MT, and extended. The purpose of this fourth examination at the midpoint of the extended phase with a burnup of 40 GWd/MT is to monitor the progress of the irradiation so that it can be determined if the fuel is behaving in accordance with the performance models utilized in the pretest safety analyses. The two capsules undergoing the 40 GWd/MT PIE are Capsule 4, which provided containment during the irradiation for Fuel Pin 7, and Capsule 13, which served as containment for Fuel Pin 16. The MOX fuel within Fuel Pin 16 was created from PuO_2 that was treated by a TIGR (Thermally-Induced Gallium Removal) process before being blended with UO_2 and pressed into pellets. The MOX within Fuel Pin 7 was untreated.

As the first step of the PIE, both capsules were examined and gamma-scanned before opening. Both fuel pins were straightforwardly removed from the capsules and were found to be in excellent condition. Visual and dimensional inspections revealed no abnormalities. The pretest CARTS code application had predicted no clad contact at the pellet centerline during the irradiation, with a widening of the pellet-clad gap when the fuel cooled down. The PIE showed minor pellet-clad contact due to thermal expansion of the pellet edges ("hourglassing") that left very small (0.3 mil) ridges in the clad at the pellet interfaces. No evidence of bulk pellet expansion into the clad was observed.

Gamma scans provided qualitative indications of the burnup along the fuel pin and within a pellet in agreement with the pretest neutronic predictions of the MCNP code. These inspections also showed that no axial gaps are developing within the fuel stack. Fission gas pressures were measured and the fractional fission gas releases were determined to be between 8.4 and 9.5%, which are appropriate for the high linear heat generation rate that these capsules experienced during their irradiations.

Metallographic mounts were prepared from both fuel pins and fuel behavior was found to be in accordance with expectations, with no indications of significant fuel restructuring or abnormal swelling. Pellet cracking was evident, but the extent is considered normal in view of the thermal cycling experienced during the irradiation. Thin (a few microns) oxide layers are beginning to form in the areas of pellet-clad contact. The fuel swelling is within the range predicted by the fuel performance models.

As previously noted in the 21 and 30 GWd/MT PIEs, large plutonium-rich agglomerates are present. A few equivalent diameters are as large as 500-600 microns, several times the initial size of the agglomerates present in modern commercial fuel. In addition, the agglomerates appear to be surrounded by halos of fission products (gases) in the surrounding matrix. No irradiation difficulties have been experienced with these agglomerates, but their large size range indicates less than optimum powder mixing, more typical of the early MOX fuels.

The grain structure of the pellet was observed to change modestly over the radius of the pellet with the grain size being somewhat larger in the interior of the pellet. This is expected as grain growth often occurs at higher temperatures.

A SEM/Microprobe examination of the fuel and clad revealed no abnormal behavior of either the fuel or clad. The oxide layers at the clad inner surface were thicker and involved some minor fuel diffusion in the regions of a surface agglomerate. At this point in the irradiation, the microstructure of the two fuel types appears to be behaving in a similar fashion, except for the greater fission gas release associated with the TIGR-treated material. Both types had "bubble trails" on the grain faces at exposed fracture surfaces. Elemental mapping confirmed that the agglomerates are rich in plutonium and that the fission products Ru and Pd are localized to the agglomerates. It also identified xenon diffusing from the agglomerates as a fission product component in the haloes appearing around the agglomerates.

Radiochemical determination of burnup is in good agreement with the code-predicted capsule-average value of about 40 GWd/MT. All indications are that the irradiation is proceeding as planned and that the fuel is performing normally.

Both fuel pins were sectioned to facilitate the tracking of gallium within the fuel pin clad, with the additional purpose of preserving specimen material for ductility testing. The gallium content of the clad was in the sub ppm range indicating no significant migration of gallium from the fuel to the clad (gallium in the sub ppm range is present in unirradiated clad). Gallium contents of selected pellets were as expected as well.

The archiving of the clad samples pertains to the ultimate need to determine the effects, if any, of the transported gallium (if any) upon the clad. Toward this end, clad specimens from all the PIEs done to date have been saved for ductility testing at a future time when apparatus for the destructive testing of clad specimens from this test series is operational.

The important lessons learned from this PIE of the two capsules withdrawn at 40 GWd/MT are

as follows:

1. This test MOX fuel prepared with weapons-derived plutonium has behaved as expected and there is no cause to reconsider the extension of its test irradiation to higher burnups. Only minor differences between the treated and untreated fuel were noted, primarily in the area of fission gas release.

2. Densification of the test fuel appears to be normal and prototypic of commercial fuel.

3. Permanent outward relocation of the clad has been confirmed. The irradiation-enhanced outward creep (0.3%) is considered consistent with the operating conditions (positive outward pressure gradient across the fuel pin wall) and the accumulated fast neutron fluence. This clad displacement is appropriately modeled in code calculations for this test irradiation.

4. Ridging of the clad from pellet end-clad interactions continues to be evident and is minor. It is typical of the pellet "hourglassing" effects discussed in the literature, which are caused by differential axial thermal expansion of the radially cracked pellets when initially taken to operating temperature.

5. Measurement of capsule and fuel pin internal pressures and ^{85}Kr activities were successful. The implied gas release fractions from the fuel matrix are within the expectations based on the European MOX fuel experience for fuel operated at similar power levels.

6. The results of the gamma scans and radiochemical burnup analyses are in accordance with the predictions of the MCNP code. The observed fuel swelling is as expected from CARTS code predictions and higher dimensional thermophysical calculations explain the local pellet end effects. There is no reason to question the use of either the MCNP or CARTS codes in performing the safety analyses for irradiation of the test fuel to higher burnups.

7. Any gallium migration to the clad has been insignificant. In this context, it is important to recognize that the fuel linear heat generation rates and the pellet-to-clad temperature differences have been much larger for these test capsules than are expected for the mission fuel.

8. Thin corrosion layers are observed on the cladding inner surface, particularly in regions where a plutonium-rich agglomerate was located at or near the pellet edge during the irradiation.

The implications of these PIE findings are discussed in greater detail in Volume 2 of this report.

1. INTRODUCTION

1.1 General

This is the eighth report in a series of reports detailing the post-irradiation examination (PIE) of the Fissile Materials Disposition Program (FMDP) MOX irradiation tests [References 10-16]. These tests are investigating the use of weapons grade (WG) plutonium in mixed oxide (MOX) fuel for light-water reactors (LWRs) to demonstrate that the substitution of weapons-derived plutonium for the reactor grade (RG) plutonium used in commercial MOX fuel does not negatively affect the performance of the fuel system and, thus, that the commercial database is applicable. To meet this end, this test program was created to fabricate, assemble, and irradiate small test capsules containing weapons-derived MOX fuels at higher than expected average powers, 6-10 kW/ft [References 1-8].

Simple, uninstrumented, drop-in capsules with local flux monitor wires were fabricated and placed in the Advanced Test Reactor (ATR) at the Idaho National Engineering and Environmental Laboratory (INEEL). The test program comprises 13 capsules, 7 of which contain MOX fuel prepared without a gallium removal step, and 6 of which contain fuel in which the PuO_2 was treated with a special gallium removal step. The target irradiation goal is 50 GWd/MT for three capsules, while other capsules have been removed at 8, 21, 30, and 40 GWd/MT for the purpose of monitoring the irradiation. Two capsules have been designated as unirradiated archives. The topic of Reference 16 and this report is the examination of the two capsules that have been withdrawn after irradiation to 40 GWd/MT; six previous reports have dealt with the PIEs at 8 GWd/MT, 21 GWd/MT, and 30 GWd/MT [References 10-15].

As in the previous PIEs, the examination of the MOX capsules removed at 40 GWd/MT was conducted in two steps. The first step was a "Quick Look", whose purpose was to determine the gross physical state of the capsule, cladding, and fuel [Reference 16]. The major goal of the Quick Look is to provide feedback to the irradiation group on issues that may impact the continued and safe operation of the capsules remaining in the ATR. This step also evaluates the usefulness of the current test apparatus and techniques for their role in the MOX irradiation task.

The second PIE step is a more detailed examination of the capsule constituents for the purpose of collecting specific cladding and fuel performance data, including radiochemical analyses, for the FMDP program. The results of this detailed examination are discussed in this final report for the 40 GWd/MT PIE.

1.2 Scope

The purpose of this report is to document the PIE effort conducted on the fourth set of two MOX test capsules withdrawn from the ATR. The first three Chapters of this report summarize the fuel, the irradiation history, and performance predictions. The reader is referred to the references for greater detail concerning fuel preparation, test conduct, and for the results of the first three

PIEs.
The remaining chapters of this report detail the PIE work conducted and the results obtained. Capsule metrology and fuel mount metallography are discussed in Chapter 4 and 5, respectively. Radiochemistry results are discussed in Chapter 6. The goal was to perform a materials compatibility test rather than a fuels test, so the emphasis of the examination has been on the behavior of the fuel pin as a unit; however, the fuel was examined to a degree sufficient to establish that no significant deviations from the expected are present. A qualitative gamma scan of a fuel segment has exhibited the expected off-center burnup profile. The clad is found to have behaved as expected during the irradiation.

1.3 Gallium Migration

The test fuel contains gallium in excess of the upper concentration limit set for the mission fuel, but still only at low ppm levels. Very large amounts of gallium are known to adversely affect Zircaloy clad. Accordingly, it is of interest for this PIE to determine if gallium has migrated during the irradiation from the fuel to the clad. Results for the current PIE are discussed in Section 6.2.

1.4 Findings Concerning Code Representation and Predictions

Fuel Performance Models taken from the ESCORE and FRAPCON-3 codes were applied before this PIE to predict the fuel configurations to be observed in the hot cell examinations. The predictions for the current PIE are described in Chapter 3. With respect to fuel densification, the current hot cell observations provide the fifth data point (following the unirradiated, the early, the intermediate, and the 30 GWd/MT values), and thereby permit continued refinement of the assumptions used in the code predictions. Measurements of the clad outer diameter allow comparison with the clad creep models.

The implications of the PIE findings, including fission gas release, agglomerate size, pellet behavior, clad dimensions, and post-PIE code calculations are discussed in Volume 2 of this report.

2. PREIRRADIATION CHARACTERIZATION

2.1 Fuel Types

Two fuel types, which differ in their treatment of a common PuO_2 source, are included in the MOX test irradiation. Fuel type B was fabricated with plutonium dioxide that was subjected to a thermal treatment ("TIGR") for gallium removal prior to pellet fabrication. Fuel type A was fabricated with plutonium dioxide that was not treated. Ten pellets of each batch were analyzed at ORNL for gallium content [Ref 17]. Batch A had an average gallium content of 2.97 ppm (mass) while Batch B had an average gallium content of 1.33 ppm (mass). The 95% confidence interval for Batch A is 1.00 to 4.95 ppm and for Batch B, 0.79 to 1.88.

Tests were performed on the fuel during fabrication and the resulting characterization information was summarized in two pellet data packages prepared by Los Alamos National Laboratory (LANL). One archive capsule assembly of each fuel type was also prepared and sent to Oak Ridge National Laboratory (ORNL) unirradiated. These archives are available for future examination if questions arise regarding in-reactor performance. The unique fuel fabrication process and processing parameters that were utilized may influence the in-reactor performance of the test fuel; the postirradiation examinations are meant to detect any such nonstandard behavior. No unusual behavior has been seen to date.

A longitudinal (pellet resting on side) cross section of the unirradiated fuel, Fig. 2.1, reveals the dish and chamfer of the pellets as well as the uniformity of the microstructure. Both batches of fuel contain 5% plutonium by weight (the plutonium-rich agglomerates are approximately 30% PuO_2). Chemical impurity analyses performed at LANL confirmed the presence of no contaminants above acceptable levels.

Both batches of fuel achieved high density in part due to the extended sintering schedule. Average immersion densities of 94.5 % TD and 95.3 % TD were measured on fuel types A and B respectively. Essentially no density change was achieved during a subsequent 24-hour thermal densification test. The porosity distribution includes a uniform distribution of fine pores, as shown in Fig. 2.2. The average grain size is 10 µm (fuel type A) and 11 µm (fuel type B). The unirradiated etched microstructure is also shown in Fig. 2.2. A typical pellet is shown in Fig. 2.3.

Figure 2.1 Longitudinal cross section of the as- fabricated MOX fuel.

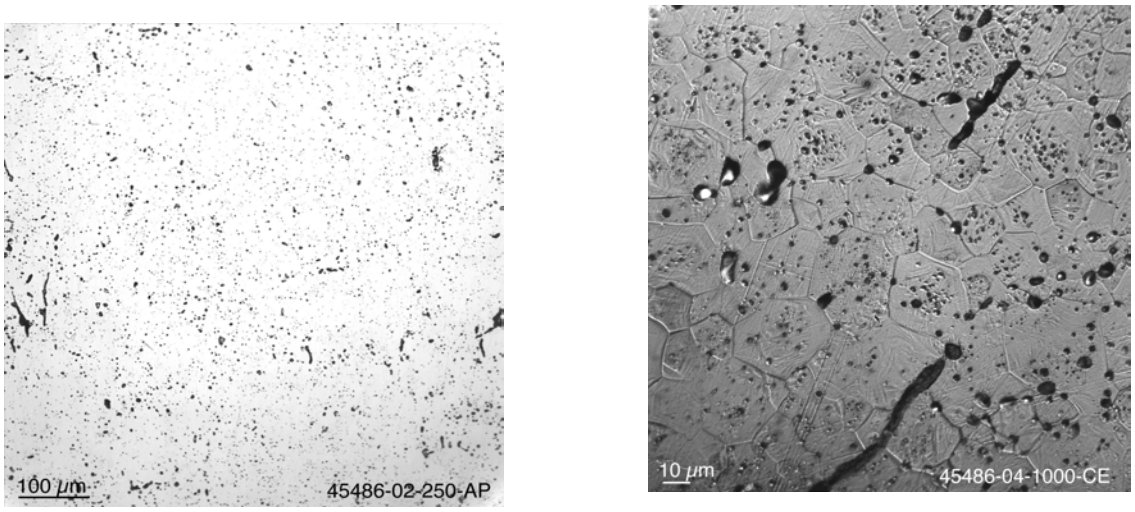

Figure 2.2 Micrograph of unetched (left) and etched (right) as-fabricated microstructure detailing porosity distribution.

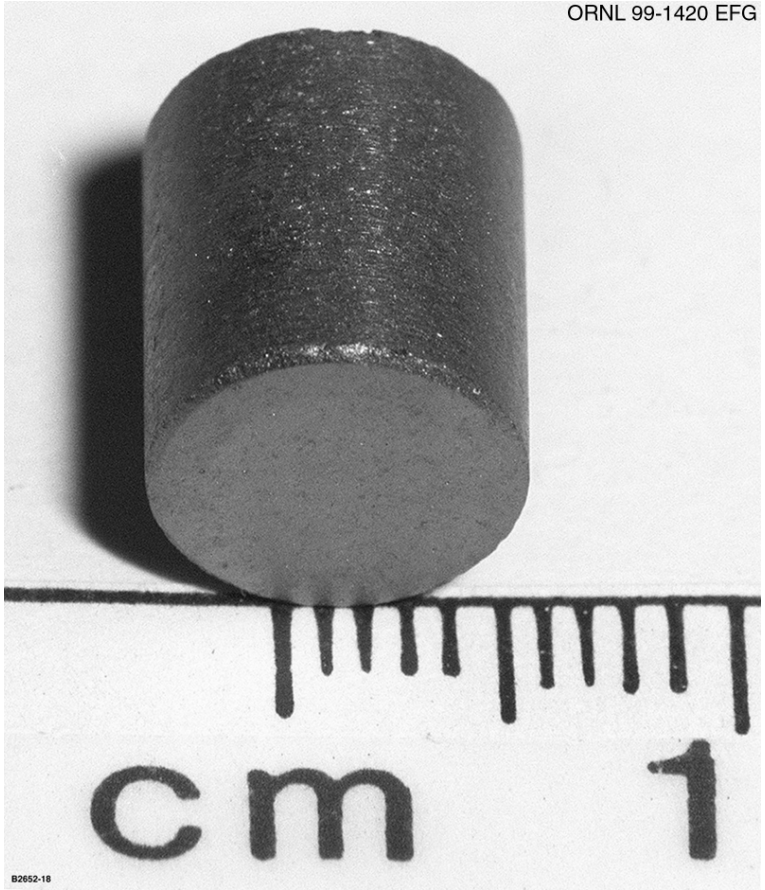

Figure 2.3 Typical MOX pellet as fabricated at LANL for the MOX test irradiation.

2.2 Irradiation Geometry

The fuel pellets and stainless steel springs were loaded into Zircaloy clad fuel pins and the pins sealed by welding at Los Alamos. The pins were then transferred to the Idaho National Engineering and Environmental Laboratory (INEEL), where they were loaded and seal welded into closely fitting stainless steel capsules (to meet the ATR pressure vessel operational requirements for this type of experiment as loaded into the reflector I-holes). Finally, the capsules were loaded into a basket assembly that was subsequently inserted into the ATR reflector for irradiation. Figures 2.4 through 2.6 show the geometry of the configuration.

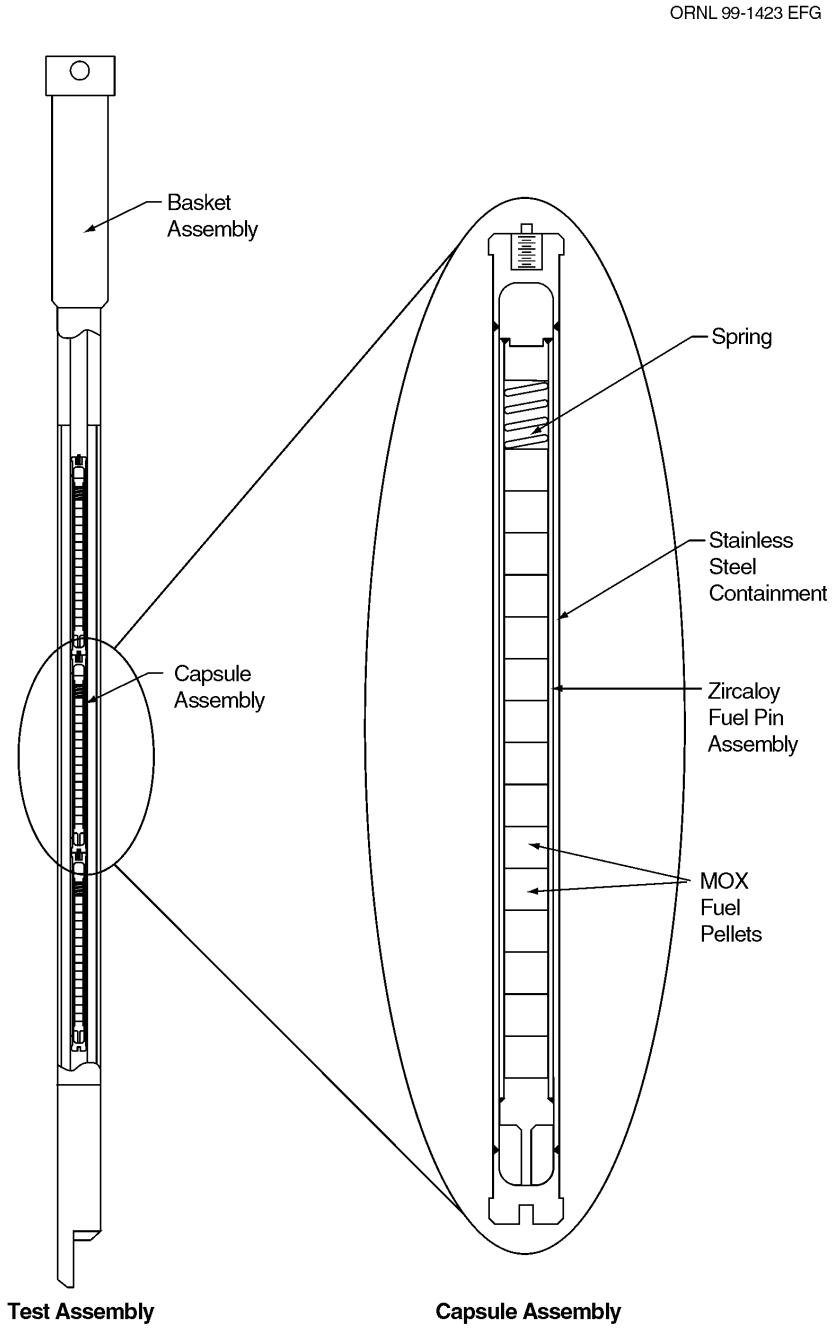

Figure 2.4 Capsule, fuel pin, and basket assemblies.

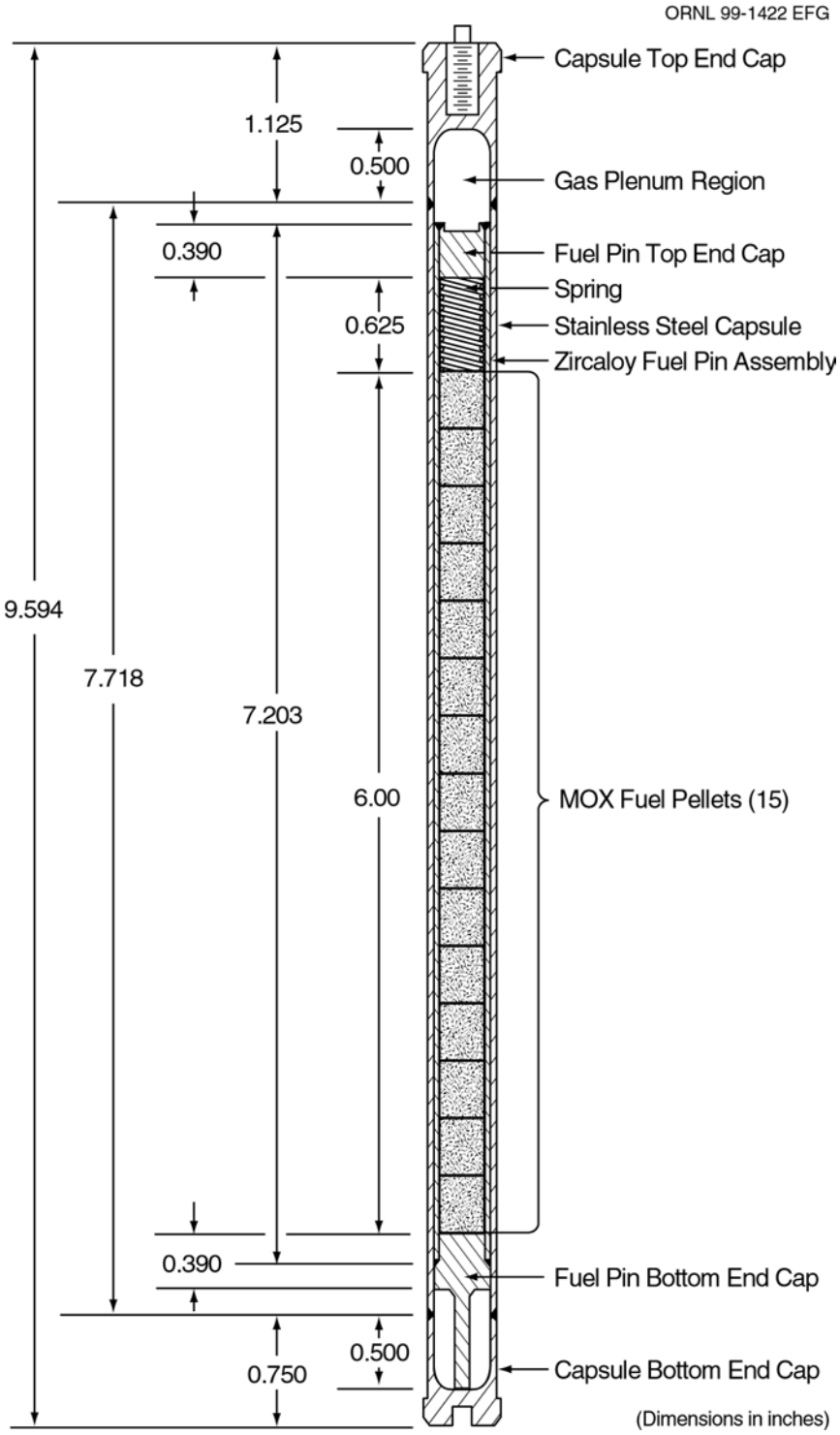

Figure 2.5 Capsule and fuel pin axial dimensions.

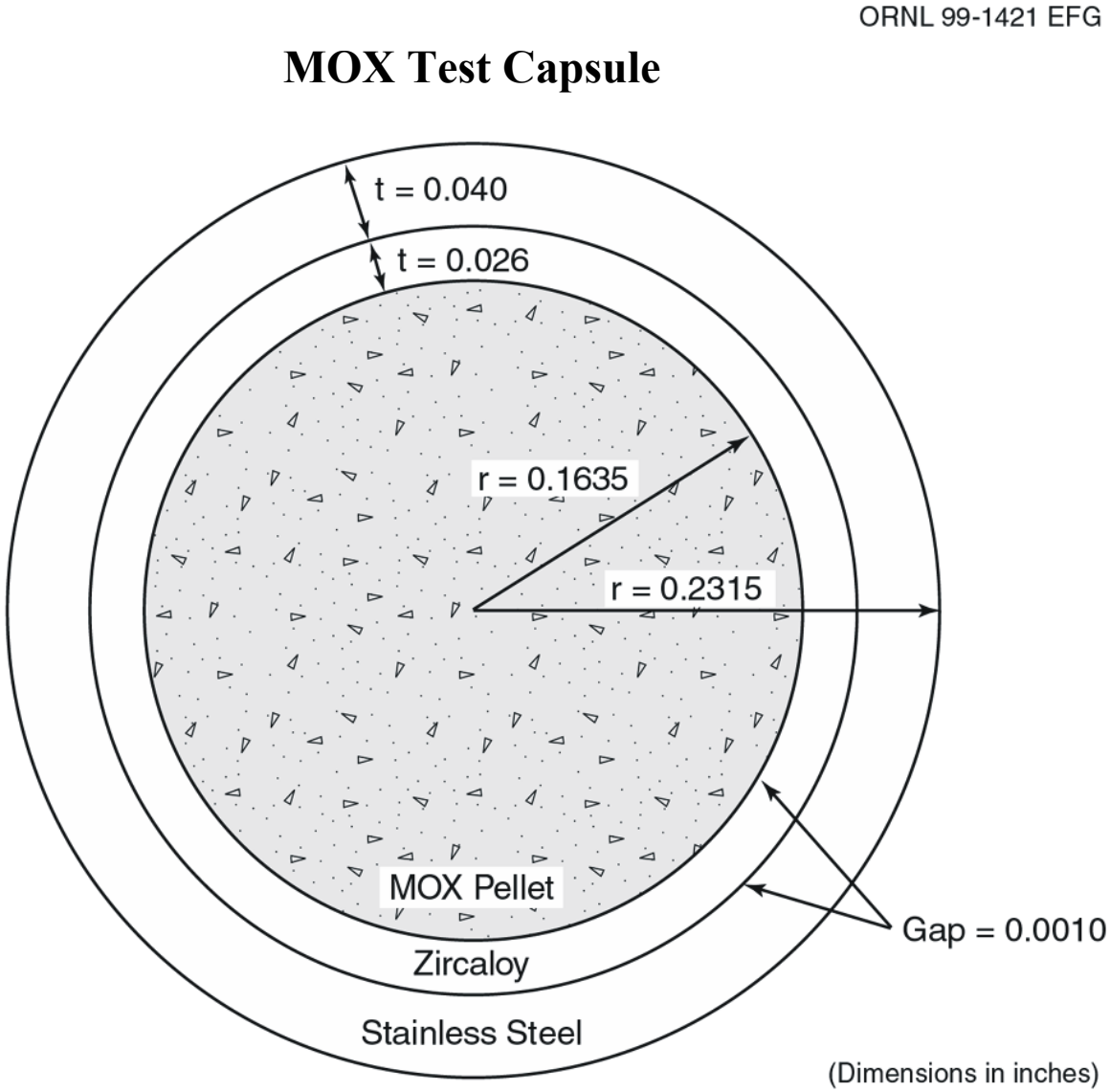

Figure 2.6 Pellet, fuel pin, and capsule radial dimensions.

2.3 Preirradiation Dimensional Data

Table 2.1 lists the dimensional data and part identification of the fuel capsule components prior to assembly.

Table 2.1 ATR-MOX Capsule Preirradiation Information

Capsule Number	**1**	**2**	**3**	**4**	**5**	**6**	**7**
Fuel Pin Number	2	5	6	7	8	9	10
Zr Tube Number	2	5	6	7	8	9	10
Zr Top Number	2	5	1	7	8	9	10
Zr Bottom Number	2	5	6	7	8	9	10
Zr Tube OD (inches)[1]	0.3806 0.3808	0.3806 0.3808	0.3805 0.3808	0.3805 0.3807	0.3806 0.3808	0.3805 0.3809	0.3806 0.3808
Zr Tube ID (inches)[1]	0.3290 0.3292	0.3290 0.3294	0.3290 0.3292	0.3290 0.3294	0.3290 0.3293	0.3290 0.3294	0.3292 0.3293
SS Tube OD (inches)[1]	0.4643 0.4649	0.4643 0.4649	0.4643 0.4649	0.4643 0.4649	0.4643 0.4649	0.4643 0.4649	0.4643 0.4649
SS Tube ID (inches)[1]	0.3830 0.3835	0.3830 0.3835	0.3830 0.3835	0.3830 0.3835	0.3830 0.3835	0.3830 0.3835	0.3830 0.3835
SS Top Number	1	2	3	4	5	6	7
Fuel Stack Height (inches)	5.821	5.833	5.859	5.816	5.816	5.829	5.823
Fuel Mass (grams)	81.41	81.63	80.51	81.40	81.31	81.66	81.47
Pellet Batch[2]	A	A	A	A	A	A	A
Burnup (GWd/MT)	8.6	21	30	40	50 (Planned)	50 (Planned)	None (Archive)

Table 2.1 (Cont.) ATR-MOX Capsule Preirradiation Information

Capsule Number	8	9	10	11	12	13
Fuel Pin Number	11	12	13	14	15	16
Zr Tube Number	11	12	13	14	15	16
Zr Top Number	11	12	13	14	15	16
Zr Bottom Number	11	12	13	14	15	16
Zr Tube OD (inches)[1]	0.3806 0.3808	0.3806 0.3808	0.3805 0.3808	0.3805 0.3807	0.3805 0.3807	0.3806 0.3808
Zr Tube ID (inches)[1]	0.3292 0.3294	0.3290 0.3293	0.3291 0.3294	0.3290 0.3294	0.3290 0.3293	0.3291 0.3292
SS Tube OD (inches)[1]	0.4643 0.4649	0.4643 0.4649	0.4643 0.4649	0.4643 0.4649	0.4643 0.4649	0.4643 0.4649
SS Tube ID (inches)[1]	0.3830 0.3835	0.3830 0.3835	0.3830 0.3835	0.3830 0.3835	0.3830 0.3835	0.3830 0.3835
SS Top Number	8	9	10	11	12	13
Fuel Stack Height (inches)	5.810	5.810	5.813	5.810	5.795	5.790
Fuel Mass (grams)	82.26	82.23	82.29	82.20	82.00	81.84
Pellet Batch[2]	B	B	B	B	B	B
Burnup (GWd/MT)	8.6	21	30	None (Archive)	50 (Planned)	40

[1] Numerator is the smallest measurement, denominator is the largest measurement.
[2] Pellet batch A was fabricated with PuO_2 that was not treated. Pellet batch B was fabricated with PuO_2 that was thermally treated ("TIGR") for Ga removal prior to pellet fabrication.

3. IRRADIATION HISTORY FOR CAPSULES 4 AND 13 AND ACCURACY OF CARTS CODE PREDICTIONS

S. A. Hodge **L. J. Ott**

Capsules 4 and 13 occupied various symmetric test assembly positions during irradiation Phases I, II, III Part 1, and IV Part 1, thereby accumulating a total of 904.1 EFPDs. Sections 3.1 through 3.4 describe these irradiation phases. Capsule 4 carried Fuel Pin 7 with a pellet stack height of 5.82 inch and a heavy metal mass of 71.754 gm. Capsule 13 carried Fuel Pin 16 with TIGR-treated fuel, a stack height of 5.79 inch and a heavy metal mass of 72.142 gm.

The pellet, fuel pin, and capsule behaviors across an average pellet midplane during the as-run irradiations were calculated in advance of the post-irradiation examinations (PIE) by application of the Capsule Assembly Response-Thermal Swelling (CARTS) code. Chapter 2 of the MOX Average Power Test 40 GWd/MT PIE: Quick Look, ORNL/MD/LTR-236 (issued November 2002) reports these results for Capsules 4 and 13. Now that the PIE has been completed, a consideration of the accuracy of these predictions provides a measure of the reliability to be expected from future CARTS applications. The extent to which the pre-PIE predictions for Capsules 4 and 13 have been found to match the PIE observations is discussed in Section 3.5.

3.1 Irradiation History for Phase I

The 155 effective full power days (EFPDs) leading up to the withdrawal of Capsules 1 and 8 for the early PIE collectively constitute irradiation Phase I. This phase, which extended from February 5 until September 13, 1998, comprises Advanced Test Reactor (ATR) Cycles 115C through 117B. The Inconel shield basket assembly (Model 1) was installed in the Northwest I-hole position I-24 throughout the irradiation. Capsules 4 and 13 occupied, respectively, the upper and lower back positions within the test assembly.

The irradiation history and subsequent PIE of the early-withdrawal capsules (1 and 8) are described in Reference 11. Figure 3.1 illustrates the Phase-I irradiation cycles with their calendar dates and the associated accumulations of EFPDs and burnups for the 40-GWd/MT Capsules 4 and 13.

The energy releases, associated average linear heat generation rates (LHGRs), and accumulated burnups for Capsules 4 and 13 during the individual irradiation cycles of Phase I are listed in Table 3.1.

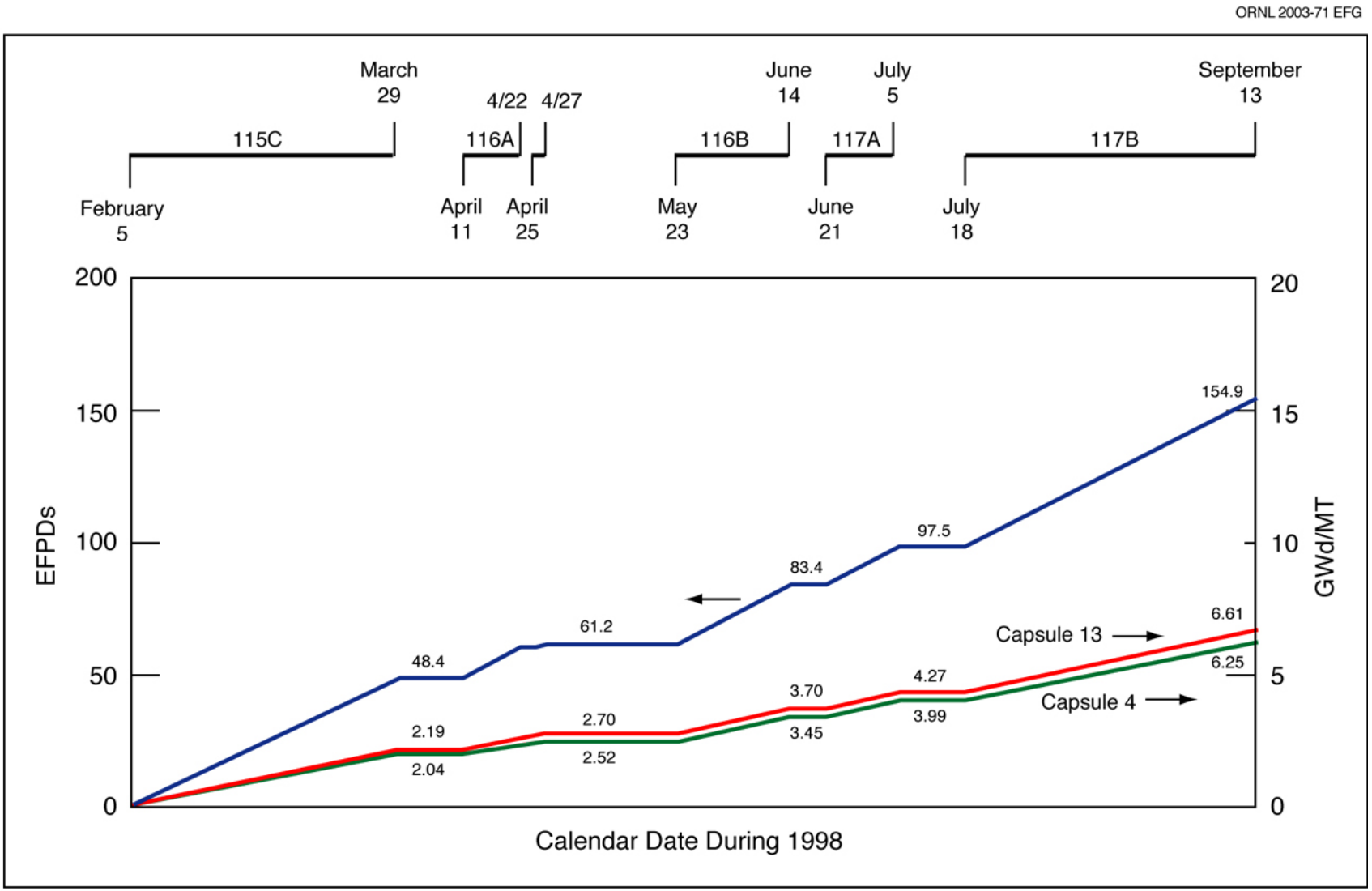

Figure 3.1 Dates, effective full-power days, and accumulated burnups for Capsules 4 and 13 during the Phase-I irradiation cycles.

Table 3.1 Capsule heating rates for Phase I

Cycle	EFPDs	Capsule 4			Capsule 13		
		MWd	Average LHGR KW/ft	End-cycle burnup GWd/MT	MWd	Average LHGR KW/ft	End-cycle burnup GWd/MT
115C	48.4	0.1435	6.118	2.04	0.1457	6.240	2.19
116A	12.8	0.0337	5.436	2.52	0.0346	5.607	2.70
116B	22.2	0.0653	6.069	3.45	0.0664	6.196	3.70
117A	14.1	0.0380	5.565	3.99	0.0382	5.620	4.27
117B	57.4	0.1593	5.726	6.25	0.1558	5.626	6.61

These EFPD totals for each cycle are as reported in Reference 18. The end-cycle burnups and the associated cycle-averaged LHGRs are obtained from the MCNP (Monte Carlo N-Particle) code results calculated at Idaho National Engineering and Environmental Laboratory (INEEL).

The test assembly capsule-loading pattern for Phase I is shown as Figure 2 of Reference 8. The LHGR values listed in Table 3.1 are lower than those experienced by the capsules withdrawn for previous PIEs because Capsules 4 and 13 occupied positions of lower neutron flux during the Phase-I irradiation.

There were two brief unplanned ATR shutdowns during Cycle 115C and another during Cycle 116A. Thus, the test capsules were thermally cycled eight times during the five ATR operating cycles of the Phase-I irradiation. Capsules 1 and 8 were withdrawn at the completion of Phase I and shipped to ORNL for PIE.

3.2 Irradiation History for Phase II

The Phase-II irradiation began November 9, 1998, with ATR Cycle 118A and continued through Cycle 120A, which ended September 12, 1999. The Model 2 aluminum-shield basket was employed throughout. The test assembly was loaded with seven irradiated capsules carried over from Phase I, plus two new fresh fuel capsules (6 and 12) to replace Capsules 1 and 8. Capsules 4 and 13 occupied the front middle positions, as shown in the loading pattern diagram included as Figure 3 of Reference 8. Figure 3.2 illustrates the Phase II irradiation periods with their calendar dates and the associated accumulations of Capsule 4 and 13 burnups.

During Phase II, the test assembly accumulated 227.7 EFPDs in the Northwest I-hole position I-24. The per-cycle energy releases, average cycle LHGRs, and accumulated burnups for Capsules 4 and 13 are listed in Table 3.2.

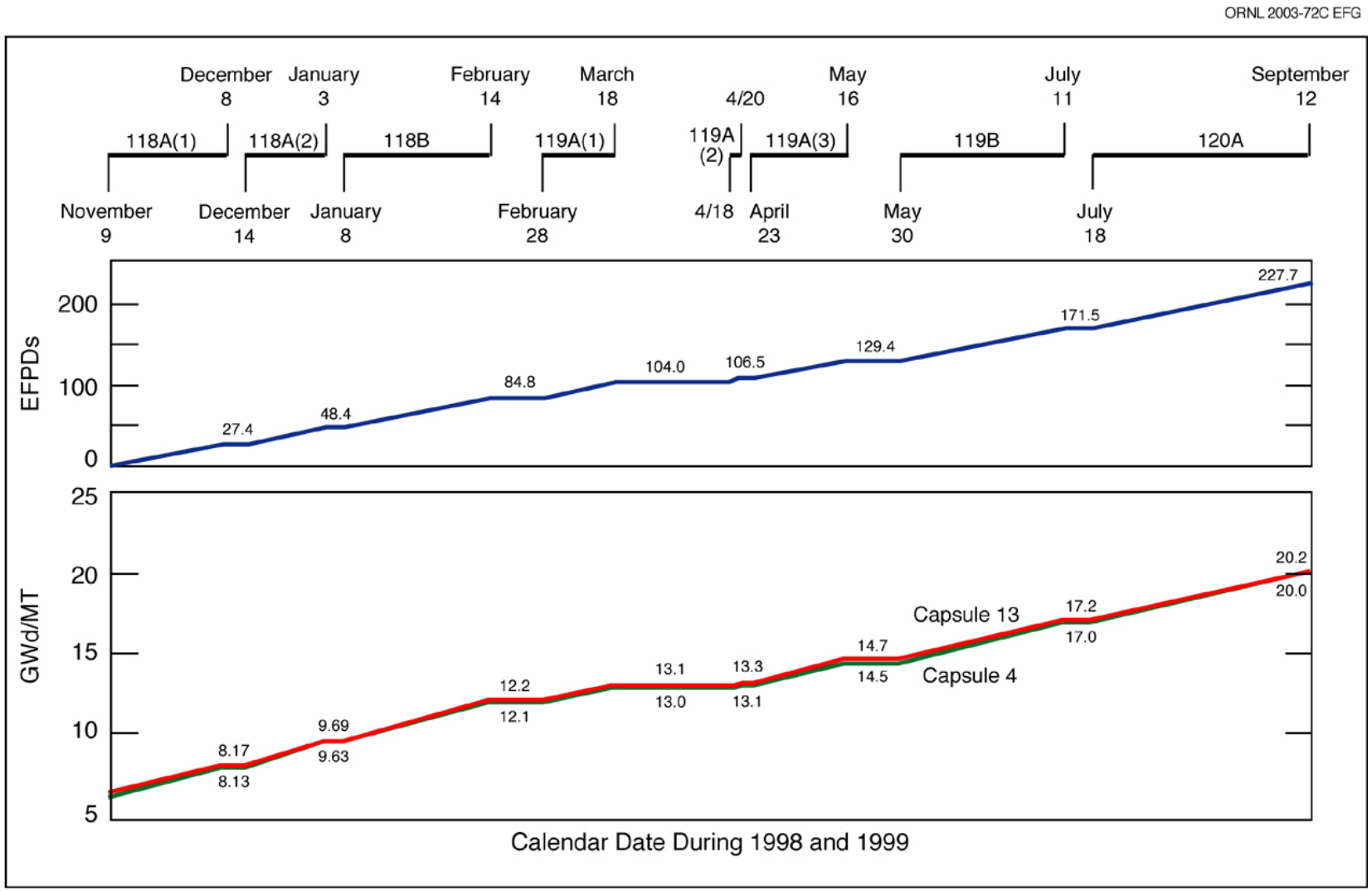

Figure 3.2 Dates, effective full-power days, and accumulated burnups for Capsules 4 and 13 during the Phase-II irradiation cycles.

Table 3.2 Capsule heating rates for Phase II

Cycle	EFPDs	Capsule 4			Capsule 13		
		MWd	Average LHGR KW/ft	End-cycle burnup GWd/MT	MWd	Average LHGR KW/ft	End-cycle burnup GWd/MT
118A(1)	27.4	0.1414	10.644	8.13	0.1421	10.750	8.17
118A(2)	21.0	0.1069	10.504	9.63	0.1082	10.680	9.69
118B	36.4	0.1772	10.046	12.11	0.1811	10.310	12.22
119A(1)	19.2	0.0619	6.654	12.97	0.0631	6.806	13.10
119A(2)	2.5	0.0105	8.646	13.12	0.0107	8.851	13.26
119A(3)	22.9	0.0984	8.864	14.50	0.1001	9.062	14.66
119B	42.1	0.1787	8.756	17.00	0.1782	8.772	17.16
120A	56.2	0.2174	7.982	20.04	0.2179	8.035	20.21

With two brief unplanned shutdowns during Cycle 118B and one during Cycle 120A, the test capsules were thermally cycled 11 times during the eight operating cycles of Phase II. The LHGRs of greater than 10 kW/ft produced within Capsules 4 and 13 during Cycles 118A and 118B are the highest experienced by any capsule during this test irradiation.

Capsules 2 and 9 were withdrawn at the end of Phase II and shipped to ORNL for PIE. The irradiation history and subsequent PIE for these intermediate-withdrawal capsules are reported in Reference 13.

3.3 Irradiation History for Phase III Part 1

The Phase-III irradiation began October 9, 1999, with ATR Cycle 120C. Part 1 continued through Cycle 122C, which ended July 23, 2000. The Model-2 aluminum-shield basket assembly was employed throughout. The test assembly was loaded with seven capsules carried over from Phase II. Capsules 4 and 13 occupied the front bottom positions during Phase III Part 1.

Figure 4 of Reference 8 illustrates the test assembly-loading pattern for Phase III Part 1. To complete the pattern, the seven mixed-oxide (MOX) test capsules were augmented by two solid stainless steel dummy capsules, which occupied the two front middle positions within the test assembly.

The test assembly accumulated 232.4 EFPDs in the Northwest I-hole position I-24 during Phase III Part 1. Figure 3.3 illustrates the irradiation periods with their calendar dates and the associated burnup accumulations for Capsules 4 and 13.

The energy releases, average LHGRs, and accumulated burnups for Capsules 4 and 13 during each of the individual irradiation cycles of Phase III Part 1 are listed in Table 3.3.

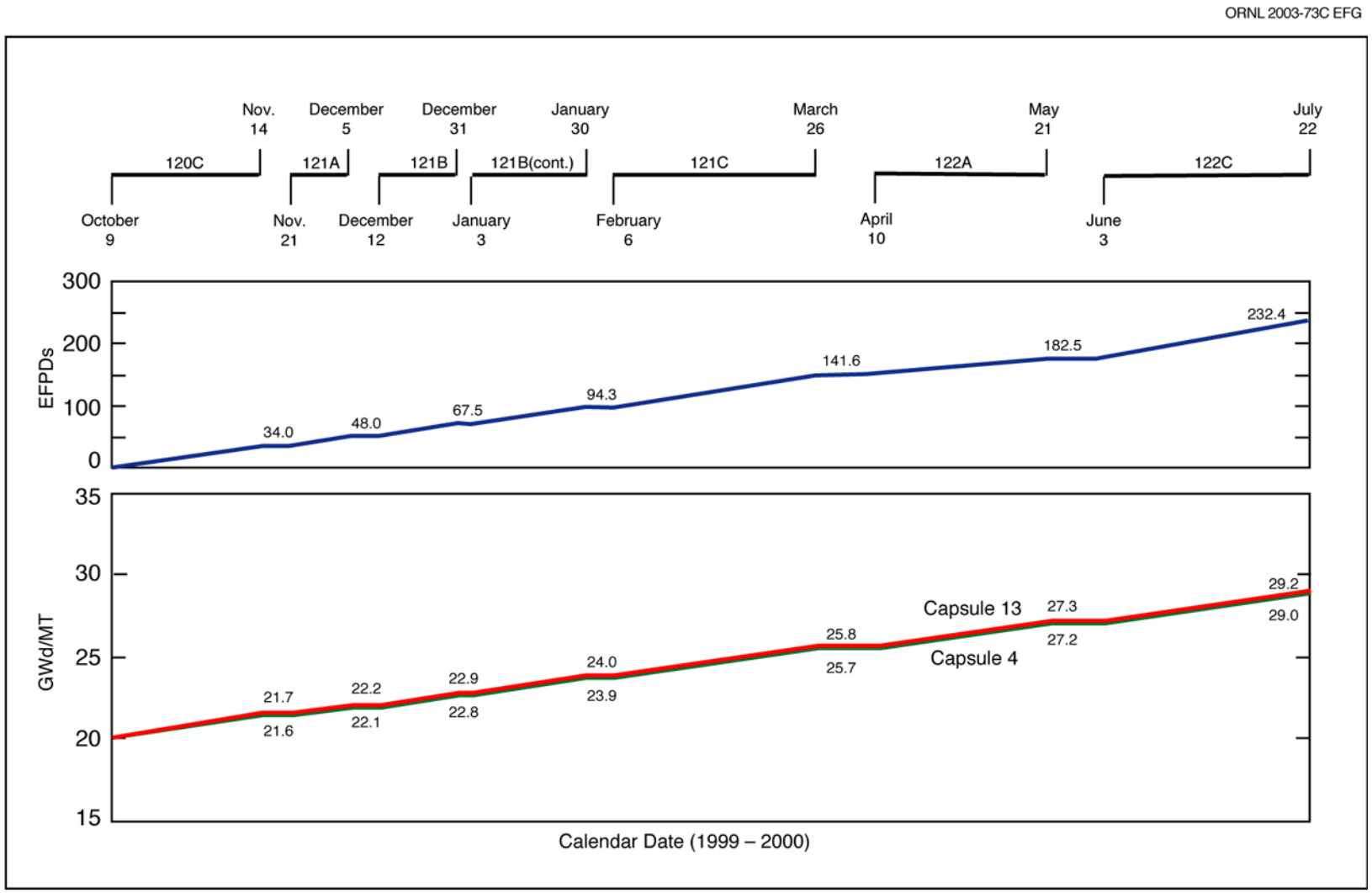

Figure 3.3 Dates, effective full-power days, and accumulated burnups for Capsules 4 and 13 during the Phase-III Part 1 irradiation cycles.

Table 3.3 Capsule heating rates for Phase III Part 1

Cycle	EFPDs	Capsule 4			Capsule 13		
		MWd	Average LHGR KW/ft	End-cycle burnup GWd/MT	MWd	Average LHGR KW/ft	End-cycle burnup GWd/MT
120C	34.0	0.1091	6.619	21.59	0.1089	6.640	21.69
121A	14.0	0.0344	5.076	22.07	0.0361	5.340	22.19
121B(1)	19.5	0.0496	5.246	22.77	0.0534	5.674	22.94
121B(2)	26.8	0.0817	6.292	23.91	0.0786	6.081	24.04
121C	47.3	0.1277	5.571	25.70	0.1291	5.658	25.84
122A	40.9	0.1055	5.321	27.18	0.1053	5.337	27.31
122C	49.9	0.1306	5.400	29.01	0.1313	5.453	29.15

With single unplanned shutdowns during Cycles 120C, 121B(2), 121C, and 122C, the test capsules were thermally cycled 11 times during the seven operating cycles of Phase III Part 1.

Capsules 3 and 10 were withdrawn at the completion of Phase III Part 1 and sent to ORNL for PIE. The irradiation history and subsequent PIE for these 30-GWd/MT-withdrawal capsules are reported in References 15 and 19.

Phase III Part 2 comprised 113 EFPDs over three ATR cycles devoted to increasing the burnup of lag Capsules 5, 6, and 12. Capsules 4 and 13 rested in the ATR canal throughout the approximately five months of the Part 2 irradiation.

3.4 Irradiation History for Phase IV Part 1

Irradiation for Phase IV Part 1 began with Cycle 124C on January 27, 2001, and continued through Cycle 127A, ending on March 9, 2002. The Model-2 aluminum-shield basket assembly was employed throughout. The test assembly carried five MOX capsules and four stainless steel dummy capsules configured as shown in Figure 6 of Reference 8. Capsules 4 and 13 occupied the front middle positions (the same as they had occupied during the Phase-II irradiation).

The test assembly accumulated 289.1 EFPDs of irradiation during Phase IV Part 1. Figure 3.4 illustrates the irradiation periods with their calendar dates and the associated burnup accumulations for Capsules 4 and 13. Following Cycle 126A, the test assembly was shifted from the Northwest I-hole Position I-24 to the Southwest I-hole Position I-23 in the ATR reflector.

The energy releases, average LHGRs, and accumulated burnups for Capsules 4 and 13 during each of the individual irradiation cycles of Phase IV Part 1 are listed in Table 3.4.

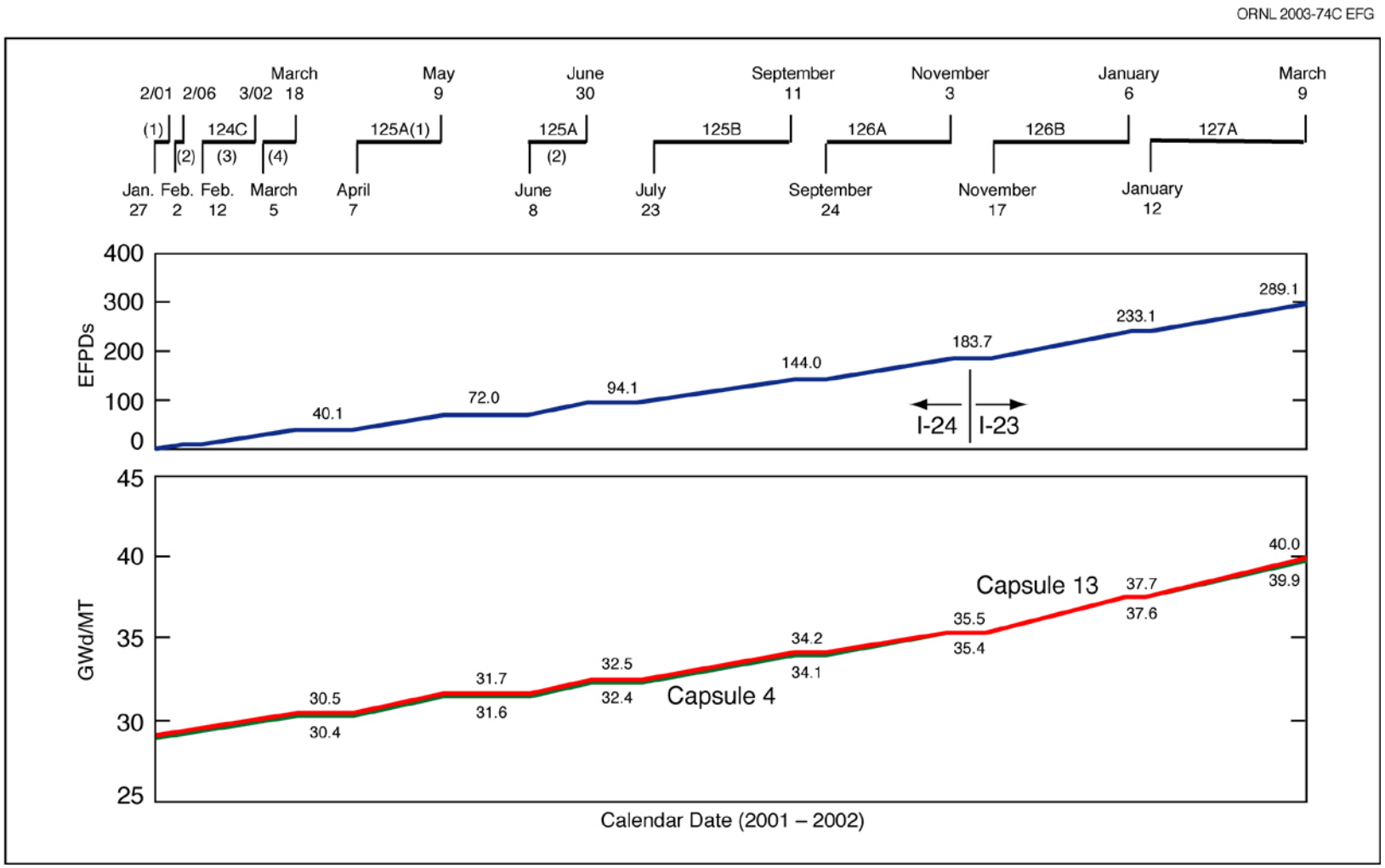

Figure 3.4 Dates, effective full-power days, and accumulated burnups for Capsules 4 and 13 during the Phase-IV Part 1 irradiation cycles.

Table 3.4 Capsule heating rates for Phase IV Part 1

Cycle	EFPDs	Capsule 4			Capsule 13		
		MWd	Average LHGR KW/ft	End-cycle burnup GWd/MT	MWd	Average LHGR KW/ft	End-cycle burnup GWd/MT
124C(1)	5.0	0.0125	5.152	29.21	0.0124	5.143	29.35
124C(2)	3.4	0.0084	5.095	29.33	0.0084	5.101	29.46
124C(3)	18.7	0.0423	4.671	29.96	0.0428	4.741	30.09
124C(4)	13.0	0.0294	4.658	30.40	0.0288	4.589	30.53
125A(1)	31.9	0.0768	4.966	31.57	0.0765	4.968	31.68
125A(2)	22.1	0.0567	5.292	32.41	0.0563	5.277	32.51
125B	49.9	0.1076	4.450	34.11	0.1082	4.494	34.20
126A	39.7	0.0861	4.475	35.40	0.0859	4.482	35.49
126B	49.4	0.1528	6.383	37.67	0.1529	6.417	37.74
127A	56.0	0.1536	5.658	39.88	0.1551	5.740	39.96

The higher power in the ATR core Southwest Lobe (23 versus 17 MW) produced the higher test capsule LHGRs as listed in Table 3.4 for the final two irradiation Cycles 126B and 127A.

With one unplanned shutdown-startup combination in both Cycles 125A(2) and 127A, the test capsules were thermally cycled 12 times during the ten operating cycles of Phase IV Part 1.

Capsules 4 and 13 were withdrawn at the completion of Phase IV Part 1 and shipped to ORNL for PIE. The results of the CARTS pre-PIE predictions and the findings of the initial PIE steps for these 40-GWd/MT capsules are described in Reference 16.

3.5. Irradiation Summary and CARTS Predictions Accuracy for Capsules 4 and 13

This Section provides an evaluation of the accuracy of the CARTS calculations run in advance of the PIE for Capsules 4 and 13. As described in the previous Sections, these capsules occupied a series of paired test assembly locations, symmetric with respect to the ATR core. Hence, their irradiation histories are similar.

Combining the Phase I, Phase II, Phase III Part 1, and Phase IV Part 1 experience, Capsules 4 and 13 were irradiated for 30 ATR operational cycles, accumulating 904.1 EFPDs (2.5 EFPY) and 42 thermal cycles. The final Fissions per Initial Metal Atom (FIMA) values are 4.15% for Capsule 4 and 4.16% for Capsule 13 (using a conversion factor of 9.60 GWd/MT per FIMA percent). The overall EFPD-averaged LHGR for these capsules is about 6.4 kW/ft, with a highest value of about 10.7 kW/ft at the beginning of Phase II. The integrated fast fluxes (n/cm^2; E>1.0 MeV) are calculated (MCNP) as 1.5E21 (fuel), 1.1E21 (Zircaloy clad) and 1.0E21 (steel capsule).

The CARTS input includes the average energy release rate (LHGR) for the test capsule during each irradiation cycle. Cycle-by-cycle energy releases for Capsules 4 and 13 are taken from the as-run Monte Carlo N-Particle (MCNP) code results obtained at INEEL at the conclusion of each

ATR operating cycle. These capsule energy releases (expressed as GWd/MT) are the sum of both fission of the test fuel and gamma heating by the ATR core, and therefore differ (slightly) from the burnups listed in Tables 3.1 through 3.4, which represent fission energy only. Uncertainties in these MCNP results are estimated to be ±7% of the calculated value. An average LHGR is then derived for each cycle based on the cycle duration (EFPDs) and the actual test capsule fuel mass, pellet stack length, and power history. Tables 3.1 through 3.4 list the average LHGRs as used for CARTS input.

As described in Chapter 2 of the Quick Look report (Reference 16), the CARTS calculations predict the conditions at the pellet midplane as a function of increasing burnup, and do not include representation of pellet cracking, or end-effects such as hourglassing. Parameters varied are the initial pellet-to-clad and clad-to-capsule gap widths (minimum, mean, and maximum), and the extent of fission gas release (best-estimate and conservative). The extent to which the PIE observations confirm the CARTS predictions is discussed in the following subsections.

3.5.1. Pellet Temperatures

When discussing calculated pellet temperatures, it is important to recall that each MOX test fuel pin contains 15 fuel pellets, each with unique dimensions within the specified fabrication tolerances. Thus, a spectrum of initial pellet-to-clad gaps exists within each pin. The gap widths, which widen in response to fuel densification and pellet temperature decrease and narrow with fuel swelling and pellet temperature increase, play an important role in establishing the burnup-dependent changes in pellet centerline temperatures as the irradiation proceeds. Accordingly, CARTS results for each fuel pin are reported for the minimum, mean, and maximum initial gap widths as defined by the clad inner diameter (measured) and the tolerance range for pellet outer diameter.

For all three assumptions regarding initial gap width, the pellet centerline temperatures predicted by CARTS exceed the Halden empirical threshold (described in Reference 20) for greater than one percent gas release. This occurs during almost all of irradiation Phase II for both fuel pins. The gas release fractions (0.0837 for Pin 7 and 0.0951 for Pin 16) measured during the PIE tend to confirm that the fuel centerline temperatures were this high.

On the other hand, PIE observations of the fuel condition near the pellet center indicate that the centerline temperatures did not approach melting. The highest pellet centerline temperature predicted by CARTS was 1601°C (for Pin 16 at the end of the second irradiation cycle for Phase II). This is more than 1000°C below the fuel melting temperature, which conforms to the observed fuel state.

Finally, the CARTS-predicted pellet centerline temperatures are less than 1100°C for all of the irradiation cycles after about 20 GWd/MT burnup. These relatively low local temperatures during the latter half of the irradiation permit formation of the characteristic high-burnup structure to outline the MOX agglomerates in the central portion of the fuel. (Such agglomerate outlining is common in the cooler outer radial portions of the fuel cross-sections.) Indeed, some of the MOX agglomerates are visible in the central portion of the fuel, which was not the case in

previous PIEs where centerline temperatures in excess of 1100°C were experienced during the final cycles of irradiation.

Without fuel thermocouples, it is impossible to precisely evaluate the accuracy of the temperature traces calculated for the fuel during the irradiation. Nevertheless, it is fair to say that the temperature traces predicted by CARTS for the irradiation of Capsules 4 and 13 are consistent with the fuel observations during the current PIE.

For the capsules in the hot cells, temperatures were predicted [Table 2.6 of the Quick Look report (Reference 16)] to be about 44.5°C in mid-July, for a decay heat at that time of about 2.15 Watts with an assumed cell ambient temperature of 33.3°C. This is consistent with the measured temperature of about 56.6°C taken during the last week of April when decay heating was about 3.33 kW/ft and the cell ambient temperature was 29.9°C.

3.5.2. Pellet – Clad Interface

The CARTS code includes models for irradiation-induced fuel densification and swelling, as well as for pellet dimension changes caused by temperature variation (fuel heatup and cooldown). For Capsules 4 and 13 with burnups of 39.9 GWd/MT, CARTS predicted that the 15 pellets within each fuel pin would exhibit, under hot cell conditions, individual pellet-to-clad diametral gap widths ranging from 2.1 to 3.0 mils. Since open internal cracks are evident in almost all irradiated fuel cross-sections, it is important to note that this is an "equivalent" gap defined as twice the radial gap that would exist if the pellet were centered with all of the internal cracks completely closed. Such "equivalent" gaps are indeed inferred from the fuel cross-section MET mount photographs.

Clad contact at the pellet midplane was not predicted to have occurred at any time during the irradiation. However, an outward clad creep at this location was modeled as an extrapolation of the progressively increased clad diameters observed in previous PIEs. This outward movement of the cladding adjacent to the pellet midplane is believed due to irradiation-induced creep under the impetus of internal gas pressure augmented to some extent by a local tensile stress mechanically imposed by hourglassing at the pellet-to-pellet interfaces. For the Capsule 4 and 13 predictions, the permanent clad deformation imposed by irradiation-induced outward clad creep was represented as 0.59 mil, a 0.18% increase in fuel pin outer diameter. This clad outward relocation was confirmed by the fuel pin diametral measurements shown in Figures 3.25 and 3.26 of the Quick Look report.

The diametral gap between the fuel pin and capsule was predicted to lie between 1.7 and 2.53 mils, which may be compared to the range of 2.2–3.0 mils for the initial cold capsule conditions. This prediction suggested that fuel pin removal from the capsule would be straightforward, without significant interference from pin-to-capsule binding. This was indeed the case.

Finally, the free volume measured for Fuel Pin 7 (about 1.3 cm^3) was found to agree within 0.5% with the value calculated from CARTS results for hot cell conditions. (Free volume was not measured for Fuel Pin 16.)

3.5.3 Fuel Pin Internal Pressure

It is important to recall that CARTS does not mechanistically calculate a fission gas release from which a fuel pin pressure is calculated. Rather, the user inputs a fission gas release fraction at 45 GWd/MT burnup to which CARTS applies a curve fit (release as function of burnup) to calculate the gas composition in the pellet-clad gap for heat transfer purposes and to obtain the overall pin gas content for fuel pin pressure determination. The user also inputs a release fraction for the created helium, for the same purposes.

The pre-PIE CARTS calculations were done twice for each capsule, one set using 4.2% fission gas release at 45 GWd/MT burnup, and the other using 16.9% release at the same burnup. The actual releases (based on Kr-85 activity measurements at the fuel burnup of about 40 GWd/MT) have turned out to be 8.4% for Pin 7 and 9.5% for Pin 13. Thus, the release fractions assumed for CARTS input bracket the actual values and, correspondingly, the fuel pin pressures (66–196 psia) predicted by CARTS bracket the measured (115–135 psia) pressures.

It is concluded that the pre-PIE CARTS calculations were based upon an appropriate approximate range for the effects of fission gas release upon heat transfer in the pellet-clad gap. In Volume 2 of this final PIE report for the 40 GWd/MT withdrawals, the CARTS calculations for Capsules 4 and 13 will be repeated, this time employing the information obtained during the PIE including actual fission gas release fractions and as-measured outward clad creep dimensions.

4. METROLOGY OF CAPSULES 4 AND 13

Table 4.1 details the items that have been assigned to the metrology task of the PIE effort. Note that these items form a subset of the total PIE. The capsules made available for the 40 GWd/MT PIE effort are Capsule 4 (fuel prepared without gallium removal) and Capsule 13 (fuel for which the PuO_2 was treated for gallium removal).

Table 4.1 Metrology Items.

No.	Examination	Comments
1	Capsule photo visual	Containment (capsule) integrity is major interest.
2	Capsule temperature measurement	Compare measured temperatures with predictions.
3	Capsule dimensional inspection	Containment integrity is major interest
4	Capsule gamma scan	Determine gross internal state of capsule and fuel pin.
5	Fission gas sampling	The gas pressure and ^{85}Kr content of both the containment and the fuel pin will be analyzed.
Remove fuel pin from capsule		
6	Fuel pin photo	First assessment of clad integrity.
7	Fuel pin dimensional inspection	Detailed assessment of clad integrity and local deformations caused by pellet-clad contact.
8	Fuel pin free volume measurement	Determine the total free volume within the fuel pin.

Note that the capsule and fuel pin numbering are not the same; Table 4.2 details the relationship between the two and identifies the status with respect to gallium removal treatment.

4.1 Capsule Photo Visual Inspection

The first portion of the PIE effort was to visually examine the capsule surfaces at low magnification. The capsules were not as clean and bright as previous capsules were. There appeared to be more handling scratches and some mild discoloration on the surfaces directly overlying the fuel, but no physical distortions or damage. These observations are not unexpected as both capsules were irradiated or stored in the ATR canal for long periods. In general, the stainless steel containment survived the irradiation as expected and these capsules have no less integrity than the capsules previously removed at 8, 21, and 30 GWd/MT.

Photographs of these capsules are shown in Figures 4.1 through 4.6 for a variety of views. The two appear identical except for the identification marks. The black lines near the welding border

Table 4.2 Capsule and Fuel Pin Numbering and Status

Capsule Number	Fuel Pin Number	Fuel Batch	Gallium Treatment	Exposure (GWd/MT)	PIE Status
1	2	A	None	8	Complete –Pending clad ductility testing
2	5	A	None	21	Complete –Pending clad ductility testing
3	6	A	None	30	Complete –Pending clad ductility testing
4	7	A	None	40	Underway – Subject of this report
5	8	A	None	In Reactor	
6	9	A	None	In Reactor	
7	10	A	None	Archive	
8	11	B	Thermal (TIGR)	8	Complete –Pending clad ductility testing
9	12	B	Thermal (TIGR)	21	Complete –Pending clad ductility testing
10	13	B	Thermal (TIGR)	30	Complete –Pending clad ductility testing
11	14	B	Thermal (TIGR)	Archive	
12	15	B	Thermal (TIGR)	In Reactor	
13	16	B	Thermal (TIGR)	40	Underway – Subject of this report

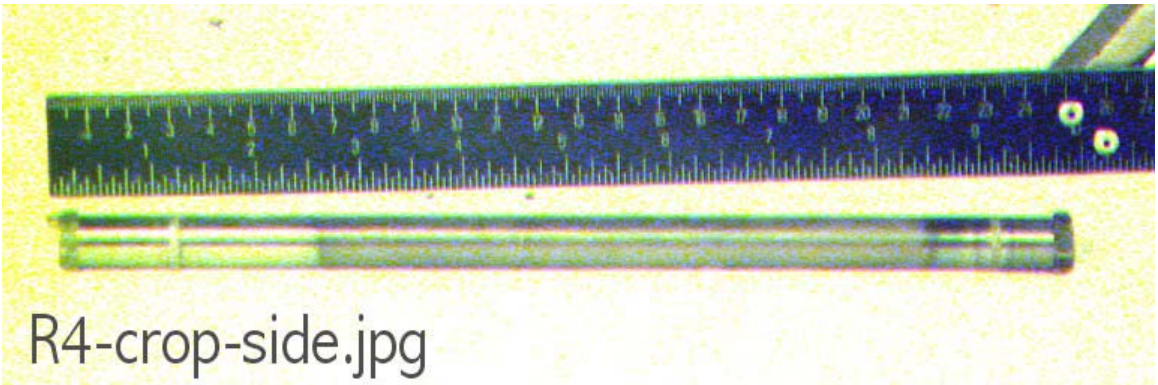

Figure 4.1 Side view of Capsule 4. Note the discoloration on the right 2/3 of the capsule.

Figure 4.2 Top view of Capsule 4.

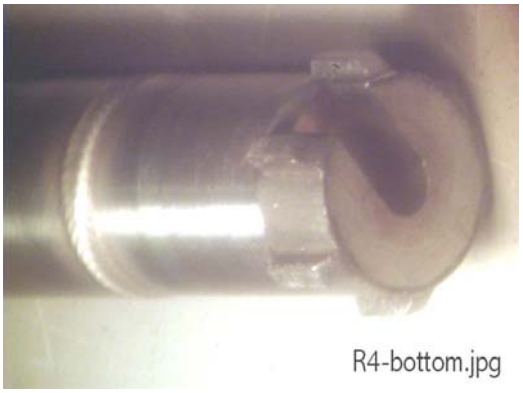

Figure 4.3 Bottom view of Capsule 4.

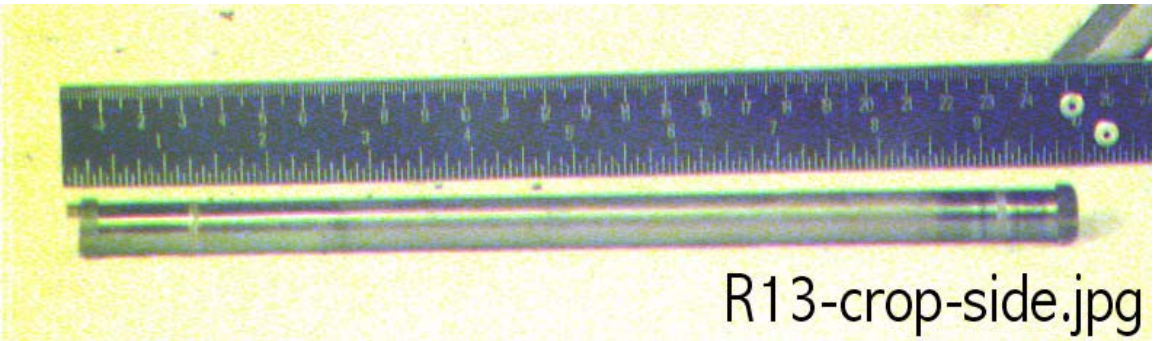

Figure 4.4 Side view of Capsule 13. The discoloration is similar to that on Capsule 4.

Figure 4.5 Top view of Capsule 13.

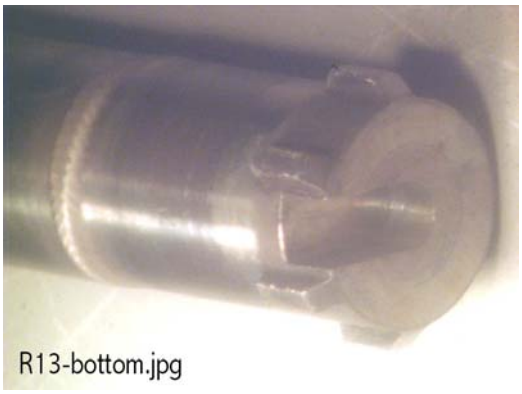

Figure 4.6 Bottom view of Capsule 13.

are the heat-affected zone and are unrelated to the irradiation. While not obvious from a comparison of the photographs shown in Figures 4.1 and 4.4, when held side-by-side both capsules have an equal amount of surface discoloration in the same location (overlying the fuel stack).

4.2 Capsule Temperature Measurements

The temperature measurements and their locations as taken on Capsules 4 and 13 are shown in Table 4.3. A photo of a capsule undergoing a measurement is shown in Fig. 4.7. The apparatus consists of a Type C thermocouple held to the capsule by a modified hose clamp.

Table 4.3 Capsule 4 and 13 Temperature Measurements

MOX Capsule 4	
Measurements taken on 04/25/2002	
Top Weld	42.7°C
Mid Point	56.5°C
Bottom Weld	48.2°C
Average	*49.1°C*
Cell Ambient	30.0°C
MOX Capsule 13	
Measurements taken on 04/26/2002	
Top Weld	40.2°C
Mid Point	56.8°C
Bottom Weld	46.3°C
Average	*47.8°C*
Cell Ambient	29.8°C

Notes:
Capsule temperature measurements were taken approximately 12" from the hot cell tabletop and allowed to stabilize for 45 minutes.

4.3 Capsule Dimensional Inspection

The results of the stainless steel capsule dimensional inspections are shown in Table 4.4. Within 0.001 inches, there were no indications of bowing or out-of-roundness. Measurements for bowing were carried out between the capsule welds. Only a slight difference between pre- and post-irradiation diametrical values was noted, 0.001 inches or less, which is attributed to the thermal expansion associated with the somewhat higher measurement temperatures in the hot cell. The lengths of the capsules were found to agree with the preirradiation values within 0.01 inches. Figure 4.8 details the measurement method for diametrical dimensions.

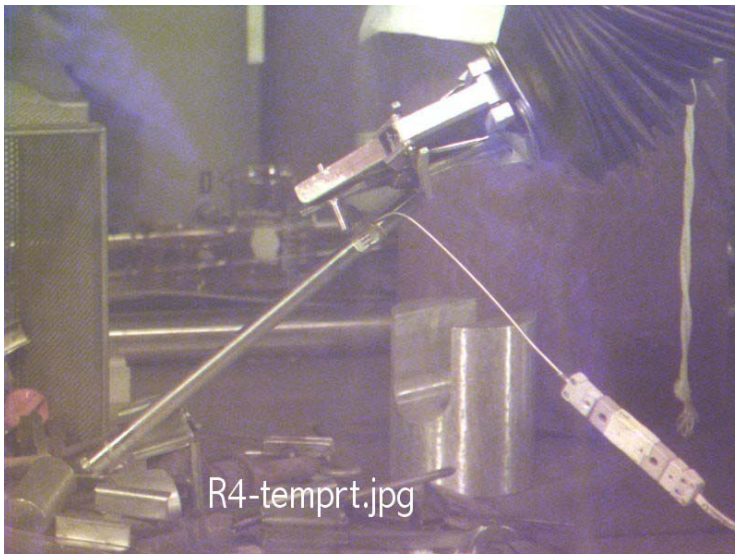

Figure 4.7 Free air temperature measurement on Capsule 4.

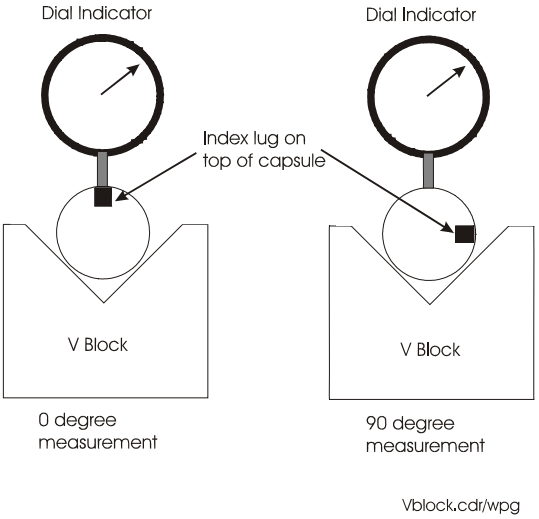

Figure 4.8 Schematic of diameter measurement.

Table 4.4 Capsule Measurements

Approximate Axial Location	Diameter Measurements (in) (±0.0005 in)		Preirradiation Value (Room Temperature) (in)
	0°	90°	
Capsule 4			
3.8” from capsule top	0.4652	0.4654	0.4643 to 0.4649
Center of capsule	0.4655	0.4655	
5.8” from capsule top	0.4655	0.4659	
Capsule 13			
3.8” from capsule top	0.4654	0.4653	0.4643 to 0.4649
Center of capsule	0.4655	0.4654	
5.8” from capsule top	0.4655	0.4654	
Length (in) (±0.005 in)			
Capsule 4	9.585		9.575 after welding (9.59 before welding)
Capsule 13	9.584		9.576 after welding (9.59 before welding)
Mass (g) (±0.1 in)			
Capsule 4	192.2		Not given
Capsule 13	192.5		Not given

4.4 Capsule Gamma Scans

Both Capsules 4 and 13 were raster-scanned to obtain two-dimensional views of the capsule internal structure. These scans comprise 6000 points and were taken with a 0.040" diameter collimator in two energy ranges. The range 400 to 700 keV was employed to broadly cover the fission products while the range 800 to 1575 keV was used to broadly cover the activation products. These two energy ranges were selected because they show the most details of interest for a general view.

In addition, both capsules underwent an axial line scan (400 points) along their length using the same collimator as was used in the two-dimensional scans. Results from these two energy ranges are presented in the following Sections. Overall, the capsules appeared to be intact with no unusual structure or abnormalities.

4.4.1 Capsule 4 Gamma Scan

Figure 4.9 shows the result of the 400 to 700 keV raster scan for Capsule 4. When compared to the schematic above, one can make out the stainless steel end caps, the fuel pin end caps, and

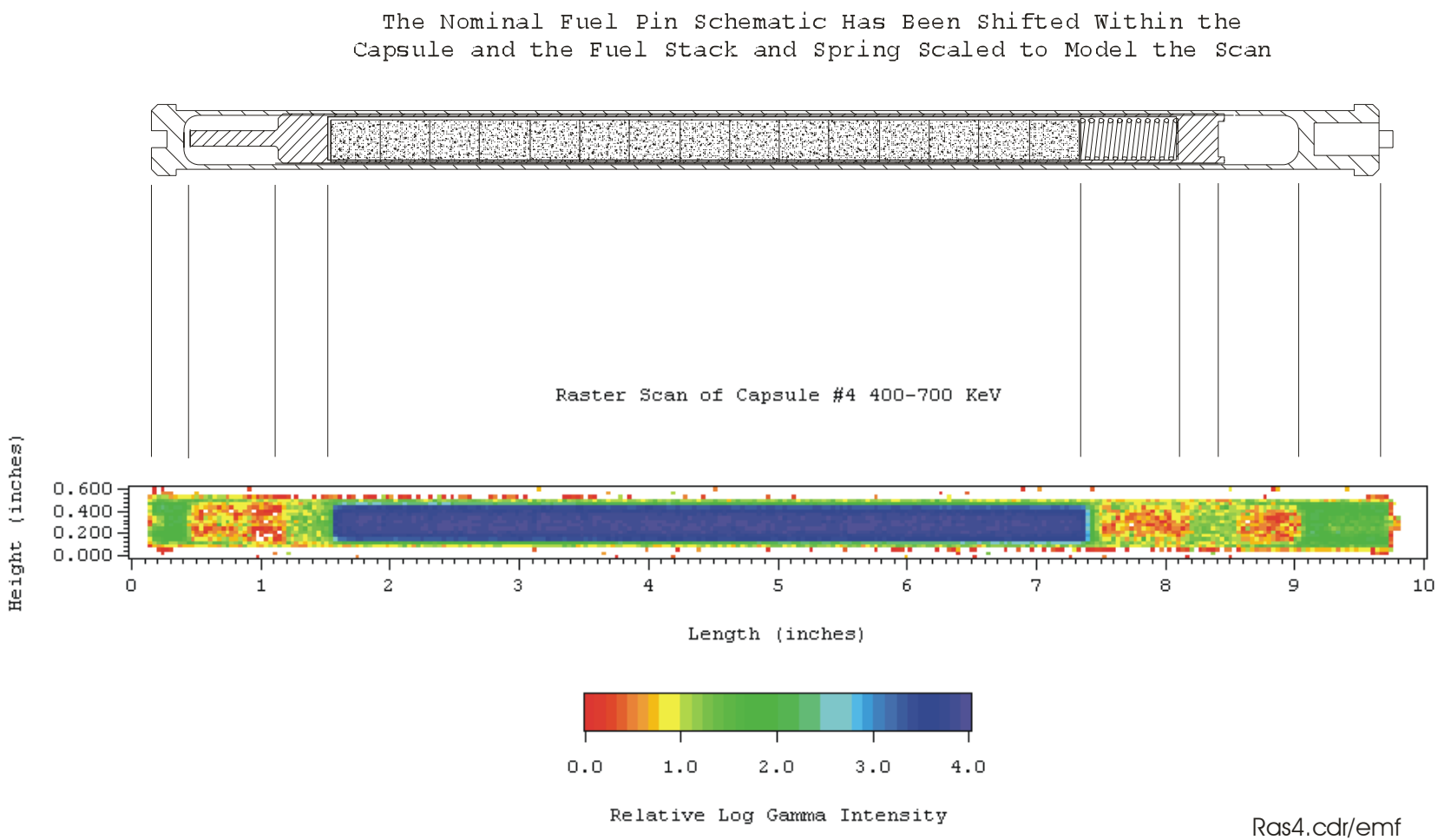

Figure 4.9 Capsule 4 mid energy gamma raster scan.

very clearly, the fuel pellet stack. The pedestal at the base of the lower fuel pin end plug is vaguely outlined as well as is the capsule boundary (the capsule bottom is to the left, the top to the right).

Figure 4.10 shows the raster scan for Capsule 4 in the 800 to 1575 keV energy range. This higher energy range outlines the stainless steel components to a greater degree.

Figure 4.11 shows an axial line scan along the capsule in the 400 to 700 keV energy range. Again, the elements of the capsule are clearly indicated. The fuel pellet stack appears to be about 5.85 inches long, within the apparatus measuring tolerance of the as-built dimension (5.82 inches). The nearly constant activity level along the pellet stack corresponds to the average of the ATR flux shapes at the positions within the test assembly where this capsule was located during the irradiation, and is as predicted by the neutronic codes.

Figure 4.12 shows an axial line scan in the energy range of 800-1575 KeV, which accents the stainless steel activation products. This figure shows the stainless steel capsule end caps and wall more clearly. The fuel can be seen because of the high-energy fission product emitters such as ^{140}La.

Overall, the capsule showed no structural problems. All components appeared to be in their proper locations and the fuel pellet stack does not appear to have swelled significantly.

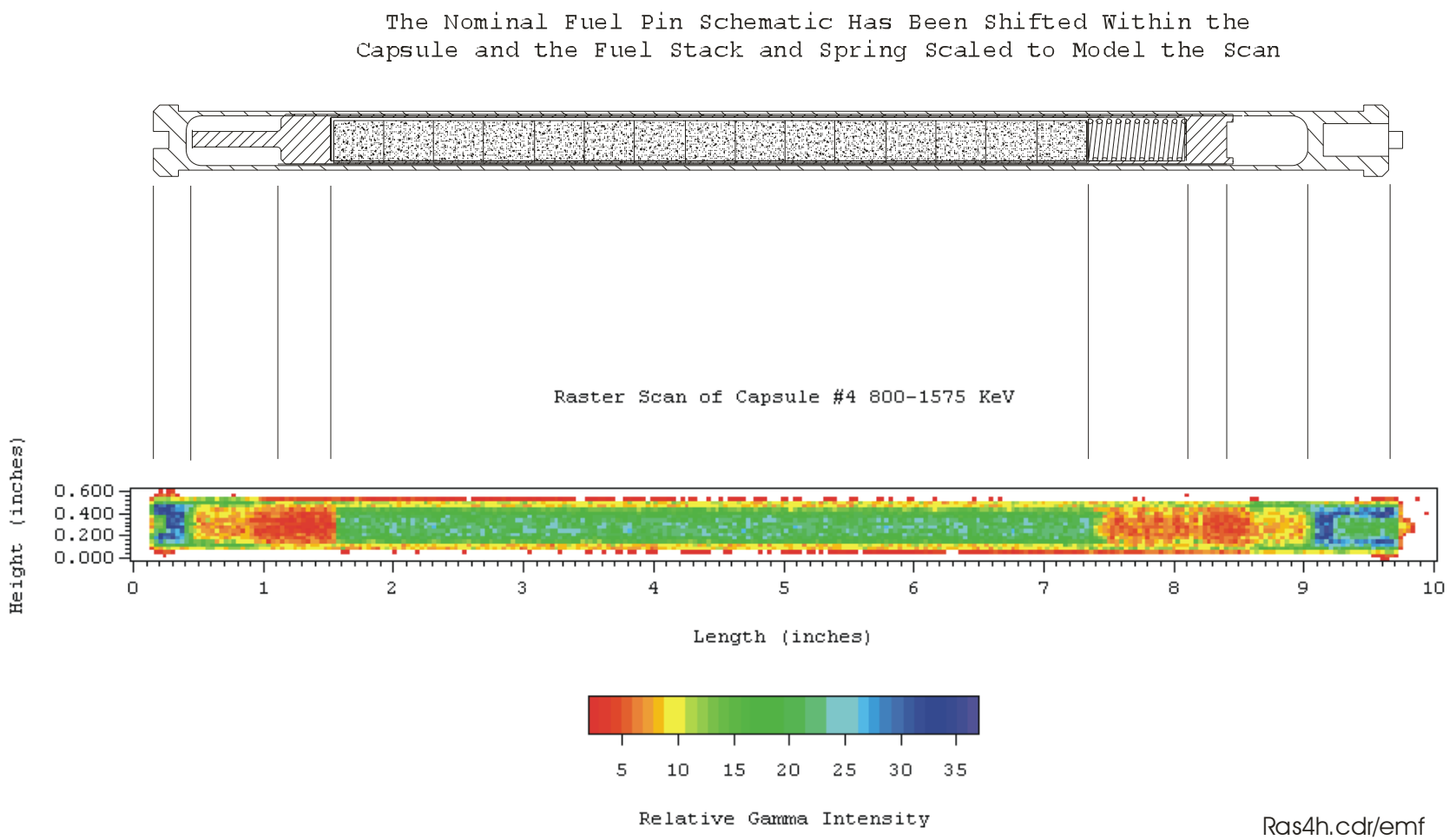

Ras4h.cdr/emf

Figure 4.10 Capsule 4 high-energy gamma raster scan.

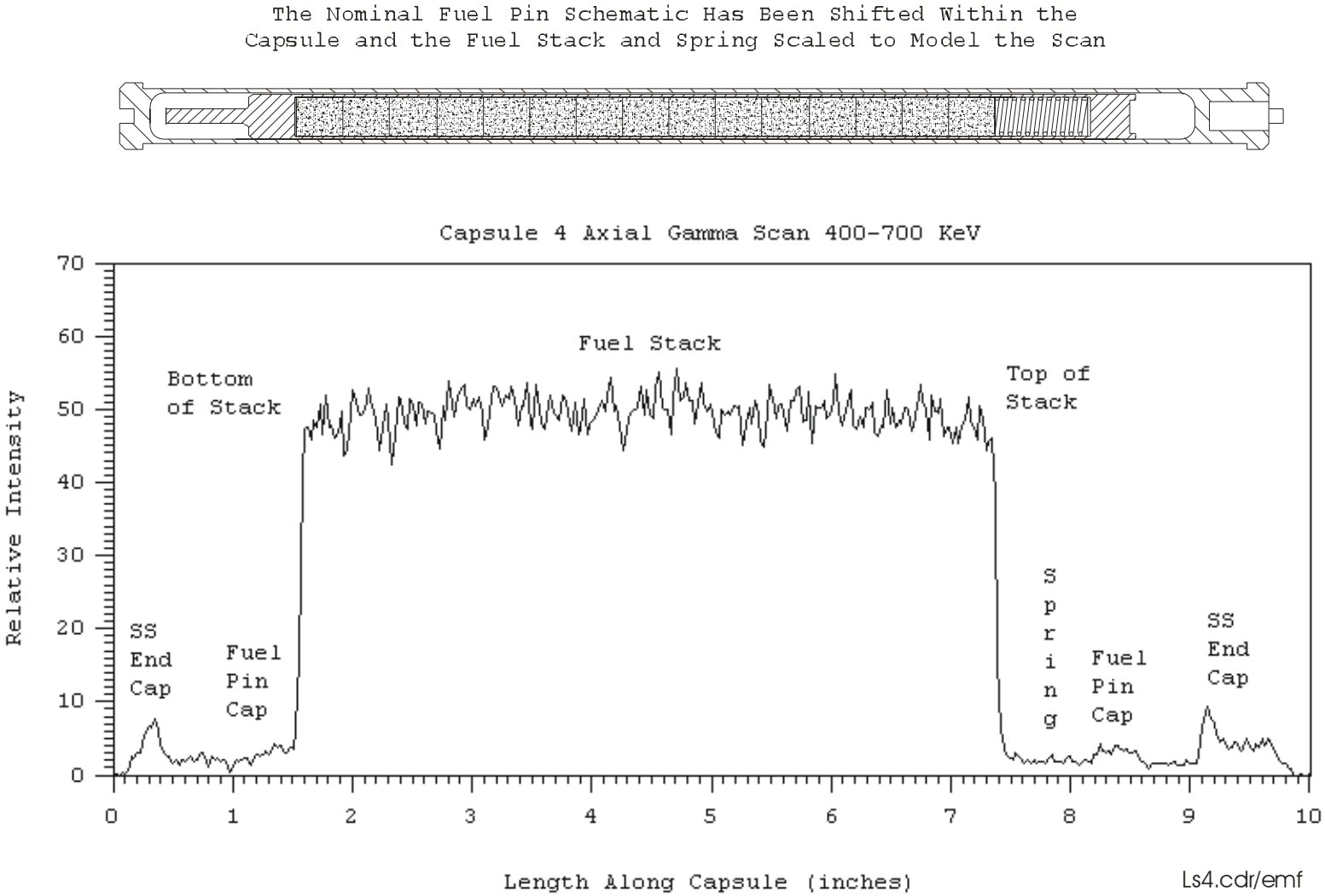

Figure 4.11 Capsule 4 mid energy gamma line scan.

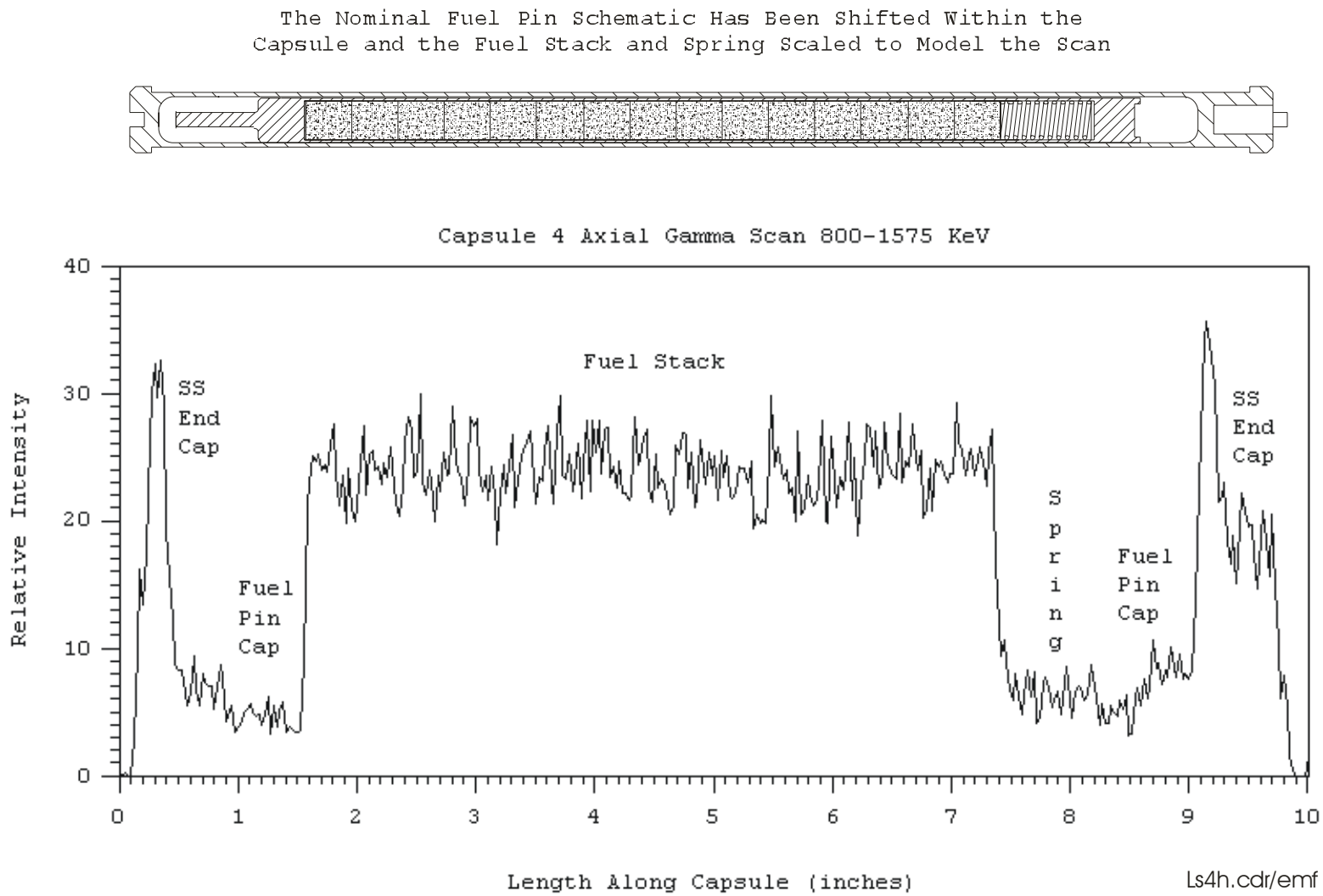

Figure 4.12 Capsule 4 high-energy gamma line scan.

4.4.2 Capsule 13 Gamma Scan

Figure 4.13 shows the results of the 400 to 700 keV raster scan for Capsule 13. As before, one can make out the stainless steel end caps, the fuel pin end caps, and the fuel pellet stack. Figure 4.14 shows the same scan in the 800 to 1575 energy range. No inconsistencies or abnormalities in internal component locations were noted.

Figure 4.15 shows an axial line scan along Capsule 13 in the 400 to 700 keV energy range. Again, the elements of the capsule are visible. The fuel stack appears to be approximately 5.8 inches long, which compares well with the as-built measurement of 5.79 inches. Unlike past PIE work, the pellet dish locations could not be discerned in either capsule gamma scan. This could be due to the high powers at which the fuel pins were operated and the associated movement of volatile fission products. Reference 27 explains how the axial migration of cesium can affect the pin activity profile. The fission product activity is also flat along the pellet stack as was seen in Capsule 4.

Figure 4.16 shows an axial line scan in the energy range of 800-1575 KeV, which accents the stainless steel activation products.

Similar to Capsule 4, Capsule 13 appears to have no structural problems and all components appear to be in their proper locations with no significant axial fuel swelling.

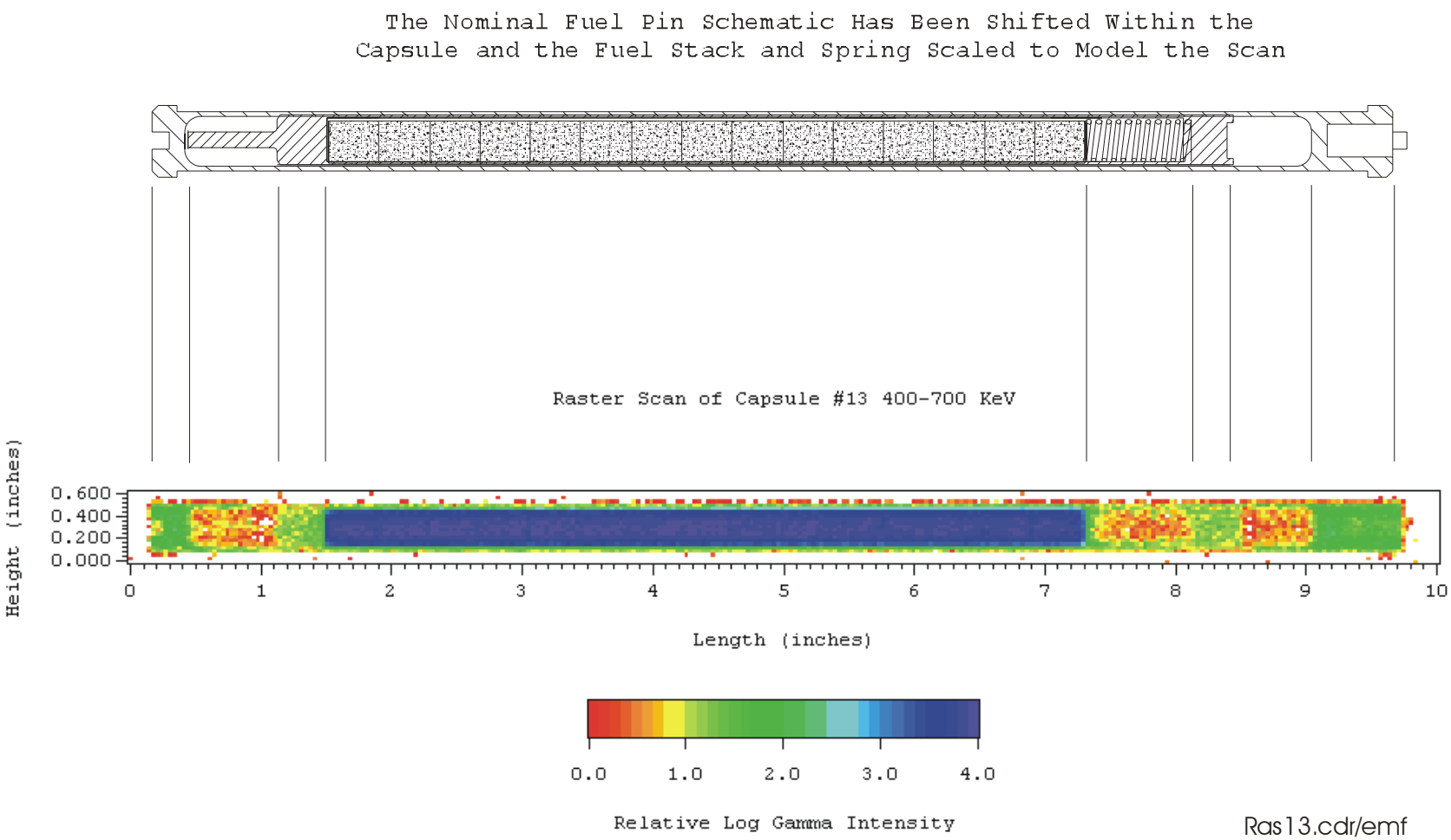

Figure 4.13 Capsule 13 mid energy gamma raster scan.

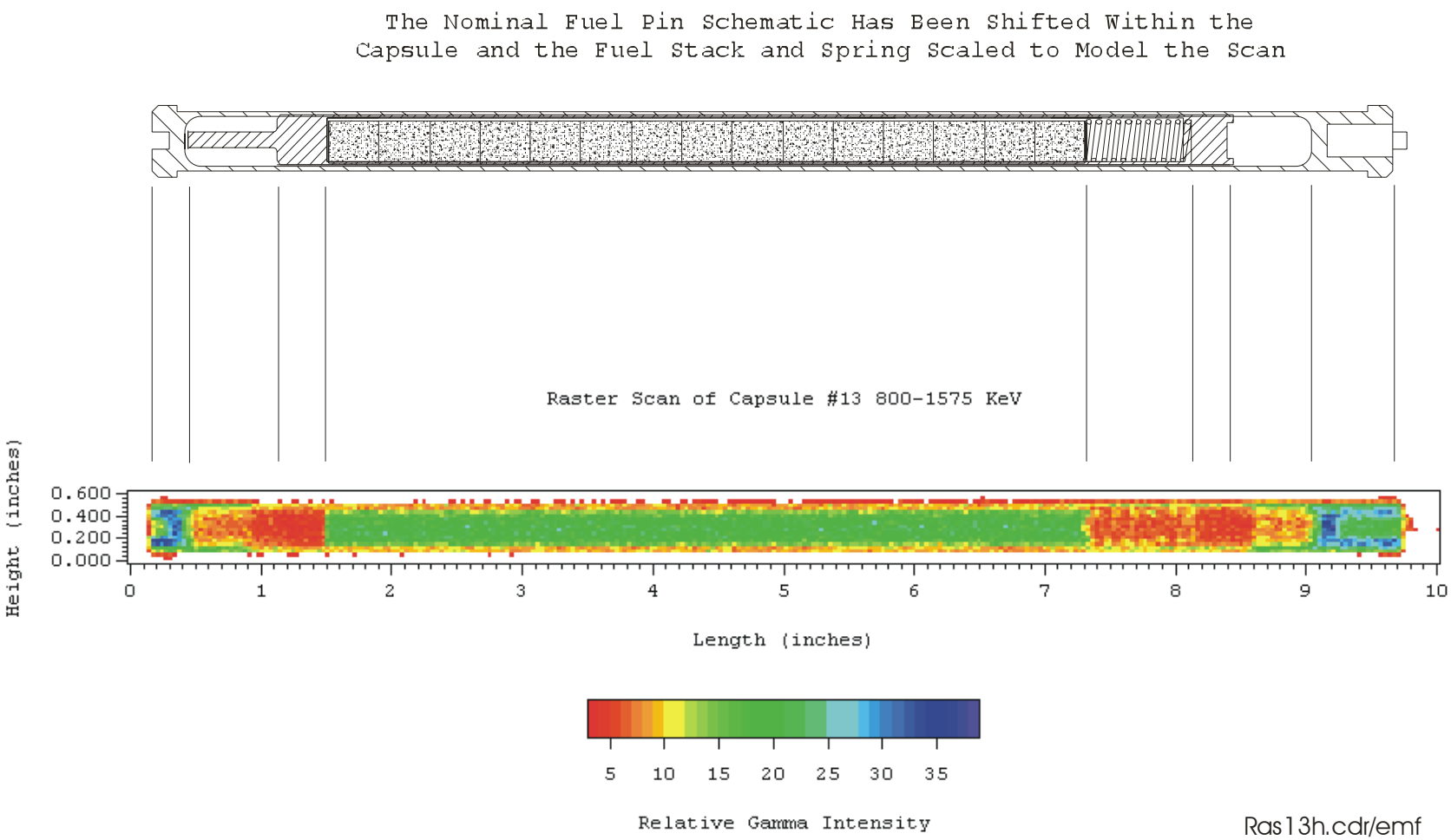

Figure 4.14 Capsule 13 high-energy gamma raster scan.

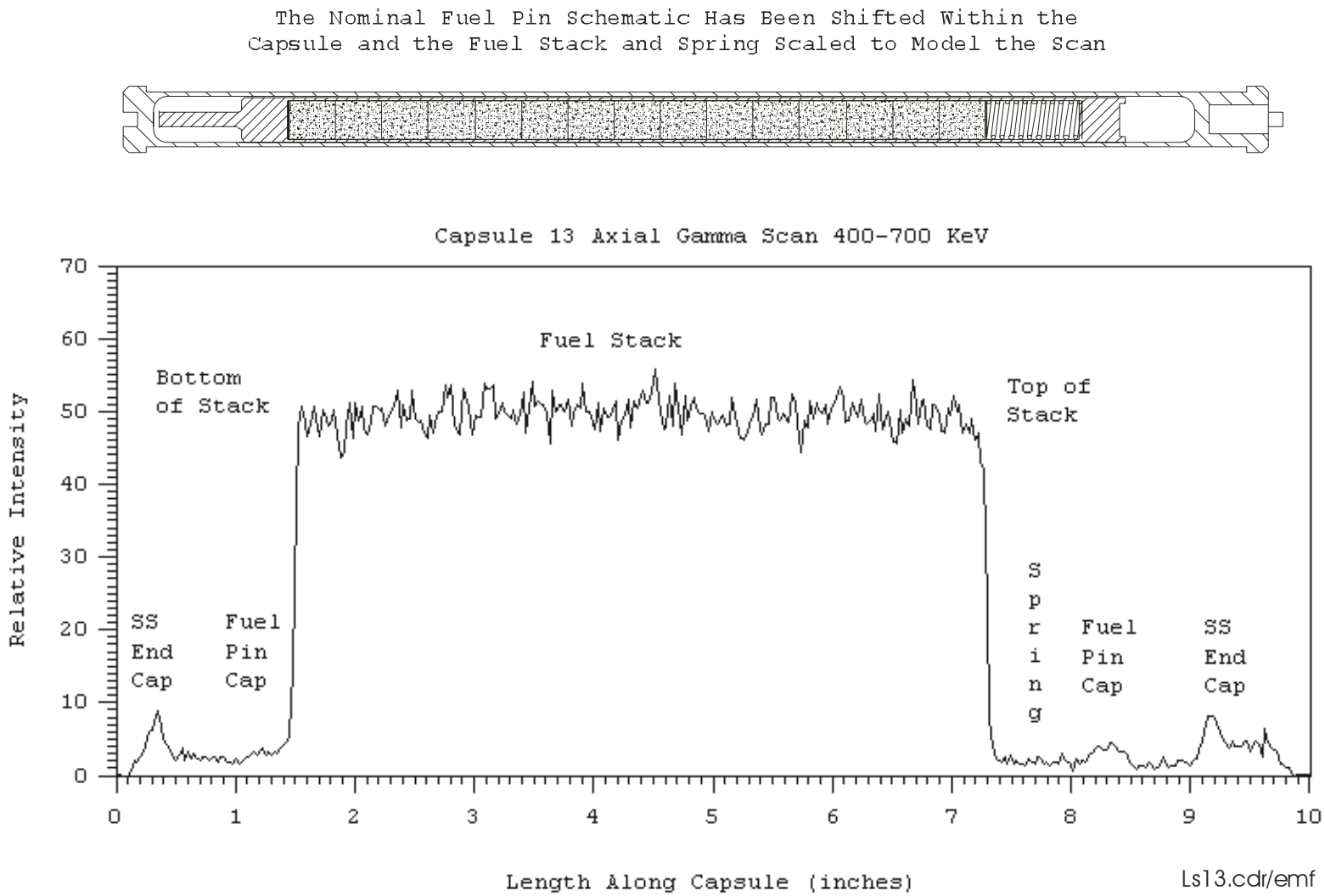

Figure 4.15 Capsule 13 mid energy gamma line scan.

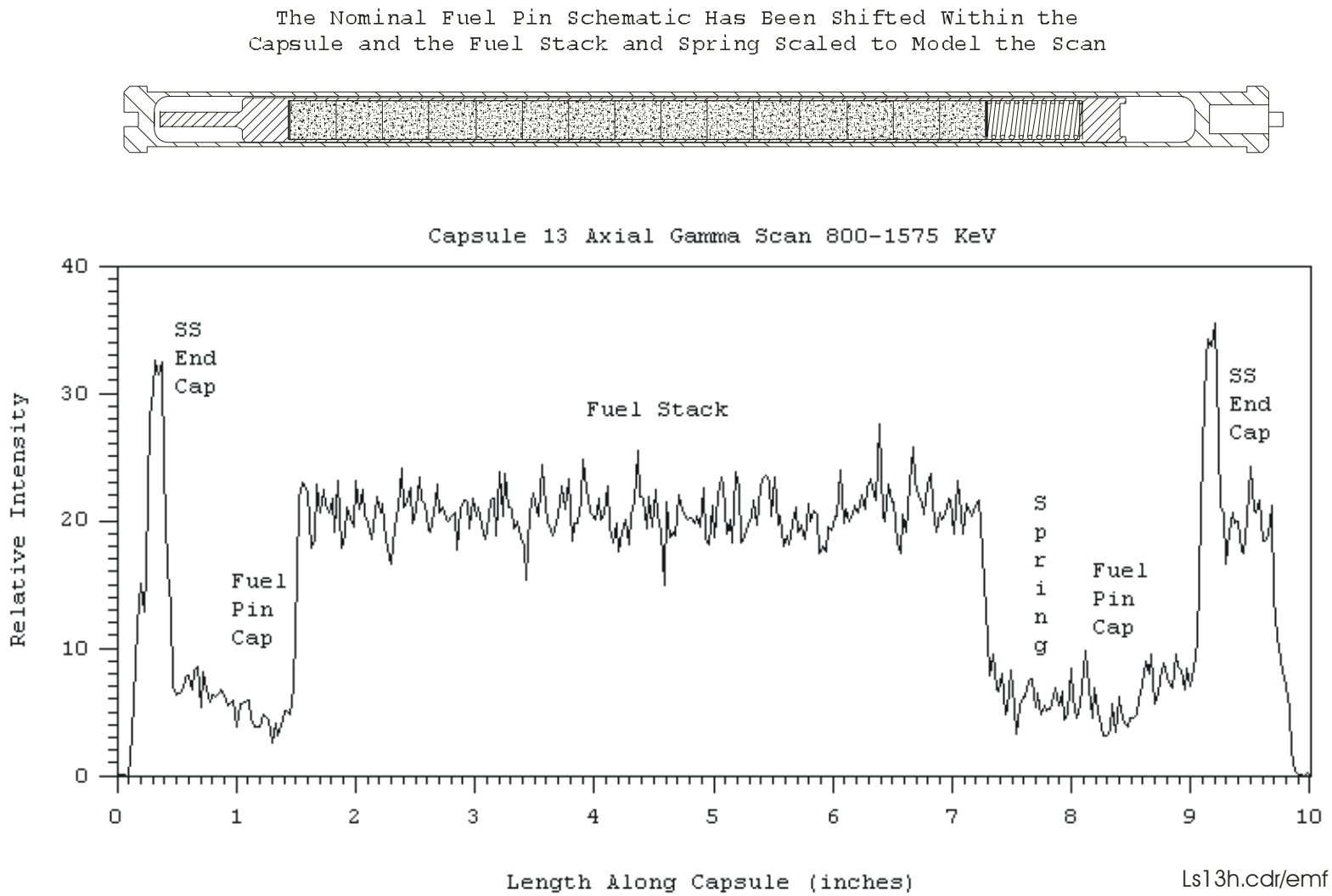

Figure 4.16 Capsule 13 high-energy gamma line scan.

4.4.3 Gamma Scanner Data Collection Orientation

The gamma intensity data was collected with the alignment lug of the capsule facing the gamma scanner detector as shown in Figure 4.17.

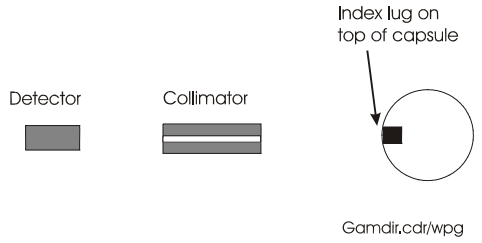

Figure 4.17 Orientation of the capsule and the gamma scanner collimator/detector.

4.5 Fission Gas Measurements

The total gas pressure and ^{85}Kr content in both Capsules 4 and 13 and their associated fuel pins were measured by use of the MOX Fission Gas Pressure Measuring Apparatus. Details of this apparatus and its calibration are described in Reference 21. This device was used previously in the PIEs of both the 21 and 30 GWd/MT capsules [References 13 and 15]. Briefly, the apparatus functions by using a vacuum sealed drill-press type action to drill first through the trimmed top of the MOX capsule and then, after sampling the gas in the capsule upper plenum region, to continue drilling into the contained fuel pin. The drilling stops as each barrier is penetrated to permit measurement of the gas pressure and sweeping of the released gases through a cold trap system to trap and determine the ^{85}Kr quantity. A diagram of the device is shown in Figure 4.18.

The drilling proceeded as planned for Capsule 4, but the drill bit broke before the fuel pin could be punctured in Capsule 13. To recover, Fuel Pin 16 was removed from its capsule, most of the drill fragments extracted from its top cap, and the fuel pin alone remounted. The drill bit in the apparatus was replaced by a mill bit and the weld on the top of the fuel pin was machined away until the seal was broken. The gas release took considerably longer (~2 hours vs. a few seconds) than normal, but no other problems were encountered. The gas was collected in the usual manner.

No anomalous fission gas release was observed in either capsule. The capsule pressures were subatmospheric, as expected since they were sealed at the elevation of INEEL, where the atmospheric pressure is about 12.5 psia. (The actual pressure in the capsule during welding could not be recorded.) The fuel pins were found to be sealed with internal pressures in excess of 100 psia. The fission gas release was found to be in the range of 8.4 to 9.5% (based on ^{85}Kr). The detailed results are summarized in Table 4.5.

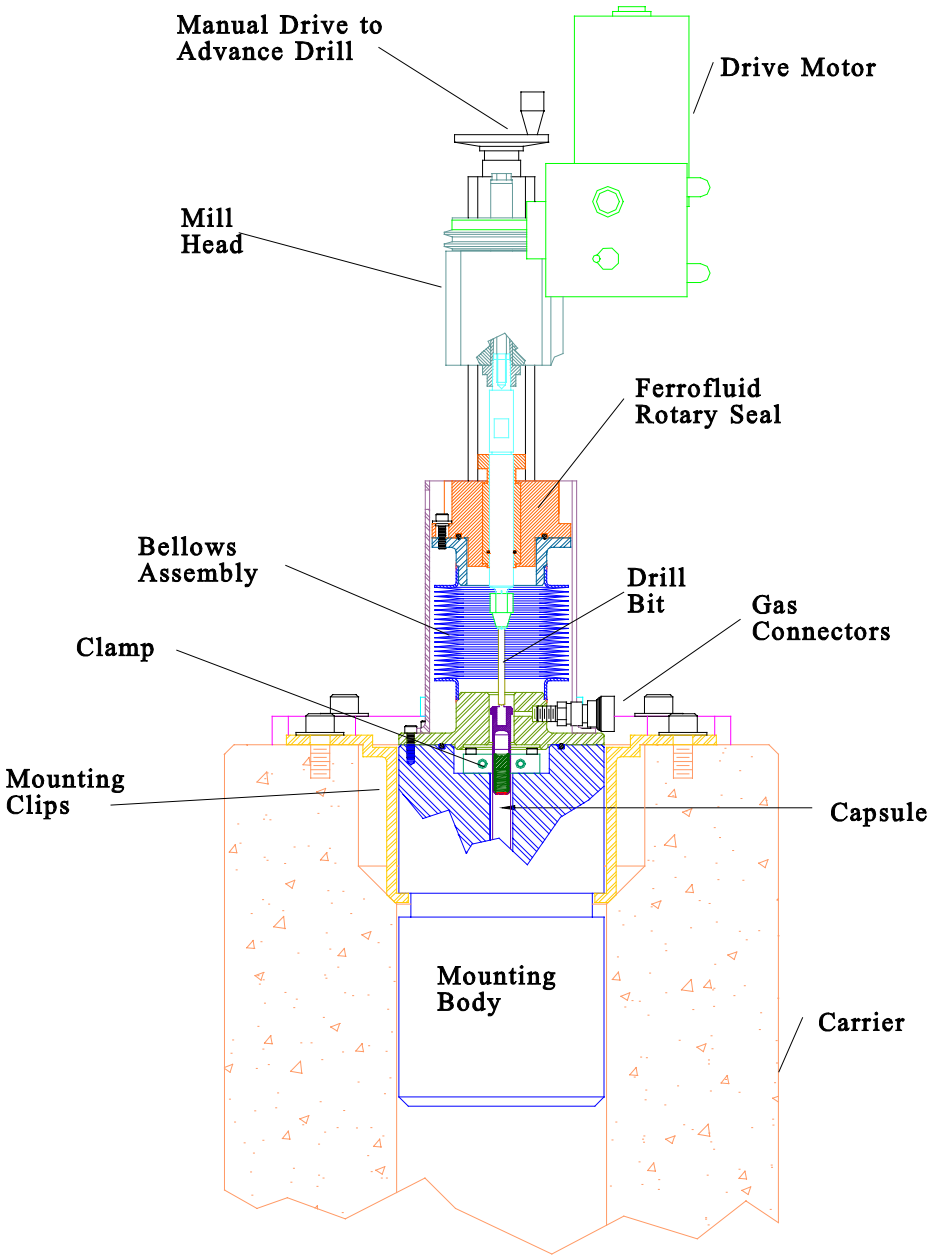

Figure 4.18 Cross sectional view of the Fission Gas Pressure Measuring Apparatus. [Drill Schematic 3.wpg]

Table 4.5 Fission Gas Measurements

Item	Best Estimate Free Volume[1] (cc)	Measured Pressure (psia)	Measured ^{85}Kr in Free Volume (mCi)	Best Estimate for Total ^{85}Kr Inventory[2] (mCi)	Model Predicted Pressure[3] (psia)	Release Fraction Based on ^{85}Kr Measurement
Capsule 4	2.405	9.84	0.00	0	N/A	N/A
Fuel Pin 7	1.323	114.8	39.6	473	66-196	0.0837
Capsule 13	2.390	9.95	0.00	0	N/A	N/A
Fuel Pin 16	1.347	134.8	44.8	471	66-196	0.0951

[1]Based on as-built dimensional measurements (capsule), volume measurements (Fuel Pin 7), and code predictions (Fuel Pin 16)
[2]Based on ORIGEN calculations (Reference 22) for the time of drilling
[3]Based on CARTS calculations with estimated release fractions corresponding to 4.2 and 16.9% at 45 GWd/MT, minimum pellet-clad gaps, and nominal fuel pellet stack length dimensions (Chapter 3)
Ambient temperature approximately 23°C
Measured values are approximately ±5% for pressure and ±8% for ^{85}Kr

With respect to the fission gas release fraction results, it should be noted that the values reported in the Quick Look report (Section 3.5 of Reference 16) are too low. Subsequent data analyses revealed that the fuel pin pressures corresponding to these gas release fractions were significantly lower than the measured pressures. It developed that the activity associated with the fuel pin gas samples was higher than the accurate range of the detector calibration curve then in use. A set of qualified ^{85}Kr gas sources was procured and a new calibration curve, accurate throughout the range of interest, was developed as described in Reference 25. Use of the new calibration curve with the original activity readings then permitted accurate determination of the gas release fractions as listed in Table 4.5.

4.6 Fuel Pin Photo Visual Inspections

Fuel Pin 7 was removed from Capsule 4 by cutting off the bottom of the capsule just above the weld. For this PIE a different technique was used to avoid cutting off the pedestal at the base of the fuel pin. After deburring the capsule body, the fuel pin was removed by grasping and pulling on the full-length pedestal. The pin slid out without difficulty. After removal, the pin was photographed and measured. The exterior of Fuel Pin 7 was found to be in excellent condition.

No attempt was made to maintain the angular orientation of the fuel pin relative to the capsule index lug because the fuel pin is not locked within the capsule during irradiation. Photographs of the fuel pin are shown in Figures 4.19 through 4.21.

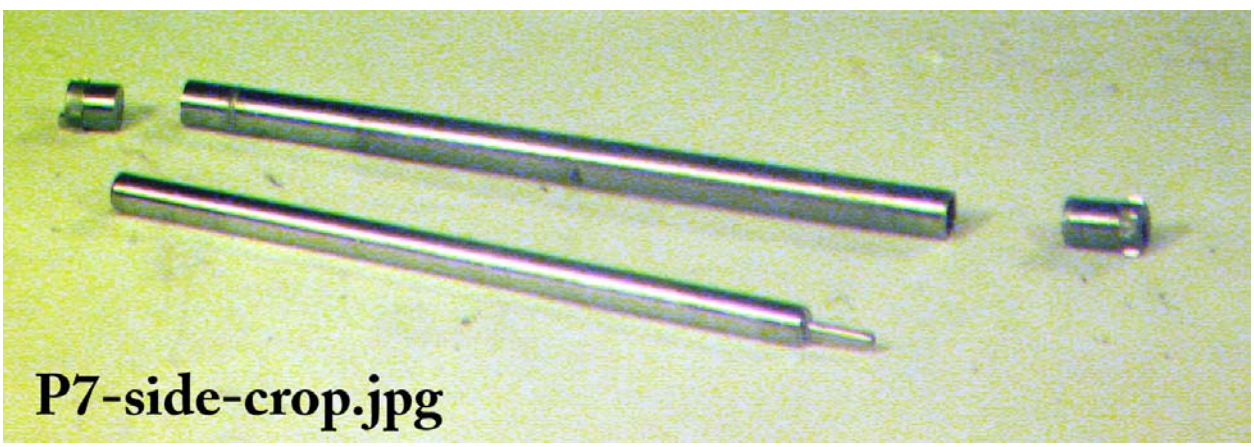

Figure 4.19 Side view of Fuel Pin 7 (foreground). Shown in the background are the components of the capsule.

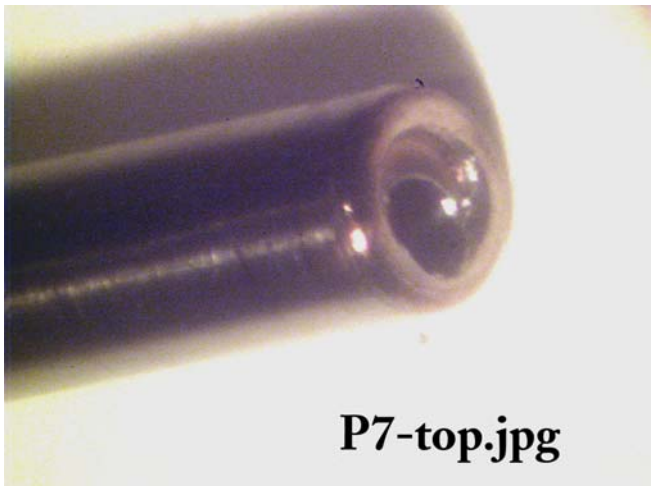

Figure 4.20 Top view of Fuel Pin 7. The puncture hole can be seen.

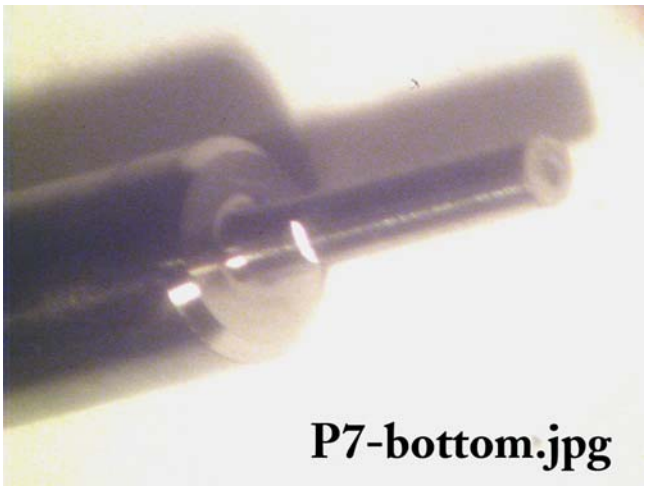

Figure 4.21 Bottom view of Fuel Pin 7. The vertical mark on the pedestal is a nick made when sawing the capsule bottom off.

Fuel pin 16 was removed from Capsule 13 in the same manner that Fuel Pin 7 was removed from Capsule 4. Slightly more force was required to pull the pin free. The exterior of Fuel Pin 16 was found to be in excellent condition. Photographs of Fuel Pin 16 are shown in Figs. 4.22 through 4.24.

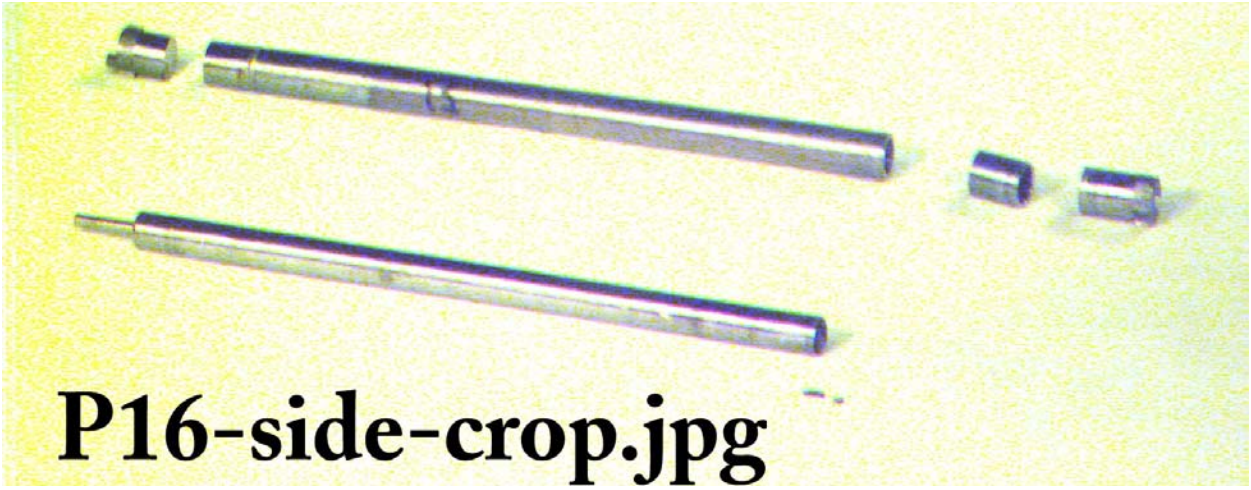

Figure 4.22 Side view of Fuel Pin 16 (foreground). Shown in the background are the components of the capsule. The small cut off piece of the capsule was used as a spacer when resolving the broken drill problem.

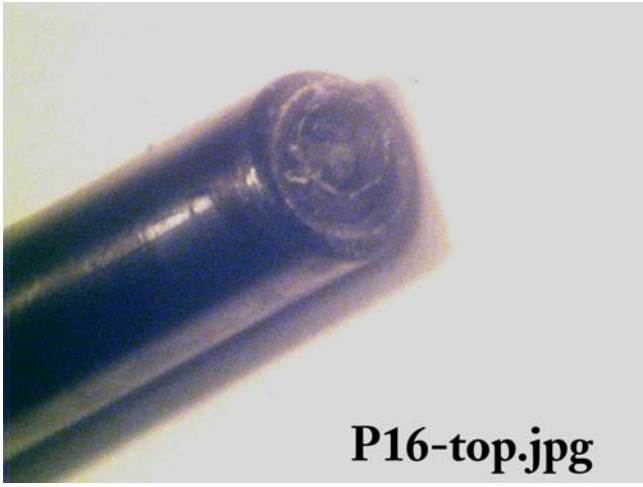

Figure 4.23 Top view of Fuel Pin 16. A piece of the broken drill bit can be seen in the partially drilled hole.

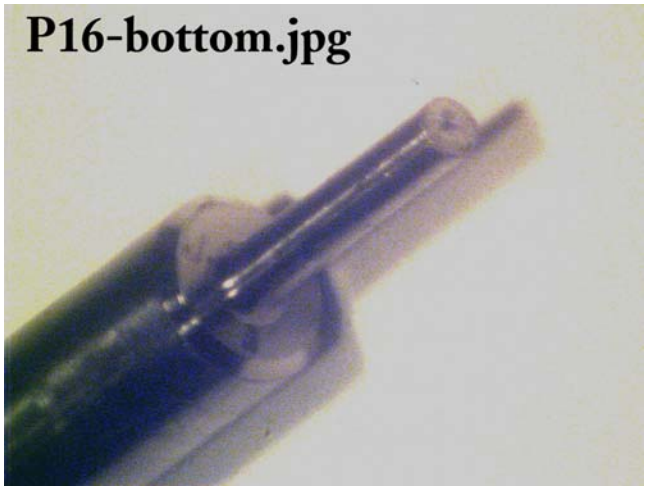

Figure 4.24 Bottom view of Fuel Pin 16.

4.7 Fuel Pin Dimensional Inspections

The results of the Fuel Pin 7 dimensional inspections are shown in Figure 4.25. These continuous profile measurements were taken using the Fuel Pin Measuring Apparatus (FPMA) as detailed in Reference 23. Accuracy is estimated to be ±0.1 mil. The zero reference point is the bottom of the pin; the pedestal region is not measured. The peaks and valleys associated with clad primary ridging are clearly outlined. The profile as measured for Fuel Pin 16 is shown in Figure 4.26.

A first set of FPMA readings was taken for Fuel Pin 16 in late September 2002. This is the only fuel pin for which the profile was measured while the pin remained internally pressurized. Similar to Pin 7, both outward clad expansion and clad primary ridges are evident. Pin 16 was found to have a slightly larger mean diameter (0.3820") than Pin 7 (0.3815"), which tends to explain the small additional force required when Pin 16 was extracted. There is no indication of surface discoloration, either in the area over the pellets (where the capsule surface was discolored), or elsewhere.

After Fuel Pin 16 was opened (as described in Section 4.5), a second set of clad profile measurements (to determine the average diameter in the absence of internal pressurization) was taken in early November 2002. As expected, the average diameter over the fueled region was slightly smaller, 0.3818 Vs 0.3820 for the pressurized case. (The internal pressure of about 135 psia had maintained a small wall tensile stress of about 5.5 MPa after the pellet shrank away from the clad as the pin cooled after irradiation.)

Other than a decrease of 0.2 mil in average diameter, the peaks and valleys of the clad profiles are virtually identical in the two measurements. Thus, an excellent reproducibility of the clad profile measurements has been demonstrated.

Primary ridging and outward clad creep were also seen in earlier PIEs and are predicted by the ABAQUS pellet hourglassing calculations. Any out-of-roundness, bowing (as judged by the fact that the fuel pins could be removed from the tight fitting capsule), and bambooing are insignificant. Other Fuel Pin 7 and 16 measurements are recorded in Table 4.6.

Table 4.6 Fuel Pin 7 and 16 Length and Weight

Fuel Pin	Length (in) Less Pedestal ±0.005	Preirradiation Length (in) Less Pedestal	Mass (g)	Preirradiation Mass (g)
Fuel Pin 7	7.411	7.41	111.5	Not given
Fuel Pin 16	7.413	7.41	112.6	Not given

4.7.1 Fuel Pin Volume Measurement

The free volume of Fuel Pin 7 was measured by using the Fuel Pin Volume Measuring Apparatus, specially designed and fabricated for this test irradiation project and detailed in Reference 24. A schematic view of the apparatus is shown in Figure 4.27. This was the first use of this device, which makes use of a simple gas compression technique and a precision pressure gauge to provide a good (1%) precision measurement of the fuel pin free volume.

The free volume within a fuel pin is determined by placing the (drilled) opened pin in an apparatus with a changeable volume (piston and cylinder) and measuring the pressure of the system both before and after the known change in volume. A big advantage of this compact design is that there are no valves, gas fill lines, or vacuum lines and it can be easily calibrated with a set of known volumes.

The measured free volume is shown as an entry in Table 4.5 and was used when computing the gas pressure (this measured value is within 1% of the calculated estimate). The temperatures of the apparatus and fuel pin exterior were within a few degrees of each other so no correction was applied for temperature in this case. A compensation factor for greater temperature differences is explained in Reference 24. Because the upper end of Fuel Pin 16 was deformed when the pressure measurement was taken (see Section 4.5), a tight seal could not be established and hence the pin free volume could not be measured. Table 4.5 shows the calculated estimate for Fuel Pin 16.

4.7.2 Fuel Density Measurement

The same apparatus described in the previous Section was used to measure the volume (for use in a fuel density calculation) of a fuel pin segment consisting of both clad and fuel (FP-7-C-5 as shown in Figure 6.2). A small chamber that fits into the apparatus in the same manner as a fuel pin was used to hold the sample for measurement (see Figure 4.27). Several stainless steel

cylinders of diameters somewhat larger and smaller than the expected volume of the sample were used to calibrate the apparatus for this volume measurement.

The sample was weighed on a milligram scale to determine its mass. A segment of un-irradiated clad was also weighed and measured to determine the volume and mass of the cladding. The volume and mass of the fuel was determined by subtracting the clad mass and volume. Additional detail concerning this method is provided in Reference 24. Table 4.7 details the measurement results. The fuel density as obtained in this PIE agrees well with the code predictions (see Volume II of this report).

Table 4.7 Fuel Pin 7 Density Measurement

Item	Measurement
Mass of FP-7-C-5	9.628 g
Volume of FP-7-C-5	1.036 cm^3
Mass of clad	1.742 g
Volume of clad	0.2647 cm^3
Mass of fuel	7.886 g
Volume of fuel	0.7717 cm^3
Pellet Density	10.22 g/cm^3
Estimated Uncertainty	± 0.5%

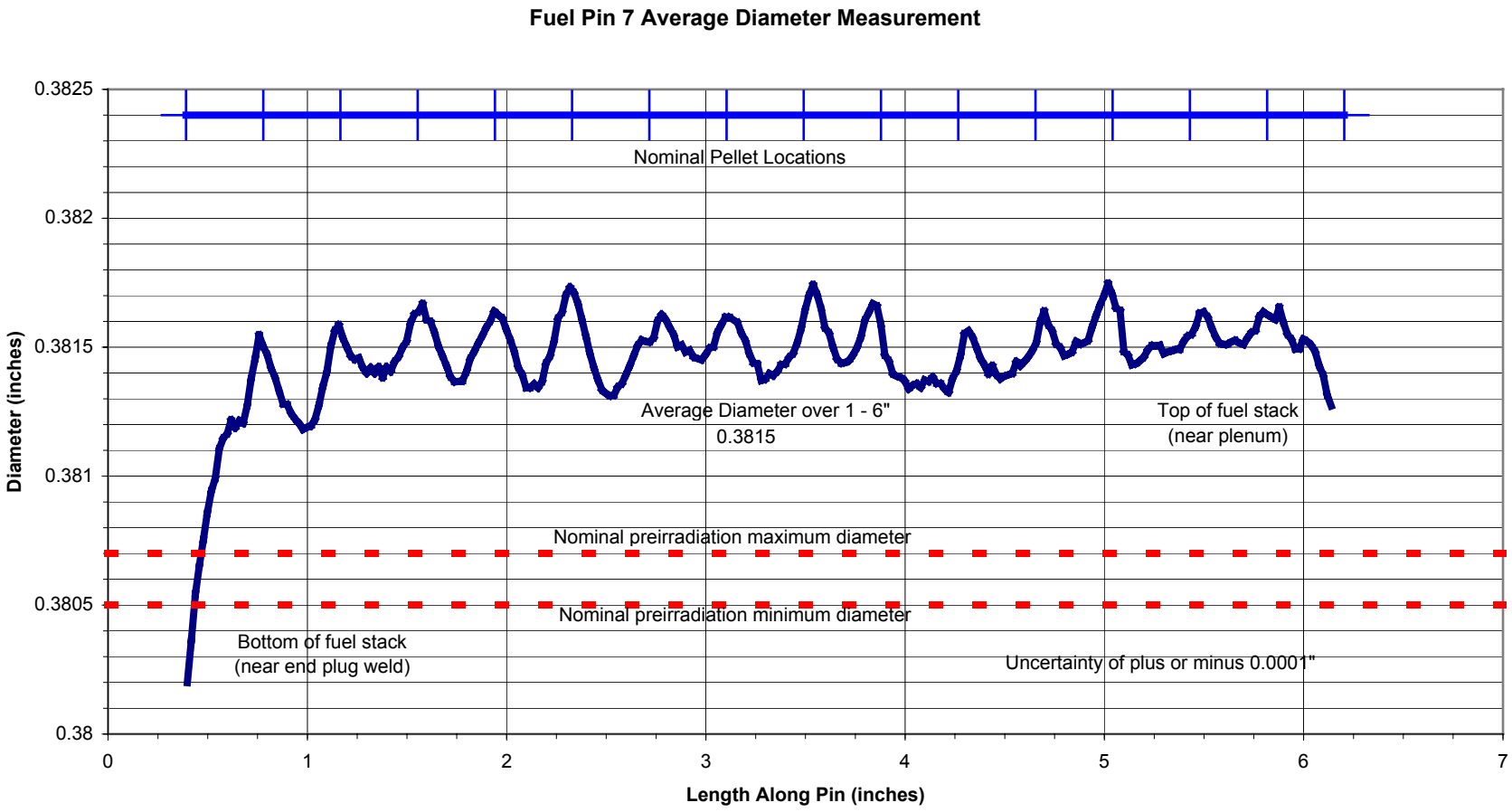

Figure 4.25 Graph of Fuel Pin 7 diametrical measurements.

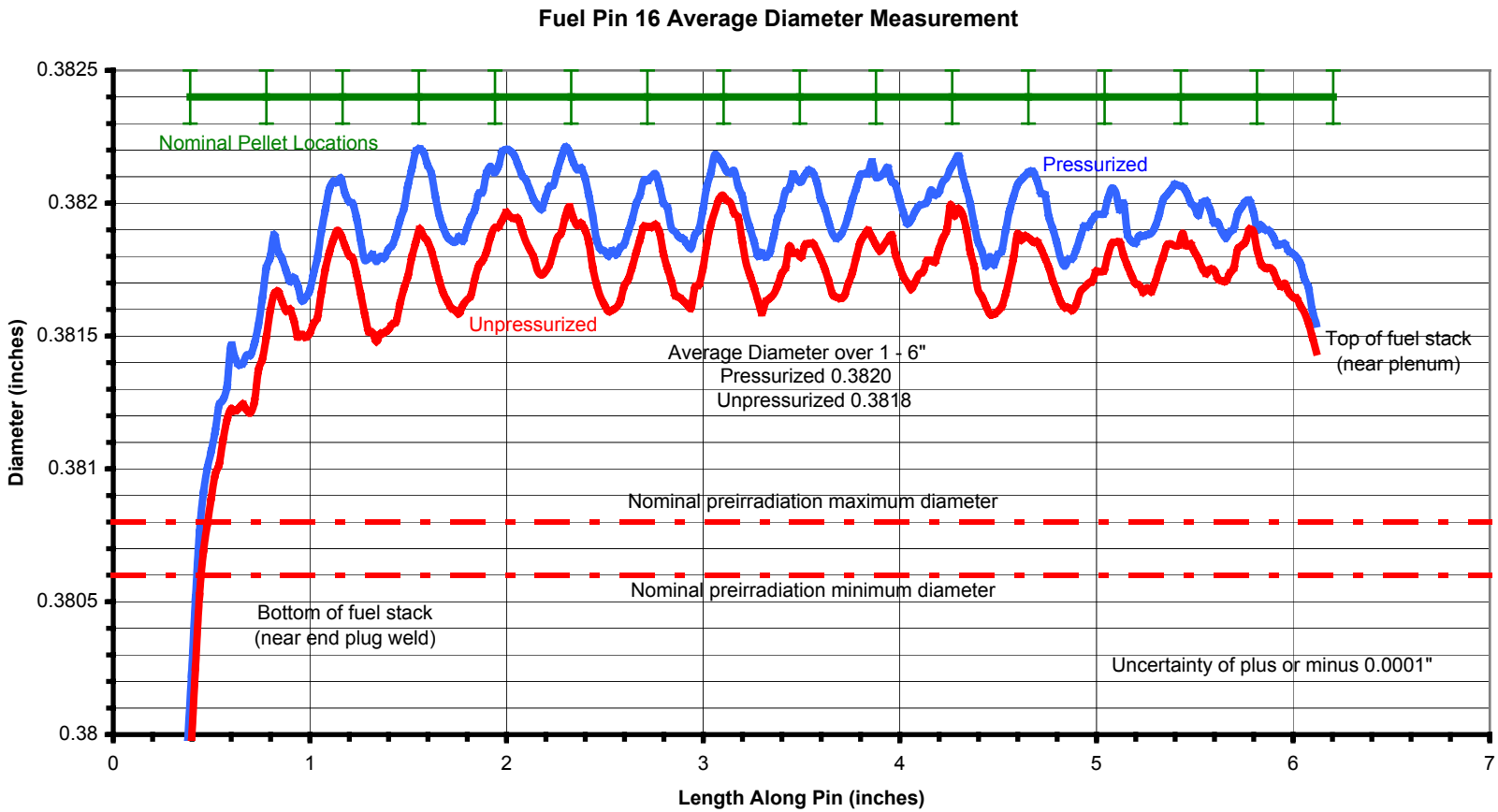

Figure 4.26 Graph of Fuel Pin 16 diametrical measurements. Both pressurized and unpressurized measurements are shown. (The unpressurized measurement had three small handling scratches at approximately 1.8, 2, and 3", which were removed from the graph for clarity)

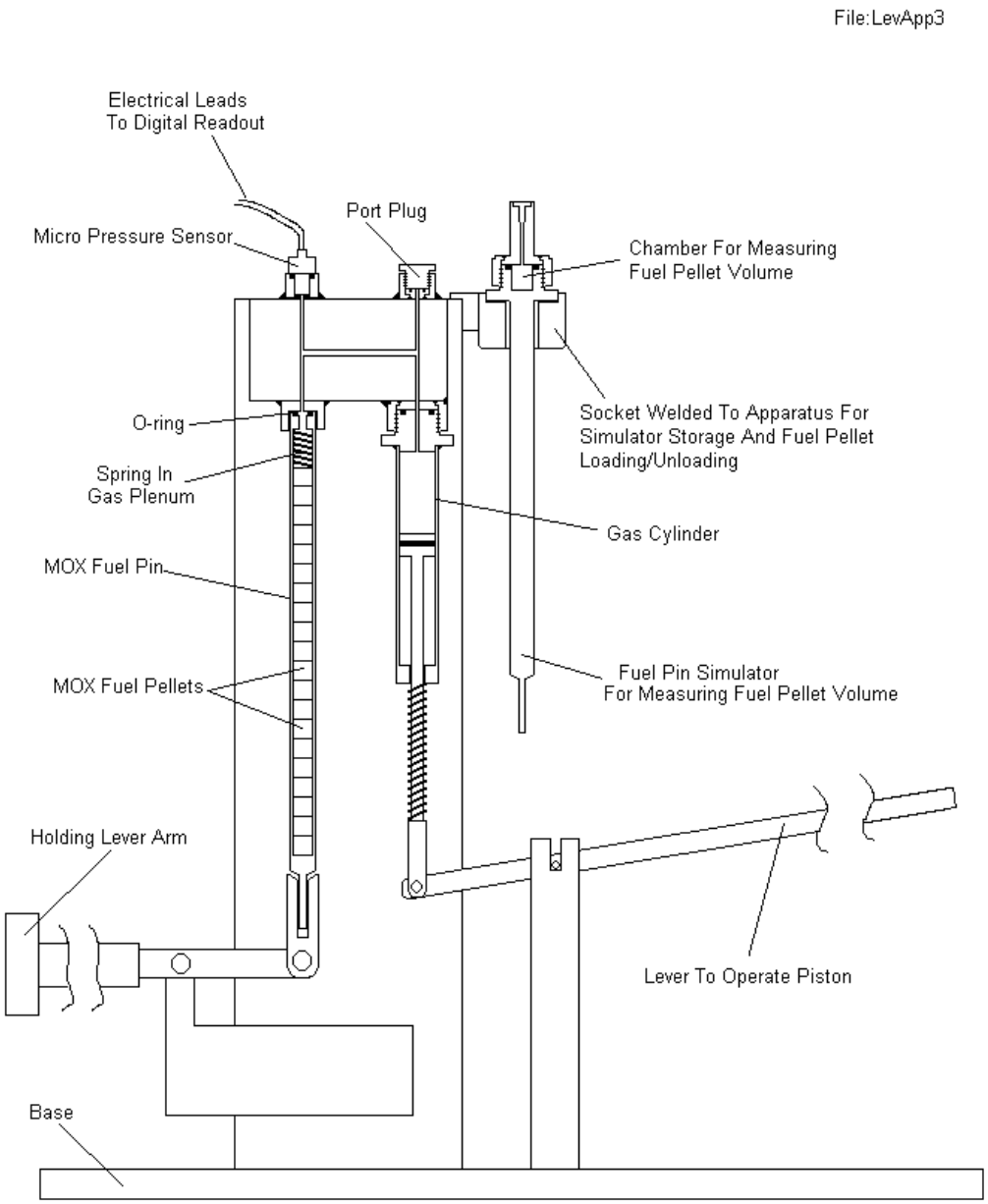

Figure 4.27 Schematic of the Fuel Pin Volume Measuring Apparatus.

5. METALLOGRAPHY

5.1 Introduction

This Chapter details the examination of the microstructure of the Type A fuel (non-TIGR plutonium oxide feed) contained in Capsule 4 (Fuel Pin 7) and the Type B fuel (TIGR plutonium oxide feed) contained in Capsule 13 (Fuel Pin 16) of the MOX test irradiation. Specimens were cut from locations within the pellet stack near the top and bottom of both fuel pins along with additional middle cross section and axial cuts from Pin 7. No significant differences were noted between the two fuel types except that the TIGR treated fuel is more friable. All pellets became more friable with increasing irradiation time; polishing was more difficult and one mount was abandoned because of excessive pullout. As was noted with the previous PIEs, several large plutonium-rich agglomerates are present in the fuel, with equivalent diameters as large as 500-600 microns. Despite this evidence of less than optimal powder mixing during fabrication, no irradiation difficulties have been noted for this fuel.

5.2 Sample Preparation

Nine specimens were cut from the two fuel pins at various locations. Both pins had specimens prepared from near the top of the pin (pellets 1 and 2) and near the bottom of the pin (pellet 15). The fifteen MOX pellets are numbered sequentially downward from the fuel pin gas plenum (Figure 2.5) (See Figures 6.1 through 6.4 for details of the cutting locations). In addition, cross sectional mounts were prepared from the central region of Fuel Pin 7 as well as one axial cut (pellets 11 to 13) for examination of the pellet edges and nearby clad effects. No axial cuts were prepared for Fuel Pin 16 because of a desire to preserve clad material for later ductility testing.

Each specimen was mounted in a metallographic mount by epoxy potting. Subsequently, each mount was rough ground and then polished with progressively finer diamond compounds. Additional potting epoxy was added between grinding and polishing steps to minimize the amount of pullout; these mounts were more friable than the mounts prepared during previous PIEs.

Each mount was assigned a unique number. Table 5.1 shows the relationship between the specimen numbers and the mount identity number and describes the location within the pellet stack where the fuel sample was taken. The mounts were photographed in sections and a composite image assembled. Higher magnification was used to examine specific details. Of particular interest was the pellet-clad interface as one of the goals of this test is to see if unusual interactions are taking place.

5.3 Results of the Polishing

The results of the polishing are shown in Figures 5.1 through 5.36 for seven of the nine mounts. Mount 6217 suffered extensive pullout and was considered unusable, but the other mounts were of good to excellent quality. Four of the eight mounts were selected for expanded illustration to

show the pellet-clad interface details.

Table 5.1 Mount ID Numbers and Fuel Pellet Locations

Specimen Number	Mount ID	Fuel Pin Location
FP-7-M-1	6217	Fuel Pin 7 Pellet 1 lower end
FP-7-SEM-1	6218	Fuel Pin 7 Pellet 2 upper end (SEM)
FP-7-M-2	6219	Fuel Pin 7 Pellet 10 upper end
FP-7-M-3	6220	Fuel Pin 7 Pellet 10 upper surface of lower half
FP-7-M-4	6221	Fuel Pin 7 Pellets 11-13 axial section
FP-7-M-5	6222	Fuel Pin 7 Pellet 15 upper end (etched)
FP-16-M-1	6223	Fuel Pin 16 Pellet 1 upper end
FP-16-SEM-1	6240	Fuel Pin 16 Pellet 2 (SEM)
FP-16-M-2	6225	Fuel Pin 16 Pellet 15 upper end (etched)

Three mounts were selected from Fuel Pin 7 and one from Fuel Pin 16 for detailed illustration. For Fuel Pin 7, the cross sectional Mounts 6218 (least) and 6220 (most) show the varying amounts of oxidation on the clad inner surface. Views around the circumference of the clad are provided as Figures 5.1 through 5.7 and 5.9 through 5.15, respectively.

The axial Mount 6221 appears to support the contention that significant clad oxide formation requires that the pellet be in close physical contact with the clad. See Figures 5.16 to 5.27.

For Fuel Pin 16, Mount 6223 showed the greatest oxide effect. See Figures 5.29 to 5.35. In general, the oxide layer thickness was on the order of a few microns and very uneven, indicating very minor corrosion, typical of what one would expect. The exception was oxide layers adjacent to agglomerates located very close to the pellet surface, which are 2 to 3 times as thick (roughly 10-20 microns and also uneven). No differences in oxide layer behavior were observed due to TIGR or untreated fuel types.

No abnormal fuel behavior was seen; the cracking is normal for LWR fuel. The cracking is somewhat greater than was seen at 30 GWd/MT and may have been exasperated by the increased number of thermal cycles. Note the cylinder-like islands in the central regions of the mounts isolated by circumferential cracks.

Plutonium-rich agglomerates are evident, particularly in the outer regions of the fuel. These are the “blemish-like” light gray patches. The locally high burnup due to the high local plutonium concentration results in a high concentration of gas bubbles that gives the agglomerate its distinctive shape when fuel temperatures are low enough to permit development of the high-burnup structure. Unlike previous PIEs, in which agglomerates were clearly visible only in the outer ¾ of the cross section, the agglomerates can be seen throughout the pellet cross section. This implies that during this last irradiation phase, the central temperature was low enough for the classical agglomerate structure to form. The maximum size of the agglomerates, about 500-600 microns, is comparable to that seen in the earlier PIEs.

Figure 5.16 shows an axial cross section comprising portions of three pellets from Fuel Pin 7. This section clearly shows that the fuel is behaving in a stable manner. Note that the pellet dishing and chamfer can be clearly seen, a small gap is present between the pellet and the clad, and no effects of significant mechanical interaction are indicated. A close-up of the pellet-pellet interface is shown in Figure 5.17, showing details of the chamfer and dishing.

No significant appearance of the "rim effect" was noted in the examination of these mounts. This is not unexpected as the burnup in the matrix is too low at this point in the irradiation for the structure to develop. A "halo" region around each large agglomerate is clearly observable and is believed to be due to fission products (gases) diffusing out of the agglomerate into the nearby matrix (discussed in the SEM section). The polishing properties of the three regions, agglomerate, halo, and matrix are different enough that the structures show up clearly.

Even with sporadic bonding to the clad (also seen in the 21 GWd/MT PIE), the agglomerates do not appear to be causing any difficulties with either the fuel or clad; no detrimental interactions have been noted. The detailed relationship between preirradiation agglomerate size and postirradiation agglomerate size is not known, so the extent to which the agglomerates have expanded with the internal accumulation of fission products is not precisely known.

One new feature seen in this irradiation is the apparent selective oxidation of the fuel clad. Referring to Figure 5.18 and the following figures for the axial section, one can see that oxide formation is generally greater on one side of the clad (left in the figures) than the other, even in the presence of agglomerates. Figures 5.20 and 5.21 show that the fuel adhered to the side (left) where the corrosion is greatest, implying that the pellets were in closer contact with that side. The right side lacks strong evidence of fuel adhesion.

Figure 5.22 shows a thicker oxide layer near an agglomerate on the left side, while in Figures 5.24 and 5.27, none of the agglomerates on the right side show the same degree of nearby oxide build up. The only exception is a small region in the center of Figure 5.20, where there is some minor corrosion in between a couple of surface agglomerates. Examination of the other mount figures also indicates that the oxide layer is not uniform and is often greatest where fuel has adhered to the clad. This implies that close contact between the fuel and clad is a precursor for oxide formation. Reference 28 shows similar experimental observations and describes an athermal diffusion mechanism (fission recoil driven) for this behavior.

The fuel cross sections show no indications of unstable or abnormal behavior; the irradiation behavior to date has been typical of that expected from MOX fuel.

ORNL 2003-115 EFG

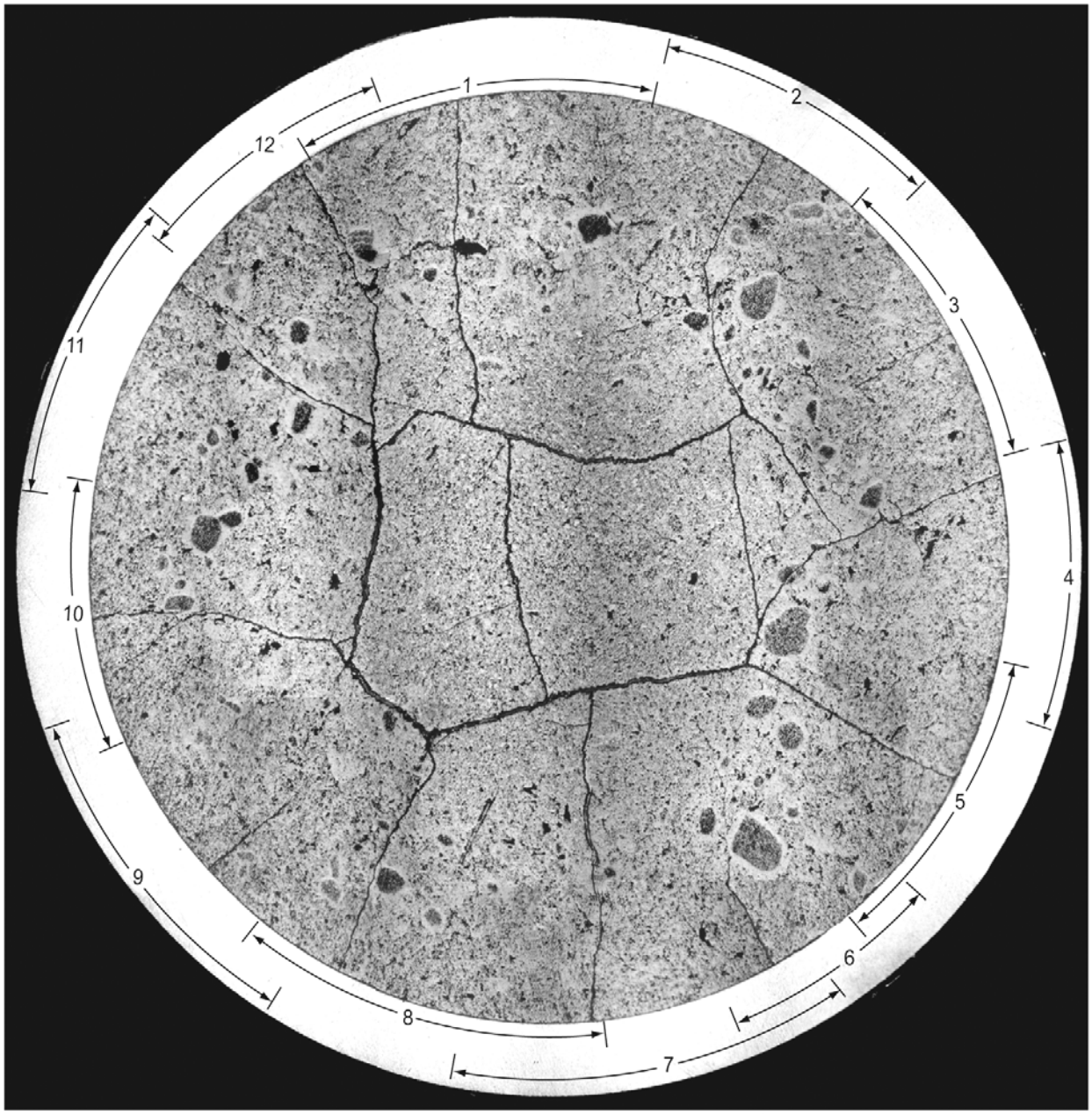

Fuel Pin 7 – Pellet 2 – Upper End – Mount 6218

500μm

as polished

Figure 5.1 Mount 6218 from Pellet 2, Fuel Pin 7. Note the rectangular island in the center, the large agglomerates, and the "halos" around the agglomerates. The sector numbers locate the pellet-clad interfaces in the next figures.

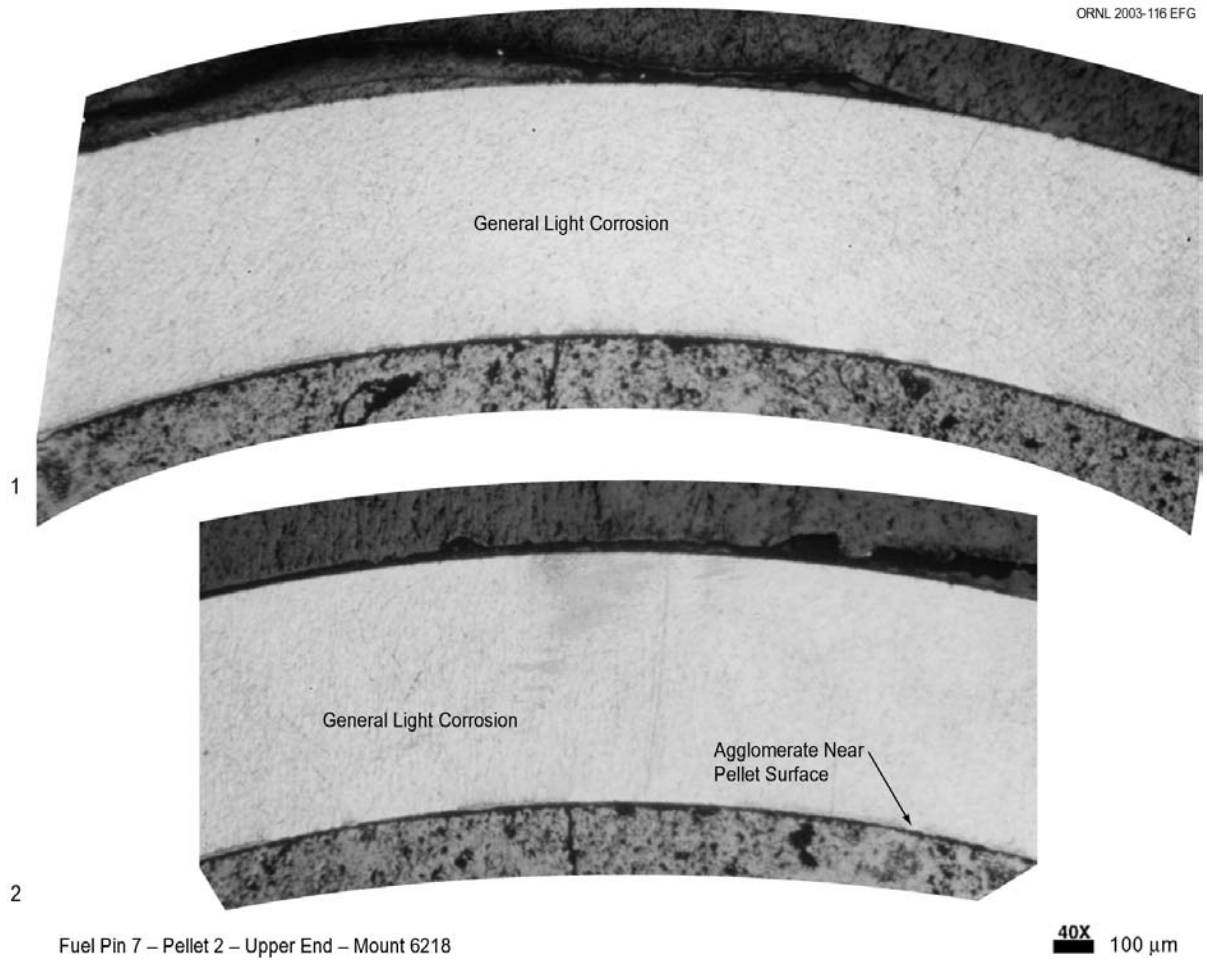

Figure 5.2 Clad sectors 1 and 2 of Mount 6218.

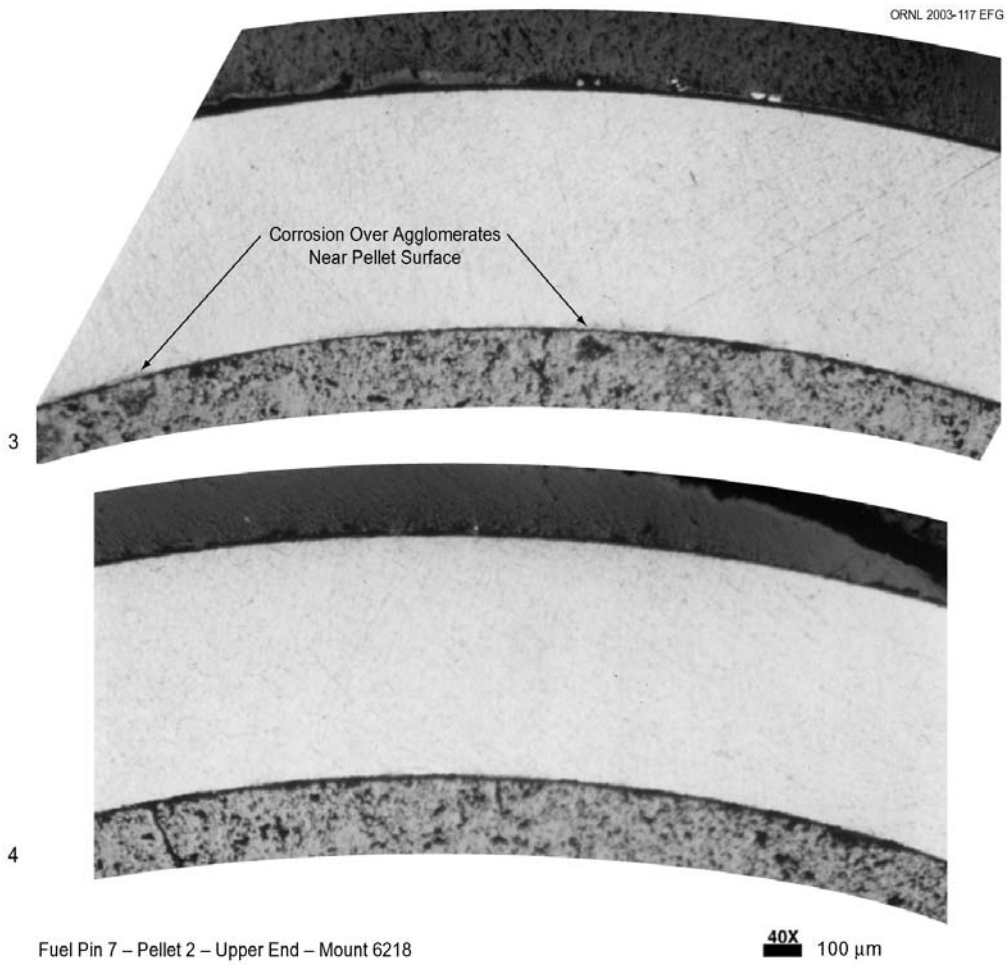

Figure 5.3 Sectors 3 and 4 of Mount 6218.

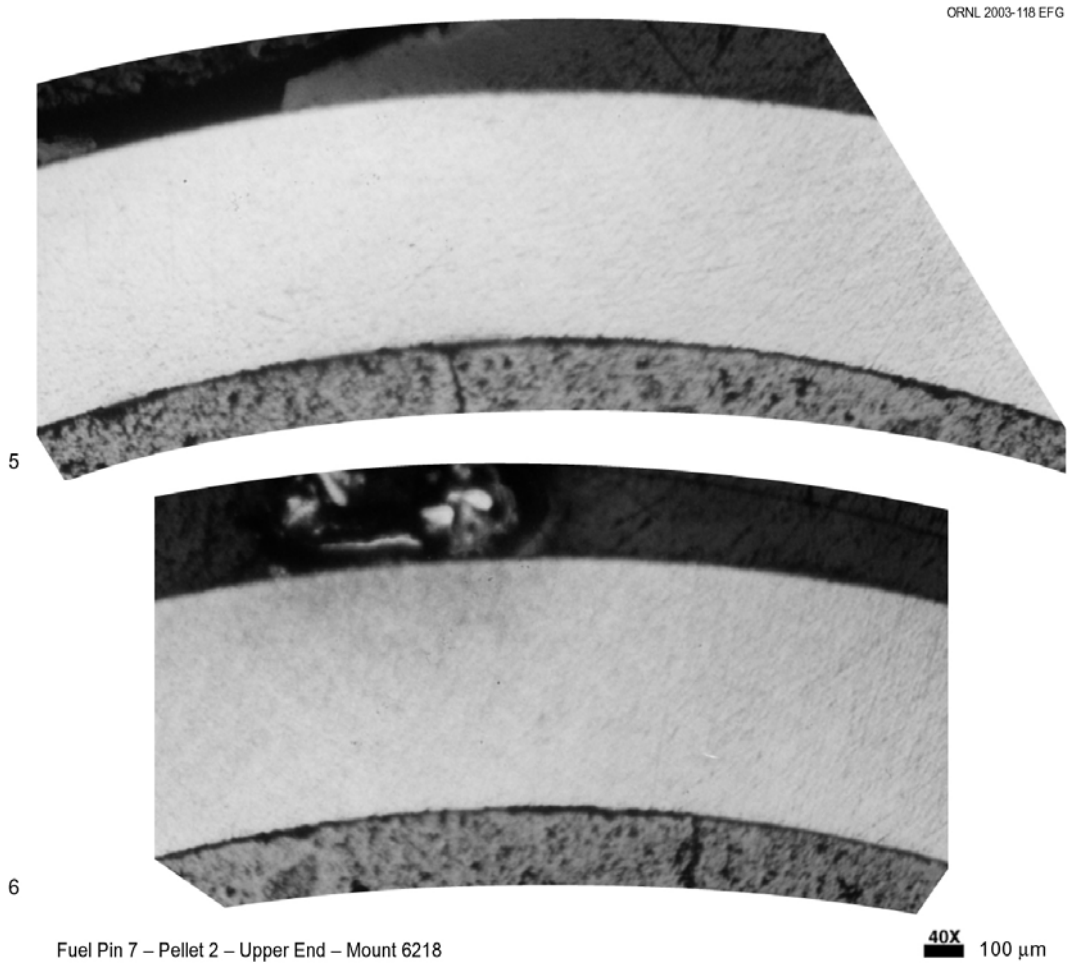

Figure 5.4 Sectors 5 and 6 of Mount 6218.

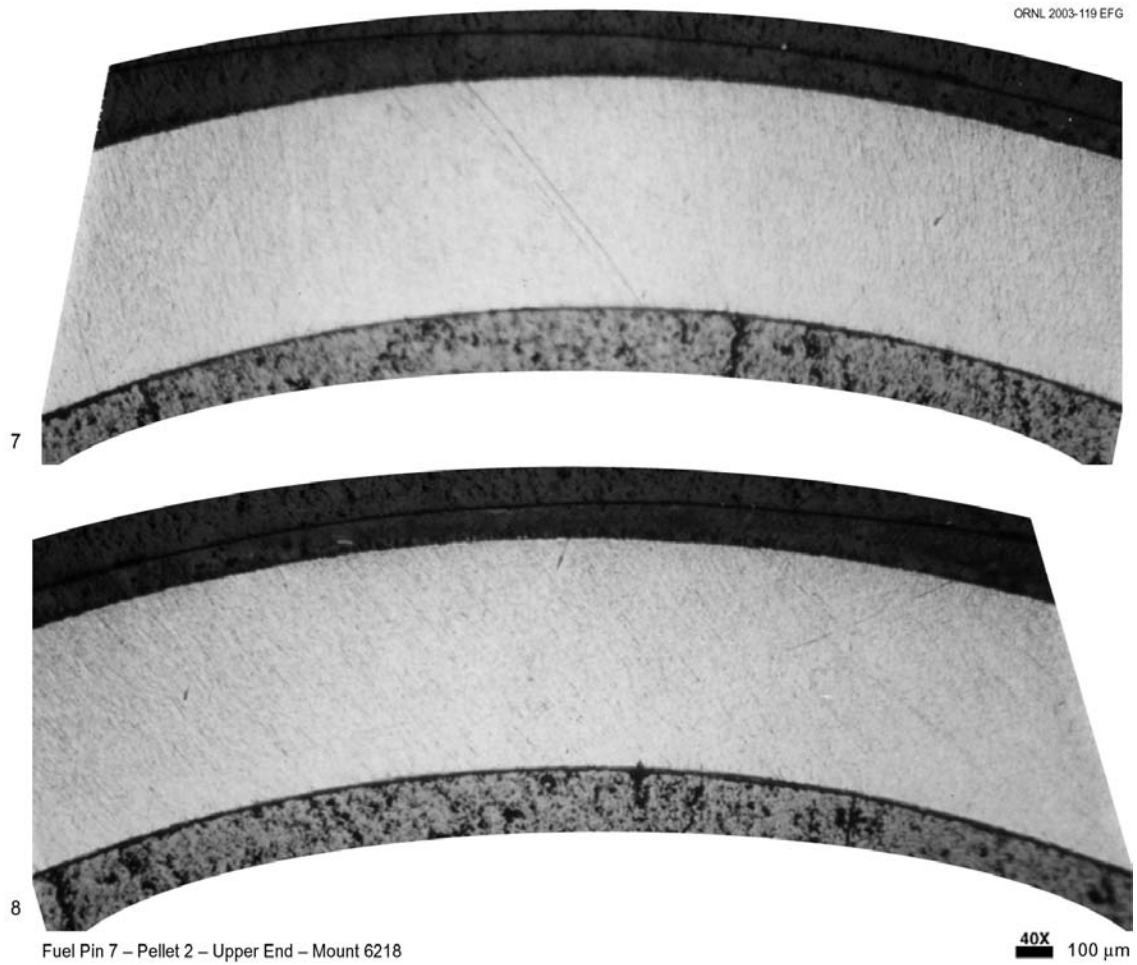

Figure 5.5 Sectors 7 and 8 of Mount 6218.

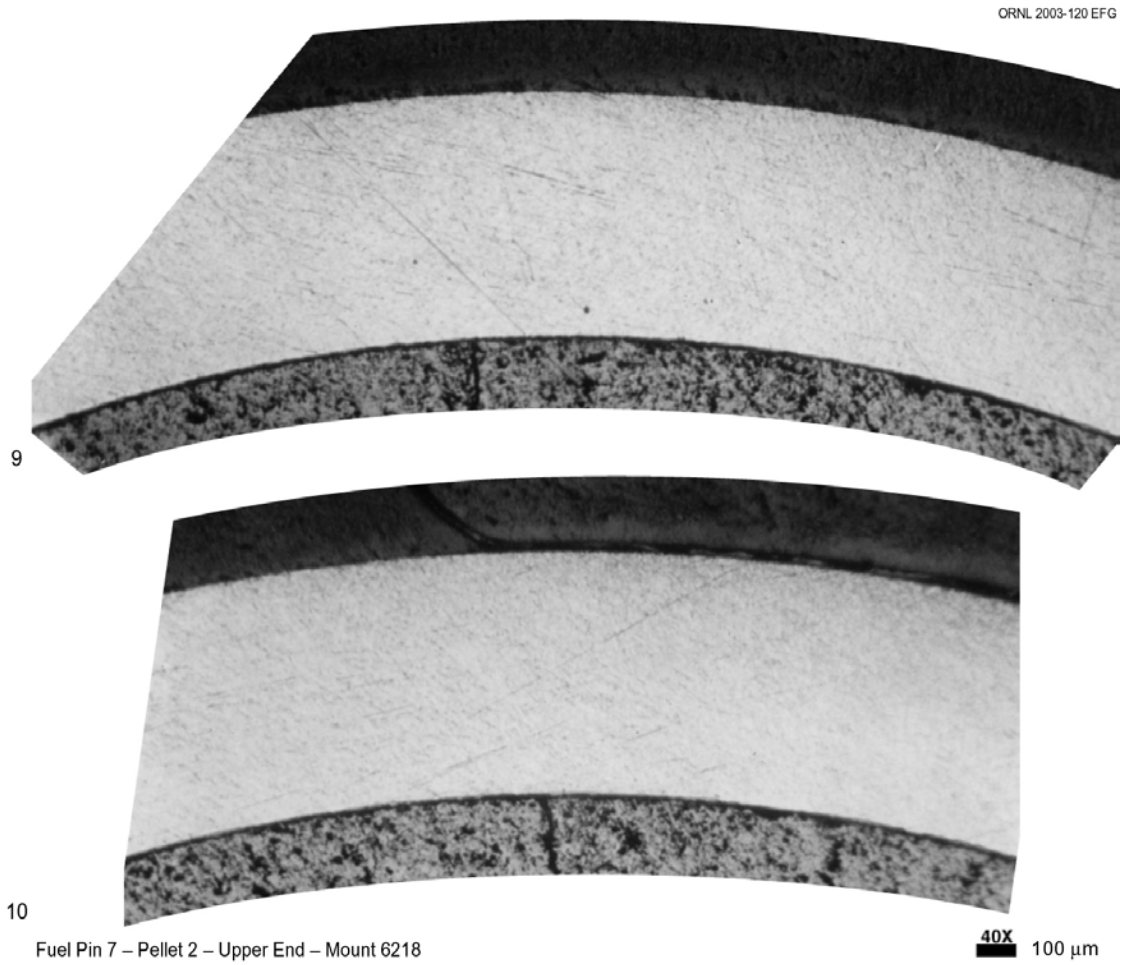

Figure 5.6 Sectors 9 and 10 of Mount 6218.

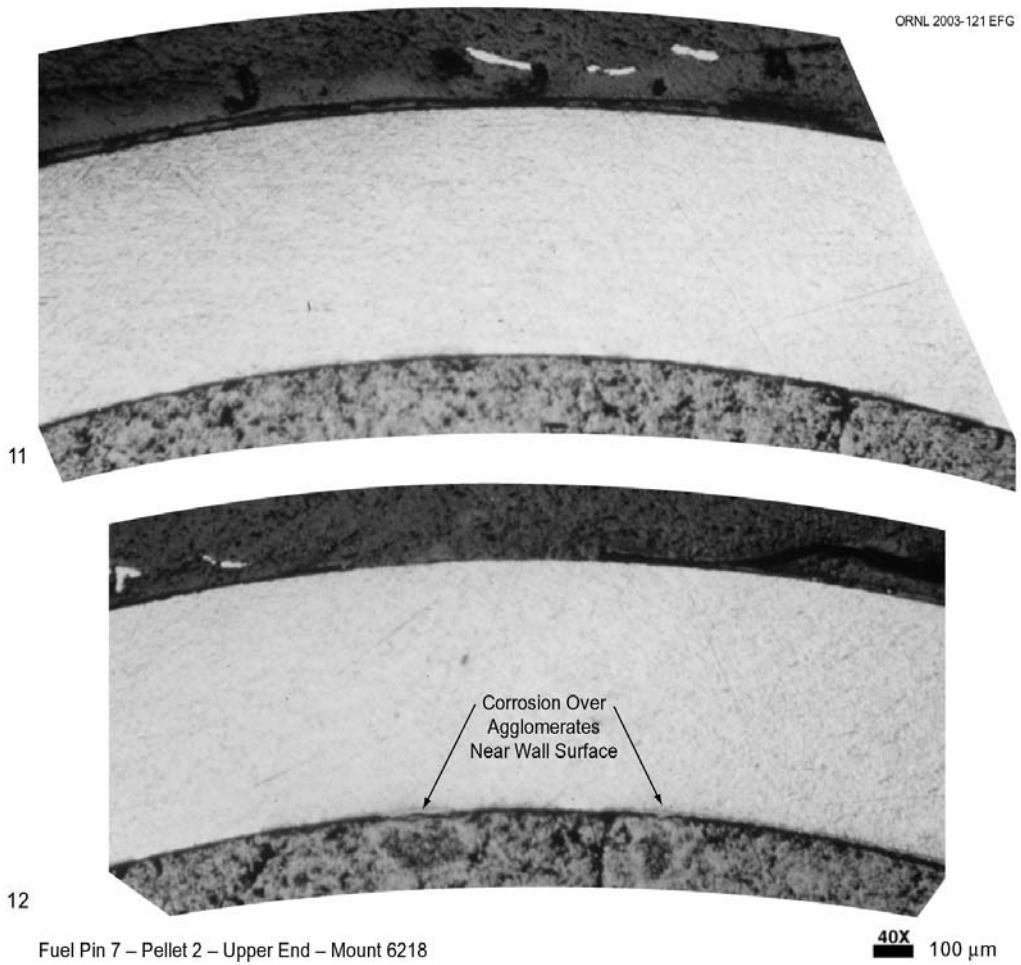

Figure 5.7 Sectors 11 and 12 of Mount 6218.

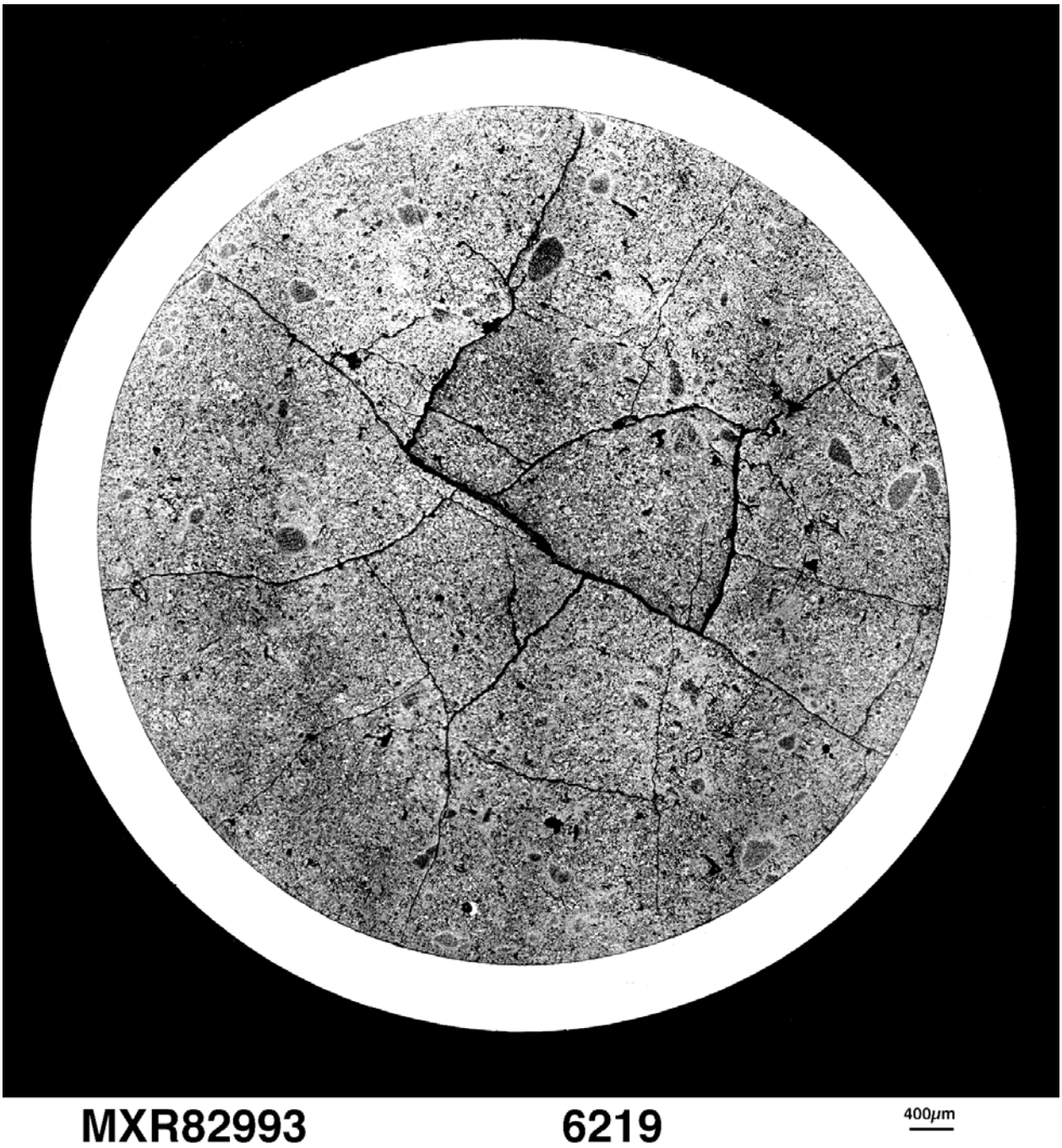

Figure 5.8 Metallographic cross section prepared from Fuel Pin 7 specimen, FP-7-M-2. Note the triangle like "core" piece isolated by cracks near the center. Agglomerates are as before.

ORNL 2003-15 EFG

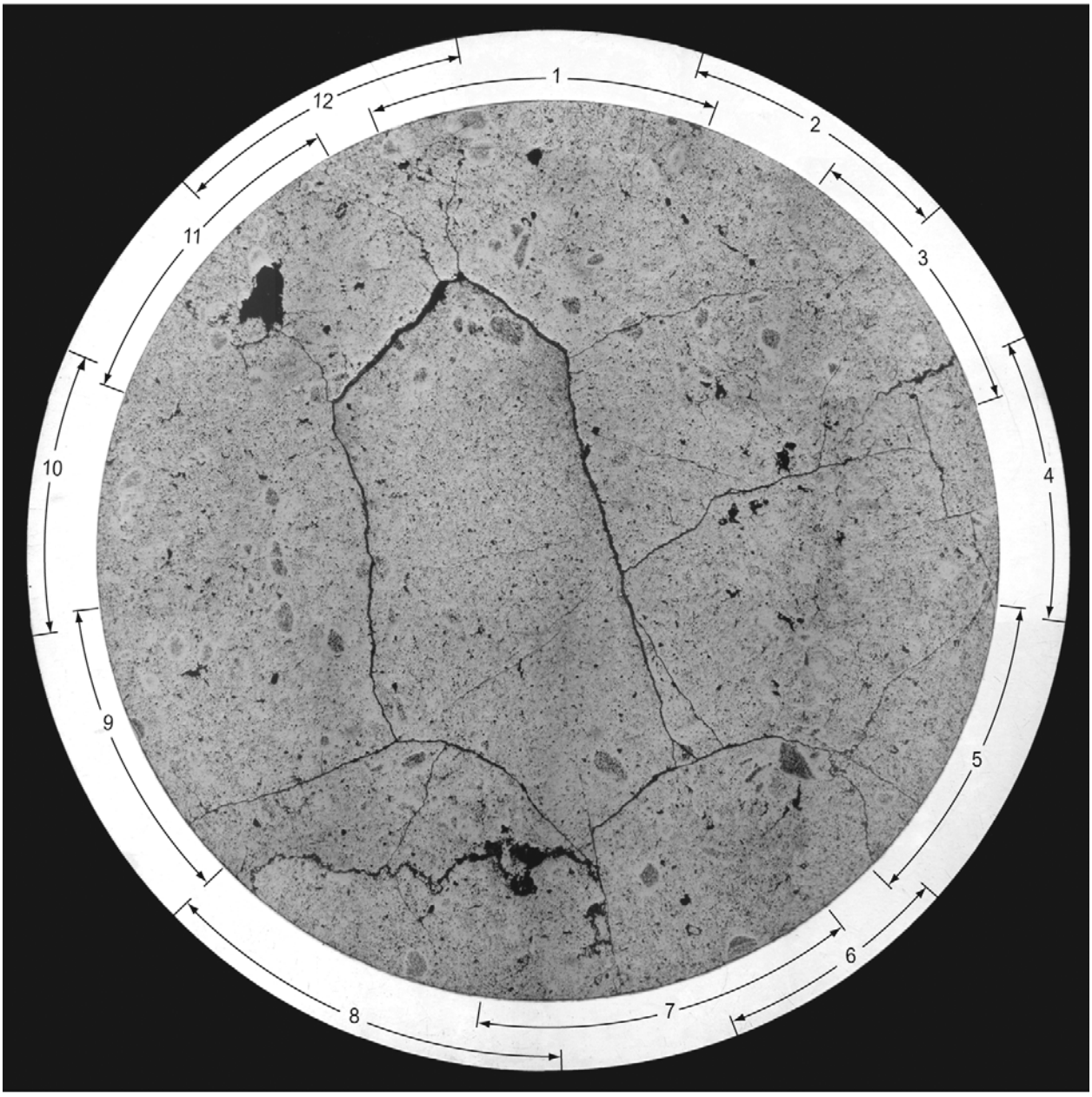

Fuel Pin 7 – Pellet 10 – Middle (upper face of lower half – pellet) – Mount 6220

400μm

Figure 5.9 Metallographic cross section prepared from Fuel Pin 7 specimen, FP-7-M-3. Note the rectangle like piece isolated by cracks near the center. The black spots are pullout.

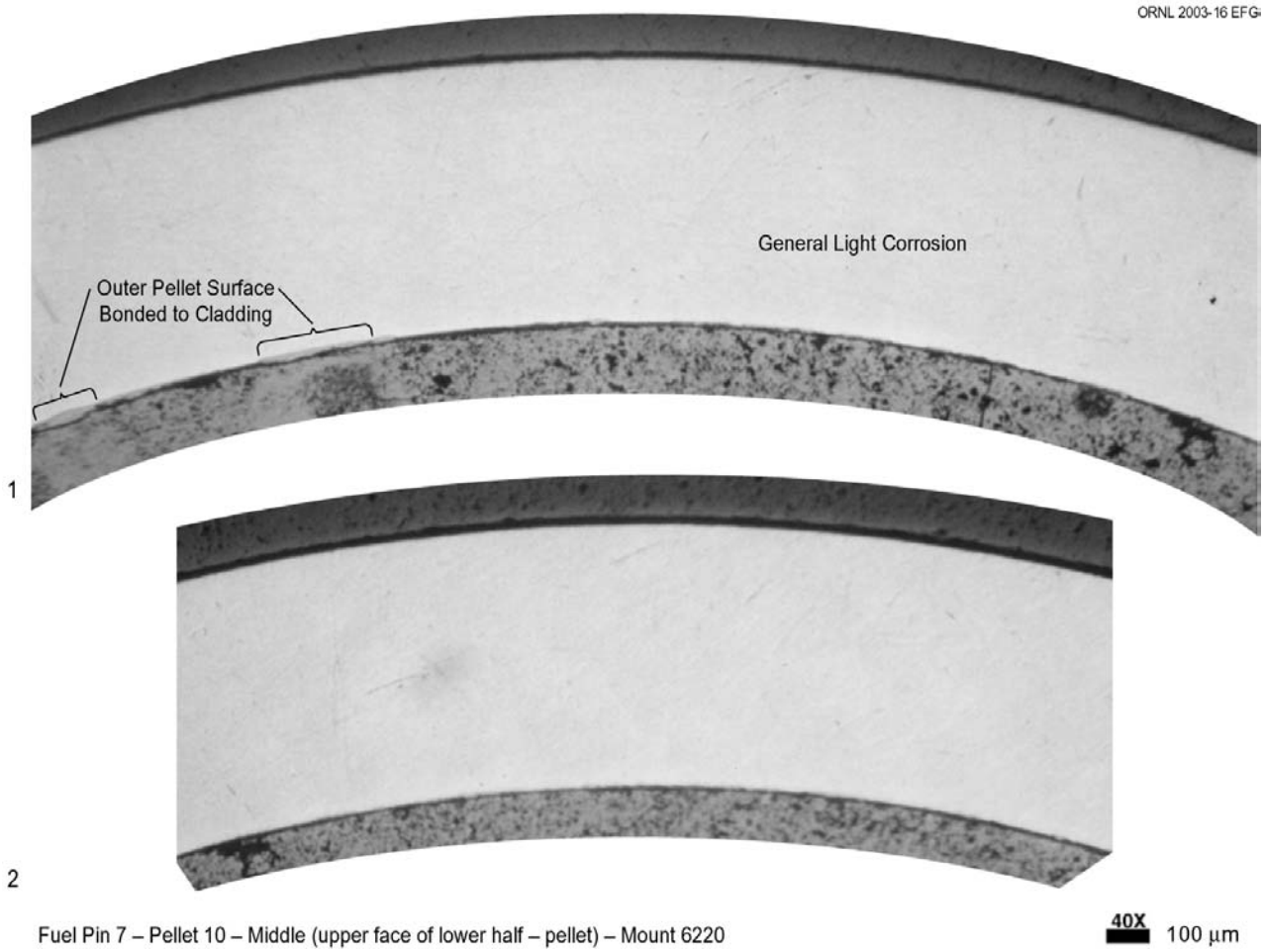

Figure 5.10 Sectors 1 and 2 of Mount 6220.

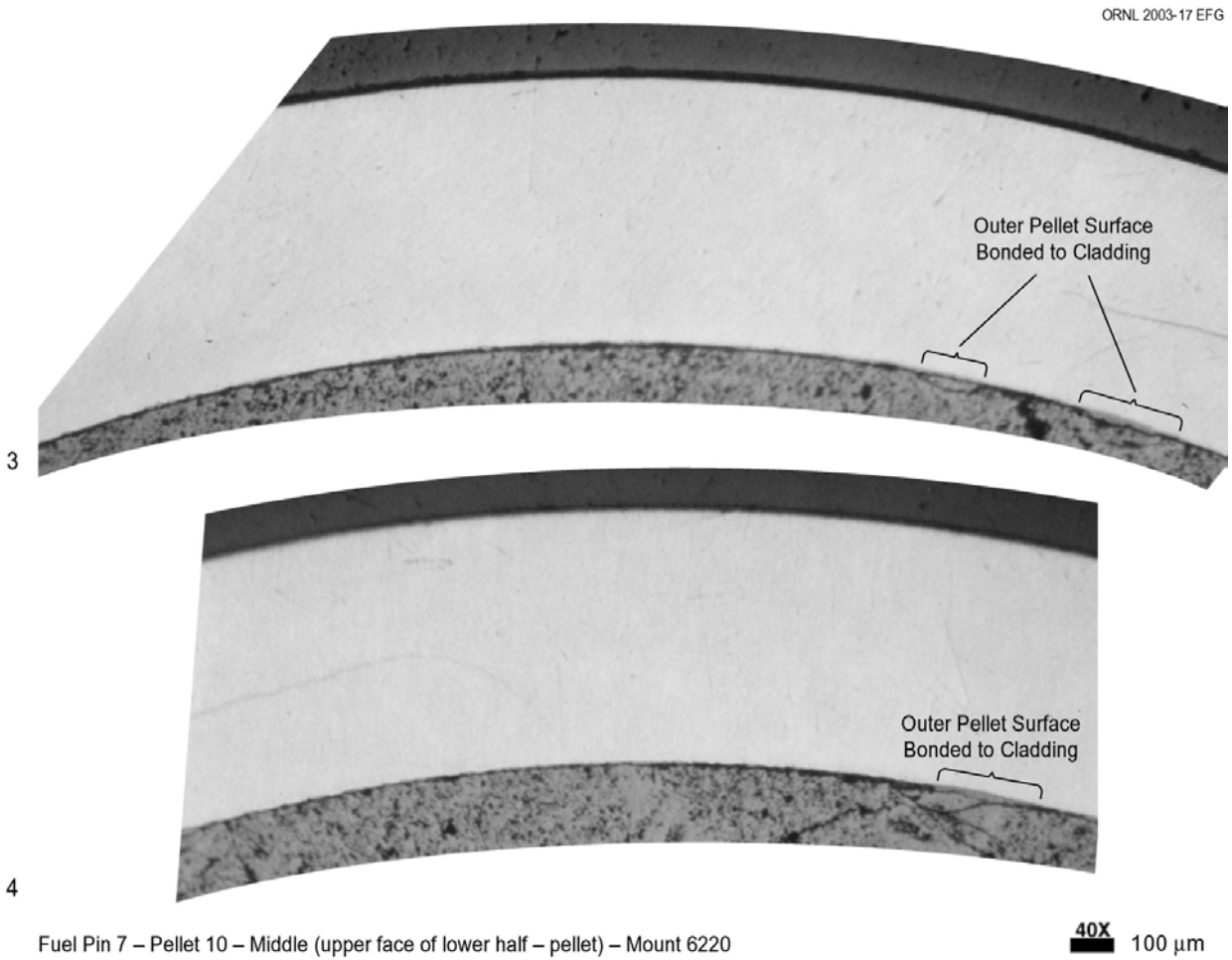

Figure 5.11 Sectors 3 and 4 from Mount 6220.

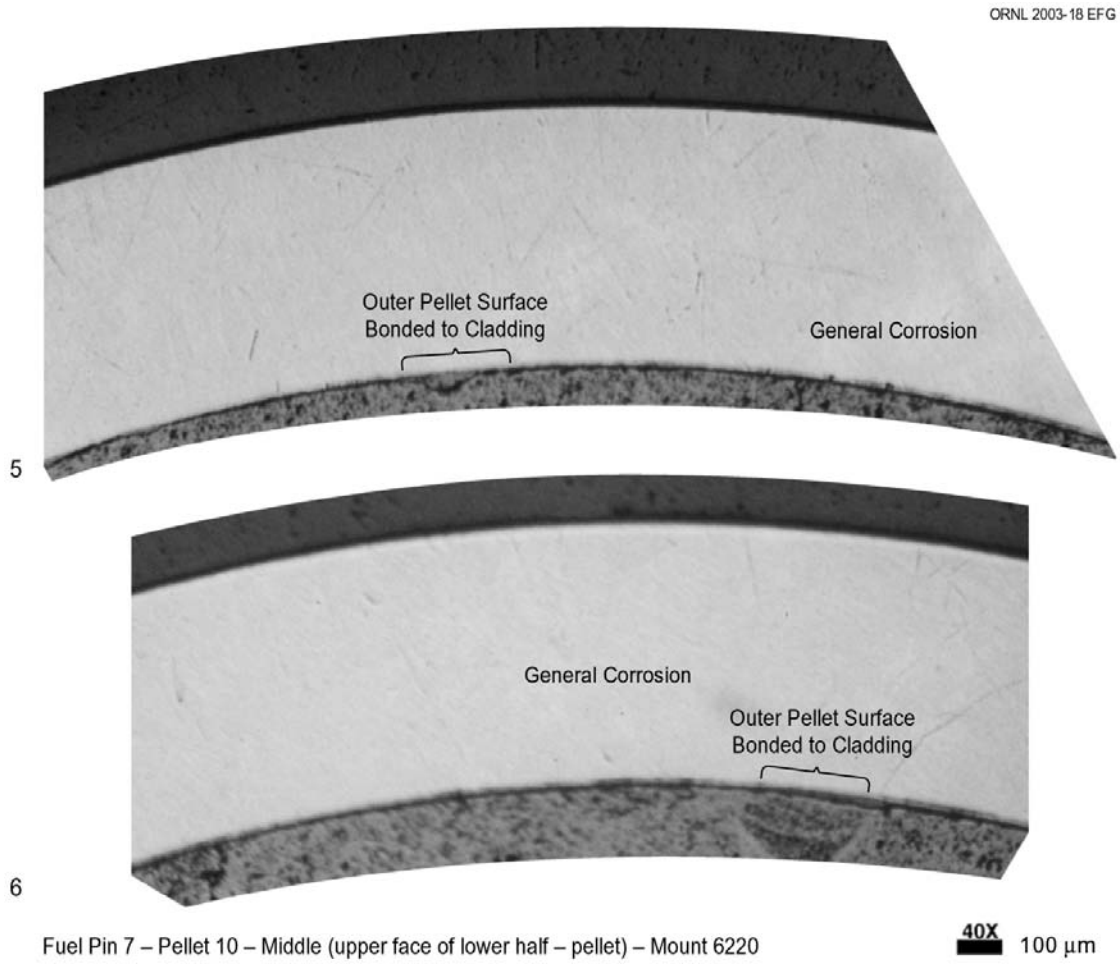

Figure 5.12 Sectors 5 and 6 from Mount 6220.

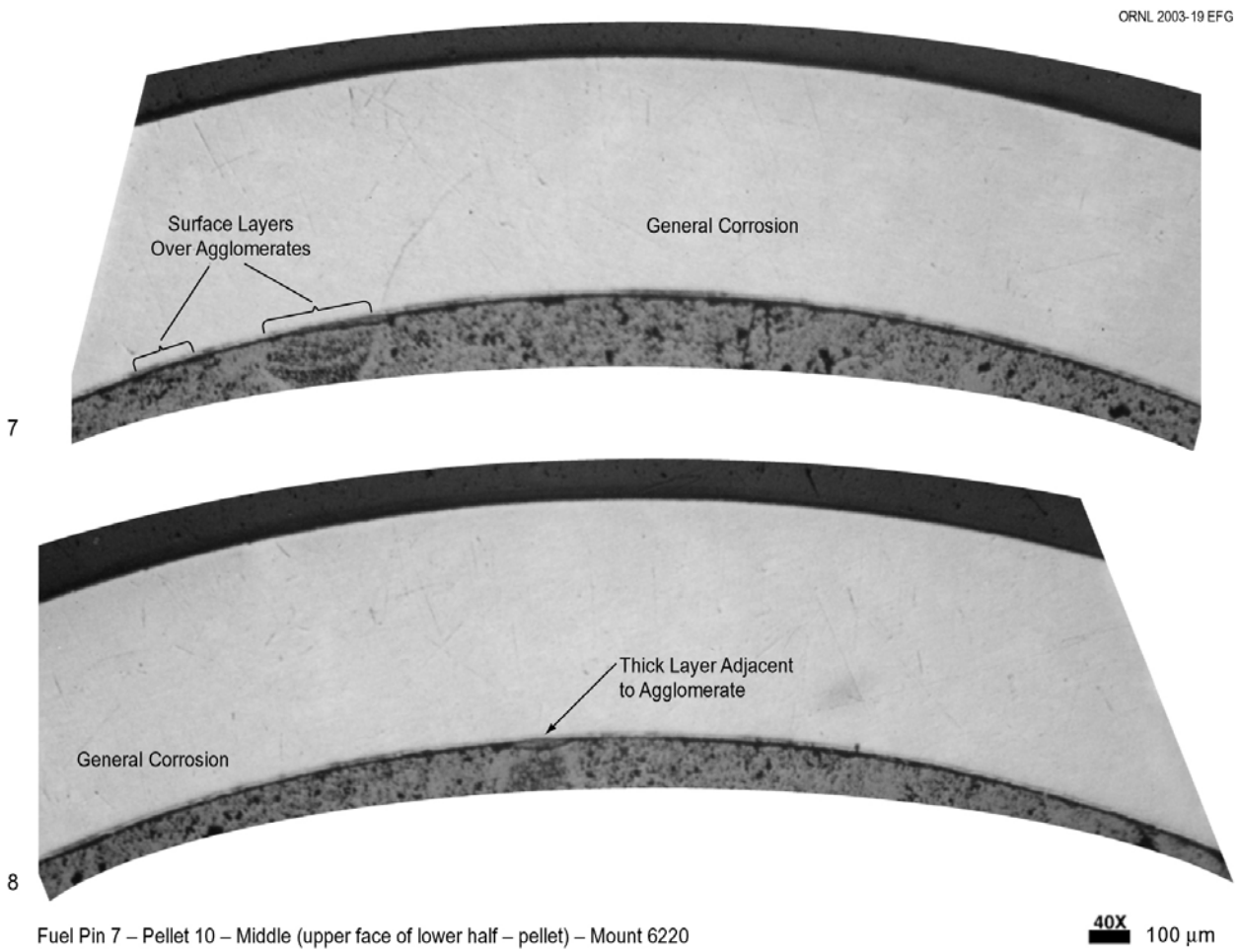

Figure 5.13 Sectors 7 and 8 from Mount 6220.

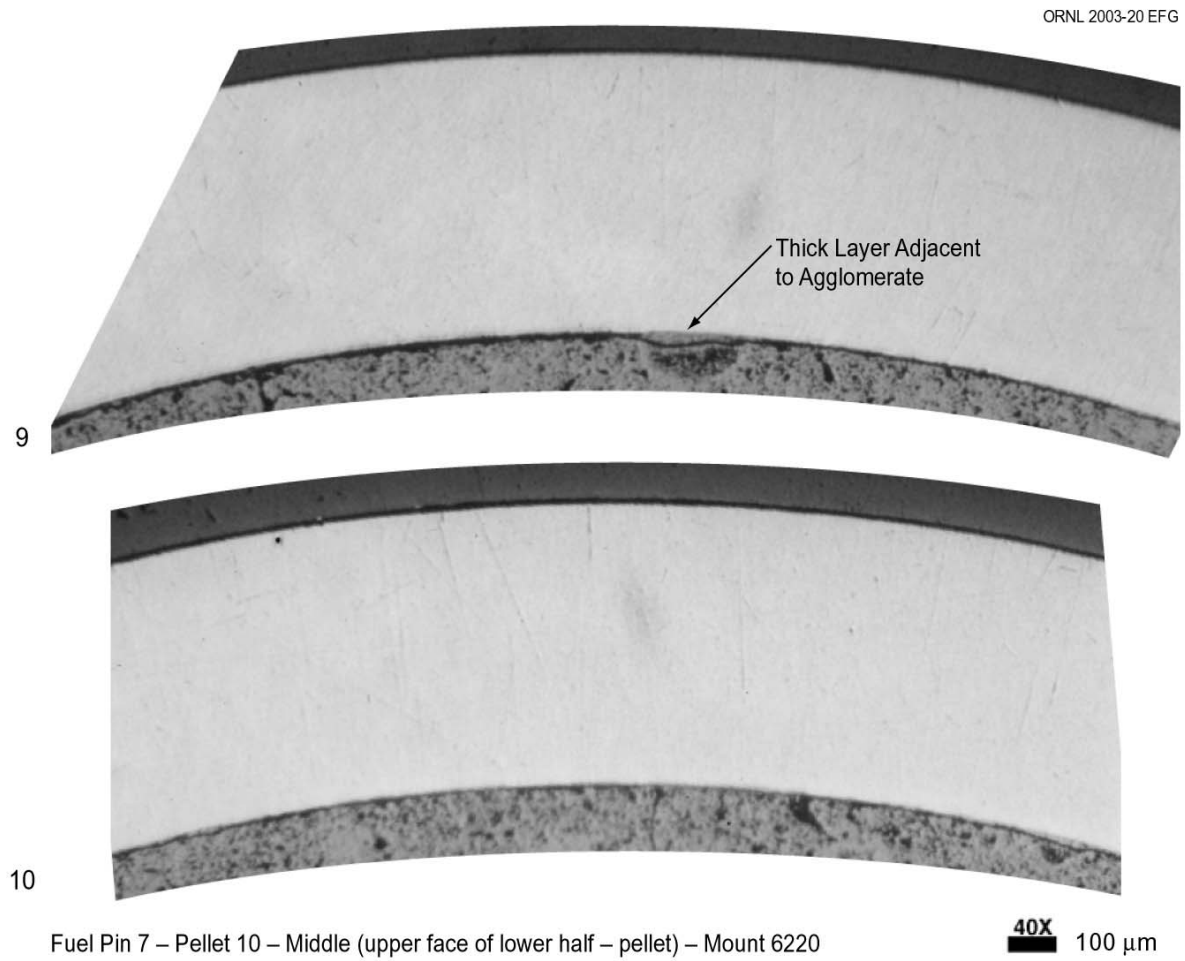

Figure 5.14 Sectors 9 and 10 from Mount 6220.

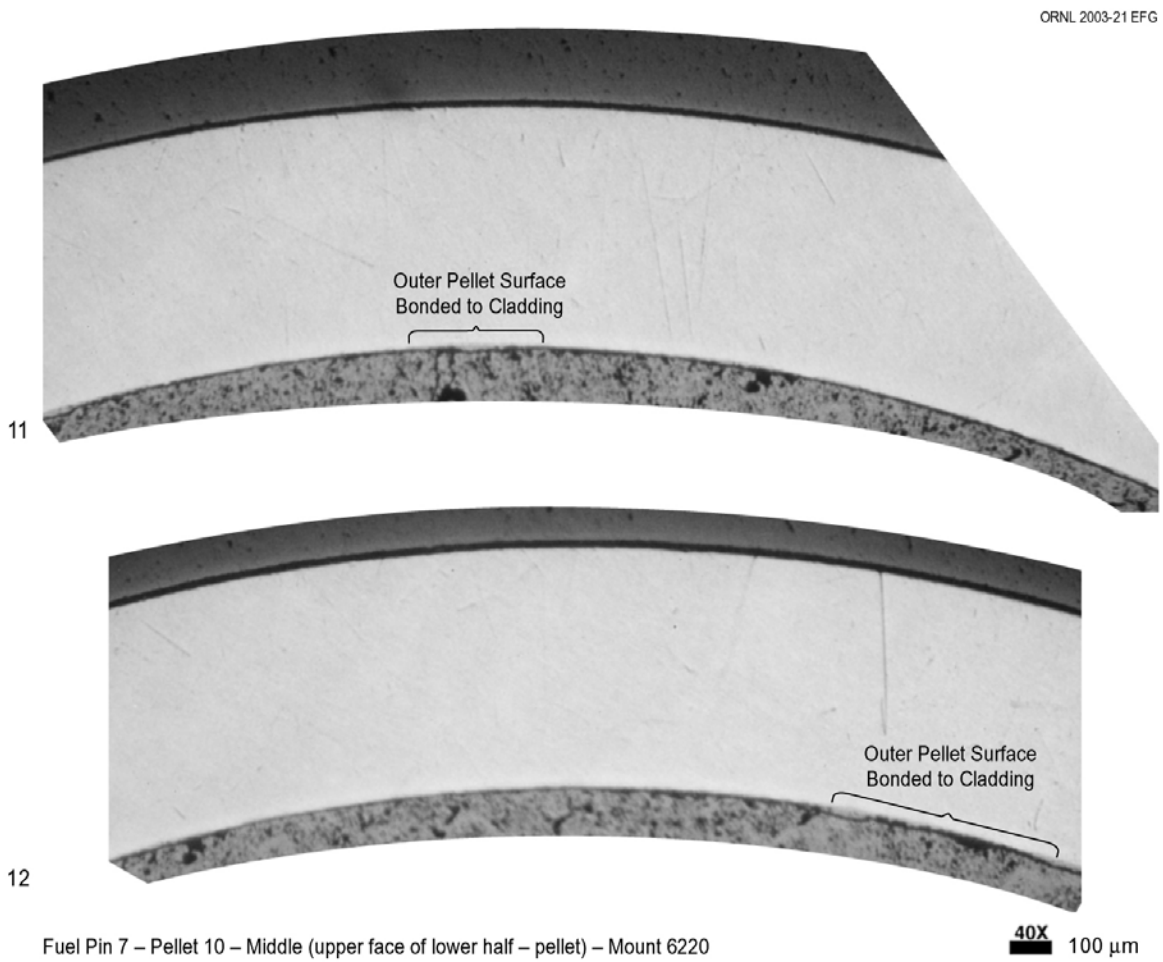

Figure 5.15 Sectors 11 and 12 from Mount 6220.

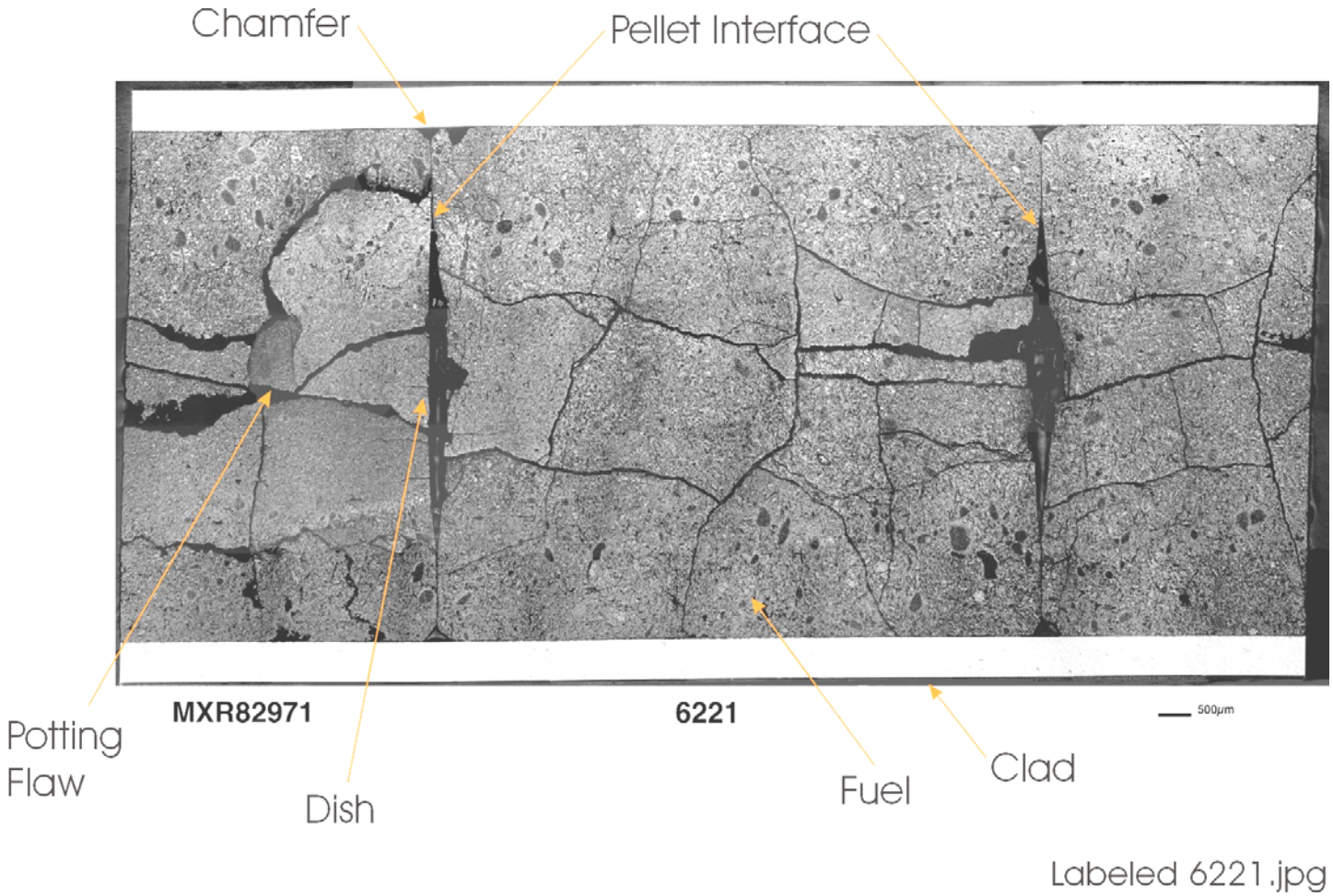

Figure 5.16 Axial section of Fuel Pin 7, specimen FP-7-M-4. Note that the pellet dish and chamfer can be seen indicating excellent irradiation behavior. Agglomerates can be seen throughout the section. Note that they are somewhat lighter, less developed, near the pellet axis than near the clad. The black regions are pull out.

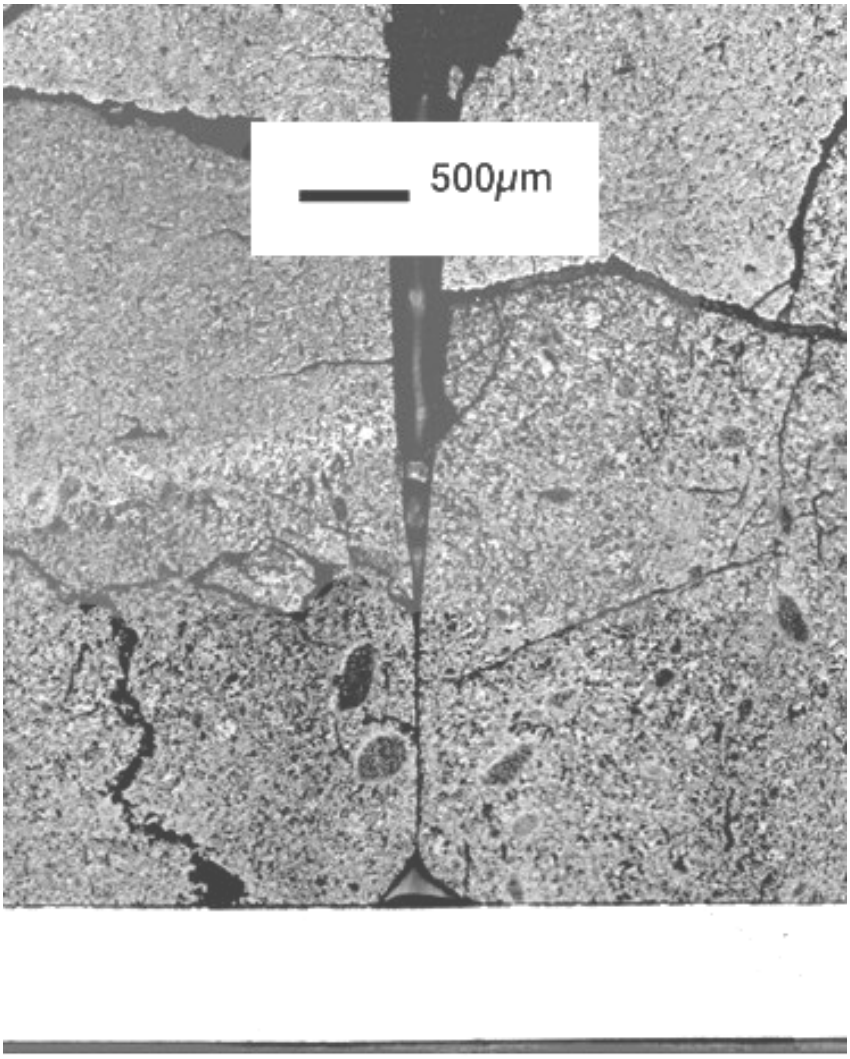

Figure 5.17 Close up view of pellet interface showing the chamfer and dishing. The small "triangle" in the chamfer space is a potting artifact (low spot or bubble).

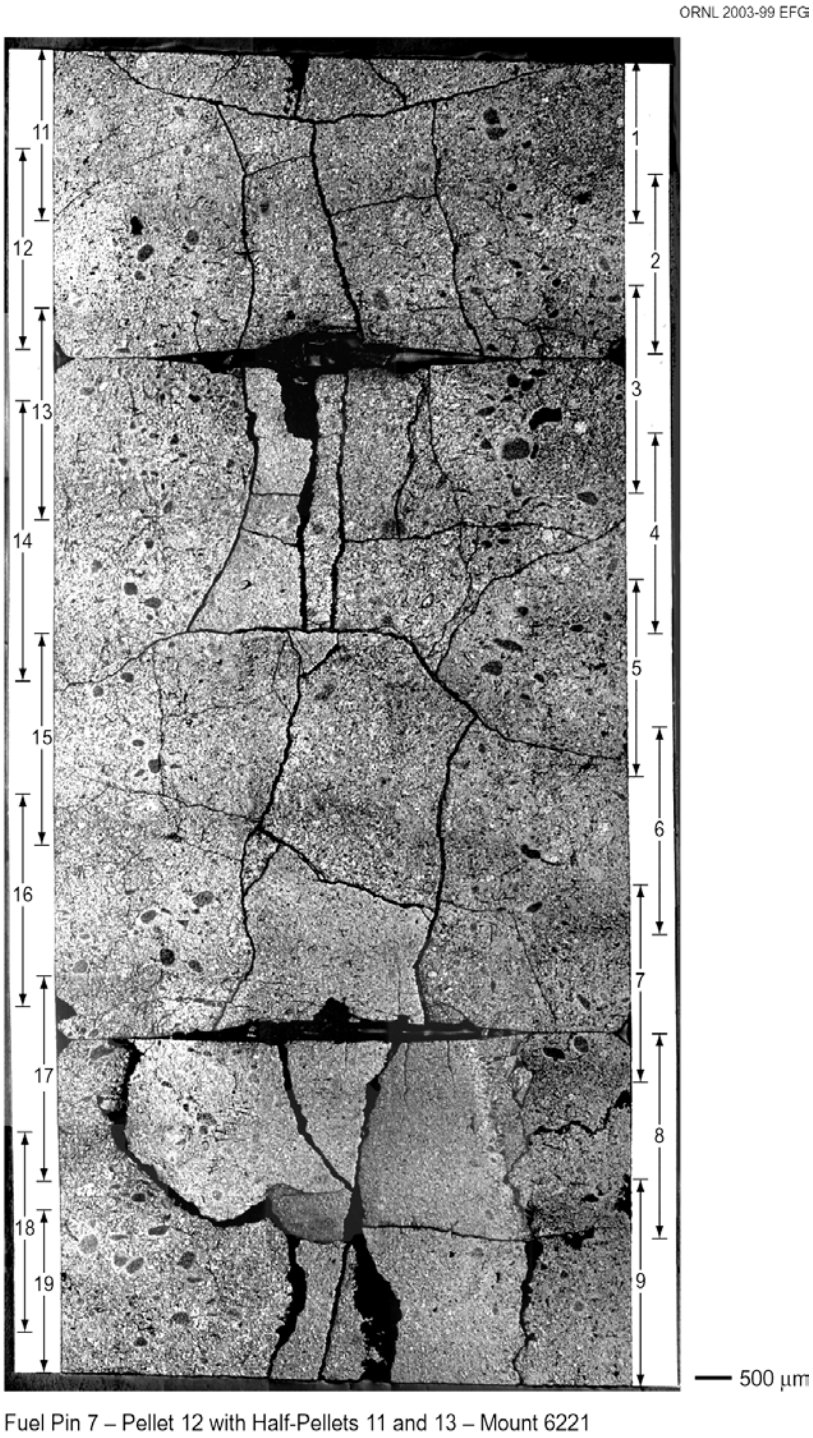

Figure 5.18 Mount 6221 with sector definitions. Note that in the following figures one side (right) has less corrosion than the other (left).

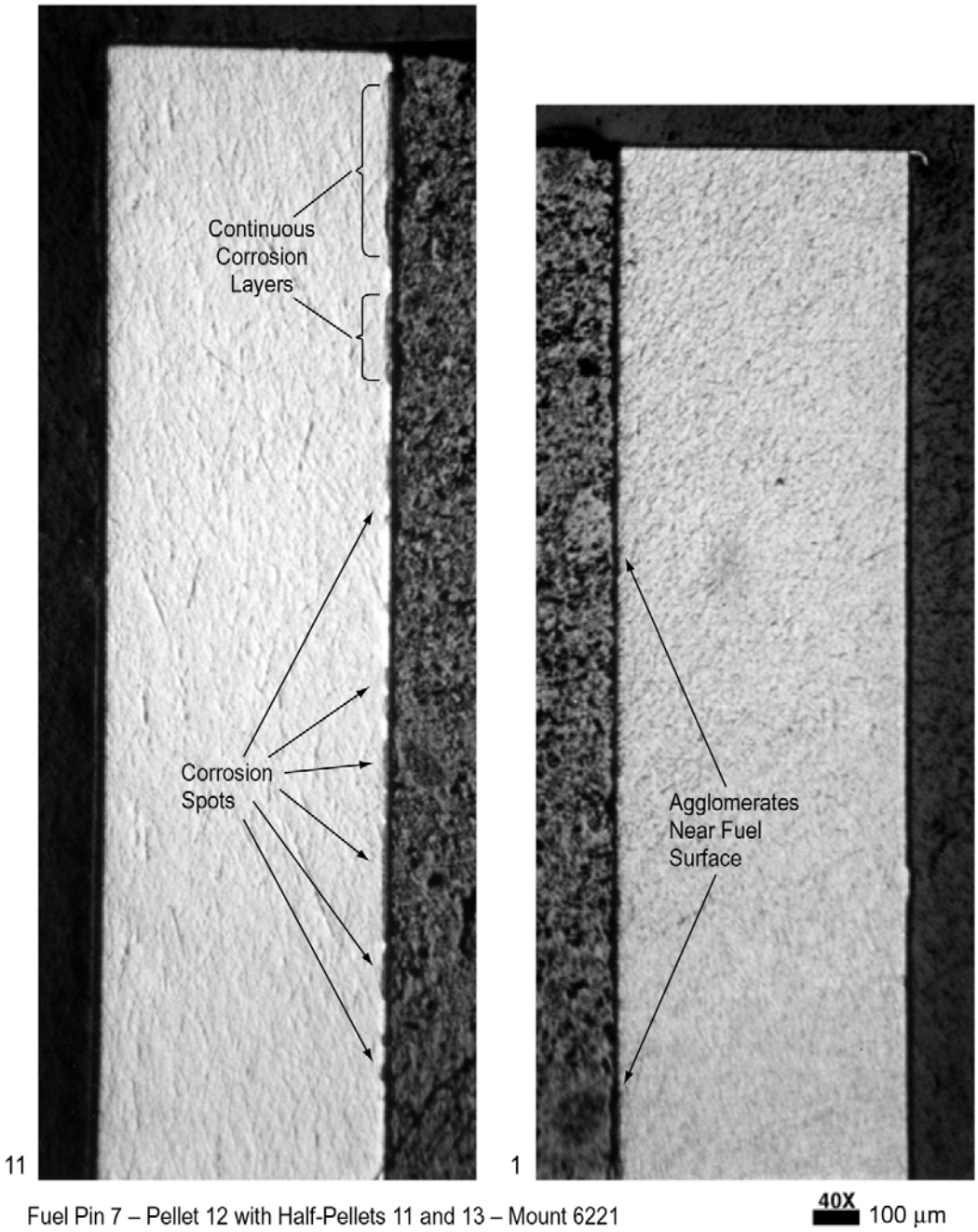

Figure 5.19 Left and right side sectors 11 and 1 from Mount 6221.

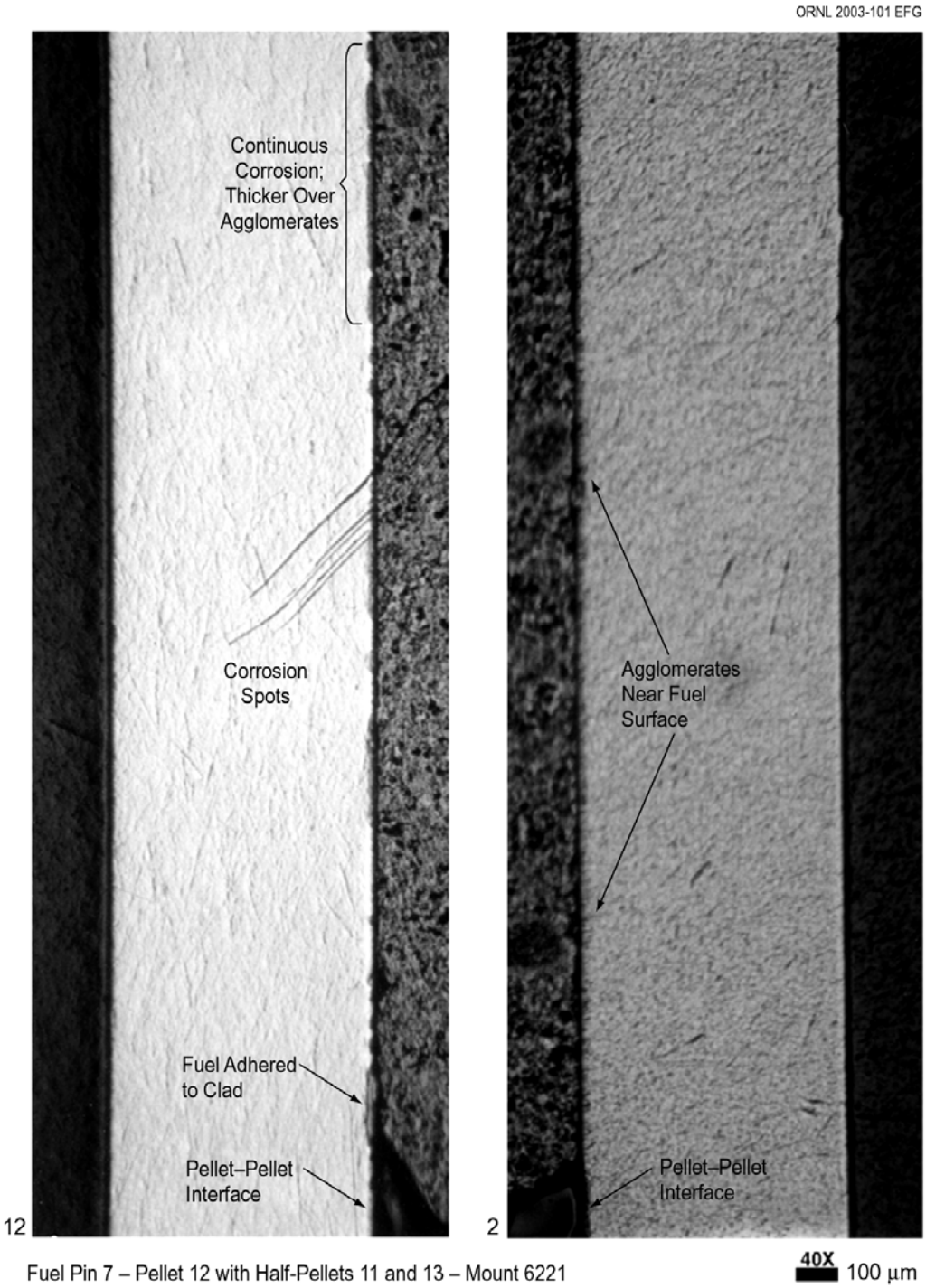

Figure 5.20 Left and right side sectors 12 and 2 from Mount 6221.

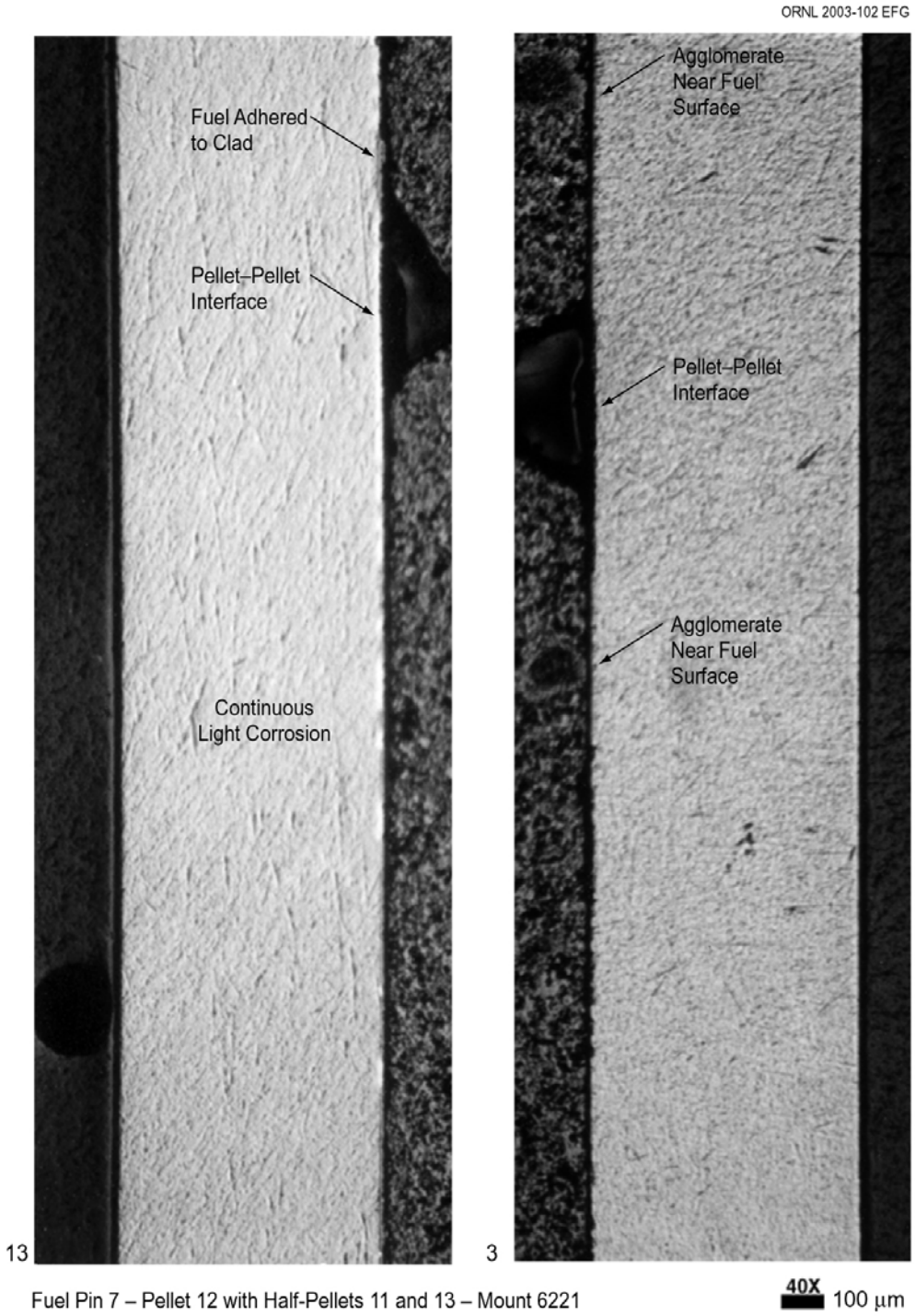

Figure 5.21 Left and right side sectors 13 and 3 from Mount 6221.

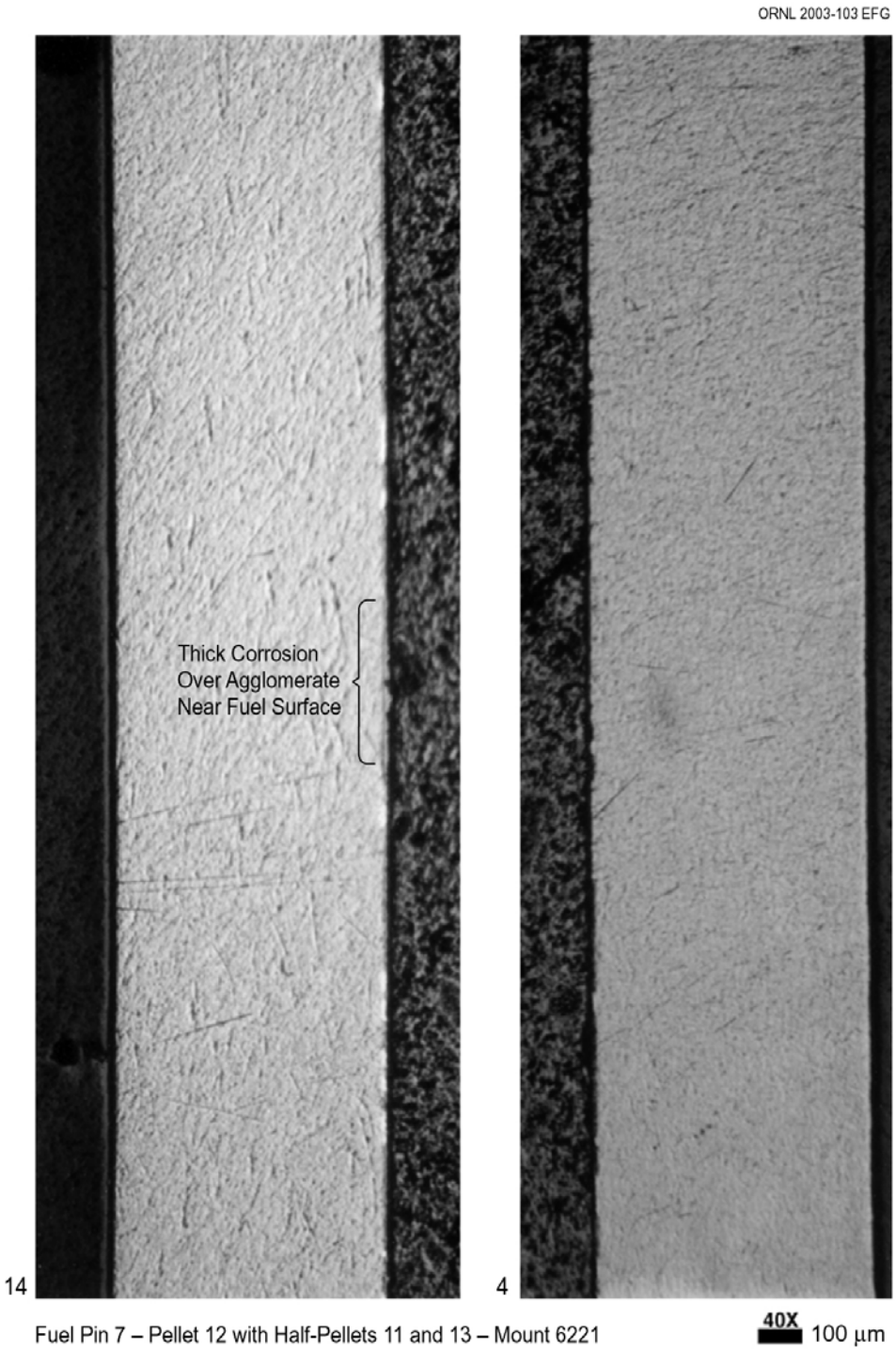

Figure 5.22 Left and right side sectors 14 and 4 from Mount 6221.

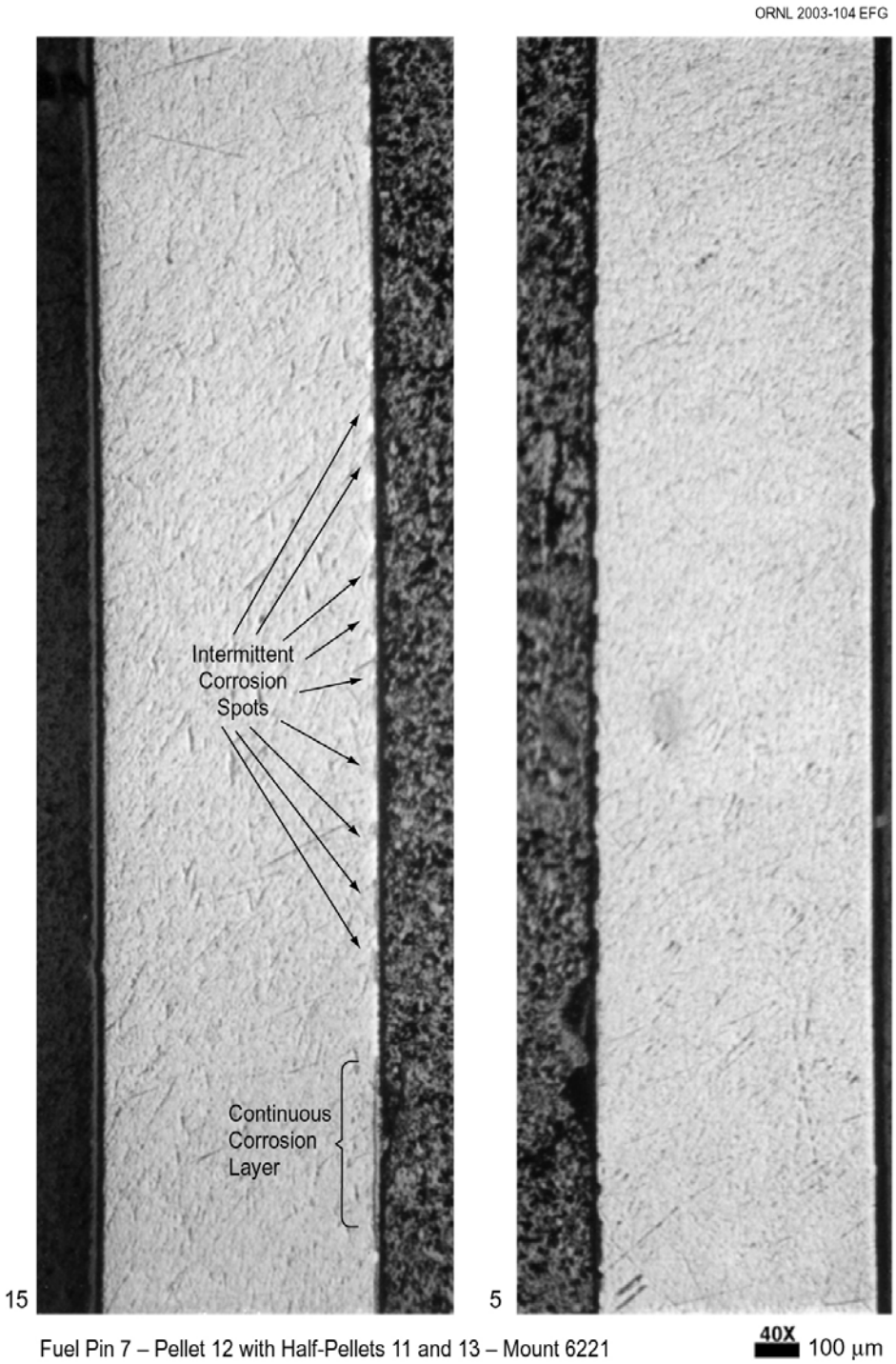

Figure 5.23 Left and right side sectors 15 and 5 from Mount 6221.

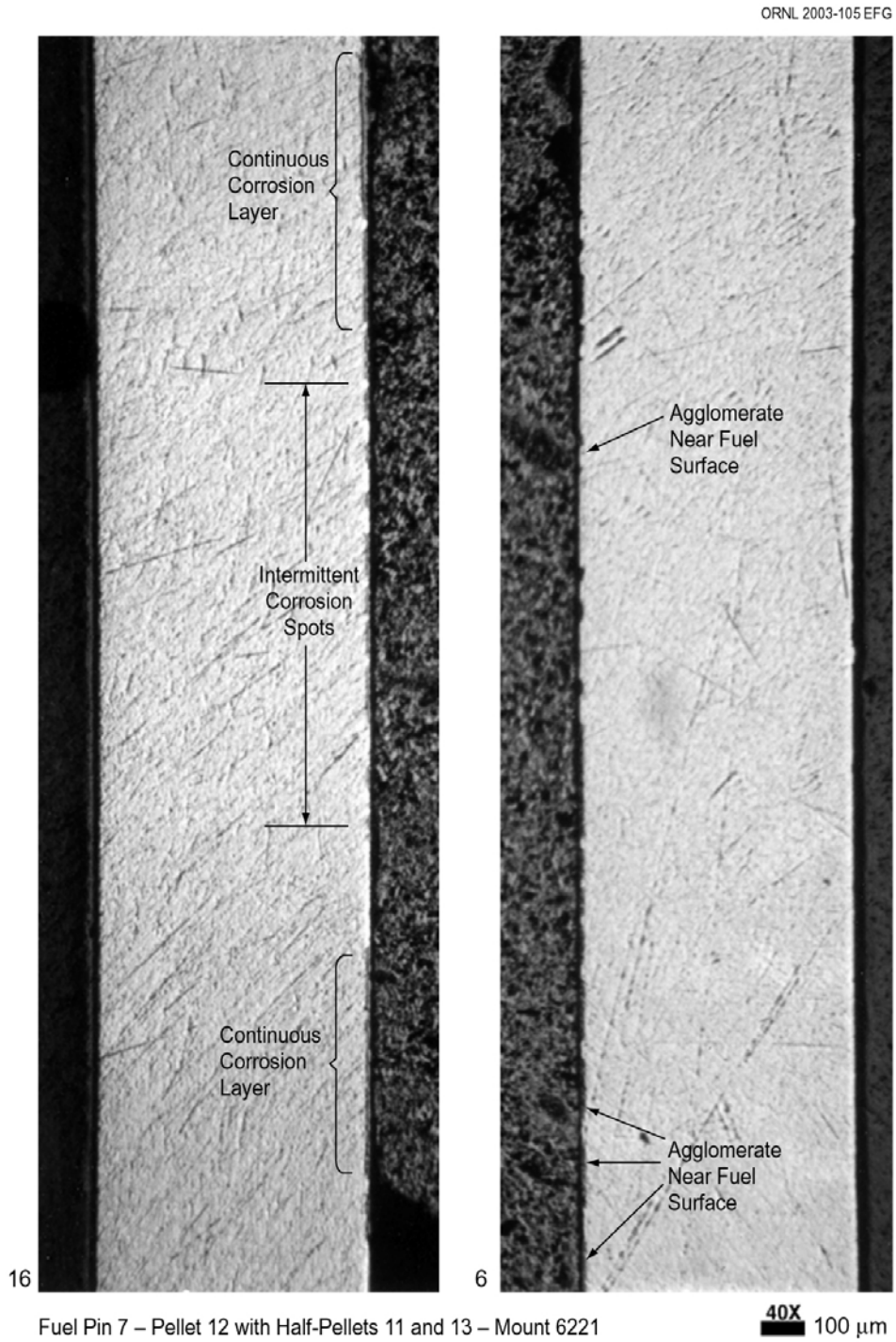

Figure 5.24 Left and right side sectors 16 and 6 from Mount 6221.

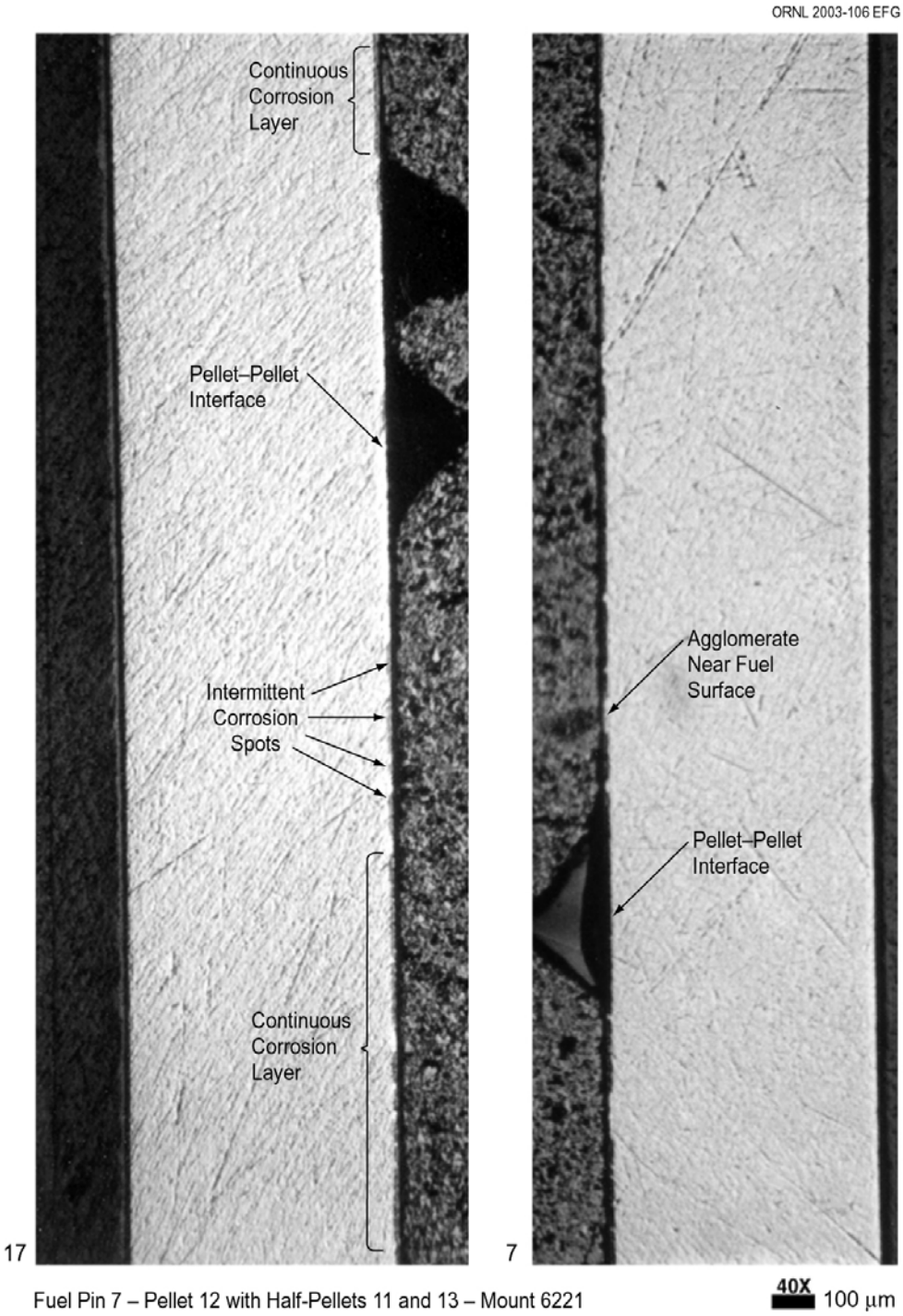

Figure 5.25 Left and right side sectors 17 and 7 from Mount 6221.

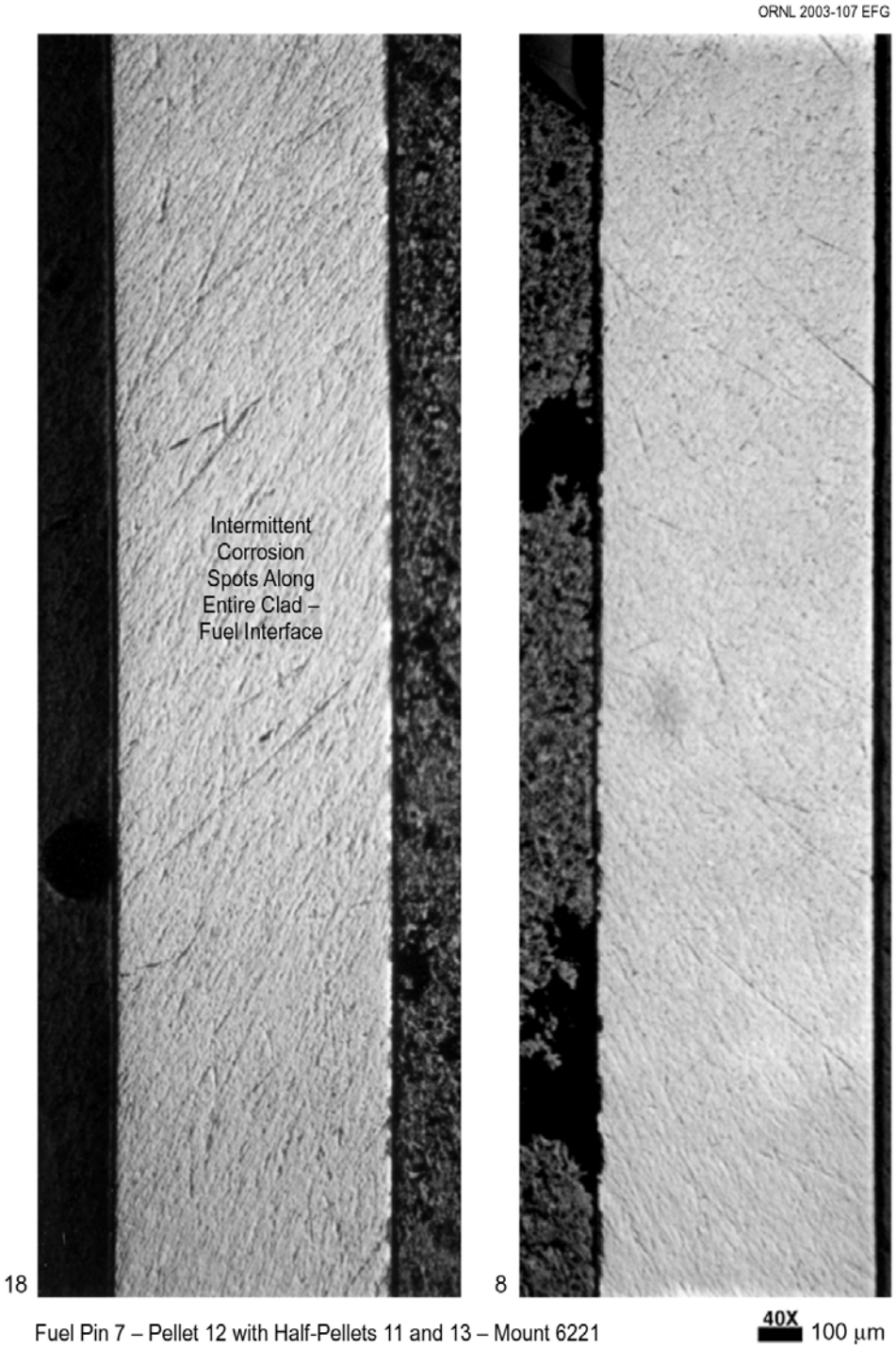

Figure 5.26 Left and right side sectors 18 and 8 from Mount 6221.

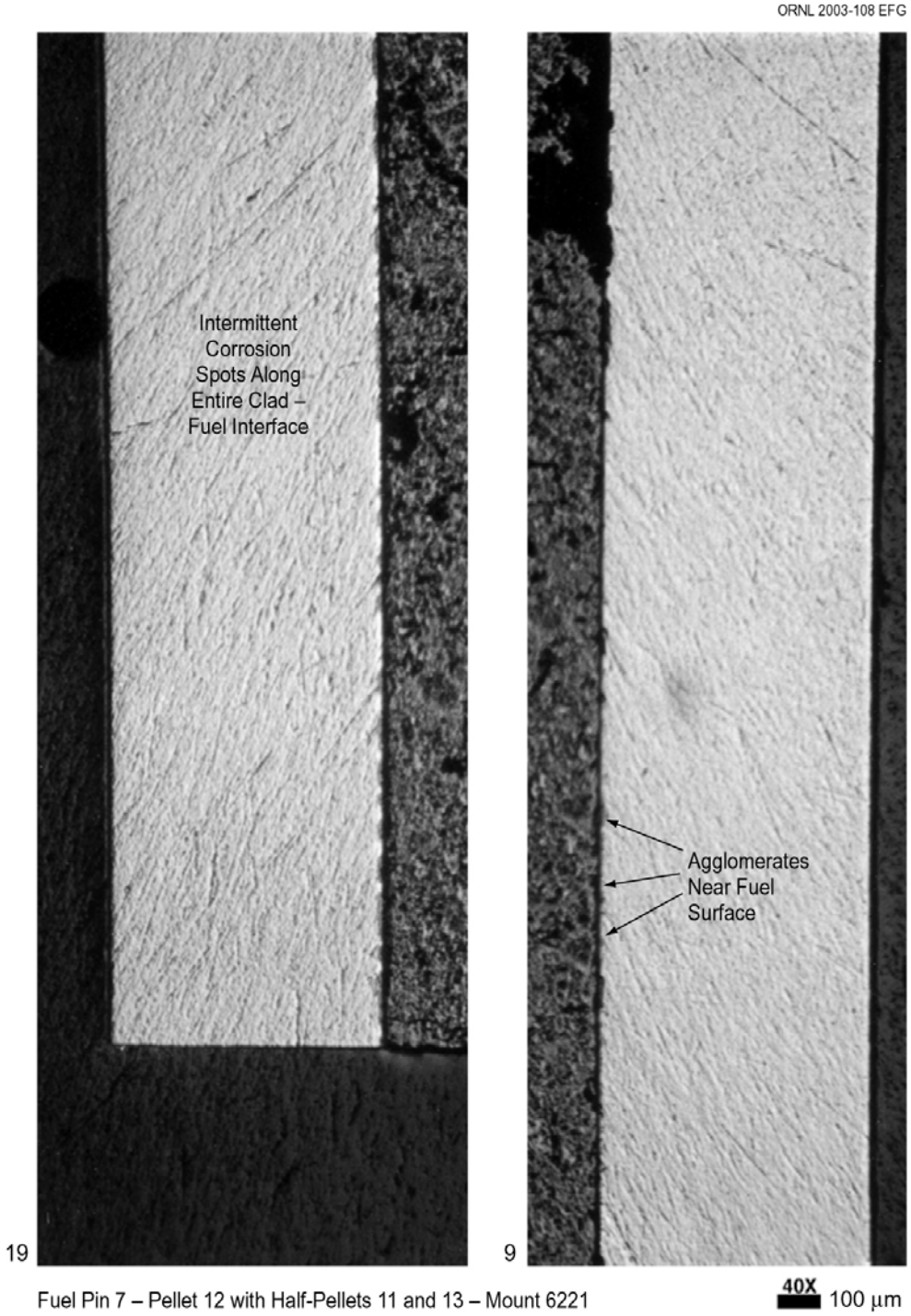

Figure 5.27 Left and right side sectors 19 and 9 from Mount 6221.

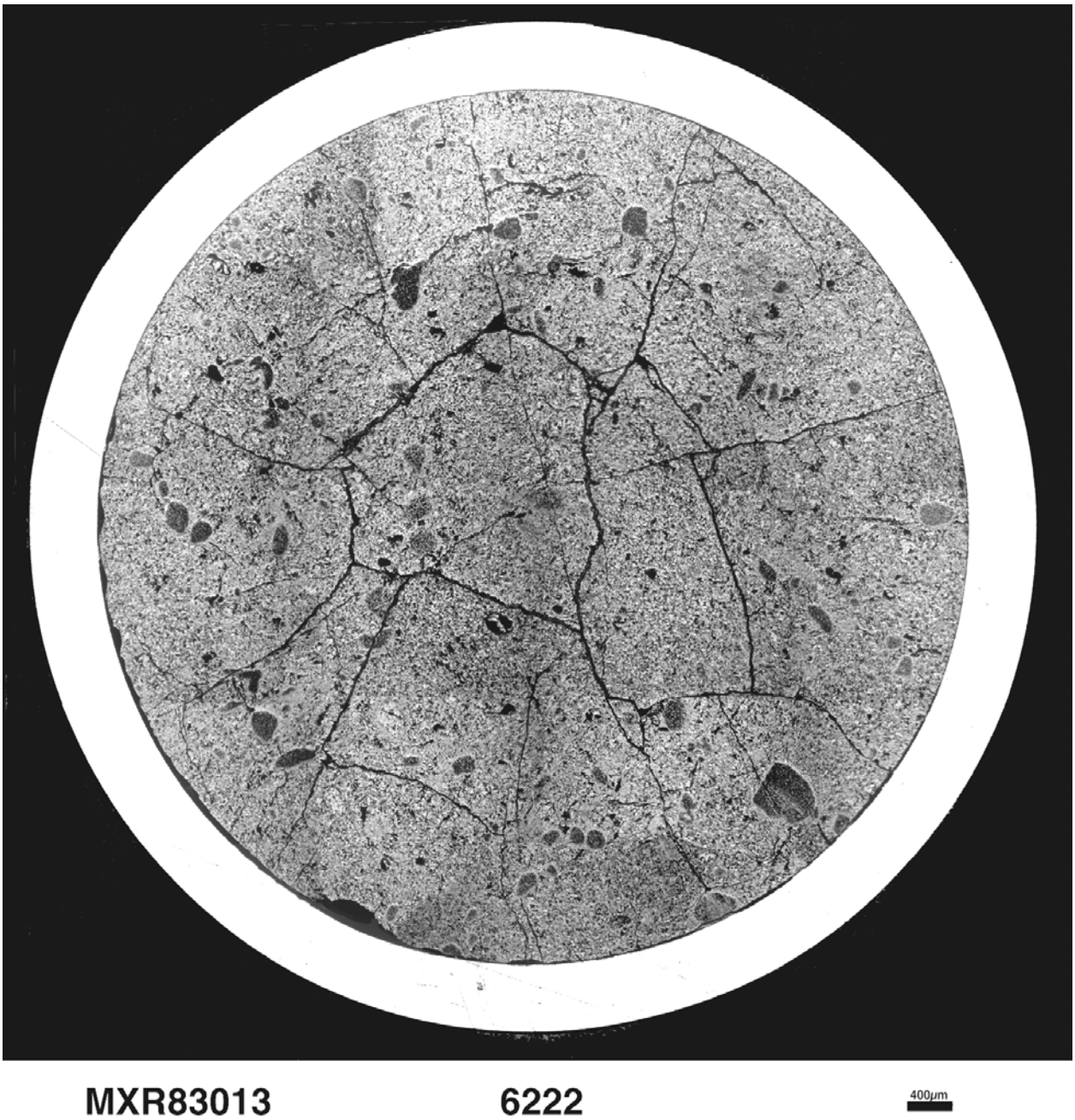

Figure 5.28 Cross section of Fuel Pin 7, specimen FP-7-M-5. Note that the agglomerates can be seen throughout the cross section, even near the center. Note the large agglomerate at the 5 o'clock position. This mount also has a triangle like region broken out near the center.

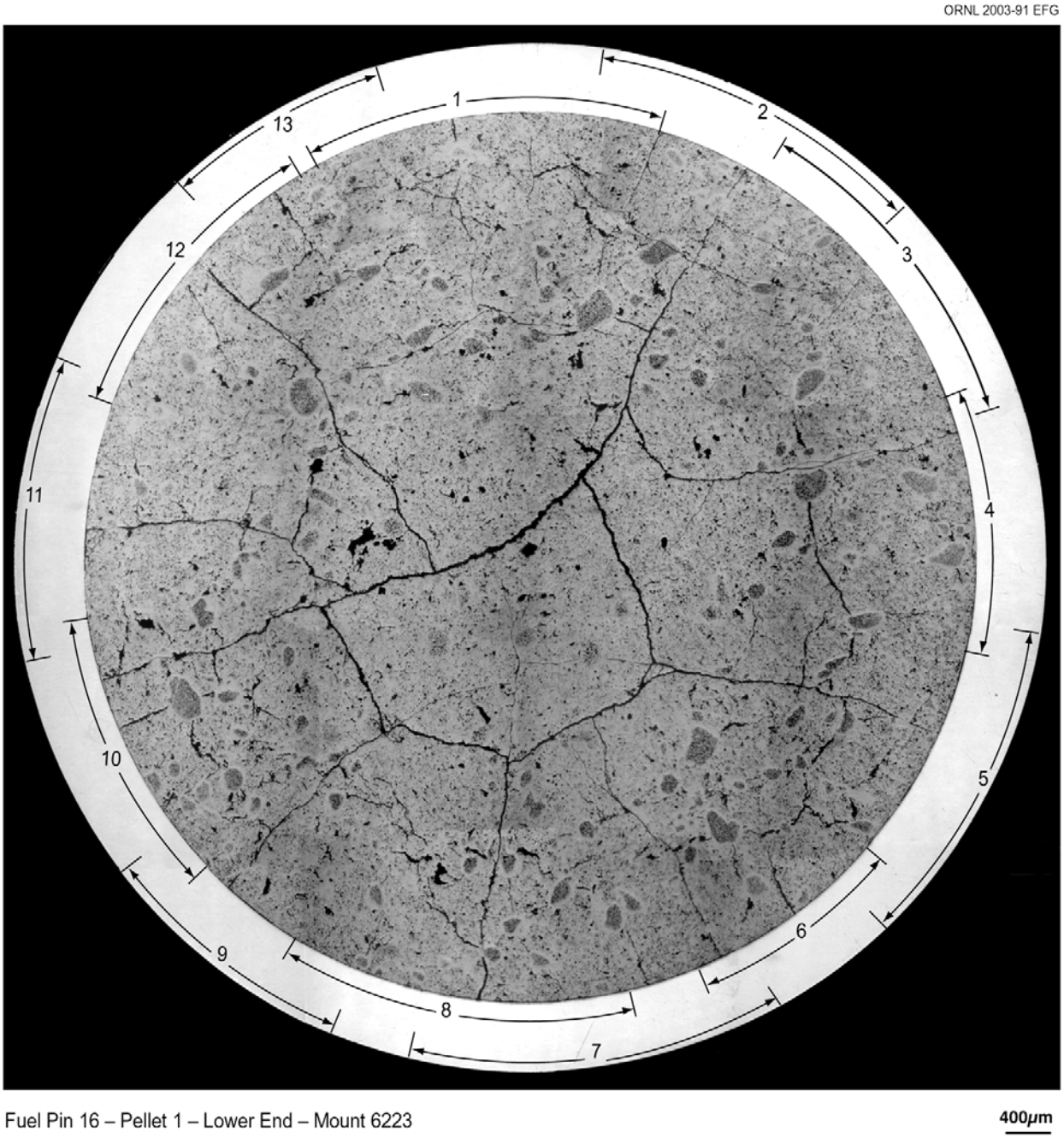

Figure 5.29 Cross section of Fuel Pin 16, specimen FP-16-M-1. Note that the agglomerates can be seen through out the cross section, even near the center. This mount also has a core like region broken out near the center.

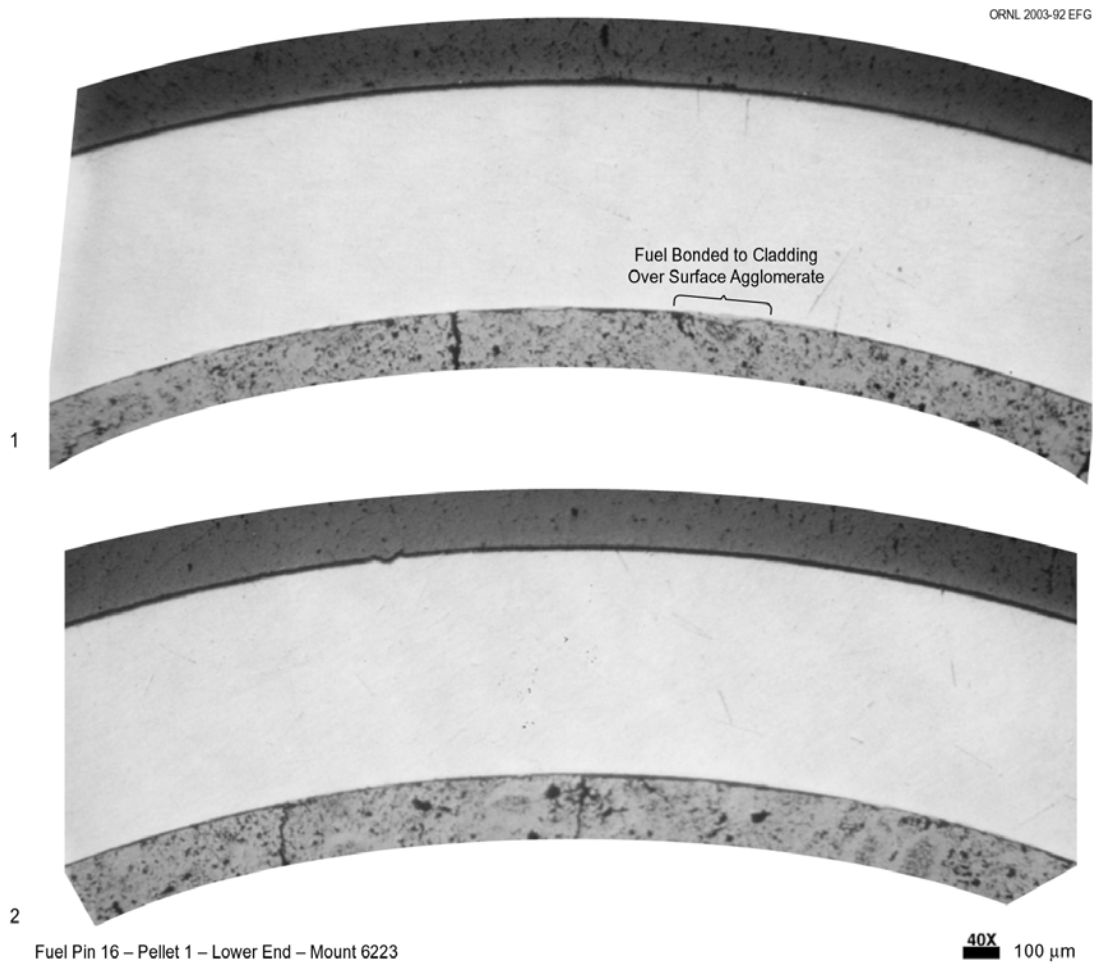

Figure 5.30 Sectors 1 and 2 of Mount 6223.

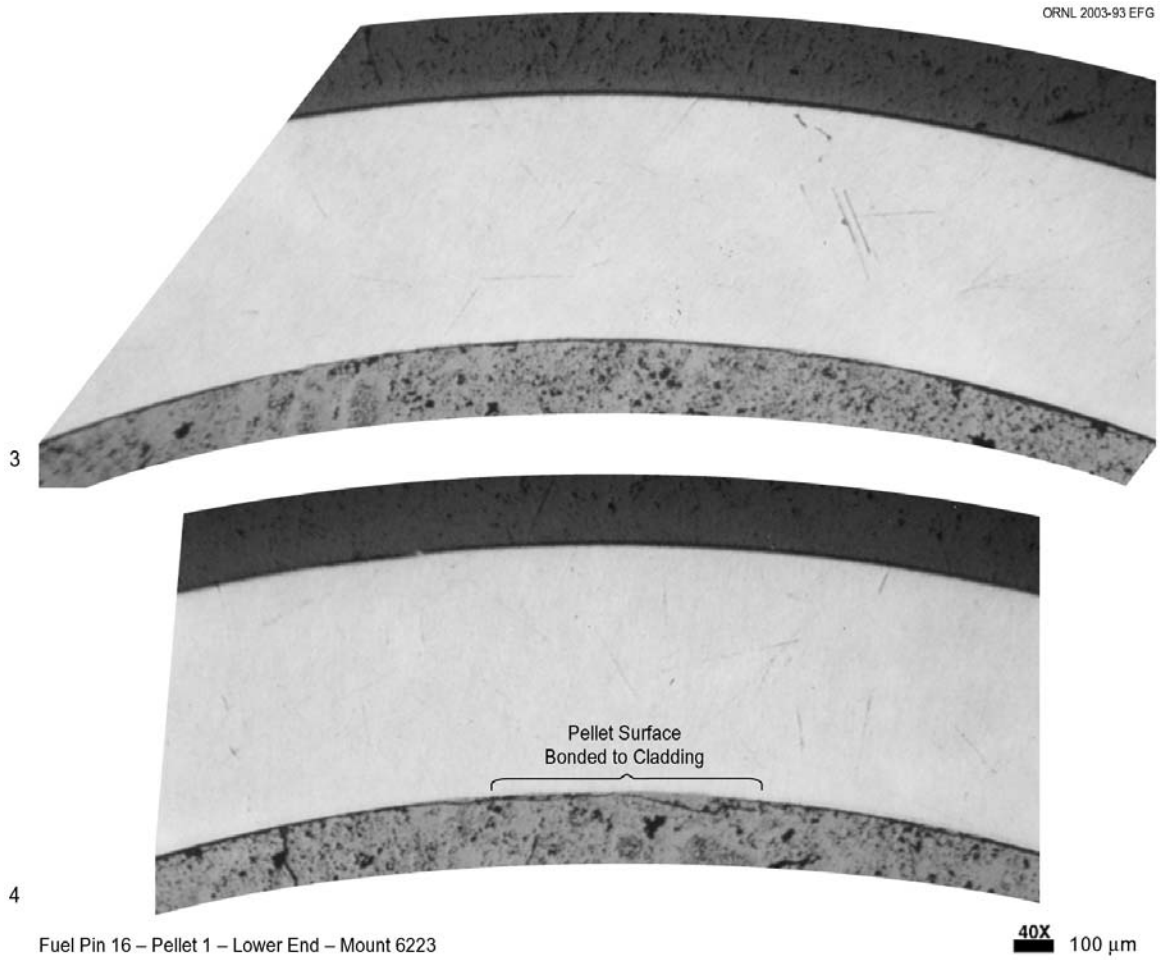

Figure 5.31 Sectors 3 and 4 of Mount 6223.

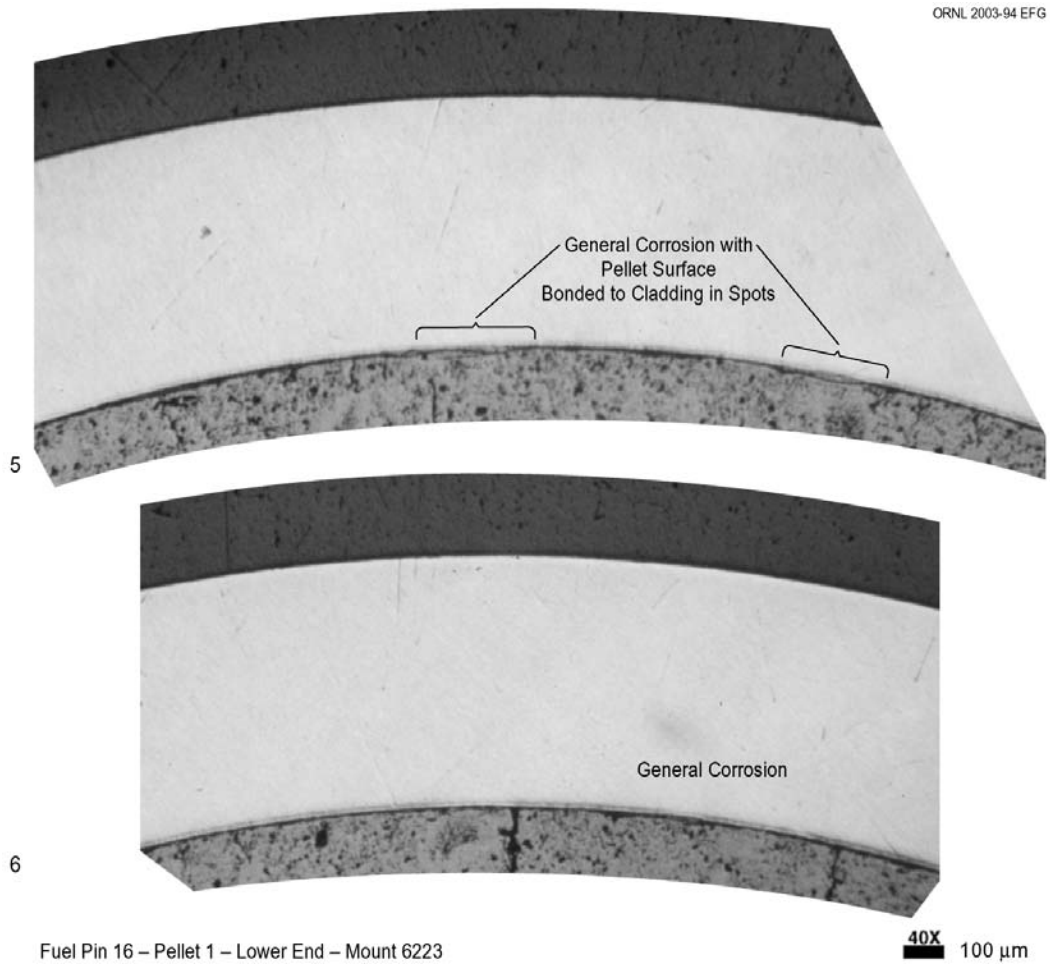

Figure 5.32 Sectors 5 and 6 of Mount 6223.

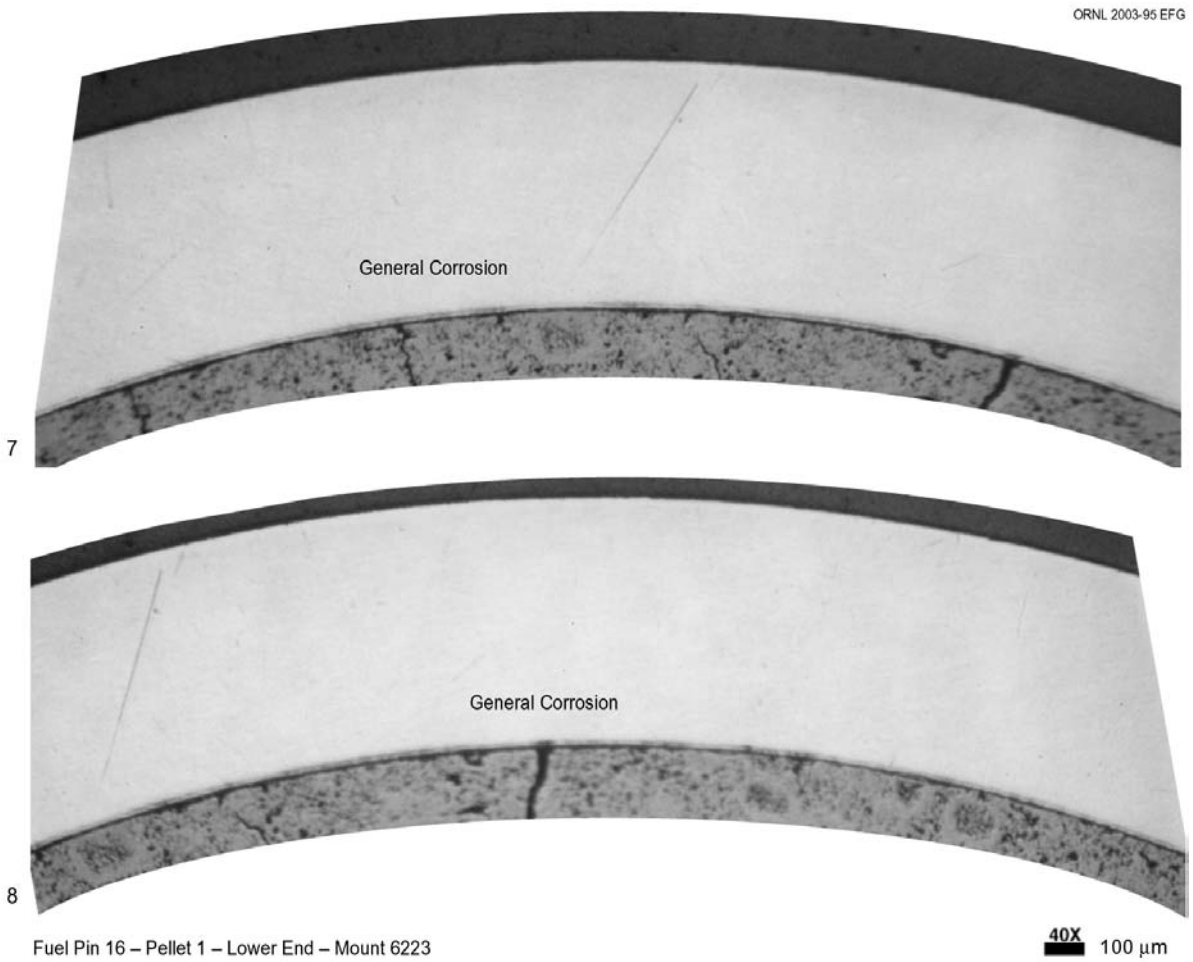

Figure 5.33 Sectors 7 and 8 of Mount 6223.

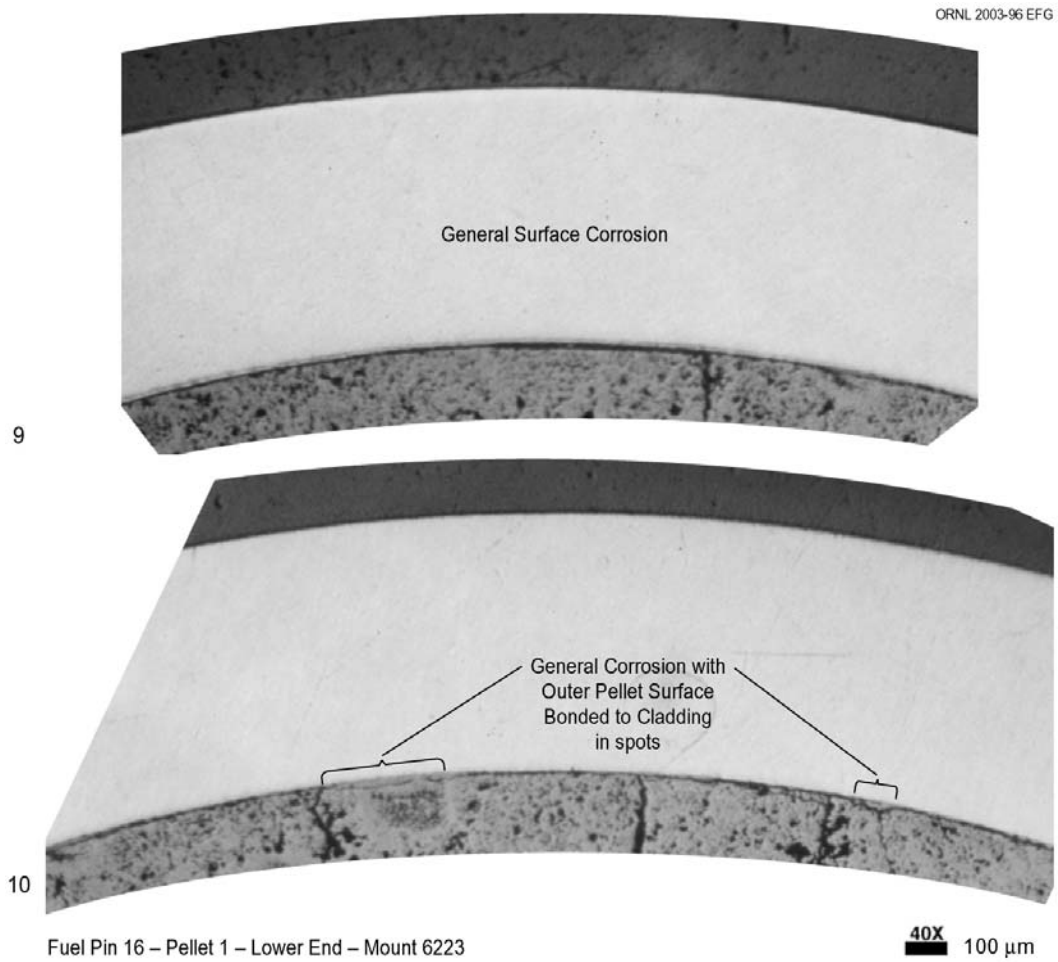

Figure 5.34 Sectors 9 and 10 of Mount 6223.

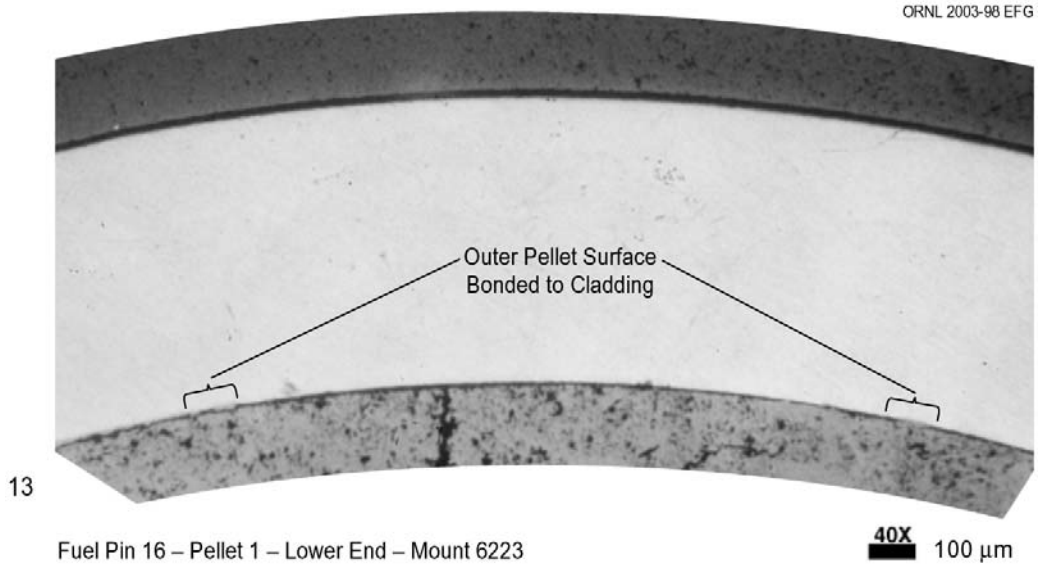

Figure 5.35 Sector 13 of Mount 6223.

Figure 5.36 Cross-section of Fuel Pin 16, specimen FP-16-M-2. Again, note that the agglomerates can be seen through out the cross-section, even near the center. Also note the trapezoid and triangle like cylinder regions isolated by cracks near the center. The black region near the bottom is pullout.

5.4 Mount Etching

Mounts 6222 and 6225 were etched to bring out the phase and grain detail by using a solution of 2.5ml H_2SO_4 + 48ml H_2O_2. The mounts were swabbed for a period of about 2-3s. These mounts did not etch as well as the mounts in the previous (30 GWd/MT) PIE and less detail is visible. The same technique was used; the reason for this less satisfactory behavior was not apparent.

Figures 5.37 and 5.38 compare the grain size at the edge (cooler) region with that of the central (hotter) region for mount 6222 (untreated fuel). While it is difficult to quantify because of the uneven etching, the central region appears to have a somewhat larger grain size, consistent with the higher temperatures in this region during irradiation.

Figures 5.39 and 5.40 compare the grain size at the edge (cooler) region with that of the central (hotter) region for mount 6225 (TIGR fuel). Again, it is difficult to quantify any differences because of the uneven etching, although the grain sizes appear slightly larger than in Figures 5.37 and 5.38.

The grain size in the edge region of both mounts is roughly the same as that in the unirradiated fuel (see Figure 2.2).

Overall, the grain differences between the center and the edge as well as between the treated and untreated material appear to be modest and probably insignificant. Larger differences were observed in the 30 GWd/MT PIE. This could be a result of the more severe thermal/power history for the current (40 GWd/MT) fuel. In addition, note that the fission gas release difference was smaller with this PIE, whereas the TIGR material had a 50% greater fission gas release fraction in the 30 GWd/MT PIE.

The actual occurrence of the High Burn-up Structure (HBS) in and near the agglomerates in this fuel could not be completely proven because an accurate assessment of the grain structure could not be obtained. Strictly defined, the HBS requires a sub-micron grain size, precipitation of fission gasses into micron-sized bubbles, and a migration of xenon. Section 5.6 will detail the gas bubbles and xenon migration, but evidence for grain size reduction was not clear.

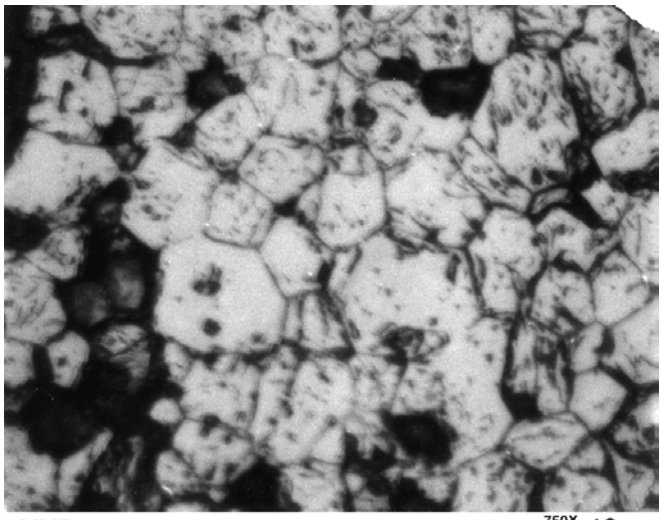

AREA 1 Near edge

Figure 5.37 Grain structure near the pellet edge in Mount 6222 (Untreated).

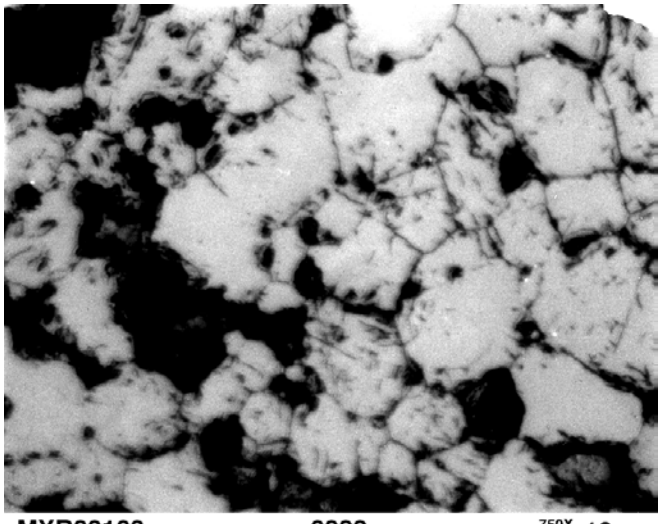

AREA 3 Near center

Figure 5.38 Grain structure near the pellet center in Mount 6222 (Untreated).

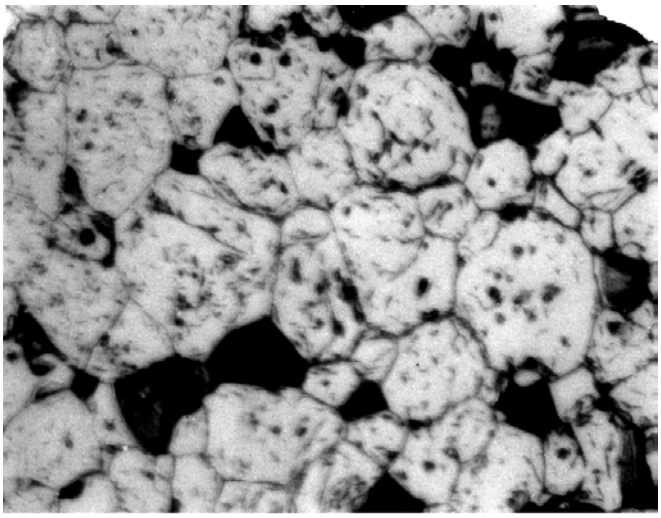

Figure 5.39 Grain structure near the pellet edge in Mount 6225 (TIGR).

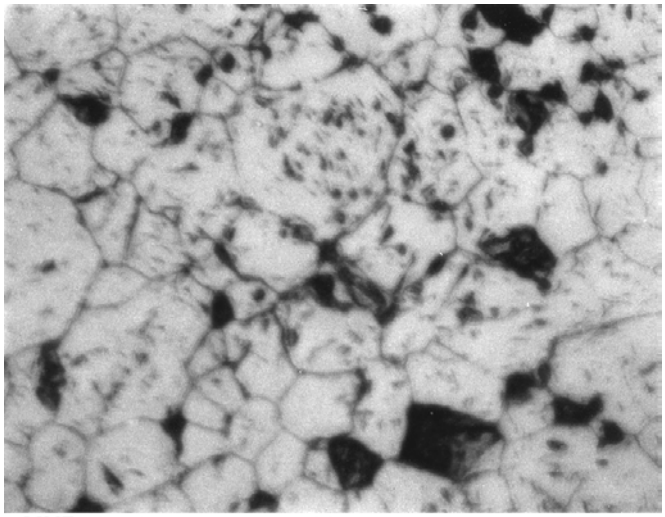

Figure 5.40 Composite photograph of etched Mount 6225 (TIGR).

5.5 Gamma Scan of Mount 6219

Mount 6219 was gamma scanned to obtain an estimate of the burnup profile as inferred from the gamma-emitting fission products. The mount was scanned using a long 1/32" collimator. The signal level was low, so long (30s) time constants were used in the signal integration as was done in the previous PIE.

Because the fuel pin is not positively locked in place in the capsule, rotation is possible during irradiation and handling. Thus, the orientation of the fuel pin relative to the reactor centerline cannot be reliably determined, and the orientation of the scanned segment is random. However, the scan does indicate a clear burnup pattern indicating minimal, if any, movement during irradiation.

The energy spectrum from 400 to 800 keV was used as the signal source. Figure 5.41 shows the results of the scan. The left side of the figure shows the collected data and the right side shows the smoothed color contours. The scan includes about four times as many total points as necessary for the collimator resolution and there is some noise on the signal, so the reader is cautioned to avoid reading much fine detail into the scans. However, there is considerable point-to-point variation in the burnup pattern (as outlined by the larger color islands in Figure 5.41), which is likely due to the relatively uneven distribution of large agglomerates in the fuel. While the resolution is not detailed enough to resolve individual agglomerates, it does indicate a coarse grained distribution of fission products. Its also shows that the burnup is asymmetric and off-center peaked as predicted by the irradiation models.

Overall, the scan verified the expected burnup profile and the effects of the agglomerates as detailed in previous Sections.

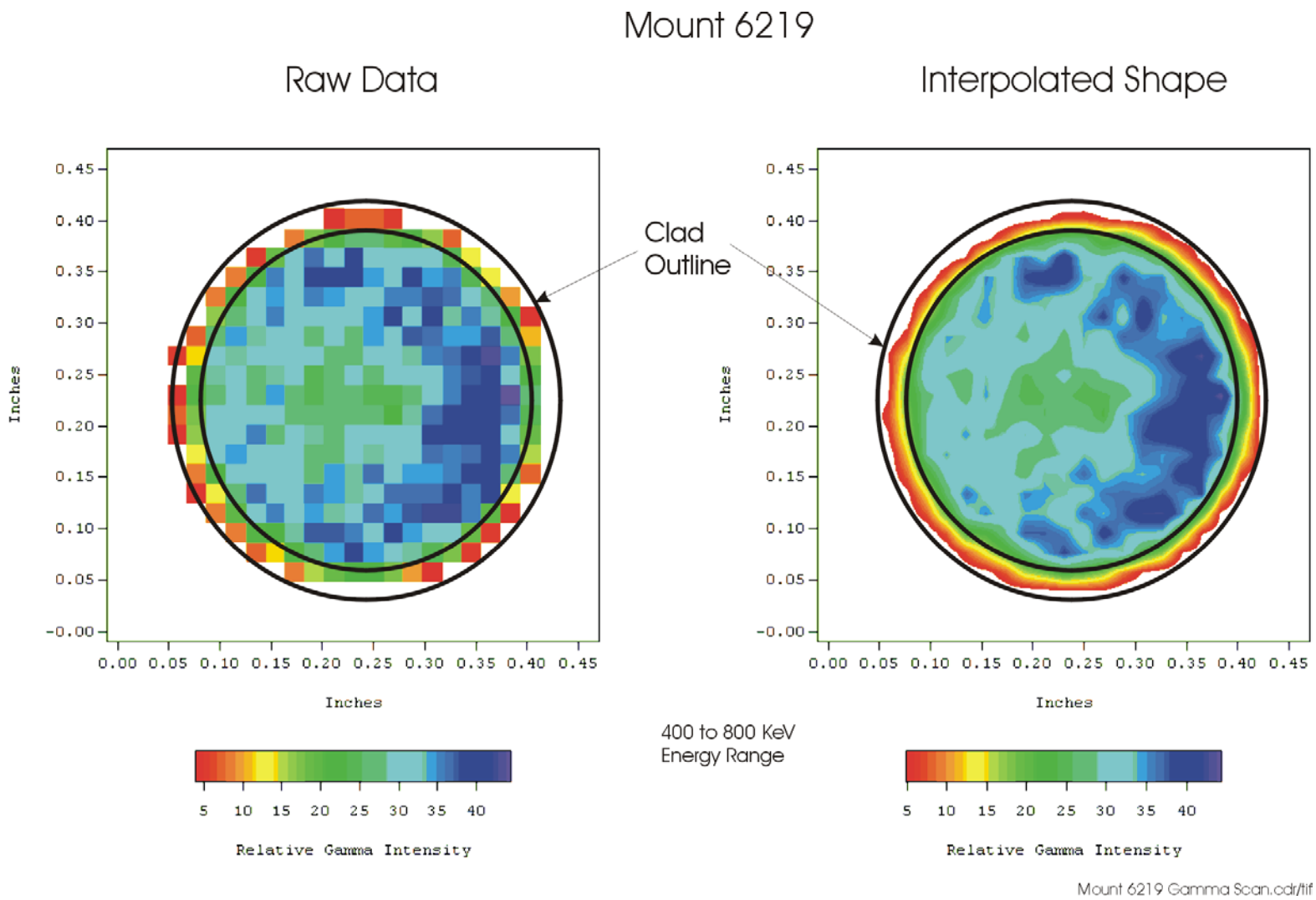

Figure 5.41 Gamma scan of Mount 6219. Note the off center burnup profile.

5.6 SEM Mounts

Two mounts were prepared for SEM/Microprobe analysis and a JEOL JXA 840A SEM/Microprobe was used for the analysis. The activity of the samples generated too much background noise for energy dispersive X-ray analysis to be employed, so only wavelength dispersive X-ray analysis was used on these specimens. The samples were prepared by epoxy mounting fuel pin sections, as was done for the metallographic mounts, and then grinding the mounts until the fuel pin section was roughly 10-25 mils thick. The mounts were then polished and photographed as was done for the metallographic mounts.

These thin-section mounts had activity levels of approximately 30 (FP-7-SEM-1) and 90 (FP-16-SEM-1) mR/hr at 12", which was low enough for handling and transfer to the SEM. Other than a special shielded transfer device for removing the specimens from the hot cell and transferring them to the SEM, no special shielding was used on the SEM. The operator and control equipment were located well away from the instrument so that the personnel radiation dose was insignificant; however, the imaging results were better (less noise) with the lower activity sample.

Table 5.2 shows the relationship between the specimen numbers and the mount identity.

Table 5.2 SEM Mount ID Numbers and Fuel Pellet Locations

Specimen Number	Mount ID	Fuel Pin Locations
FP-7-SEM-1	6218	Fuel Pin 7 Pellet 2 upper end
FP-16-SEM-1	6240	Fuel Pin 16 Pellet 2 upper end

5.6.1 Fuel Pin 7 SEM Mount

Figure 5.42 shows the polished cross section and regions of interest. Site 1 is an agglomerate near the pellet-clad interface, Site 2 is an agglomerate near the mid-radius region of the pellet, Site 3 is the pellet-clad interface in the absence of an agglomerate, and Site 4 is a grain boundary that shows the effects of fission gas accumulation and transport. The elemental mapping is qualitative because the signal to noise ratio was too low for quantitative analysis in most cases; however, the behavior of the fuel is clearly seen.

Figure 5.43 shows the mapping of Site 1, a small agglomerate near the surface of the pellet. As was seen in previous PIEs, the agglomerate is rich in plutonium and deficient in uranium (elemental concentration is proportional to brightness) and shows a much higher concentration of fission products than the nearby matrix. Ruthenium imaged well and illustrates this concentrating of fission products in the agglomerate.

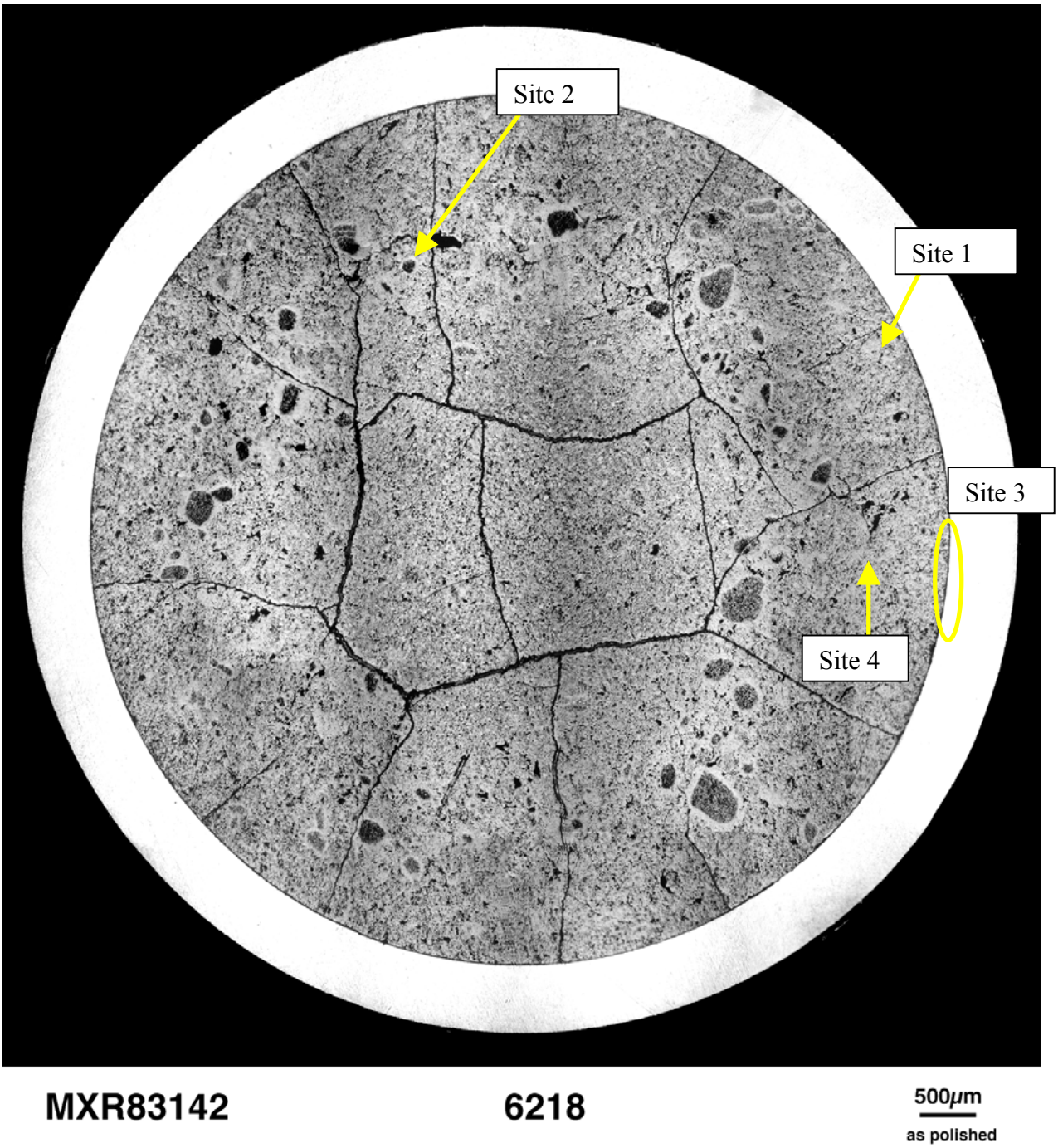

Figure 5.42 Composite photograph of mount used for SEM/Microprobe examination. (Also discussed in the metallography section)

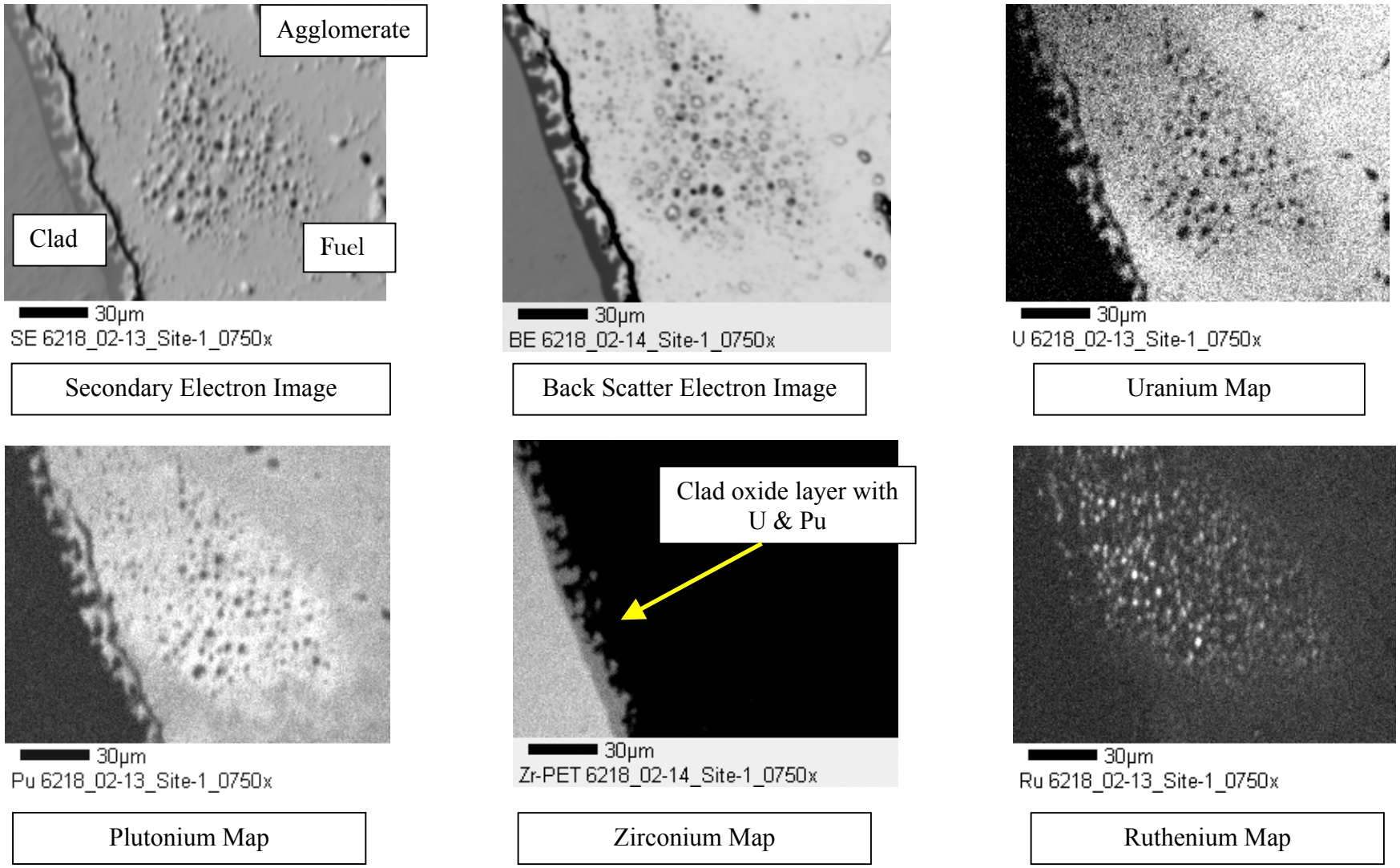

Figure 5.43 SEM/Microprobe scans of Site 1 in Mount 6218

As was detailed previously, the clad oxide layer is developing and is roughly 10 microns thick in some areas. Of particular interest is the diffusing of fuel into the clad oxide layer in the vicinity of the agglomerate. The finger like penetrations of the fuel, both Pu and U, into the oxide layer can be clearly seen in the elemental maps and in a larger back scatter image in Figure 5.44. As will be discussed shortly, this fuel diffusion did not occur in the pellet-clad regions lacking a nearby agglomerate.

Also apparent in Figure 5.44 (and Figure 5.42) is the "halo", a region of microstructure that is visibly different from either the porous agglomerate or the general fuel matrix. An elemental scan for xenon showed that xenon is diffusing out of the agglomerate region and into the nearby fuel matrix. Figure 5.45 illustrates this behavior. The xenon in the agglomerate does not image well because of its collection into macrobubbles, but the agglomerate is clearly the source of the xenon. When gases (xenon) are contained in bubbles larger than 20 angstroms in diameter, the emitted X-ray intensity is reduced and the magnitude of this signal reduction increases with bubble size [Reference 29]. The weak signal prevented a quantitative determination of the density gradient. This observation suggests that athermal (fission recoil) and thermal diffusion of fission products from the agglomerate has changed the nearby matrix in a manner that responds differently to polishing than the general matrix and thus makes these regions visible. The agglomerates appear to be able to plastically deform sufficiently so that the "halo" is unlikely to be caused by a local compressive stress field due to agglomerate swelling [References 30 and 31].

Figure 5.46 shows the imaging for Site 3, a region that did not have a surface agglomerate, but offered two fuel-clad interface conditions. The first, shown in the top of the figure, is a fuel-clad interface with a small gap. This area showed the growth of a thin oxide layer as discussed above, but the layer was only a few microns thick and lacked the feature of fuel diffusing into the oxide layer. The second condition, that of fuel adhering to the clad, is shown in the bottom of the figure. This region also showed the growth of an oxide layer, but this layer was not significantly thicker than the first case (gap). In addition, even though the fuel adhered to the clad, there was none of the "finger- like" fuel diffusion into the oxide layer. In fact, it appears to be very similar to the case with a fuel-clad gap. Thus, the agglomerate appears to be a driving force for significant fuel diffusion into the oxide layer [References 28 and 31].

No significant signs of the rim effect were seen in either Site 1 or 3, either visually or by Pu mapping. Additionally, no signs of fuel recrystallization were seen at the agglomerate boundary.

Imaging of Site 2 is shown in Figure 5.47. This site shows the usual concentration of Pu and the fission products in the agglomerate and of U outside of it. In general, it is no different from the previous agglomerates seen in this and previous PIEs. A xenon scan also revealed an apparent concentration gradient in xenon at the periphery of the agglomerate, but the signal quality was too poor to produce a clear image.

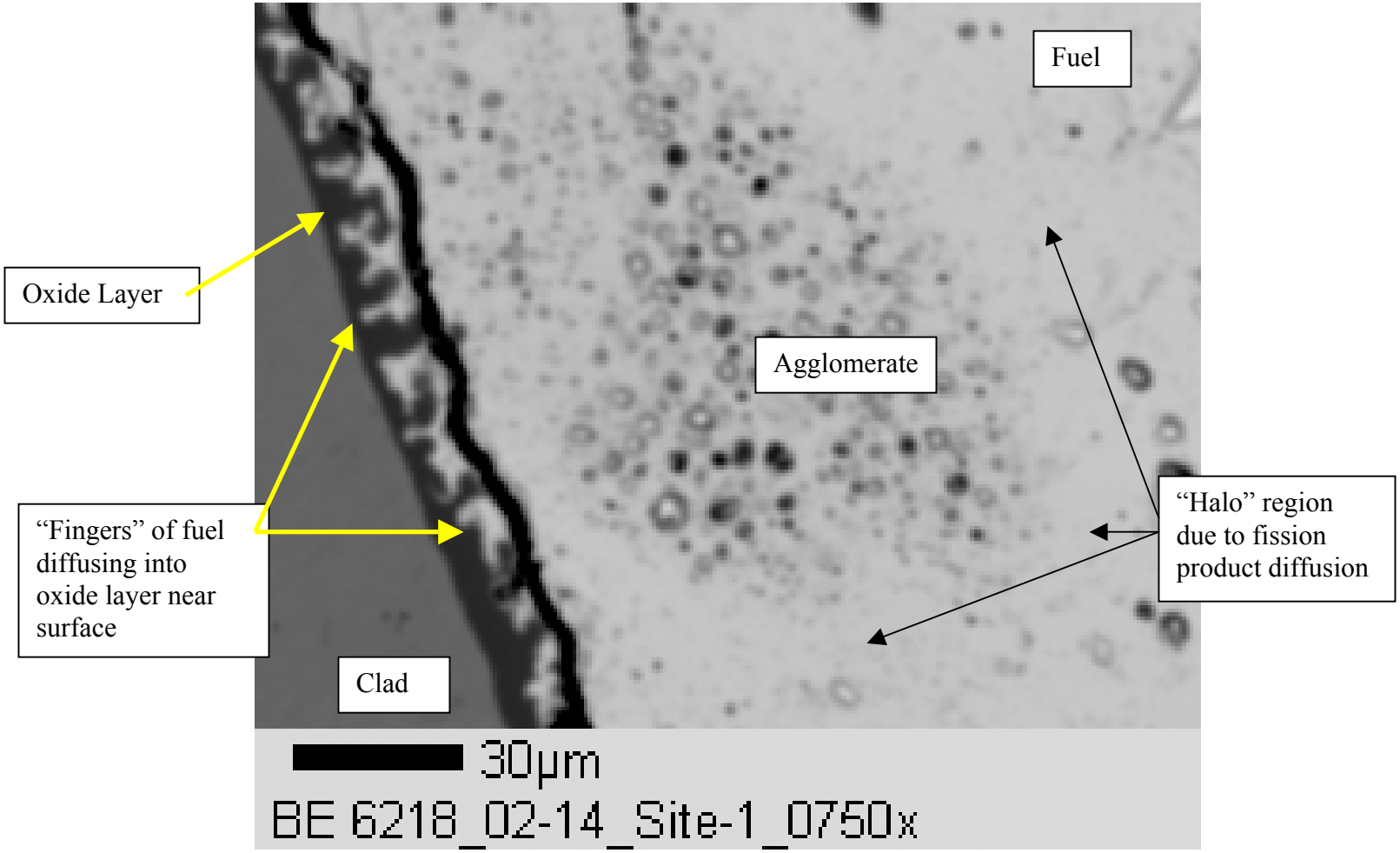

Figure 5.44 Larger view of SEM/Microprobe back scatter electron image of Site 1.

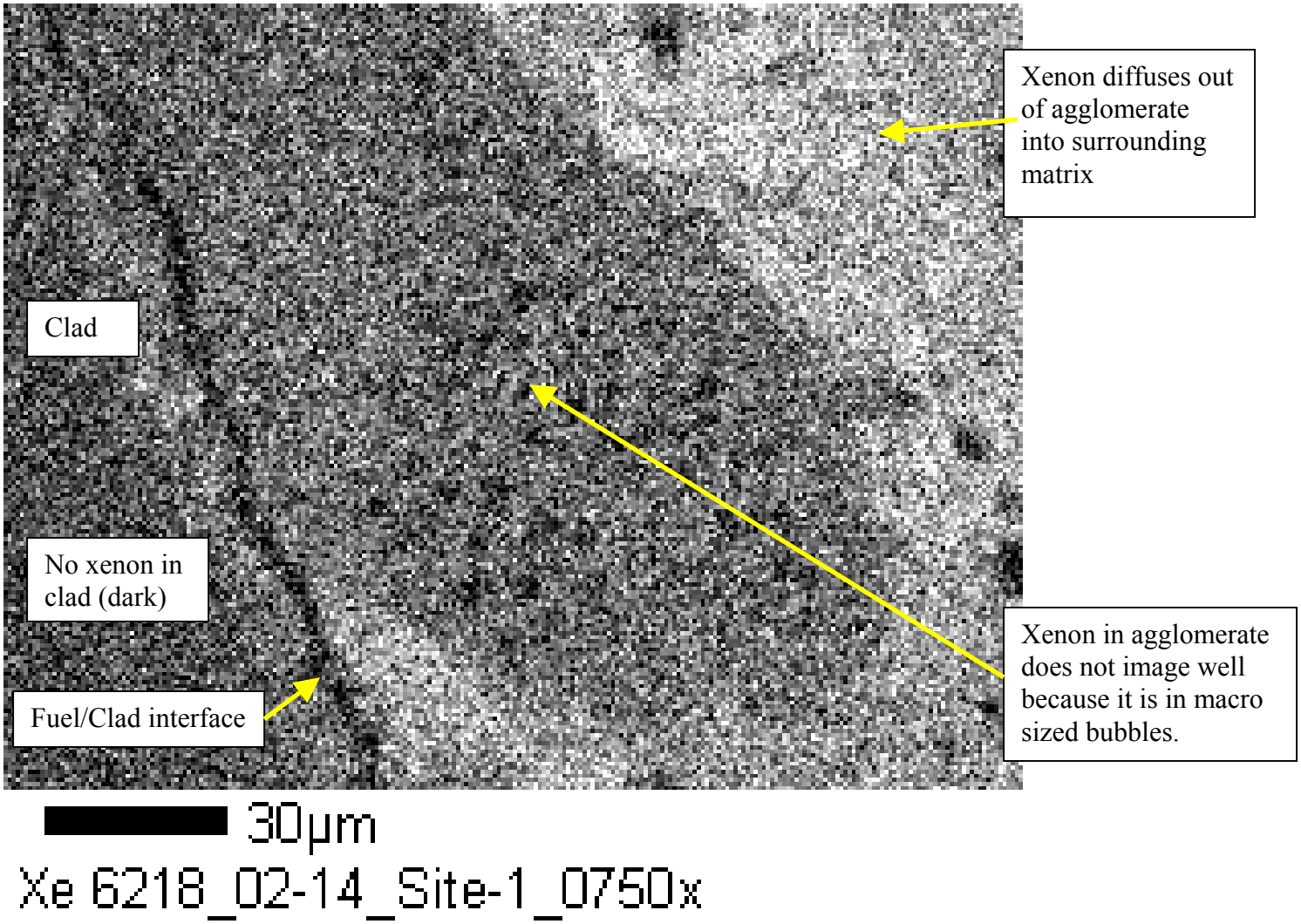

Figure 5.45 SEM/Microprobe Xe scan of Site 1 in Mount 6218.

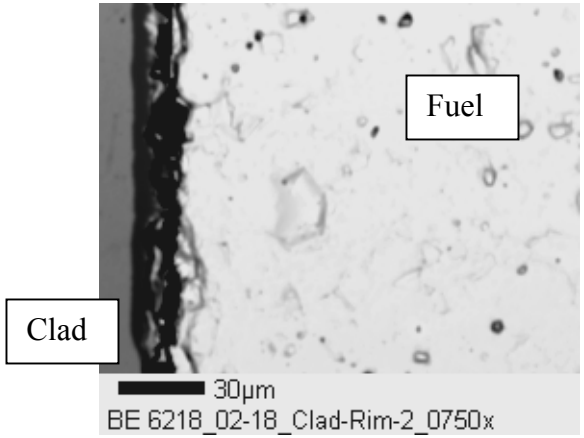

Back Scatter Electron Image

Fuel/clad region with no adhesion to clad. Note the featureless oxide layer

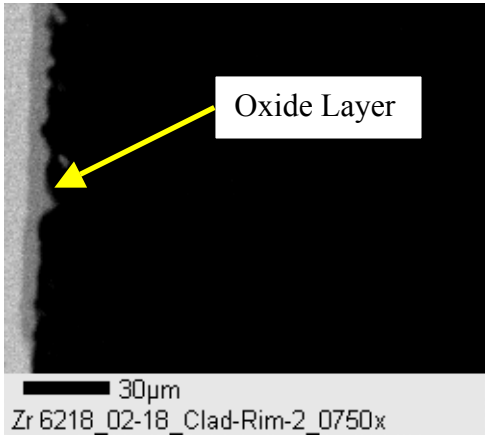

Zirconium Map

Agglomerate-free pellet/clad interfaces

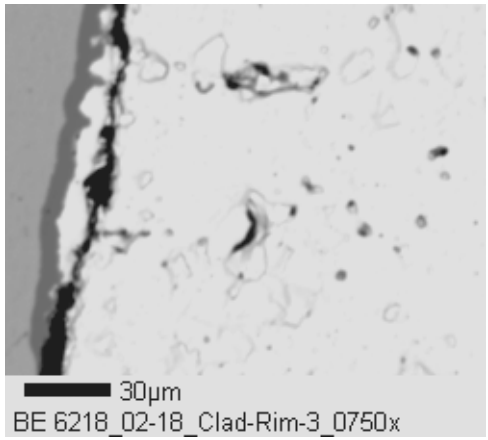

Back Scatter Electron Image

Fuel/clad region with adhesion to clad. Again, note the lack of fuel "fingers" in the oxide layer.

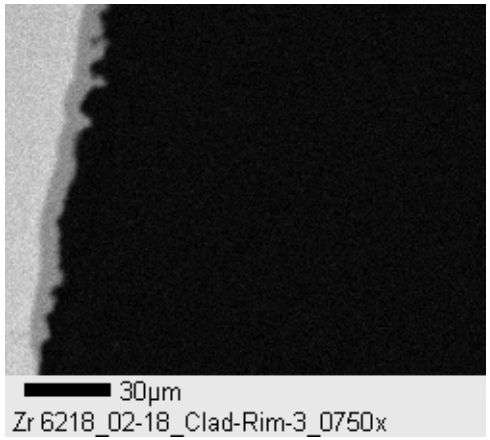

Zirconium Map

Figure 5.46 SEM/Microprobe scans for a fuel/clad region, Site 3, isolated from an agglomerate.

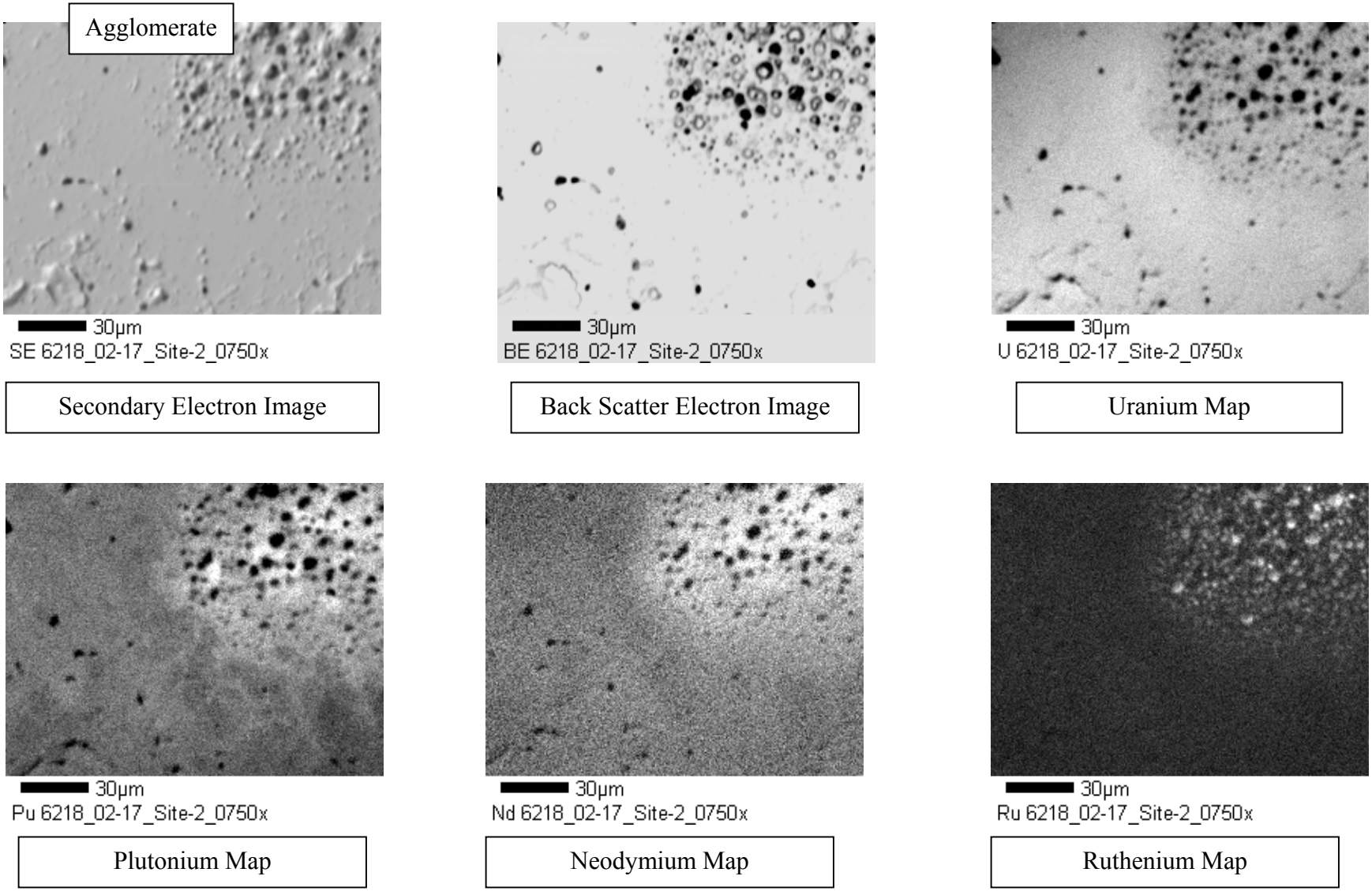

Figure 5.47 SEM/Microprobe scans for an internal agglomerate at Site 2

A small random region near the center of the pellet was also imaged, but other than some minor Pu rich regions, nothing distinctive was noted. In addition, the above sites were imaged for gallium, cesium, and oxygen, but again, no signs of any distinctive patterns were seen other than for oxygen which was concentrated in the fuel. The oxygen signal was too noisy to give decent imaging, however. Finally, a fracture surface was noted in Site 4. See Figure 5.48.

This region contained grooves and dimples that are believed to come from the accumulation and transport of fission gases. This behavior was also seen in an earlier PIE (30 GWd/MT).

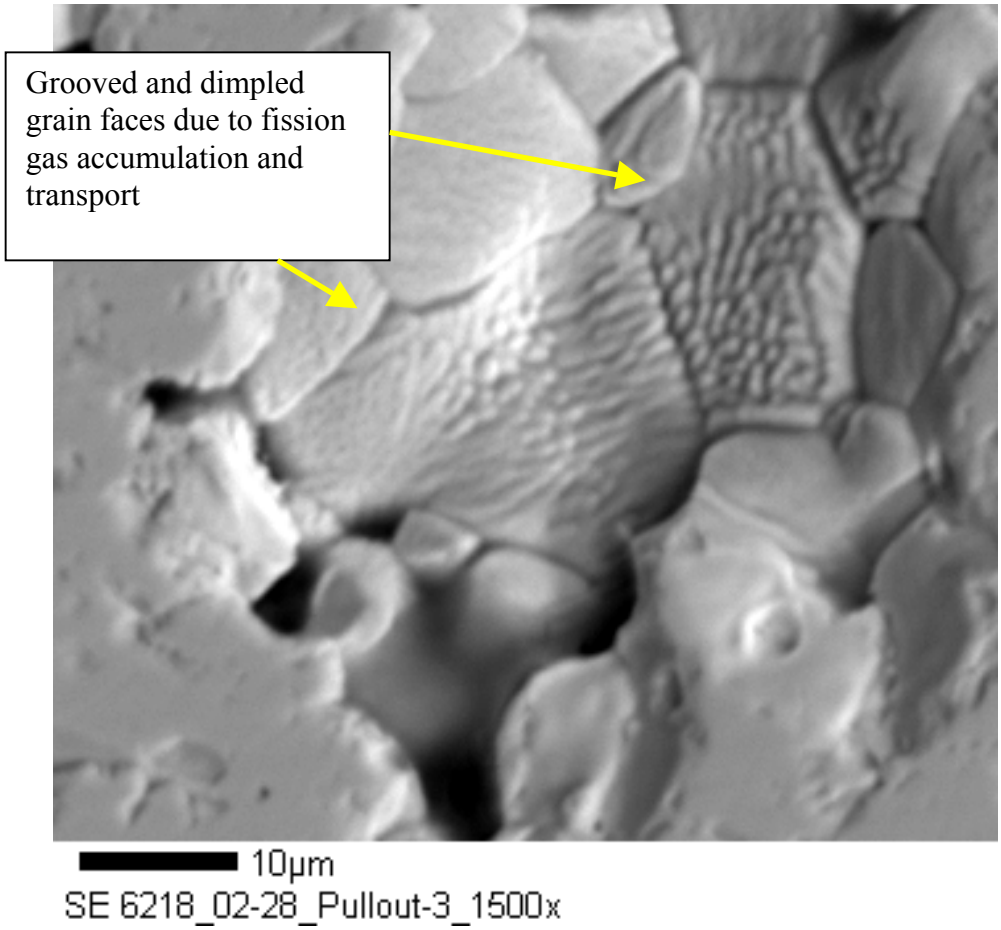

Figure 5.48 SEM/Microprobe scans for a grain boundary at Site 4.

5.6.2 Fuel Pin 16 SEM Mount

SEM examination of Fuel Pin 16 was conducted in a manner similar to that of Fuel Pin 7 and the results were also very similar. Figure 5.49 shows the polished cross section and the regions of interest. Site 1 is a set of small agglomerates near the pellet clad interface, Site 2 is an agglomerate near the mid radius of the pellet, Site 3 is the pellet clad region in the absence of a surface agglomerate, Sites 5 and 6 are agglomerates near the central region of the pellet, and Pull Out 1 is a fracture surface near the mid radius of the pellet.

Figure 5.50 shows the mapping of Site 1, two small agglomerates near the surface of the pellet. The results of this examination are very much the same as was seen in the mapping of a similar region for Fuel Pin 7. Again, one sees the concentration of plutonium and fission products in the agglomerates and the "fingers" of fuel diffusing into the clad oxide layer of similar thickness.

Mapping of Site 3, a region lacking a surface agglomerate, again shows the lack of fuel "fingers" in the clad oxide layer (Figure 5.51). A trace amount of plutonium (microagglomerate) is present about 25 microns from the clad, but it has only a minor influence on the interface behavior. The ruthenium map shows no strong presence of fission products.

Figure 5.52 is the mapping of Site 2, an internal agglomerate. The results are very similar to those seen for Pin 7, with the concentrating of plutonium and fission products in the agglomerate. Mapping the xenon is difficult (poor signal to noise ratio), but the same indications of outward diffusion from the agglomerate to the matrix can be observed.

During the irradiation, the edge regions of the pellet have always been cool enough for the characteristic agglomerate structure to develop; however, only during the last part of the irradiation has the central part of the pellet become cool enough for this structure to develop. It is useful to compare these two regions. Figure 5.53 compares these two regions and one can see that the edge agglomerate has a more complex structure and has smaller and higher density of "bubbles". The internal agglomerates lack the more complex structure, because of the much higher fission product diffusion rates at the higher temperatures seen over most of their history.

Finally, a fracture surface is shown in Figure 5.54. This image clearly shows the wavy surface tracks believed to be caused by diffusing fission gases and the grain structure. Because of the difficulty of getting uniform surfaces, no clear comparison can be made between Pin 7 and 16. However, the TIGR material has consistently had higher gas release and has been more friable during mount preparation, implying weaker bonding.

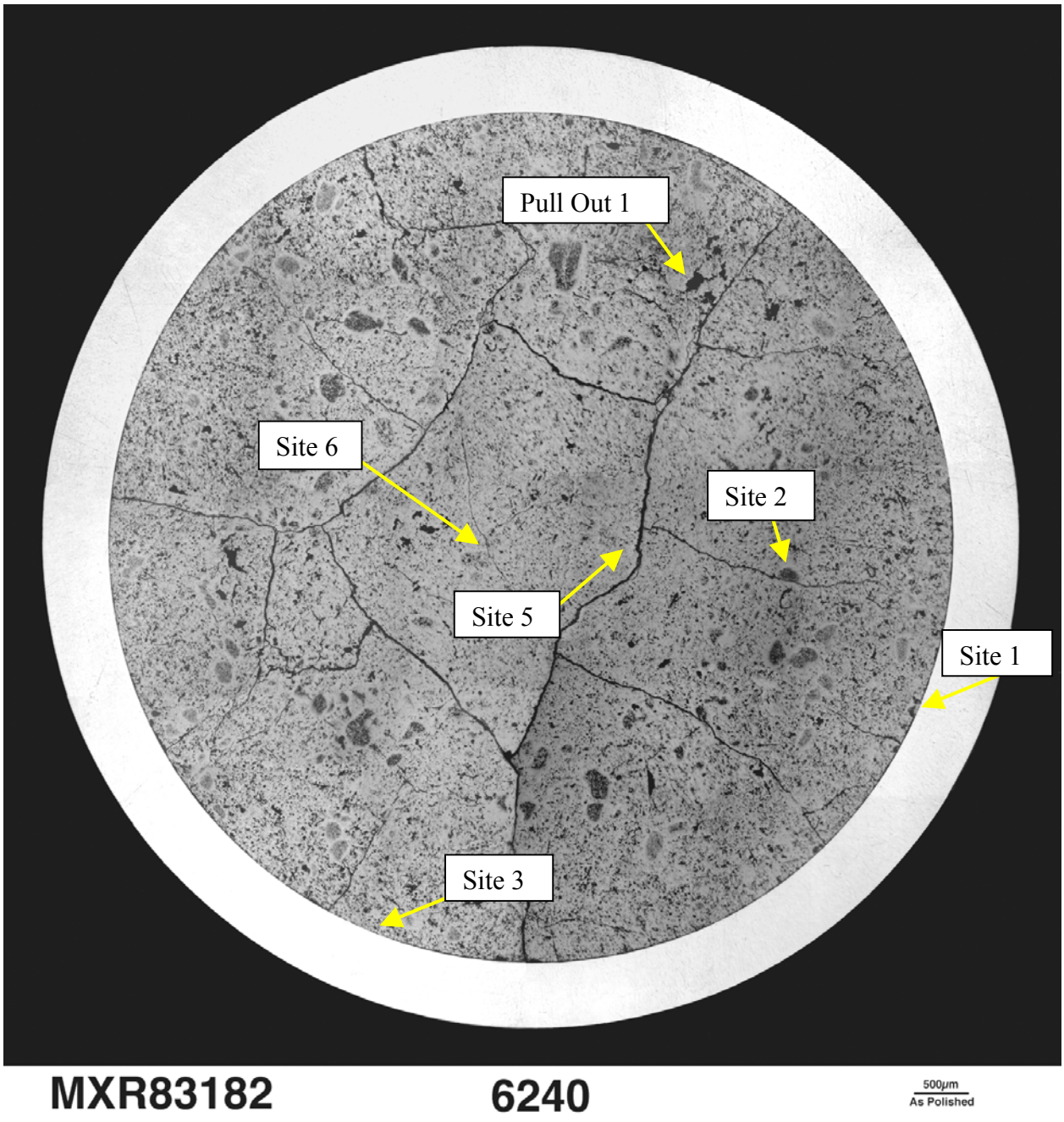

Figure 5.49 Composite photograph of mount used for SEM/Microprobe examination. (Note that there is no Site 4).

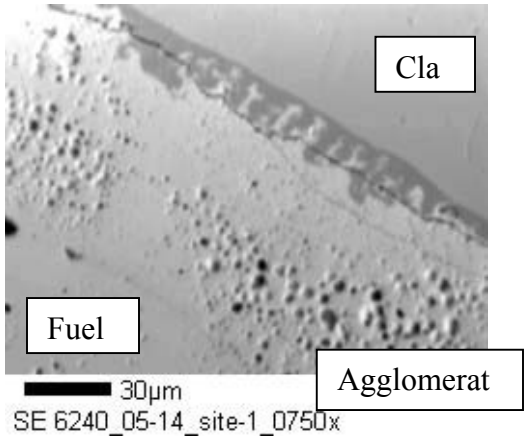

Secondary Electron Image

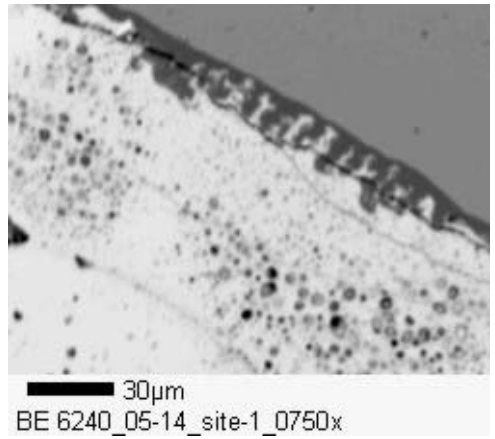

Back Scatter Electron Image

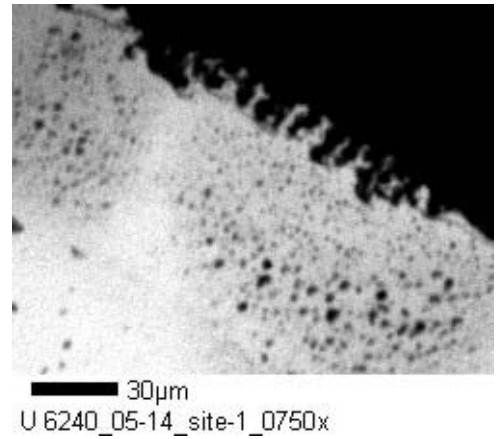

Uranium Map

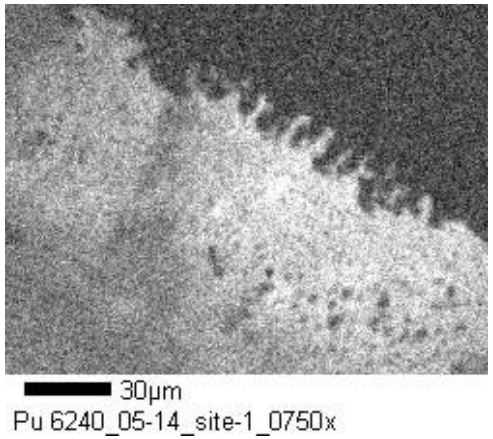

Plutonium Map

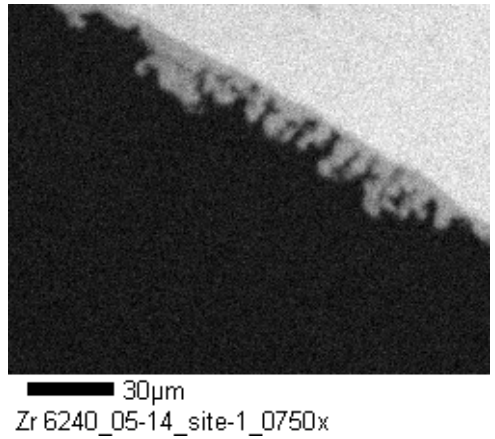

Zirconium Map

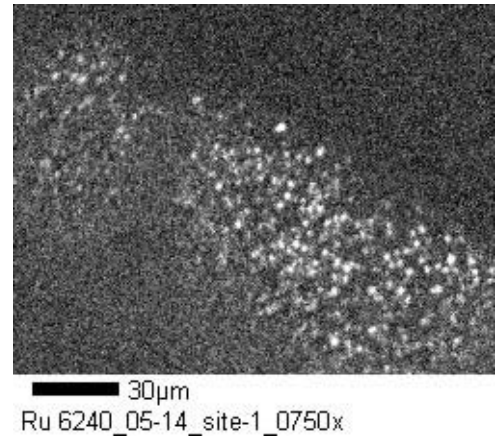

Ruthenium Map

Figure 5.50 SEM/Microprobe scans of Site 1 in Mount 6240.

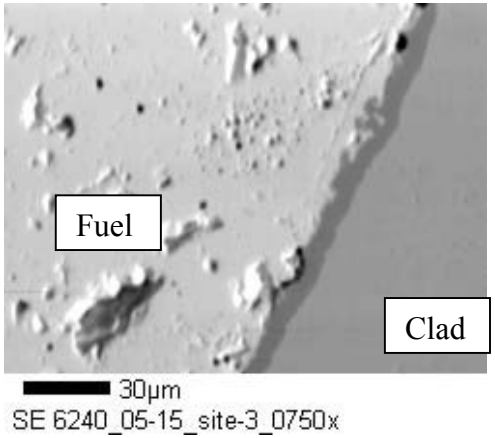

Secondary Electron Image

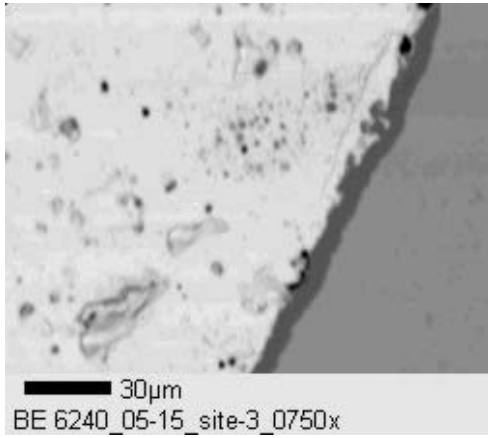

Back Scatter Electron Image

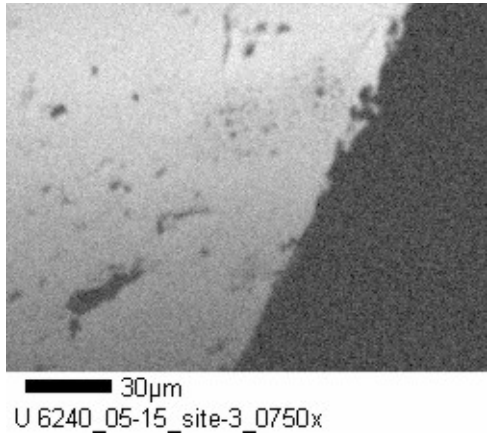

Uranium Map

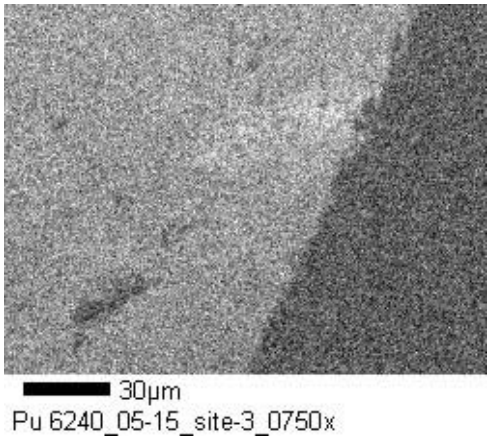

Plutonium Map

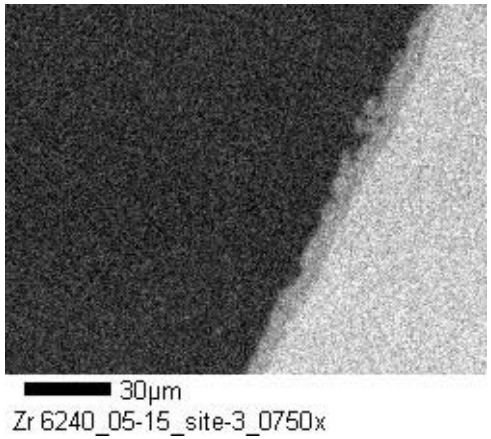

Zirconium Map

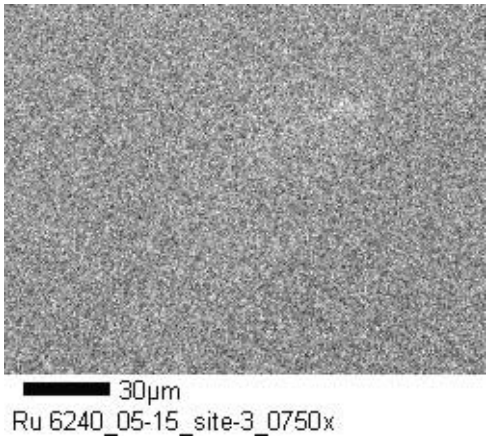

Ruthenium Map

Figure 5.51 SEM/Microprobe scans of Site 3 in Mount 6240.

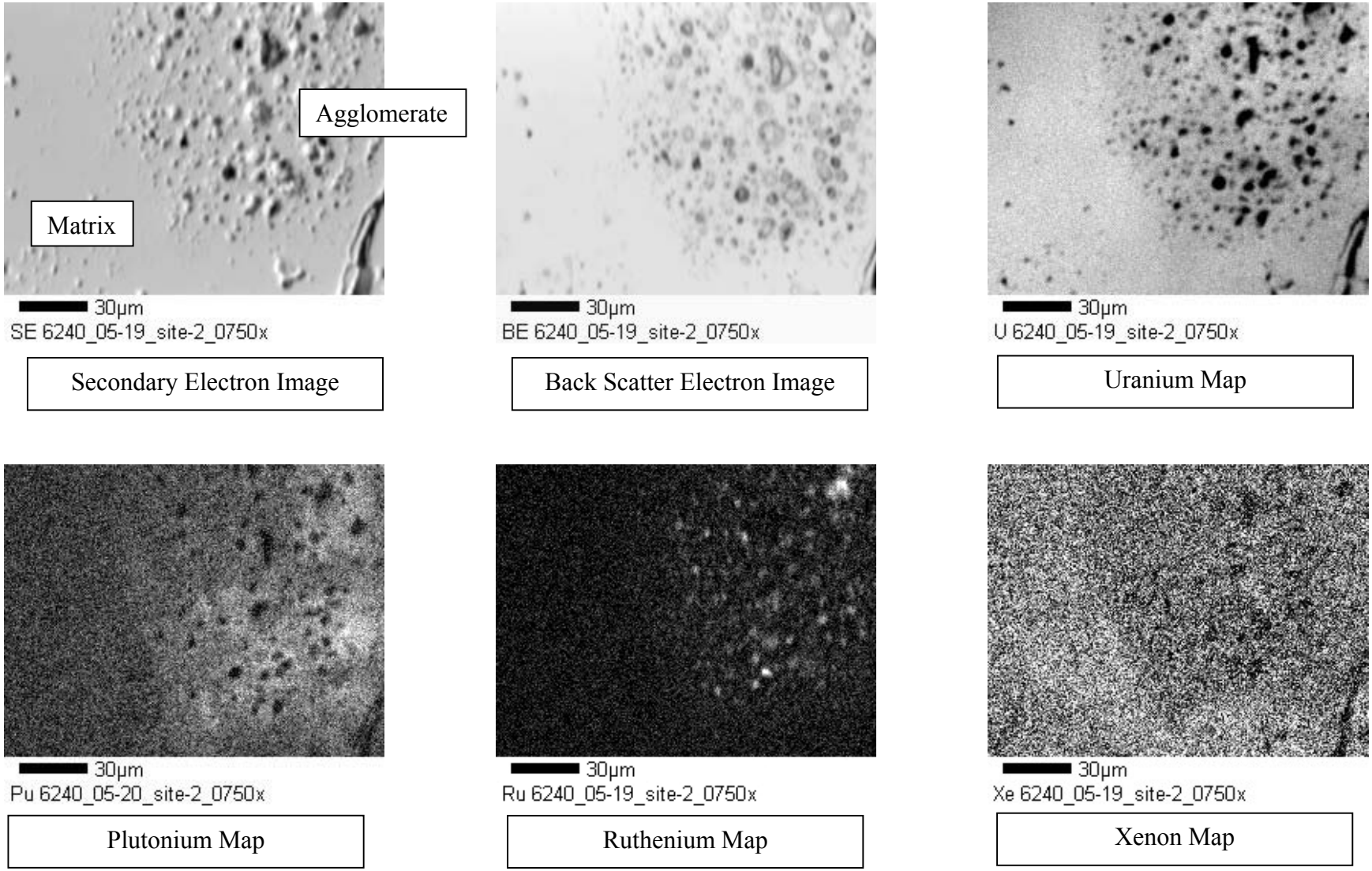

Figure 5.52 Mapping of Site 2, an internal agglomerate.

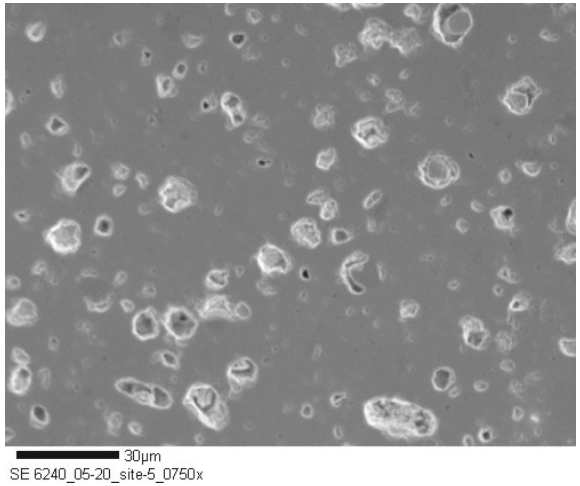

Site 5

Later forming agglomerates near the central region show a lower density of larger bubbles.

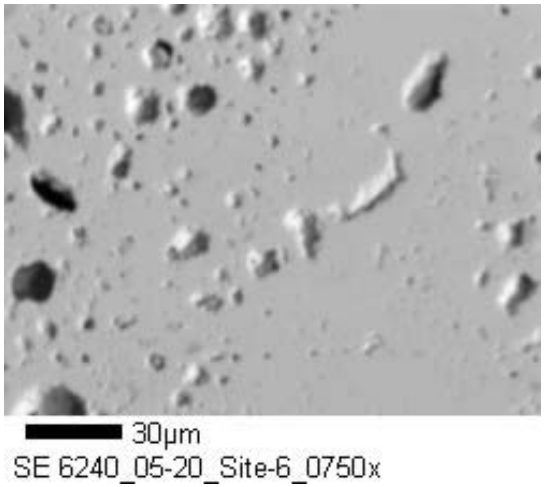

Site 6

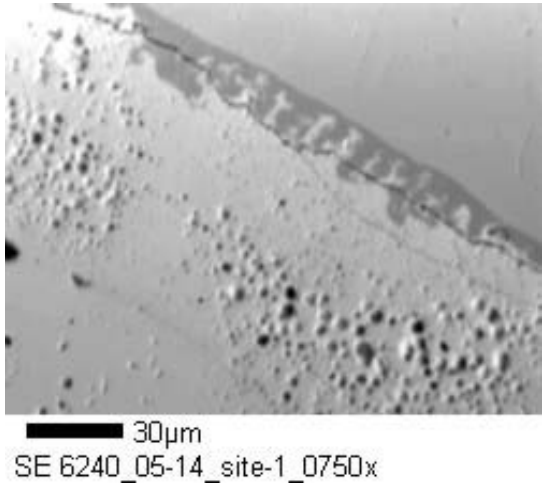

Site 1

Early forming agglomerate near the pellet edge shows high density of small bubbles

Figure 5.53 Comparison of internal and edge agglomerates.

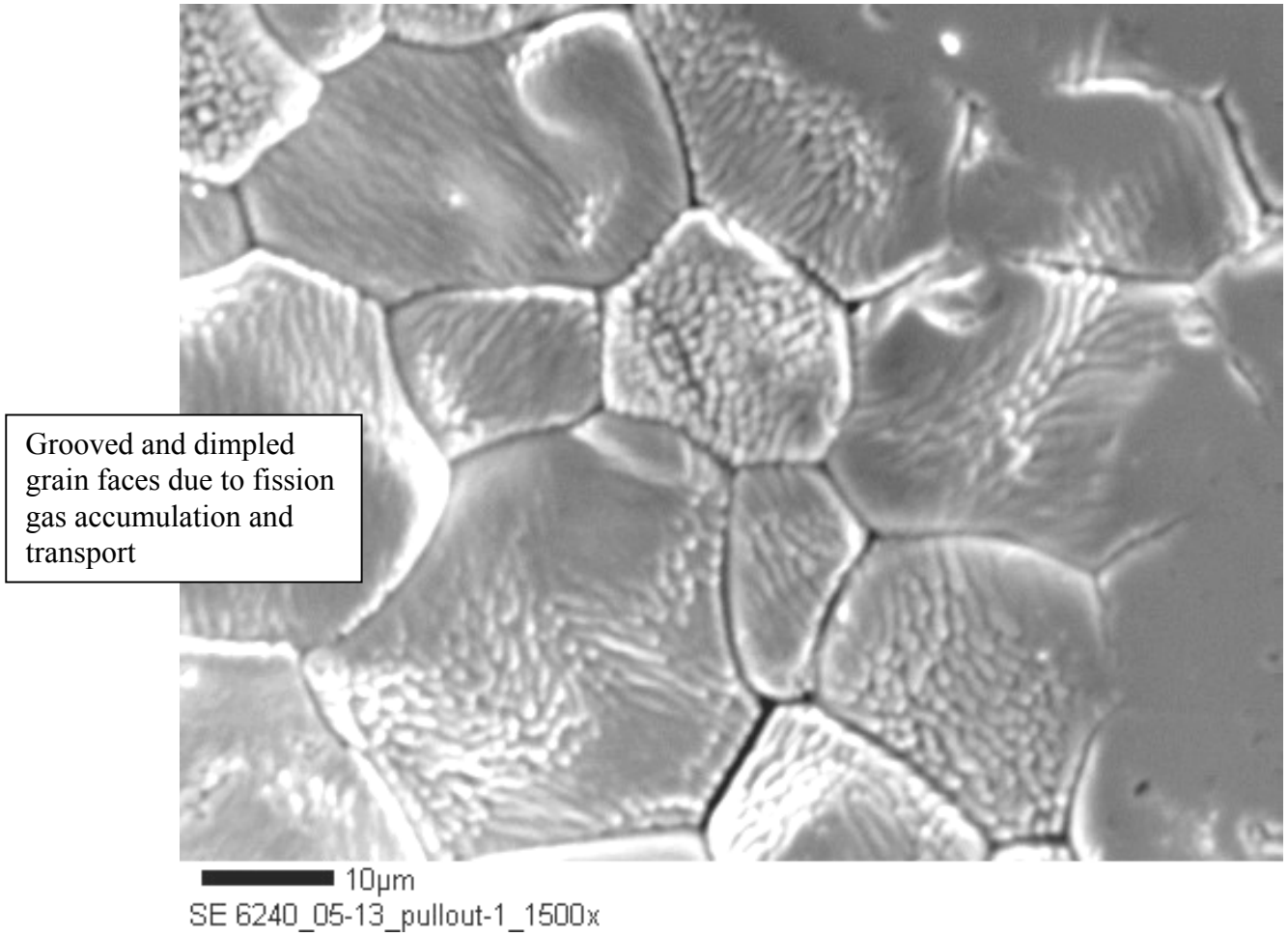

Figure 5.54 SEM image of a grain boundary at Pull Out 1.

5.7 Metallographic Summary

Seven metallographic mounts and two SEM mounts were prepared from Fuel Pins 7 and 16. All of these mounts indicate that the fuel is behaving in a normal fashion and the irradiation is proceeding as planned. Pellet cracking is similar to that seen in previous PIEs, the plutonium-rich agglomerates are similar to those seen in the 30 GWd/MT PIE, and the axial fuel section clearly shows that the pellet integrity is good and that the pellet swelling is proceeding in a predictable manner. Some differences were noted in the pellet central grain behavior, but the etching proved to be difficult to interpret. A small oxide layer is building up on the clad and it appears to be localized to regions of close pellet clad contact. A gamma scan of one mount confirmed the predicted diametral off center burnup of the pellet.

A SEM/Microprobe examination of the fuel confirmed the plutonium rich nature of the agglomerates, found no indication of a rim effect (as expected), and revealed no abnormal pellet-clad behavior. In the neighborhood of an agglomerate near the pellet surface, there are indications of fuel diffusing into the oxide layer. Mapping of the fission products Ru, Pd, and Nd showed them to be localized to the agglomerates without significant diffusion. One item of interest was the observation that the "halos" around the agglomerates are created by the diffusion of fission gas from the agglomerate. Imaging of fracture surfaces showed wavy tracks, believed to be due to the accumulation and diffusion of fission gases.

One general observation was that the TIGR treated material appeared to be more friable when making the thin SEM mounts, implying weaker internal bonding.

Details about observed pellet behavior versus modeling predictions are covered in Volume 2 of this report.

6. RADIOCHEMISTRY RESULTS

6.1 Introduction

Fuel Pin 7 (untreated fuel) was segmented as shown in Figures 6.1 and 6.2. Table 6.1 details the disposition of the specimens (metallographic tasks are detailed in Chapter 5.) The needs of fuel behavior, gallium tracking, and ductility testing are balanced in this segmenting plan.

Fuel Pin 16 (treated fuel) was segmented as shown in Figures 6.3 and 6.4. Table 6.2 details the disposition of the specimens. The Pin 16 segmenting plan preserves more cladding material for ductility testing at the expense of fewer metallographic mounts.

Fourteen pellet and clad specimens were sent to the Radioactive Materials Analysis Laboratory (RMAL) for determination of their gallium contents. Two of these specimens were long cladding sections that were to be defueled and returned for eventual ductility testing. In all, 7 clad specimens and 7 pellet specimens were to be analyzed for gallium (including the fuel containing ductility specimens), and 7 pellet specimens were to be analyzed for burnup (including the fuel-containing ductility specimens). Table 6.3 identifies the source (fuel pin location) for all of the gallium and burnup analyses.

In addition, a portion of the Capsule 4 stainless steel containment was also sent to Building 2026 to determine the source of the discoloration (see Section 6.4).

6.2 Gallium Analysis Results

The results of the fuel pin clad gallium analyses are shown in Table 6.4, and the results of the fuel pin pellet analyses are shown in Table 6.5. The fuel was removed from the clad specimens to be used for ductility testing by immersion in nitric acid. The fuel was dissolved in about three days time using concentrated (16 molar) nitric acid (HNO_3) at 120ºC.

After dissolution, the irradiated clad and pellet samples underwent a first separation step to remove the uranium and plutonium from the samples; a second separation step to remove the barium was then performed. Barium separation is useful because barium interferes with one of the gallium mass signals (number 69), forcing the analyst to rely only on the mass 71 signal (gallium has two stable isotopes of mass 69 and 71). Having clear signals on both mass 69 and 71 is useful because the ratio between the two signals can be compared to the naturally occurring mass ratio as a check on the accuracy of the analysis.

The plenum regions of the clad have somewhat lower gallium levels than the cladding located next to the fuel, but this may be consistent with the adherence of some fuel (and associated gallium) to the inner surface of the clad. The clad specimens were only lightly brushed, not scraped, to avoid removing any surface layers. It should be noted that even if some gallium transfer from the fuel to the clad occurred, the magnitude of the transfer is insignificant.

As a reference, the un-irradiated clad average gallium content is 589 ppb, the untreated fuel average gallium content is 2.97 ppm, and the average TIGR treated fuel gallium content is 1.33 ppm [Reference 17].

The sample with the greatest observed clad gallium concentration, FP-16-C-4, was from a fuel pin containing TIGR treated material (Table 6.4). The fuel enclosed by this clad specimen, FP-16-P-2, also had its gallium content measured (Table 6.5) and the mass ratio of the fuel to its surrounding clad is 4.56 (column 3 of Tables 6.4 and 6.5). If one assumes that all the additional gallium in the clad came from the enclosed fuel, then the initial gallium concentration in the fuel would be:

$$C_{initial} = C_{final} + \frac{\Delta C_{clad}}{M_r}$$

where $C_{initial}$ is the fuel initial gallium concentration, C_{final} is the post irradiation measured gallium concentration, ΔC_{clad} is the measured change in the clad gallium concentration, and M_r is the enclosed fuel to clad mass ratio. Using the above numerical values gives a $C_{initial}$ for FP-16-P-2 of 1.49 ppm.

The fraction of gallium transferred to the clad is:

$$F = \frac{\Delta C_{clad}}{M_r C_{initial}}$$

where F is the fraction transferred. For the fuel and clad specimens under study, F is 7.4%, assuming no fuel carryover contamination. Thus, the worst case gallium transfer can be estimated at 7.4%. The rest of the samples had gallium concentrations near (or somewhat lower than) their pre-irradiation values.

Overall, the difference between the unirradiated and the irradiated clad gallium concentrations indicates negligible transfer of gallium to the cladding, with the specimen average gallium concentrations of 605 and 699 ng/g within 20% of the unirradiated value. The mass average clad values of 514 and 523 ng/g were also near the unirradiated cladding average of 589 ng/g. The larger mass and lower gallium concentrations of the plenum regions tend to reduce the mass average.

The plenum region of both fuel pins has a somewhat lower (approximately one standard deviation) gallium concentration value. The 30 GWd/MT clad plenum regions had gallium concentrations of 472 and 492 ng/g, also lower than the unirradiated average. This phenomenon will be reviewed at the next PIE to determine if it is an actual trend.

The pellet gallium levels vary as has been seen in the past, with the mass average for each pellet stack comparable to the previously measured unirradiated values of 2.97 ppm for untreated fuel and 1.33 ppm for TIGR fuel.

Detailed Cutting Guide for Top Half of Fuel Pin 7

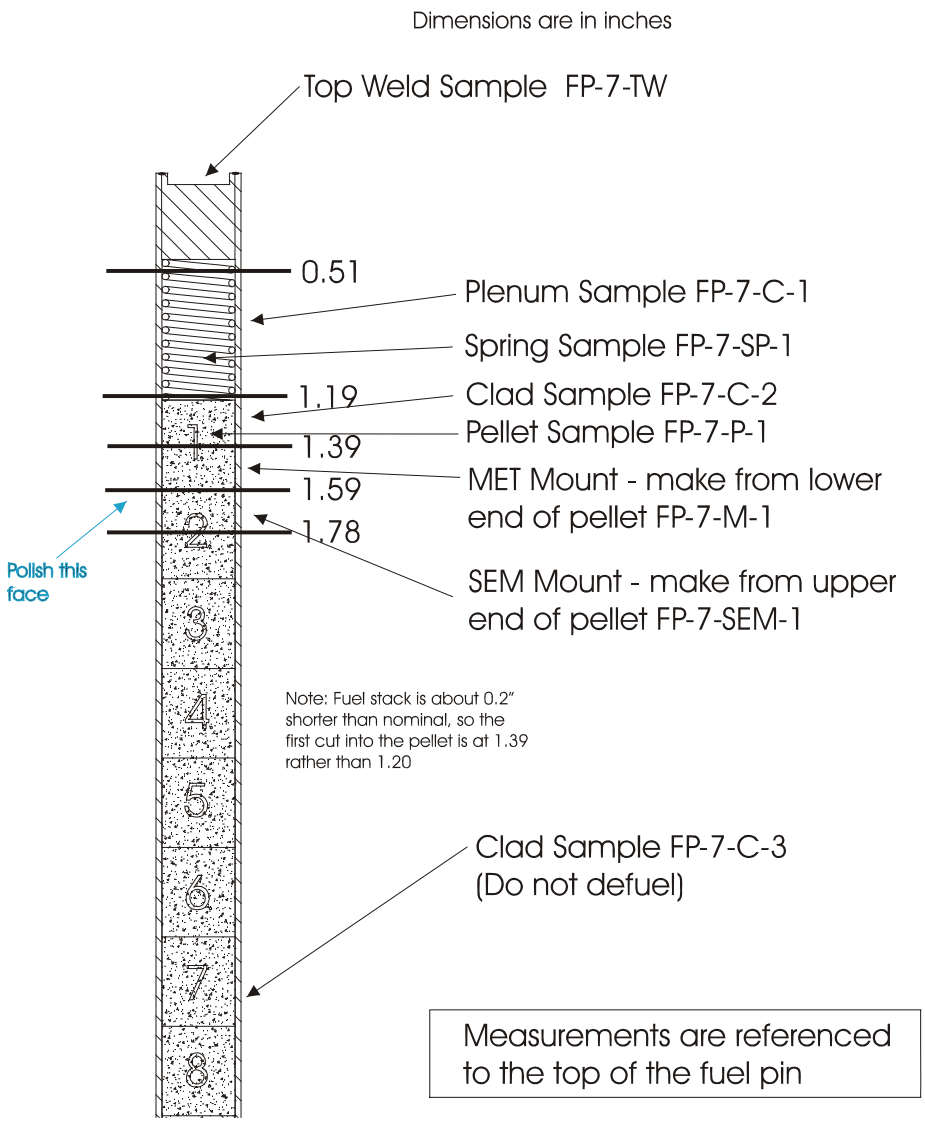

Figure 6.1 Fuel Pin 7 top cutting guide.

Detailed Cutting Guide for Bottom Half of Fuel Pin 7

Dimensions are in inches

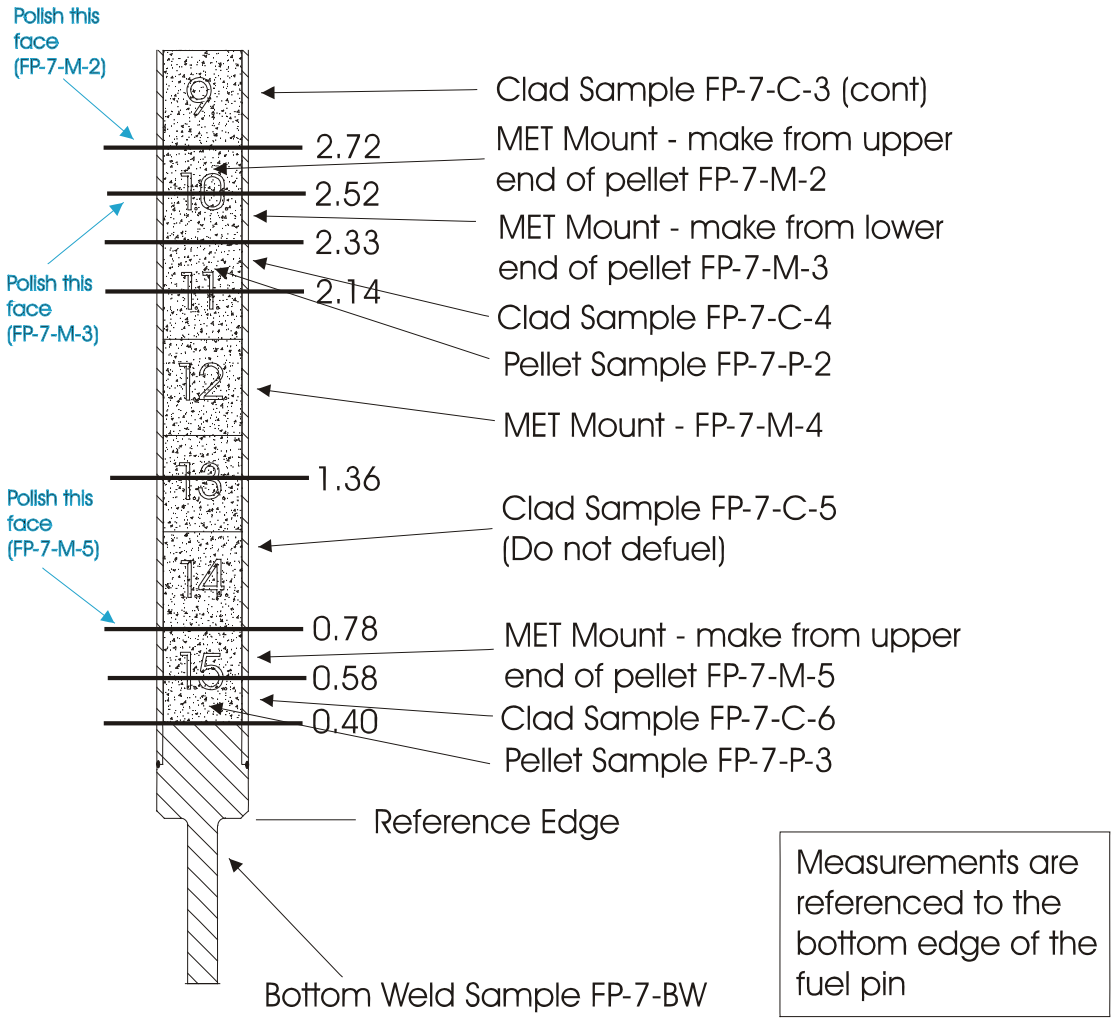

Figure 6.2 Fuel Pin 7 bottom cutting guide.

Detailed Cutting Guide for Top Half of Fuel Pin 16

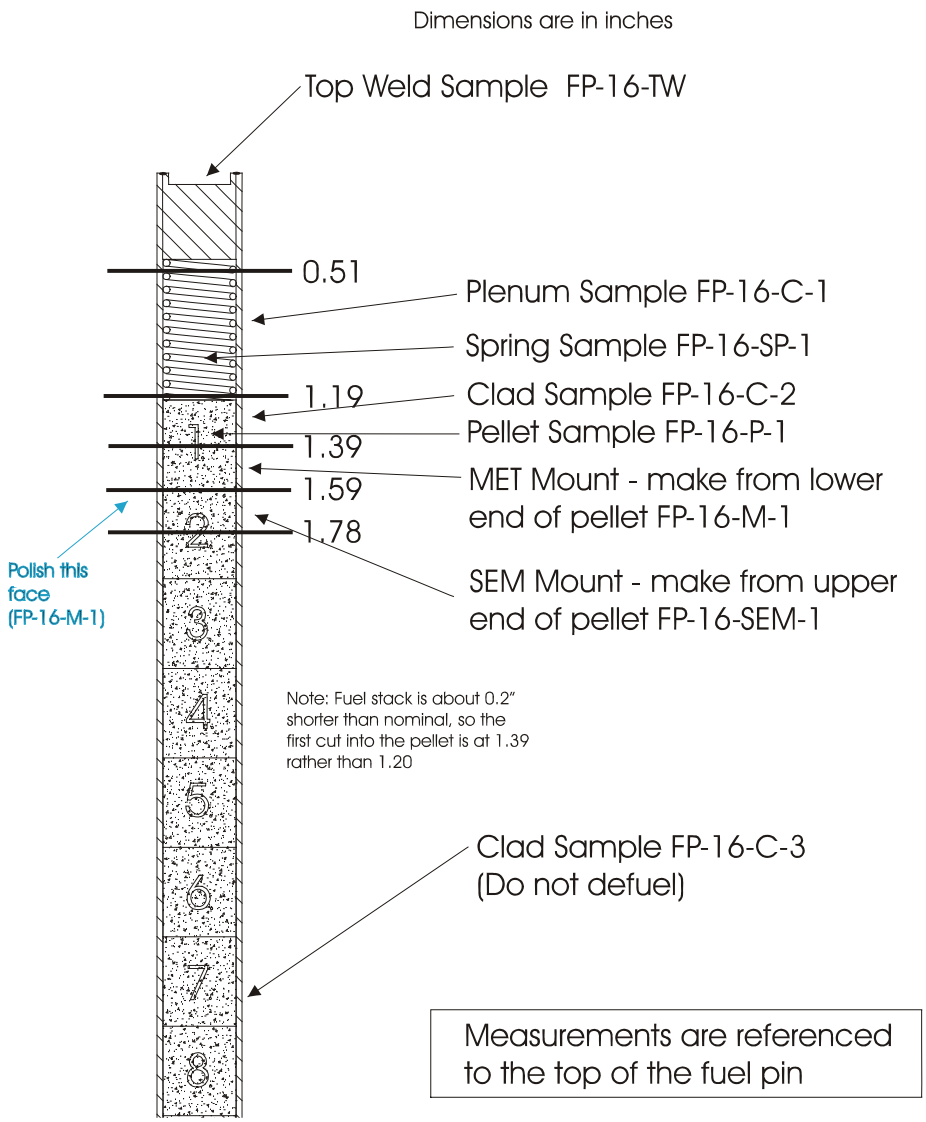

Figure 6.3 Fuel Pin 16 top cutting guide.

Detailed Cutting Guide for Bottom Half of Fuel Pin 16

Dimensions are in inches

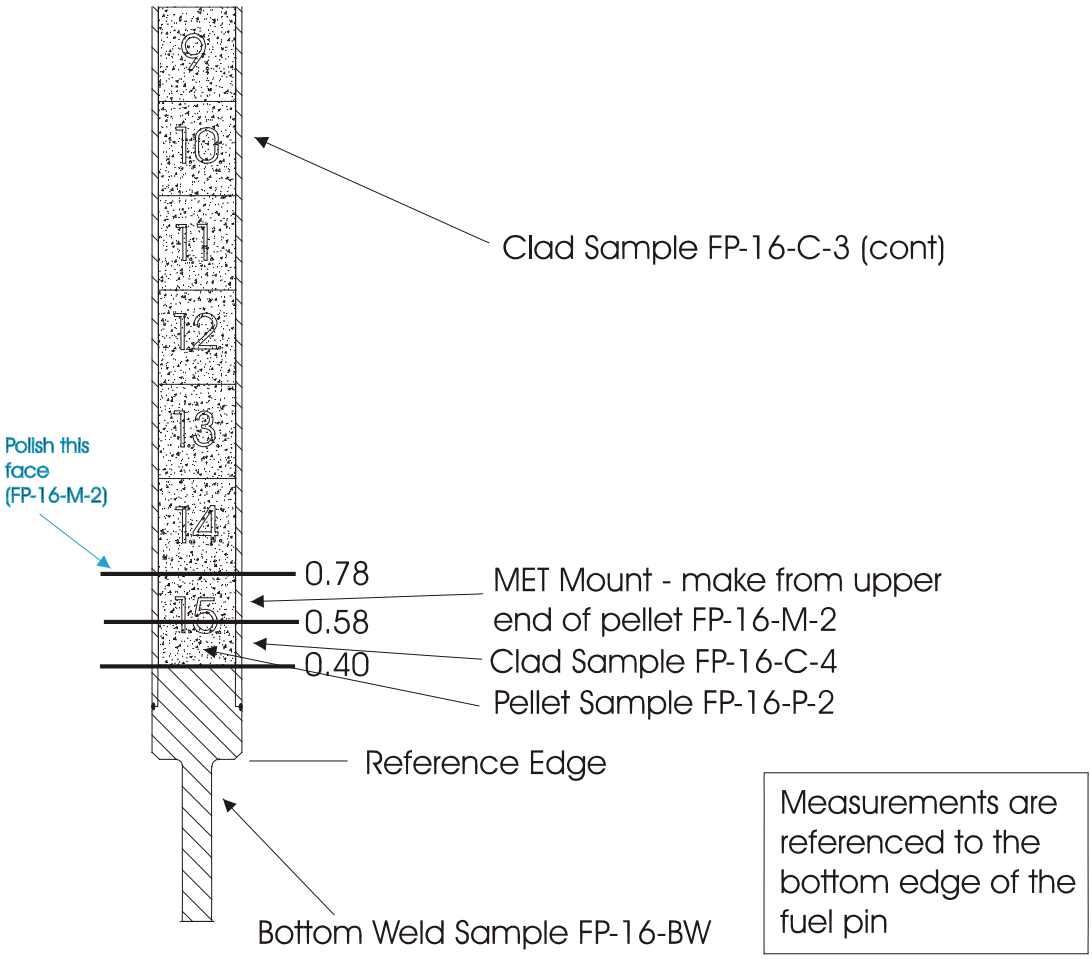

Figure 6.4 Fuel Pin 16 bottom cutting guide.

Table 6.1 Fuel Pin 7 Sampling

Specimen	Location	Interest	Disposition
FP-7-C-1	Plenum Clad	Ga Analysis	Radiochemistry
FP-7-C-2	Top ½ of Pellet 1 Clad	Ga Analysis	Radiochemistry
FP-7-C-3	Pellets 1½ to 9 Clad	Ductility Testing, burnup, and gallium	Clad ductility testing, radiochemistry (Fuel will be removed at 2026 as a batch and analyzed)
FP-7-C-4	Top ½ of Pellet 11 Clad	Ga Analysis	Radiochemistry
FP-7-C-5	Pellets 13½ to 14 with Clad	Reserve	Archive (Fuel will be left in clad)
FP-7-C-6	Bottom ½ of Pellet 15 Clad	Ga Analysis	Radiochemistry
FP-7-P-1	Top ½ of Pellet 1	Ga Analysis and Burnup	Radiochemistry
FP-7-P-2	Top ½ of Pellet 11	Ga Analysis and Burnup	Radiochemistry
FP-7-P-3	Bottom ½ of Pellet 15	Ga Analysis and Burnup	Radiochemistry
FP-7-TW	Top Weld	Reserve	Archive
FP-7-BW	Bottom Weld	Reserve	Archive
FP-7-SP-1	Spring	Reserve	Archive
FP-7-M-1	Bottom ½ of Pellet 1 with clad	Microstructure	Metallography
FP-7-M-2	Top ½ of Pellet 10 with clad	Microstructure	Metallography
FP-7-M-3	Bottom ½ of Pellet 10 with clad	Microstructure	Metallography
FP-7-M-4	Pellets 11½ through 12½ with clad (axial)	Microstructure	Metallography
FP-7-M-5	Top ½ of Pellet 15 with Clad	Microstructure	Metallography
FP-7-SEM-1	Top ½ of Pellet 2 with Clad	Microstructure	SEM/Microprobe

Table 6.2 Fuel Pin 16 Sampling

Specimen	Location	Interest	Disposition
FP-16-C-1	Plenum Clad	Ga Analysis	Radiochemistry
FP-16-C-2	Top ½ of Pellet 1 Clad	Ga Analysis	Radiochemistry
FP-16-C-3	Pellets 1½ to 14 Clad	Ductility Testing, burnup, and gallium	Clad ductility testing, radiochemistry (Fuel will be removed at 2026 as a batch and analyzed)
FP-16-C-4	Bottom ½ of Pellet 15 Clad	Ga Analysis	Radiochemistry
FP-16-P-1	Top ½ of Pellet 1	Ga Analysis and Burnup	Radiochemistry
FP-16-P-2	Bottom ½ of Pellet 15	Ga Analysis and Burnup	Radiochemistry
FP-16-TW	Top Weld	Reserve	Archive
FP-16-BW	Bottom Weld	Reserve	Archive
FP-16-SP-1	Spring	Reserve	Archive
FP-16-M-1	Bottom ½ of Pellet 1 with clad	Microstructure	Metallography
FP-16-M-2	Top ½ of Pellet 15 with clad	Microstructure	Metallography
FP-16-SEM-1	Top ½ of Pellet 2 with Clad	Microstructure	SEM/Microprobe

Table 6.3 Radiochemical Samples for Building 2026

Specimen	Location	Interest	Disposition
FP-7-C-1	Plenum Clad	Ga Analysis	Radiochemistry
FP-7-C-2	Top ½ of Pellet 1 Clad	Ga Analysis	Radiochemistry
FP-7-C-3	Pellets 1½ to 9 Clad	Ductility Testing, burnup, and gallium	Clad ductility testing, radiochemistry (Fuel will be removed at 2026 as a batch and analyzed, see note.)
FP-7-C-4	Top ½ of Pellet 11 Clad	Ga Analysis	Radiochemistry
FP-7-C-6	Bottom ½ of Pellet 15 Clad	Ga Analysis	Radiochemistry
FP-7-P-1	Top ½ of Pellet 1	Ga Analysis and Burnup	Radiochemistry
FP-7-P-2	Top ½ of Pellet 11	Ga Analysis and Burnup	Radiochemistry
FP-7-P-3	Bottom ½ of Pellet 15	Ga Analysis and Burnup	Radiochemistry
FP-16-C-1	Plenum Clad	Ga Analysis	Radiochemistry
FP-16-C-2	Top ½ of Pellet 1 Clad	Ga Analysis	Radiochemistry
FP-16-C-3	Pellets 1½ to 14 Clad	Ductility Testing, burnup, and gallium	Clad ductility testing, radiochemistry (Fuel will be removed at 2026 as a batch and analyzed, see note.)
FP-16-C-4	Bottom ½ of Pellet 15 Clad	Ga Analysis	Radiochemistry
FP-16-P-1	Top ½ of Pellet 1	Ga Analysis and Burnup	Radiochemistry
FP-16-P-2	Bottom ½ of Pellet 15	Ga Analysis and Burnup	Radiochemistry

Note: The fuel will be removed from specimens FP-7-C-3 and FP-16-C-3, individually, at Building 2026 by soaking in nitric acid (no halogens). The clad will then be washed and shipped back to Building 3525 for ductility testing. The remaining fuel will then be completely dissolved and analyzed for burnup and gallium.

Table 6.4 Irradiated Clad Results

Specimen	Location	Mass (grams)	Measured Gallium Concentration (ng/g)
FP-7-C-1	Plenum Clad	2.132	389 ±20%
FP-7-C-2	Top ½ of Pellet 1 Clad	0.586	734 ±10%
FP-7-C-4	Top ½ of Pellet 11 Clad	0.515	657 ±10%
FP-7-C-6	Bottom ½ of Pellet 15 Clad	0.505	639 ±10%
Fuel Pin 7 Average			605
Standard Deviation			150
Mass Average			514
FP-16-C-1	Plenum Clad	1.983	338 ±20%
FP-16-C-2	Top ½ of Pellet 1 Clad	0.576	668 ±10%
FP-16-C-4	Bottom ½ of Pellet 15 Clad	0.501	1090 ±10%
Fuel Pin 16 Average			699
Standard Deviation			377
Mass Average			523

Table 6.5 Pellet Results

Specimen	Location	Mass (grams)	Measured Gallium Concentration (µg/g)
FP-7-C-3	Pellets 1½ to 9	39.98	2.45 ±10%
FP-7-P-1	Top ½ of Pellet 1	2.479	5.33 ±10%
FP-7-P-2	Top ½ of Pellet 11	2.267	2.15 ±10%
FP-7-P-3	Bottom ½ of Pellet 15	2.244	4.49 ±10%
Fuel Pin 7 Average			3.61
Standard Deviation			1.55
Mass Average			2.68
FP-16-C-3	Pellets 1½ to 14	67.89	1.00 ±10%
FP-16-P-1	Top ½ of Pellet 1	2.428	2.20 ±10%
FP-16-P-2	Bottom ½ of Pellet 15	2.285	1.38 ±10%
Fuel Pin 16 Average			1.53
Standard Deviation			0.61
Mass Average			1.05

6.3 Burnup Analysis

The results of the burnup analysis are shown in Tables 6.6 through 6.13. Fuel Pin 7 has a mass averaged measured burnup value of 38.9 GWd/MT and Fuel Pin 16 has a mass averaged burnup value of 39.4 GWd/MT. The burnup peaking on the fuel stack ends is expected. The agreement between the measured average and the calculated average is within approximately 2%. The greatest individual difference is less than 5%.

The burnup analysis method was essentially that detailed in *ASTM E 321 Standard Test for Atom Percent Fission in Uranium and Plutonium Fuel (Neodymium-148 Method).* The fuel burnup is derived from knowledge of the number of fissions that have occurred in a given fuel mass. The number of fissions is derived from the number of Neodymium (in particular, ^{148}Nd) atoms present (determined via radiochemistry and mass spectrometry) and knowledge of the Nd yield (Nd atoms produced per fission).

In practice, since each fissioning isotope has its own Nd yield, an effective Nd yield is calculated from a breakdown of the fission total into the fractions by ^{239}Pu, ^{241}Pu, ^{235}U, and ^{238}U (fast). An additional adjustment is necessary because a small portion of the ^{148}Nd is not generated directly by fission, but rather by neutron capture in ^{147}Nd. The overall correction factor for these effects as a function of burnup was taken from the curve in Figure 3 of Reference 26. The MCNP calculations from which this curve was developed are specific to this MOX irradiation test.

At 40 GWd/MT, this overall correction factor is 0.9770. For the irradiation history of these capsules, the composite ^{148}Nd yield is 0.016422. The effective ^{148}Nd yield appropriate to the current 40 GWd/MT fuel is then 0.016422/0.9770, or 0.016809 ^{148}Nd atoms per fission.

The estimated accuracy of the radiochemistry burnup determination is approximately 5%; the estimated code accuracy (MCNP and FRAPCON codes) is 7%.

6.4 Capsule 4 & 13 Surface Investigation

The surface discolorations on both capsules were investigated by visual, metallographic, and radiochemical means. Lengths from Capsules 4 and 13 were prepared by first cutting a ring from the capsule and then splitting this ring into two half sections so that the inside surface could be easily viewed. Three areas were examined. The first was the heat-affected zone from the weld near the bottom of Capsule 4. Examination revealed that the discoloration due to the welding was observable on both the inside and outside of the weld, implying that discoloration due to overheating would be visible on both the inside and outside surfaces of the capsule.

This same ring cutting and splitting was conducted on a discolored section of Capsule 4 and at the interface of the discoloration and shiny part of Capsule 13. Both examinations showed that the inside surfaces of the capsule were not discolored. Finally, a ring section of Capsule 4 was mounted and polished. The layer was too thin to be observed visually, so it was examined by SEM. This capsule wall mount is shown in Figure 6.5.

Table 6.6 Pellet Burnup Results

Specimen	Location	Mass (grams)	Measured Burnup (GWd/MT)	Calculated Burnup (GWd/MT)
FP-7-P-1	Top ½ of Pellet 1	2.479	41.8	42.9
FP-7-P-2	Top ½ of Pellet 11	2.267	38.0	39.4
FP-7-C-3	Bottom ½ of Pellet 2 through Pellet 9	39.981	38.7	39.5
FP-7-P-3	Bottom ½ of Pellet 15	2.244	41.1	41.7
Fuel Pin 7 Mass Average			38.9	39.8
FP-16-P-1	Top ½ of Pellet 1	2.428	41.9	43.8
FP-16-C-3	Bottom ½ of Pellet 2 through Pellet 14	67.889	39.2	39.6
FP-16-P-2	Bottom ½ of Pellet 15	2.428	41.1	40.8
Fuel Pin 16 Mass Average			39.4	39.8

The only information that could be obtained from this mount was that the surface layer is very thin, beyond what could be imaged by the equipment. No elemental analysis was obtained. The bright regions at the interface between the clad and the mounting medium are artifacts of the imaging and not indications of any specific element.

The film on Capsule 4 also underwent some chemical testing. Unirradiated stainless steel specimens heated in air (from the INEEL) were etched in nitric acid to determine the relative rates of material removal as a function of heating temperature. Less metallic material was removed from the specimens heated at higher temperatures (more discolored), apparently because the oxide layer impedes transfer of the underlying metals.

A section of Capsule 4 containing both shiny and discolored regions was etched in a similar manner and it was noted that the shiny end transferred more metallic material to the solution than the discolored end. However, it was also noted that the amount of metal transferred to solution was much greater than that seen with the heated unirradiated samples.

These two sets of results imply that the discoloration is not due to a temperature effect (capsule overheating). The discoloration is a very thin surface film, source unknown.

6.5 Radiochemical Summary

The analysis of the irradiated clad indicated negligible transfer of gallium from the fuel to the clad. At this point, it may be safely assumed that the trace gallium present in the fuel is not migrating out to the clad at a significant rate and presents no credible danger to the continued irradiation of the fuel pins.

Burnup analyses for these 40 GWd/MT fuel specimens proceeded very smoothly. Individual

fuel pin burnup results are within 5% of the calculated value and the two-pin burnup average essentially agrees with the calculations.

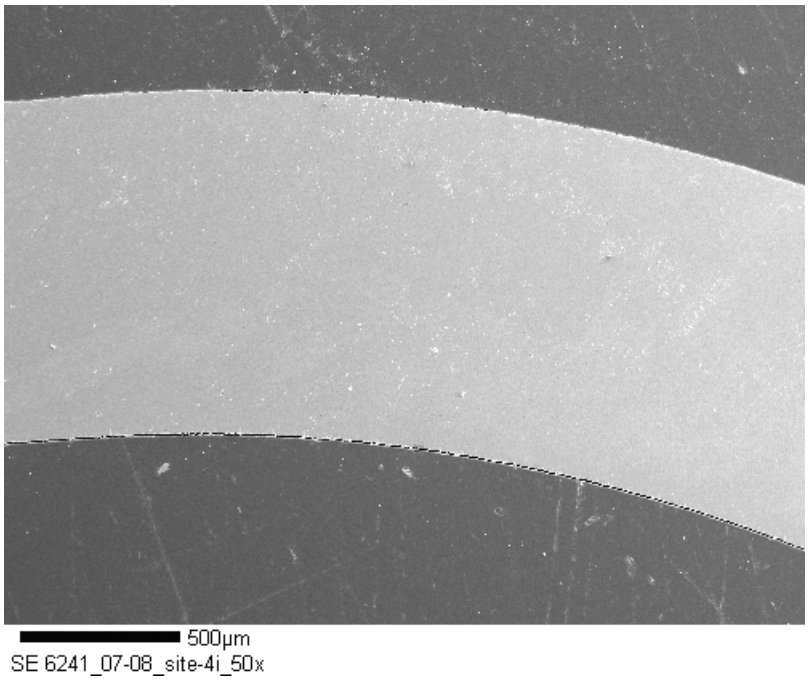

Figure 6.5 Capsule 4 wall MET mount.

Table 6.7 Burnup Results for FP-7-P-1.

ICPMS Burn-up Data **Sample: FP-7-P-1**

2.479 g fuel pellet N_A = 6.02E+23 atoms/mole

Uranium	wt. %	Plutonium	wt. %	Neodymium	wt. %
				^{140}Nd	
				^{142}Nd	0.0000%
^{233}U	0.0001%	^{238}Pu	0.0000%	^{143}Nd	15.5735%
^{234}U	0.0007%	^{239}Pu	25.0499%	^{144}Nd	31.6719%
^{235}U	0.0440%	^{240}Pu	50.8443%	^{145}Nd	17.4889%
^{236}U	0.0349%	^{241}Pu	13.4306%	^{146}Nd	17.7771%
^{238}U	99.9203%	^{242}Pu	10.6752%	^{148}Nd	10.9518%
		^{244}Pu	0.0000%	^{150}Nd	6.5368%
	100.0000%		100.0000%		100.0000%
Total (mg/g)[1]	**835.43**		**15.97**		**3.688**
Total (mg)	**2071**		**39.59**		**9.14**

[1] Concentration in sample with units of mg of element per gram of sample.

$^{235}U_R$	0.367	mg/g	$^{239}Pu_R$	3.982	mg/g
$^{235}U_R$	9.42E+17	atoms/g	$^{239}Pu_R$	1.00E+19	atoms/g
$^{238}U_R$	834.760	mg/g	$^{240}Pu_R$	8.116	mg/g
$^{238}U_R$	2.11E+21	atoms/g	$^{240}Pu_R$	2.04E+19	atoms/g
^{148}Nd	0.4039	mg/g	$^{241}Pu_R$	2.153	mg/g
^{148}Nd	1.64E+18	atoms/g produced	$^{241}Pu_R$	5.40E+18	atoms/g

Nd to Fission Conversion for ^{239}Pu 0.016809 ^{148}Nd effective yield from fission and capture

$(^{235}U+^{238}U+^{239}Pu+^{240}Pu+^{241}Pu)_R$ 2.15E+21 atoms/g remaining (dominate contributors)

$(^{235}U+^{239}Pu)_C$ 9.78E+19 atoms/g consumed (assume dominated by ^{239}Pu)

Burnup = 4.35% 41.80 GWD/MT

Table 6.8 Burnup Results for FP-7-P-2.

ICPMS Burn-up Data **Sample: FP-7-P-2**

2.267 g fuel pellet N_A = 6.02E+23 atoms/mole

Uranium	wt. %	Plutonium	wt. %	Neodymium	wt. %
				^{140}Nd	
				^{142}Nd	0.0000%
^{233}U	0.0001%	^{238}Pu	0.0000%	^{143}Nd	16.7581%
^{234}U	0.0007%	^{239}Pu	28.3327%	^{144}Nd	31.2833%
^{235}U	0.0567%	^{240}Pu	50.6485%	^{145}Nd	17.4456%
^{236}U	0.0314%	^{241}Pu	12.6601%	^{146}Nd	17.1516%
^{238}U	99.9111%	^{242}Pu	8.3587%	^{148}Nd	10.8878%
		^{244}Pu	0.0000%	^{150}Nd	6.4736%
	100.0000%		100.0000%		100.0000%
Total (mg/g)[1]	**867.62**		**18.56**		**3.494**
Total (mg)	**1967**		**42.07**		**7.92**

[1] Concentration in sample with units of mg of element per gram of sample.

$^{235}U_R$	0.492	mg/g	$^{239}Pu_R$	5.236	mg/g
$^{235}U_R$	1.26E+18	atoms/g	$^{239}Pu_R$	1.32E+19	atoms/g
$^{238}U_R$	866.851	mg/g	$^{240}Pu_R$	9.400	mg/g
$^{238}U_R$	2.19E+21	atoms/g	$^{240}Pu_R$	2.36E+19	atoms/g
^{148}Nd	0.3804	mg/g	$^{241}Pu_R$	2.359	mg/g
^{148}Nd	1.55E+18	atoms/g produced	$^{241}Pu_R$	5.92E+18	atoms/g

Nd to Fission Conversion for ^{239}Pu 0.016809 ^{148}Nd effective yield from fission and capture

$(^{235}U+^{238}U+^{239}Pu+^{240}Pu+^{241}Pu)_R$ 2.24E+21 atoms/g remaining (dominate contributors)

$(^{235}U+^{239}Pu)_C$ 9.21E+19 atoms/g consumed (assume dominated by ^{239}Pu)

Burnup = 3.96% 37.97 GWD/MT

Table 6.9 Burnup Results for FP-7-P-3.

ICPMS Burn-up Data — Sample: FP-7-P-3

2.244 g fuel pellet — N_A = 6.02E+23 atoms/mole

Uranium	wt. %	Plutonium	wt. %	Neodymium	wt. %
				^{140}Nd	
				^{142}Nd	0.0000%
^{233}U	0.0001%	^{238}Pu	0.0000%	^{143}Nd	15.6165%
^{234}U	0.0007%	^{239}Pu	25.0354%	^{144}Nd	32.1119%
^{235}U	0.0501%	^{240}Pu	50.9407%	^{145}Nd	17.3613%
^{236}U	0.0343%	^{241}Pu	13.7984%	^{146}Nd	17.3890%
^{238}U	99.9149%	^{242}Pu	10.2162%	^{148}Nd	10.9285%
		^{244}Pu	0.0092%	^{150}Nd	6.5928%
	100.0000%		100.0000%		100.0000%
Total (mg/g)[1]	**832.89**		**15.82**		**3.618**
Total (mg)	**1869**		**35.49**		**8.12**

[1] Concentration in sample with units of mg of element per gram of sample.

$^{235}U_R$	0.417	mg/g	$^{239}Pu_R$	3.942	mg/g
$^{235}U_R$	1.07E+18	atoms/g	$^{239}Pu_R$	9.93E+18	atoms/g
$^{238}U_R$	832.183	mg/g	$^{240}Pu_R$	8.054	mg/g
$^{238}U_R$	2.11E+21	atoms/g	$^{240}Pu_R$	2.02E+19	atoms/g
^{148}Nd	0.3954	mg/g	$^{241}Pu_R$	2.191	mg/g
^{148}Nd	1.61E+18	atoms/g produced	$^{241}Pu_R$	5.50E+18	atoms/g

Nd to Fission Conversion for ^{239}Pu — 0.016809 ^{148}Nd effective yield from fission and capture

$(^{235}U+^{238}U+^{239}Pu+^{240}Pu+^{241}Pu)_R$ — 2.14E+21 atoms/g remaining (dominate contributors)

$(^{235}U+^{239}Pu)_C$ — 9.58E+19 atoms/g consumed (assume dominated by ^{239}Pu)

Burnup = 4.28% 41.08 GWD/MT

Table 6.10 Burnup Results for FP-7-C-3.

ICPMS Burn-up Data — Sample: FP-7-C-3

39.981 g fuel pellet — N_A = 6.02E+23 atoms/mole

Uranium	wt. %	Plutonium	wt. %	Neodymium	wt. %
				^{140}Nd	
				^{142}Nd	0.0000%
^{233}U	0.0000%	^{238}Pu	0.0000%	^{143}Nd	16.6979%
^{234}U	0.0013%	^{239}Pu	28.1143%	^{144}Nd	31.2705%
^{235}U	0.0550%	^{240}Pu	51.0827%	^{145}Nd	17.4834%
^{236}U	0.0326%	^{241}Pu	12.4953%	^{146}Nd	17.1751%
^{238}U	99.9110%	^{242}Pu	8.2975%	^{148}Nd	10.9342%
		^{244}Pu	0.0101%	^{150}Nd	6.4388%
	100.0000%		100.0000%		100.0000%
Total (mg/g)[1]	**902.51**		**19.99**		**3.696**
Total (mg)	**36083**		**799.17**		**147.76**

[1] Concentration in sample with units of mg of element per gram of sample.

$^{235}U_R$	0.497	mg/g	$^{239}Pu_R$	5.596	mg/g
$^{235}U_R$	1.27E+18	atoms/g	$^{239}Pu_R$	1.41E+19	atoms/g
$^{238}U_R$	901.712	mg/g	$^{240}Pu_R$	10.210	mg/g
$^{238}U_R$	2.28E+21	atoms/g	$^{240}Pu_R$	2.56E+19	atoms/g
^{148}Nd	0.4041	mg/g	$^{241}Pu_R$	2.508	mg/g
^{148}Nd	1.65E+18	atoms/g produced	$^{241}Pu_R$	6.29E+18	atoms/g

Nd to Fission Conversion for ^{239}Pu — 0.016809 ^{148}Nd effective yield from fission and capture

$(^{235}U+^{238}U+^{239}Pu+^{240}Pu+^{241}Pu)_R$ — 2.33E+21 atoms/g remaining (dominate contributors)

$(^{235}U+^{239}Pu)_C$ — 9.79E+19 atoms/g consumed (assume dominated by ^{239}Pu)

Burnup = 4.03% 38.72 GWD/MT

Table 6.11 Burnup Results for FP-16-P-1.

ICPMS Burn-up Data — Sample: FP-16-P-1

2.428 g fuel pellet — N_A = 6.02E+23 atoms/mole

Uranium	wt. %	Plutonium	wt. %	Neodymium	wt. %
				^{140}Nd	
				^{142}Nd	0.0000%
^{233}U	0.0000%	^{238}Pu	0.0000%	^{143}Nd	14.9814%
^{234}U	0.0011%	^{239}Pu	24.4334%	^{144}Nd	33.0928%
^{235}U	0.0397%	^{240}Pu	50.5574%	^{145}Nd	17.1008%
^{236}U	0.0336%	^{241}Pu	13.6246%	^{146}Nd	17.4532%
^{238}U	99.9256%	^{242}Pu	11.3715%	^{148}Nd	10.9032%
		^{244}Pu	0.0131%	^{150}Nd	6.4686%
	100.0000%		100.0000%		100.0000%
Total (mg/g)[1]	**861.55**		**17.16**		**3.833**
Total (mg)	**2092**		**41.66**		**9.31**

[1] Concentration in sample with units of mg of element per gram of sample.

$^{235}U_R$	0.342	mg/g	$^{239}Pu_R$	4.173	mg/g
$^{235}U_R$	8.76E+17	atoms/g	$^{239}Pu_R$	1.05E+19	atoms/g
$^{238}U_R$	860.908	mg/g	$^{240}Pu_R$	8.670	mg/g
$^{238}U_R$	2.18E+21	atoms/g	$^{240}Pu_R$	2.18E+19	atoms/g
^{148}Nd	0.4179	mg/g	$^{241}Pu_R$	2.346	mg/g
^{148}Nd	1.70E+18	atoms/g produced	$^{241}Pu_R$	5.89E+18	atoms/g

Nd to Fission Conversion for ^{239}Pu — 0.016809 ^{148}Nd effective yield from fission and capture

$(^{235}U+^{238}U+^{239}Pu+^{240}Pu+^{241}Pu)_R$ — 2.22E+21 atoms/g remaining (dominate contributors)

$(^{235}U+^{239}Pu)_C$ — 1.01E+20 atoms/g consumed (assume dominated by ^{239}Pu)

Burnup = 4.37% 41.91 GWD/MT

Table 6.12 Burnup Results for FP-16-P-2.

ICPMS Burn-up Data — Sample: FP-16-P-2

2.285 g fuel pellet — N_A = 6.02E+23 atoms/mole

Uranium	wt. %	Plutonium	wt. %	Neodymium	wt. %
				^{140}Nd	
				^{142}Nd	0.0000%
^{233}U	0.0001%	^{238}Pu	0.0000%	^{143}Nd	15.6030%
^{234}U	0.0015%	^{239}Pu	26.4337%	^{144}Nd	32.0391%
^{235}U	0.0457%	^{240}Pu	49.7310%	^{145}Nd	17.3886%
^{236}U	0.0344%	^{241}Pu	13.5564%	^{146}Nd	17.4576%
^{238}U	99.9184%	^{242}Pu	10.2789%	^{148}Nd	10.9392%
		^{244}Pu	0.0000%	^{150}Nd	6.5726%
	100.0000%		100.0000%		100.0000%
Total (mg/g)[1]	**843.29**		**16.58**		**3.665**
Total (mg)	**1927**		**37.89**		**8.37**

[1] Concentration in sample with units of mg of element per gram of sample.

$^{235}U_R$	0.385	mg/g	$^{239}Pu_R$	4.364	mg/g
$^{235}U_R$	9.87E+17	atoms/g	$^{239}Pu_R$	1.10E+19	atoms/g
$^{238}U_R$	842.606	mg/g	$^{240}Pu_R$	8.244	mg/g
$^{238}U_R$	2.13E+21	atoms/g	$^{240}Pu_R$	2.07E+19	atoms/g
^{148}Nd	0.4009	mg/g	$^{241}Pu_R$	2.257	mg/g
^{148}Nd	1.63E+18	atoms/g produced	$^{241}Pu_R$	5.66E+18	atoms/g

Nd to Fission Conversion for ^{239}Pu — 0.016809 ^{148}Nd effective yield from fission and capture

$(^{235}U+^{238}U+^{239}Pu+^{240}Pu+^{241}Pu)_R$ — 2.17E+21 atoms/g remaining (dominate contributors)

$(^{235}U+^{239}Pu)_C$ — 9.71E+19 atoms/g consumed (assume dominated by ^{239}Pu)

Burnup = 4.28% 41.11 GWD/MT

Table 6.13 Burnup Results for FP-7-C-3.

ICPMS Burn-up Data — Sample: FP-16-C-3

67.889 g fuel pellet — N_A = 6.02E+23 atoms/mole

Uranium	wt. %	Plutonium	wt. %	Neodymium	wt. %
				^{140}Nd	
				^{142}Nd	0.0000%
^{233}U	0.0001%	^{238}Pu	0.0000%	^{143}Nd	16.5573%
^{234}U	0.0010%	^{239}Pu	28.2110%	^{144}Nd	31.2103%
^{235}U	0.0547%	^{240}Pu	50.4600%	^{145}Nd	17.4876%
^{236}U	0.0294%	^{241}Pu	13.0714%	^{146}Nd	16.8804%
^{238}U	99.9148%	^{242}Pu	8.2576%	^{148}Nd	10.9048%
		^{244}Pu	0.0000%	^{150}Nd	6.9596%
	100.0000%		100.0000%		100.0000%
Total (mg/g)[1]	**710.15**		**16.27**		**2.953**
Total (mg)	**48212**		**1104.50**		**200.47**

[1] Concentration in sample with units of mg of element per gram of sample.

$^{235}U_R$	0.389	mg/g	$^{239}Pu_R$	4.570	mg/g
$^{235}U_R$	9.96E+17	atoms/g	$^{239}Pu_R$	1.15E+19	atoms/g
$^{238}U_R$	709.549	mg/g	$^{240}Pu_R$	8.209	mg/g
$^{238}U_R$	1.80E+21	atoms/g	$^{240}Pu_R$	2.06E+19	atoms/g
^{148}Nd	0.3220	mg/g	$^{241}Pu_R$	2.135	mg/g
^{148}Nd	1.31E+18	atoms/g produced	$^{241}Pu_R$	5.36E+18	atoms/g

Nd to Fission Conversion for ^{239}Pu — 0.016809 ^{148}Nd effective yield from fission and capture

$(^{235}U+^{238}U+^{239}Pu+^{240}Pu+^{241}Pu)_R$ — 1.83E+21 atoms/g remaining (dominate contributors)

$(^{235}U+^{239}Pu)_C$ — 7.80E+19 atoms/g consumed (assume dominated by ^{239}Pu)

Burnup = 4.08% 39.16 GWD/MT

7. SUMMARY AND CONCLUSIONS

7.1 Fuel and Clad Performance Found Acceptable

The 40 GWd/MT PIE has been performed on two capsules irradiated in the reflector of the ATR for a total of 904.1 EFPDs with an accumulated average burnup of about 40 GWd/MT. These capsules have been irradiated during 30 ATR operational cycles and have experienced 42 thermal cycles. The average EFPD-weighted LHGR has been about 6.4 kW/ft, which is higher than normally experienced by commercial fuel reaching this burnup.

Both Capsule 4 (containing Fuel Pin 7) and Capsule 13 (containing Fuel Pin 16) were visually and dimensionally examined. No signs of capsule damage or distortion were observed. Gamma scans indicated that all internal components (pellets, end caps, and spring) were in their initial locations, and there were no signs of fuel pin damage or distortion. The extent of end-pellet peaking as exhibited by the gamma scans is in accordance with the MCNP code predictions used for the pretest thermal-hydraulic analyses. Measurement of internal gas pressure was successful, indicated no fuel pin leakage, and the pressure was within expectations. The capsules were opened by cutting at the bottom, just above the weld. After the capsules were opened, the fuel pins were removed and visually and dimensionally inspected.

Sectioned fuel was polished, etched, and gamma-scanned. Metallographic examination of fuel specimens revealed good performance; nothing detrimental or unexpected was noted. The observed plutonium-rich agglomerates were larger than is expected in mission fuel, but are not troublesome. The pellet cracking is considered normal. Thin (a few microns) oxide layers are evident in the areas of pellet-clad contact, particularly where an agglomerate lies at or very near the pellet surface. The fuel exhibited no restructuring or deleterious thermal effects.

Some modest grain growth was observed in the central hotter portion of the fuel pellets. The TIGR-treated fuel had slightly greater fission gas release than the untreated fuel. The reason for this may be the preirradiation thermal processing associated with the TIGR-treated material. The extent of fuel swelling, as inferred from polished cross sections, appears to be in accordance with expectations based on reviews of the available literature. Volume 2 discusses fuel swelling and densification in greater detail.

A SEM/Microprobe examination of the fuel and clad revealed no abnormal behavior of either the fuel or clad. The oxide layers were thicker and involved some minor fuel diffusion in the regions of a surface agglomerate. At this point in the irradiation, the microstructure of the two fuel types appears to be behaving in a similar fashion, except for the greater fission gas release from the TIGR-treated material. Both types had “bubble trails” on the fracture surfaces. Elemental mapping confirmed that the agglomerates were rich in plutonium and that the fission products Ru and Pd were localized to the agglomerates. It also identified xenon diffusing from the agglomerate as the driver for the haloes appearing in the matrix around the agglomerates.

The qualitative gamma scan indicated that the burnup profile is off-center peaked, as expected from the MNCP code pretest calculations, but the peaking is not as strong as noted in previous PIEs.

Gallium analyses of the clad specimens indicate no significant migration of the gallium to the clad. The analysis of both unirradiated archival material (as a baseline) and the irradiated cladding indicate no transfer of gallium to the cladding within the measurement uncertainty. Selected segments of the clad were set aside for later ductility testing.

Both the fuel pins containing untreated and TIGR-treated material performed in a similar manner with respect to gallium fuel-clad migration. In fact, there was no indication of significant gallium movement, which was consistent with past PIEs.

A neodymium-148 burnup analysis gave an average burnup of 38.9 GWd/MT for Fuel Pin 7 and 39.4 GWd/MT for Fuel Pin 16, very near the predicted value of 39.8 GWd/MT.

Overall, the capsules handled the irradiation without incident and there are no indications of any mechanisms that may result in threats to containment integrity from continued irradiation of the sister capsules. The only difference in the observed states of the untreated (Fuel Pin 7) and TIGR-treated (Fuel Pin 16) pellets was the fission gas release.

7.2 Permanent Clad Expansion

There is clear evidence of a progressive expansion of the clad. This expansion is permanent persisting after cooling has caused the pellet to shrink away from the inner clad surface. The extent is small, about 0.3 percent diametral. Although the direction is outward, not inward, the magnitude is consistent with the radiation-induced clad expansions and examples of clad creep documented in the literature. In addition, minor pellet edge/clad interactions have been noted, similar to the “primary ridges” found in commercial PWR fuel. The clad exterior has been measured in detail for the 8, 21, 30 and 40 GWd/MT irradiations and it has been shown that the clad creep and ridging were present in all four examinations. This indicates that the ridging and creep occurred early in the irradiation. See Volume 2 for additional discussion of this finding.

7.3 Clad Samples Identified for Future Testing

Two clad sections were prepared but not destructively tested during this PIE; they were set aside for later ductility testing when the necessary test apparatus has been fabricated and installed in the hot cell. Table 7.1 lists these items along with the clad samples stored from the previous PIE tasks. It should be noted that the Fuel Pin 2, 3, 7, 9, 10, and 16 samples are relatively long, and can be subdivided as desired in the future.

Defueling was done on two of the previous clad sections to establish an effective method for fuel removal without damage to the clad surface. Soaking the fuel pin sections in 100ºC 8M nitric acid was found to be a reasonable method for removing the fuel from the clad.

Table 7.1 Clad Samples Archived for Later Testing

Capsule	Fuel Pin	Fuel Type	Sample	Approx. Length (inches)
1	2	Non-TIGR	Upper clad region of Fuel Pin 2	1.6
8	11	TIGR	Upper clad region of Fuel Pin 11, Sample FP-11-C-6	2.4
8	11	TIGR	Lower clad region of Fuel Pin 11, Sample FP-11-C-8	2.4
2	5	Non-TIGR	Middle clad region of Fuel Pin 5, Sample FP-5-C-5	3.8
9	12	TIGR	Middle clad region of Fuel Pin 12, Sample FP-12-C-2	5.2
3	6	Non-TIGR	Middle clad region of Fuel Pin 6, Sample FP-6-C-3	3.0
3	6	Non-TIGR	Bottom clad region of Fuel Pin 6, Sample FP-6-C-5	1.6
10	13	TIGR	Middle clad region of Fuel Pin 13, Sample FP-13-C-3	2.0
10	13	TIGR	Bottom clad region of Fuel Pin 13, Sample FP-13-C-5	1.6
4	7	Non-TIGR	Middle clad region of Fuel Pin 7, Sample FP-7-C-3	3.0
13	16	TIGR	Middle clad region of Fuel Pin 16, Sample FP-16-C-3	5.0

7.4 Summary of Adjusted Pressure and Release Fraction Measurements.

During the course of this PIE the equipment used for gas pressure measurement and release fraction measurement was refined and accuracy checked with calibration runs and reexamination of past data. In addition, the volume of the fuel pins and capsule plenums were recalculated (and in one case measured) to reduce the uncertainty. Finally, the as-built fuel mass was used to estimate fission product inventories rather than the nominal values. The net result of this effort was minor changes in the reported pressure and release fraction values. The updated values are listed in Table 7.2.

Table 7.2 Adjusted Capsule and Fuel Pin Pressures and Release Fractions

Approximate Burn Up (GWd/MT)	Capsule / Fuel Pin	Pressure (psia)	Release Fraction (%)	Type
21	Capsule 2	9.79		
21	Fuel Pin 5	20.25	1.32	Non-TIGR
21	Capsule 9	9.74		
21	Fuel Pin 12	23.61	1.88	TIGR
30	Capsule 3	9.88		
30	Fuel Pin 6	26.71	1.47	Non-TIGR
30	Capsule 10	9.70		
30	Fuel Pin 13	33.21	2.30	TIGR
40	Capsule 4	9.84		
40	Fuel Pin 7	114.84	8.37	Non-TIGR
40	Capsule 13	9.95		
40	Fuel Pin 16	134.79	9.51	TIGR

8. ACKNOWLEDGMENTS

The authors wish to thank Steve Childs, Tom Kenney, Pat Howard, Jeff Moody, and Dale Caquelin of the Irradiated Fuels Examination Laboratory Staff for their help with the MOX capsule PIE task; thanks also go to Hu Longmire of the Metals and Ceramics Division for performing the metallographic work. Steve Hodge and Cindy Johnston helped with clad oxide layer photo analysis. The SEM/microprobe task was performed with assistance from Larry Walker, also from the Metals and Ceramics Division, who supported us both in the task and with equipment testing. In addition, we wish to express our appreciation to John Keller and Joseph Giaquinto of the Radioactive Materials Analysis Laboratory for performing the radiochemical analysis. Finally, we would like to thank the reviewers of this document.

9. REFERENCES

1. B.S. Cowell and S.A. Hodge, *Fissile Materials Disposition Program Light-Water Reactor Mixed Oxide Fuel Irradiation Test Project Plan*, ORNL/MD/LTR-78, Rev 2, May 2000.

2. B.S. Cowell, *Technical Specification: Mixed-Oxide Pellets for the Light-Water Reactor Irradiation Demonstration Test*, ORNL/MD/LTR-75, June 1997.

3. K.R. Thoms, *Design, Functional, and Operational Requirements for the Advanced Test Reactor Mixed Oxide Fuel Irradiation Experiment*, ORNL/MD/LTR-76, September 1997.

4. B.S. Cowell, *Purchase Order: Mixed-Oxide Pellets and Fuel Pin Assemblies*, ORNL/MD/LTR-77, August 1997.

5. S.A. Hodge, *Effects of Fission Gas Release and Pellet Swelling Within the LWR Mixed Oxide Irradiation Test Assembly*, ORNL/MD/LTR-83 Rev 1, November 1997.

6. L.J. Ott, *Thermal/Hydraulic Calculations for the LWR MOX Irradiation Test Assembly at 12 KW/FT*, ORNL/MD/LTR-85, Vol. 1&2, October 1997.

7. B.S. Cowell, *Purchase Order: Mixed-Oxide Capsule Assemblies*, ORNL/MD/LTR-90, Rev 0, August 1997.

8. B.S. Cowell and S.A. Hodge, *ATR Capsule Assembly Loading and Operation Schedule*, ORNL/MD/LTR-91 Rev 4, November 2001.

9. R.N. Morris, *Post-Irradiation Examination Plan For ATR MOX Capsules Withdrawn at 30 GWd/MT and Higher*, ORNL/MD/LTR-195, September 2000.

10. R.N. Morris, et. al., *MOX Average Power Early PIE: 8 GWd/MT Quick Look*, ORNL/MD/LTR-163 Rev. 1, February 1999.

11. R.N. Morris, et. al., *MOX Average Power Early PIE: 8 GWd/MT Final Report*, ORNL/MD/LTR-172, November 1999.

12. R.N. Morris, et. al., *MOX Average Power Intermediate PIE: 21 GWd/MT Quick Look*, ORNL/MD/LTR-185, March 2000.

13. R.N. Morris, et. al., *MOX Average Power Intermediate PIE: 21 GWd/MT Final Report*, ORNL/MD/LTR-199, December 2000.

14. R.N. Morris, et. al., *MOX Average Power Test 30 GWd/MT PIE: Quick Look*, ORNL/MD/LTR-208, February 2001.

15. R.N. Morris, et. al., *MOX Average Power 30 GWd/MT PIE: Final Report*, ORNL/MD/LTR-212, Volume 1, November 2001.

16. R.N. Morris, et. al., *MOX Average Power Test 40 GWd/MT PIE: Quick Look*, ORNL/MD/LTR-236, Volume 1, November 2002.

17. R.N. Morris, J. Giaquinto, S.A. Hodge, *MOX Average Power Test Fuel Pellet Initial Gallium Content,* ORNL/MD/LTR-182.

18. INEEL Letter *"MCNP-Recalculated MOX Fuel Capsule Burnup at the End of Phase-I, Phase-II, and Estimated Phase III Irradiation,"* ORMOX-GSC-25-99 dated December 9, 1999.

19. S. A. Hodge, et al., *Implications of the PIE Results for the 30-GWd/MT-Withdrawal MOX Capsules,* ORNL/MD/LTR-212, Volume 2, Rev 1, February 2002.

20. C. Vitanza, E. Kolstad, and U. Graziani, *Fission Gas Release From UO_2 Pellet Fuel at High Burn-up*, ANS Topical Meeting on Light Water Reactor Fuel Performance, Portland, Oregon, 29 April–3 May, 1979.

21. R.N. Morris, C.A. Baldwin, C.M. Malone, *MOX Fission Gas Pressure Measuring Apparatus*, ORNL/MD/LTR-176, January 2000.

22. W. K. Terry, *As-Run Radiological Characterization of MOX Fuel Capsules Removed From the ATR After Cycle 127A — WKT-03-02*, March 28, 2002.

23. R.N. Morris, C.A. Baldwin, *MOX Fuel Pin Measuring Apparatus*, ORNL/MD/LTR-209, March 2001.

24. R.N. Morris, D.W. Heatherly, *MOX Fuel Pin Volume Measuring Apparatus*, ORNL/MD/LTR-232, September 2002.

25. R. N. Morris, C. A. Baldwin, *CCCTF Trap Table Calibration Curves for Krypton-85 Activity Determination,* ORNL/MD/LTR-246, June 2003.

26. G. S. Chang, *ATR WG-MOX Fuel Pellet Burnup Measurement by Monte Carlo – Mass Spectrometric Method,* PHYSOR 2002, Seoul, Korea, October 7-10, 2002.

27. H. Bailly, D. Menessier, and C. Prunier, ed., *The Nuclear Fuel of Pressurized Water Reactors and Fast Reactors— Design and Behaviour,* Lavoisier Publishing Inc., Secaucus, NJ, 1999.

28. "Internal Corrosion Layer in PWR Fuel," Lionel Desgranes, **OECD Proceedings, Seminar on Thermal Performance of High Burn-up LWR Fuel**, 3-6 March 1998,

CEA, Cadarache France, 187-195

29. C. Ronchi and C.T. Walker, *Determination of Xenon Concentrations in Nuclear Fuels by Electron Microprobe Analysis*, J. Phys. D: Appl. Phys., 13 (1980) 2175

30. S.B. Fisher, et al., *Microstructure of Irradiated SBR MOX Fuel and Its Relationship to Fission Gas Release,* **Journal of Nuclear Materials,** 306, (2002), 153-172

31. C.T. Walker, W. Goll, T. Matsumura, *Further Observations on OCOM MOX Fuel; Microstructure in the Vicinity of the Pellet Rim and Fuel-Cladding Interaction,* **Journal of Nuclear Materials,** 245 (1997), 169-178

10. DISTRIBUTION

1. P.T. Rhoads, U.S. Department of Energy, MD-3, 1000 Independence Avenue SW, Forrestal Building 6G-050, Washington DC 20585
2. D. Alberstein, DOE/NNSA NN-60, 1000 Independence Avenue SW 6G069, Washington, DC 20585
3. S. Basu, RES/DST/AEB, U.S. Nuclear Regulatory Commission, MS-T 10 E45, Rockville, MD 20852

4-6. T. Blair, NMT-15, MS E530, Los Alamos National Laboratory, Los Alamos, NM 87545

7-10. R.C. Pedersen, Idaho National Engineering and Environmental Laboratory, EROB, 2525 Fremont Avenue, Idaho Falls, ID 83415-3419

11. P. Kasik, MPR Associates Inc., 320 King Street, Alexandria, VA 22314-3238

12-16. C.A. Baldwin

17. B.S. Cowell
18. S.R. Greene
19. D.W. Heatherly
20. W.R. Hendrich

21-25. S.A. Hodge

26. L.L. Horton
27. M.W. Kennard, Stoller Nuclear Fuel, 485 Washington Avenue, Pleasantville, NY 10570
28. R.Y. Lee, RES/DST/AEB, U.S. Nuclear Regulatory Commission, MS-T 10 H3, Rockville, MD 20852

29-33. J.S. Tucker, Framatome Cogema Fuels, 3315 Old Forest Road, Lynchburg, Va 24506

34. W.J. McAfee

35-39. R.N. Morris

40. L.J. Ott

41-45. N.H. Packan

46. H.H. Scott, RES/DST/RPSB U.S. Nuclear Regulatory Commission, MS-T 10 I03, Rockville, MD 20852
47. D.J. Spellman
48. K.R. Thoms
49. ORNL Laboratory Records (RC)